Contributors

Numbers in parentheses indicate the pages on which the authors' contributions begin.

Emili Besalú (1), Institut de Química Computacional, Universitat de Girona, Girona 17071, Catalonia, Spain

Joachim Brand (65), Theoretische Chemie, Universität Heidelberg, D-69120 Heidelberg, Germany

J. L. Brédas (121), Service de Chemie des Matérial Nouveaux, Centre de Recherche Electronique et Photonique Moléculaires, Université de Mons-Hainaurt, B-7000 Mons, Belgium

Ramon Carbó-Dorca (1), Institut de Química Computacional, Universitat de Girona, Girona 17071, Catalonia, Spain

Lorenz S. Cederbaum (65), Theoretische Chemie, Universität Heidelberg, D-69120 Heidelberg, Germany

Xavier Gironés (1), Institut de Química Computacional, Universitat de Girona, Girona 17071, Catalonia, Spain

Roman F. Nalewajski (217), K. Guninski Department of Theoretical Chemistry,Jagiellonian University, 30-060 Cracow, Poland

Swapan K. Pati (121), Department of Chemistry, Northwestern University, Evanston, IL 60208

S. Ramasesha (121), Solid State and Structural Chemistry Unit, Indian Institute of Science, Bangalore 560 012, India

Z. Shuai (121), Service de Chemie des Matérial Nouveaux, Centre de Recherche Electronique et Photonique Moléculaires, Université de Mons-Hainaurt B-7000 Mons, Belgium

Michael Charles Zerner

January 31, 1940—February 2, 2000

On February 2, 2000, our colleague, friend, and fellow editor Michael Zerner died after a long and difficult battle with cancer. Mike was born in Hull, Massachusetts, and graduated from Carnegie-Mellon University in 1961. Subsequent graduate study with Martin Gouterman at Harvard led to M.A. and Ph.D. degrees in chemistry in 1966, and marked the beginning of an outstanding career as a theoretical chemist. After serving for two years in the U.S. Army during which he reached the rank of Captain, he spent two years at Uppsala University in Sweden with Per-Olov Löwdin as an N.I.H. Postdoctoral Fellow. He subsequently took his first faculty position in 1970 as an assistant professor at Guelph University in Canada, where he later attained the rank of professor. In 1981 he was appointed Professor of Chemistry at the University of Florida. His productive career was marked by exemplary teaching, research and service. From 1988 to 1994 he served as Chairman of the department. His research has led to approximately 200 publications. He held visiting professor appointments at a number of universities in several countries and presented countless talks at universities, industrial laboratories, and professional meetings. He was an active participant in the Quantum Theory Project, a joint research institute of the departments of Chemistry and Physics at the University of Florida. He was one of the organizers of and a major contributor to the annual Sanibel Symposia. His leadership role in the international community of quantum chemists is reflected by his editorship of *Advances in Quantum Chemistry* his associate editorship of *International Journal of Quantum Chemistry* and his membership on several editorial boards. The ZINDO software program written by him and his students is used throughout the world for instruction and research. In 1998 he became the first member of the University of Florida chemistry department to be promoted to the rank of Distinguished Professor.

Mike will be long remembered for his boundless energy and positive attitude to almost every situation. As he was wont to say, "We can do that!"

JOHN R. SABIN

Extended Density Functions

Ramon Carbó-Dorca [☆], Emili Besalú, Xavier Gironés

Institut de Química Computacional
Universitat de Girona
Girona 17071
Catalonia (Spain)

Abstract

Density Functions play a fundamental role in the definition of Quantum Theory, due to this they are the basic materials used in order to define Quantum Objects and from this intermediate step, they constitute the support of Quantum Similarity Measures. Here, the connection of Wavefunctions with Extended Density Functions is analysed. Various products of this preliminary discussion are described, among others the concept of Kinetic Energy Distributions. Another discussed set of concepts, directly related with the present paper, is constituted by the Extended Hilbert Space definition, where their vectors are defined as column structures or diagonal matrices, containing both wavefunctions and their gradients. The shapes of new density distributions are described and analysed. All the steps above summarised are completed and illustrated, when possible, with practical application examples and visualisation pictures.

☆ To whom correspondence must be addressed.

ADVANCES IN QUANTUM CHEMISTRY, VOLUME 38

0065-3276/01 $35.00

1.Introduction.

Several years ago, Wigner [1] described how to reconcile some aspects of Quantum Mechanics, with thermodynamic statistical distributions, a question which has been raised again recently, even in close relationship with modern experimental techniques [2]. In addition, contemporary to Wigner's paper, there is a volume due to von Neumann, considered by the author itself as a proposal to clarify the ideas presented in a previous work by Dirac [3]. The concepts along with von Neumann's work appear as a result of discussions in deep of the quantum mechanical theoretical foundations [4], yielding a mathematical development, where the modern usual statistical interpretation of Quantum Theory is still to be found. With equal interest, associated to similar mathematical aspects, shall be mentioned the book of Bohm [5], where the interpretation of both wavefunction and probability density function roles was cleverly analysed, among other nonetheless interesting subjects. After this, following an exciting research path, Bell [6] produced several discussion proposals. These were mainly related to various remnant ambiguous theoretical aspects of Quantum Mechanics, among others, those raised by the so-called Einstein, Podolsky and Rosen paradox [7, 8].

The previously mentioned ideas could be considered as an inspiring source of the present work. However, one of the references, which shall be located at the real origin of this study, is the volume due to Mezey [9]. Also, large amount of previous and ulterior related studies [10] published by the same author are to be quoted due to the same inspiring aspect. Mezey has proved how electronic Density Functions (eDF) pictorial forms can be handled: analysed, computed and visualised. He has shown for the first time how eDF visualisation can be of great help for the understanding of molecular shapes. The eDF isodensity surfaces acting as a molecular microscope. Describing the eDF topology, Mezey deduced a great deal of attached applications, like the concept of molecular shape similarity [11] and the recently described holographic theorem [12]. Starting from these considerations, there may be an interesting way to show that other than eDF surfaces can be visualised and analysed, alone or added to the usual eDF to obtain enhanced pictures. On the other hand, very important precedents circumscribed on the point of view of eDF mathematical analysis, have been developed by Bader [13] in a constant, long and fruitful research period, which can be traced up to actual times [14].

The present work pretends to follow the path of these approaches, hopefully adding new ways and insights to study molecular shape and to analyse generally extended Density Function (DF) concepts. This paper do not tries to substitute in any way this previous brilliant work. On the contrary, pretends to

complement and enlarge it as much as possible, providing the chemical body of alternative tools to understand molecular structure and behaviour.

Besides of these previous considerations, the theoretical development of Density Functional techniques, which started from the seminal paper by Hohenberg and Kohn [15], has enhanced the role of the DF in all the possible aspects. In this way, this fact acts as another basis for a study like the one presented.

The actual discussion has the aim to adopt this previous spirit, but obviously choosing a much more modest point of view, attached to Quantum Similarity Measures (QSM). This work is focused to explore the various possible extensions for the study of DF, the auxiliary building block elements of QSM [16-38]. In order to fulfil such a purpose, this study will start analysing a sound formal basis as a first step to understand the role of momentum operators in computational Quantum Chemistry. From this introductory position, it will be finally obtained a general pattern enveloping the whole area of DF study, beginning at the basic aspects and ending over the final applications of extended DF definitions.

It is well known that the eDF can be used for computing molecular expectation values. However, from the point of view of the development of practical applications, first order DF beginning with *ab initio* functions and ending as well into Atomic Shell Approximation (ASA) forms [39], are accepted work candidates for QSM applications too [40]. General QSM definition proves to contain expectation values as a particular case [41], some summarised details can be found in Appendix A. First-order eDF are customarily used in QSM molecular comparisons, since the initial description of the original concept [16]. Higher order eDF can be employed as well in QSM calculations [31,33,35]. Problems consisting in systems other than molecules can be studied in the same way [41], and the QSM applications can be extended to the area of statistical mechanics distributions [43] as well.

Several new possibilities have become apparent along the path of the QSM theoretical development [44]. Among others, one can quote Electrostatic Potential distributions as well as eDF transformations. Thus, one can say that eDF analysis and the attached concept of Quantum Object (QO) [41,45,46] have opened the way towards an almost complete definition of the structure of QSM and their generalisations. At the end, a mathematical picture of the connection between chemical information and the idea of molecule emerges in the form of Tagged Sets and Ensembles [47,48], see also the Definition 1 and Definition 8 of the Appendix A.

Owing to these considerations, the present paper will be organised in the following way: Tagged Sets, eDF and QO will be first briefly discussed. Differential operators and Kinetic Energy DF will be described next. Extended DF in general and associated to the ASA DF framework will follow, and some visual examples for assorted molecules given. Finally, a diagonal representation of extended wavefunctions and some applications, which could be important to grasp the new theoretical aspects, will be analysed.

2. Density Functions as Object Tags.

In this initial section will be briefly presented the background ideas which fundament the connection between quantum systems and Tagged Sets [47]. Everybody can admit that DF are, since the early times of Quantum Mechanics, an indispensable tool to precisely define mechanical systems at the adequate microscopic scale [4,5]. Therefore, Tag Set parts made of quantum DF ought to be associated to quantum system's information [48]. The quantum theoretical structure fits perfectly into the Tagged Set formalism and permits the definition of valuable new theoretical elements [49].

2.1. Quantum Objects.

The idea of Quantum Object (QO) without a well-designed formulation has been already used in the literature [30-32,35]. Moreover, the background mathematical structure leading towards the recently published [48,49] definition of QO is to be found within the possibility to construct a new kind of sets: the Tagged Sets. In their definition, both set elements and known information on them are taken simultaneously into account. In order to obtain a sound QO definition, besides the definition of the Tagged Set concept [47], and furthermore to develop this line of thought, there are needed some preliminary considerations.

2.1.1. *Expectation Values in Classical Quantum Mechanics.*

Starting from the fact that classical quantum study of microscopic systems is essentially associated with the Algorithm 1 of Appendix B. Then, all observable property values of a known system, ω, can be formally computed as expectation values, $\langle\omega\rangle$, of the associated hermitian operator, Ω, acting over the known state DF, $\rho(\mathbf{r})$ [4,5]. In the same way as in theoretical statistics it can be written:

$$\omega = \int \Omega(\mathbf{r}) \rho(\mathbf{r}) d\mathbf{r}. \tag{1}$$

Where **r** shall be considered a p-dimensional particle co-ordinate matrix. It must be also noted that equation (1) can be interpreted as some scalar product or linear functional form:

$$\omega = \Omega | \rho \ , \tag{2}$$

defined within the spaces where both the involved $\Omega(\mathbf{r})$ and $\rho(\mathbf{r})$ p-particle operators belong. Equation (1) has been recently used to connect QSM and QSAR [51] and to extend the well known Hohenberg-Kohn theorem [52].

A quantum mechanical well known alternative definition of expectation value, ω, has been defined in parallel to equation (1), having the form:

$$\omega = \int \Psi(\mathbf{r})^* \Omega \Psi(\mathbf{r}) d\mathbf{r}, \tag{3}$$

Such computational possibility may adopt the formal structure of a weighted norm:

$$\omega = \Psi | \Omega | \Psi \ . \tag{4}$$

An elegant statistical deduction of equation (4) can be found in the reference [59].

2.1.2. *Examples.*

A practical example of the formalism provided by equation (1) may be constituted by the electronic part of Electrostatic Molecular Potentials (eEMP). The concept was first used by Bonaccorsi, Scrocco and Tomasi [53a)]. The eEMP evaluated at the position **R** in 3-dimensional space, V(**R**), computed over first order eDF, $\rho(\mathbf{r})$, is readily defined using equation (1) as:

$$\Omega(\mathbf{r}) = |\mathbf{r} - \mathbf{R}|^{-1} \wedge V(\mathbf{R}) = \int |\mathbf{r} - \mathbf{R}|^{-1} \rho(\mathbf{r}) d\mathbf{r}. \tag{5}$$

Not taking into account the electron charge, eEMP acts as a positive definite (PD) distribution, with maxima located at molecular nuclei. Thus, the

form of the eEMP, when compared with the eDF structure, must be expected to reflect the weighting presence of the Coulomb operator. This is made obvious when eDF is forced to adopt the formal definition:

$$\Omega(\mathbf{r}) = \delta(\mathbf{r}-\mathbf{R}) \wedge \rho(\mathbf{R}) = \int \delta(\mathbf{r}-\mathbf{R})\rho(\mathbf{r})\,d\mathbf{r} \ . \tag{6}$$

Equation (6), can be considered as an overlap-like QSM [33] between a molecular eDF $\rho(\mathbf{r})$ and a point charge located at position **R**, represented by the Dirac delta function: $\delta(\mathbf{r}-\mathbf{R})$. At the same time, equation (6) bears the same structure as equations (1) and (5) have. Thus, it can be also said that the eDF itself, as eEMP with respect to Coulomb operator, could formally be considered as the expectation value of a Dirac delta function acting as an operator.

Equation (5), can be also written as a Coulomb interaction between a point charge, located at the position **R**, represented by a Dirac's delta function and an eDF, $\rho(\mathbf{r})$, using the integral:

$$V(\mathbf{R}) = \iint \delta(\mathbf{s}-\mathbf{R})|\mathbf{r}-\mathbf{s}|^{-1}\rho(\mathbf{r})\,d\mathbf{s}\,d\mathbf{r}, \tag{7}$$

but it can be considered as a Coulomb-like QSM too, just as in the same way as the current QSM are defined [31-33]. See also Definition 7 in Appendix A, for more details.

2.1.3. *Quantum Object Definition and Generating Rules*

Then, after these preliminary considerations, the QO Definition 2, which can be found in Appendix A, can be made. The interesting fact, which must be stressed here, is the DF leading role played in quantum mechanical systems description and, as a consequence, in the QO definition. The DF generation in varied wavefunction environments has been studied [54] several years ago. The most interesting aspect of this situation corresponds to the way eDF, ρ, are constructed, starting from the original system's wavefunctions, Ψ. This general formation process has been called a *generating rule* [49], and has been expressed by the symbol: $\mathscr{R}(\Psi \to \rho)$, see equation (B-1) in Appendix B.

2.2. Density Functions.

It is well known [54] how eDF can be variable reduced. Integrating the raw eDF definition over the entire system particle co-ordinates, except r of them, produces a r-th order eDF. The procedure may be schematised within the third step of Algorithm 1 or using the way depicted in the generating rule of equation (B-1) of Appendix B. This kind of co-ordinate reduction has been studied in many ways [55-57] and will not be repeated here.

When the practical implementation of QSM has been considered in this laboratory, a simplified manner to construct the first-order eDF form [39] has also been proposed and named Atomic Shell Approximation (ASA) eDF. A procedure has been recently described [39e),f)], bearing the correct necessary conditions to obtain positive definite ASA eDF, possessing appropriate probability distribution properties.

2.3.Convex Conditions and ASA Fitting.

Definition 4, in appendix A, succinctly presents the structural details of first order eDF, and connects their form with the ASA eDF. The ASA eDF coefficients vector, $\mathbf{w} = \{w_i\}$ must be optimised, in order to obtain an approximate function, completely adapted to *ab initio* eDF. The **w** vector component values shall be restricted to lie within the boundaries of some Vector Semispace (VSS): $\mathscr{V}_n(\mathbf{R}^+)$, see Appendix A, and his element sum, $\|\mathbf{w}\|$, shall be unity. This feature can be cast into a unique symbol, which can be referred to as *convex conditions*, $\mathscr{K}_n(\mathbf{w})$, applying over the n-dimensional vector **w**. In appendix A details can be found within the corresponding Definition 5.

As commented in Definition 4 of Appendix A, the DF form shown in equation (A-1) can be used to build up new DF elements, while preserving $\mathscr{K}_\infty(\rho)$. If **w** is taken as a vector, assuming that $\mathscr{P}=\{\rho_i(\mathbf{r})\} \subseteq \mathscr{H}(\mathbf{R}^+)$ is used as a given set of homogeneous order DF, and that convex conditions $\mathscr{K}_n(\mathbf{w})$ hold, then the linear combination:

$$\rho(\mathbf{r}) = \sum_i w_i \rho_i(\mathbf{r}) \in \mathscr{H}(\mathbf{R}^+) \tag{8}$$

produces a new DF with the same order and characteristic properties as the ones associated to the elements of the set $\mathscr{P}$. It can be said that convex conditions over vector coefficients, affecting DF superpositions, are the way to allow the construction of new DF of the same nature. Quite a considerable proportion of chemical computations, performed over large molecular systems, is based on such principle. A recent paper [39e)] and its sequel [39f)] provide the complete up-to-date details of ASA eDF fitting.

The DF themselves may be considered as elements of a VSS or also, alternatively, as members of a PD Operator Set, which can be collected in turn into another isomorphic VSS, whose elements may be PD Operators.

The most important thing to be noted in the context of PD Operator VSS, as well as in the isomorphic VSS companions, is the *closed nature* of such VSS, when appropriate PD coefficient sets are known. That is: PD linear combinations of PD Operators remain PD Operators. Discrete matrix representations of such PD Operators are PD too, and PD linear combinations of PD matrices will remain PD in the same way. Identical properties can be described using convex conditions symbols, if $\{\mathscr{K}_\infty(\rho_i);\forall i\}$ and $\mathscr{K}_n(\mathbf{w})$ hold, then equation (8) is a convex function fulfilling $\mathscr{K}_\infty(\rho)$.

2.4. Generalised density functions.

For describing a general DF form, a definition of a new matrix product, the inward product, is needed, and it can be found in Appendix D along its properties.

These features and definitions permit to express density functions in a compact and extremely general form [92]. Such previous work may be referred to defining a matrix $\mathbf{W}$ as bearing a convex coefficient (hyper-)matrix of arbitrary dimensions: $Dim(\mathbf{W}) = \{\delta\}$. In general, this can be obtained by choosing a complex matrix $\mathbf{X}$, with adequate dimension: $Dim(\mathbf{X}) = \{\delta\}$, such that the inward product holds: $\mathbf{W} = \mathbf{X}^* * \mathbf{X}$. Then, symbolically it can be assured that: $\mathbf{W} = \left\{\forall \omega \in \mathbf{W} \rightarrow \exists \chi \in \mathbf{X} : \omega = \chi^* \chi = |\chi|^2 \in \mathbf{R}^+\right\}$. This special choice can be also described by imposing convex conditions on $\mathbf{W}$, that is: $\mathscr{K}_{\{\delta\}}(\mathbf{W}) = \left\{\forall \omega \in \mathbf{W} \rightarrow \omega \in \mathbf{R}^+ \wedge |\mathbf{W}| = 1\right\}$. In the previous definitions and in what follows, (hyper-)matrix elements are written without subindices, this is so because in inward product definitions the involved (hyper-)matrix elements have to bear the same subindex set.

Let us define now a (hyper-)matrix $\mathbf{P}$, possessing such a dimension that:

$Dim(\mathbf{P}) = Dim(\mathbf{W}) = \{\delta\}$. Also, $\mathbf{P}$ contains as elements, normalised positive definite multivariate functions of a position vector $\mathbf{R}$ of arbitrary dimension. That is, it can be formally written: $\int \mathbf{P}(\mathbf{R}) d\mathbf{R} = \mathbf{1}$, being $\mathbf{1}$ the unity (hyper-)matrix, as defined before, such that: $Dim(\mathbf{1}) = \{\delta\}$. More specifically, one can compactly write the convenient structure of (hyper-)matrix $\mathbf{P}$, using the construction rule:

$$\mathbf{P} = \left\{ \forall \mathbf{p}(\mathbf{R}) \in \mathbf{P} \rightarrow \forall \mathbf{R} : \mathbf{p}(\mathbf{R}) \in \mathbf{R}^{+} \wedge \int \mathbf{p}(\mathbf{R}) d\mathbf{R} = 1 \right\}.$$

This can be accomplished by constructing an inward product: $\mathbf{P} = \mathbf{\Psi}^{*} * \mathbf{\Psi}$, being: $Dim(\mathbf{\Psi}) = \{\delta\}$, so $\mathbf{P} = \left\{ \forall \mathbf{p} \in \mathbf{P} \rightarrow \exists \varphi \in \mathbf{\Psi} : \mathbf{p} = \varphi^{2} \right\}$. Keeping this in mind, a normalised density function of the position variables vector $\mathbf{R}$ can be also expressed as an inward product:

$$\rho(\mathbf{R}) = \mathbf{W} * \mathbf{P} \Rightarrow \int \rho(\mathbf{R}) d\mathbf{R} = 1.$$

Where have been used the matrix elements sum as in Definition 6 of Appendix A.

3.Differential Operators and Kinetic Energy.

There is another interesting question, not yet discussed in the quantum mechanical literature, as it deserves. It could be attached to the interpretation of the differential operators role, as momentum representatives within the framework of classical quantum mechanics when the position space point of view is chosen.

3.1.Statement of the Problem.

There appears to be present a formal puzzle, when one tries to connect a second order differential operator, representing a QO kinetic energy (KE), using the expression of an expectation value in the statistical formalism, represented by equation (1). KE expectation values do not fulfil the usual statistical formalism represented by equation (1) and the examples given in equations (5) and (6). On the contrary, they possess a kind of expression according equation (3), as can be found in any treatise, see for instance, the Bohm [5], Messiah [58] or Shankar [59] discussions. However, the KE expectation value adequately transformed and, avoiding some scalar factors, looks like a norm. This can be easily seen when writing the following equalities:

$$2K = -\int \Psi^* \nabla^2 \Psi dV = \int (\nabla \Psi)^* (\nabla \Psi) dV , \tag{9}$$

where the change of sign can be attributed to Green's first identity [60]. A similar technique has been also used in the evaluation of KE integral representation over atomic basis sets [61]. Equation (9) has been customarily employed since the first description of DFT [62] and used as a working tool in this context hereafter [63].

A remark shall be made here, concerning the absence of a scalar imaginary unit factor accompanying the nabla operator in expression (9) and in the following equations. There seems apparently not imperative for the purpose of the present discussion to use this imaginary scalar factor. Moreover, equation (9) tells that KE will become necessarily a DP quantity, being the result of a norm-like expression. Later, section 6.3 gives a discussion on the possible ways to define the momentum operator, as well as a possible origin of the minus sign in the KE, will be given.

Available ancient and contemporary textbooks do not explain this situation, see for a recent example reference [64]. However, the current literature presents it as a *de facto* characteristic feature of quantum mechanics. The usual trend is to classify this oddity within the fuzziness of quantum mechanical postulates*. Other authors introduce KE expectation values throughout mathematical manipulations not exempt of difficulty [5].

3.2. Extended Hilbert (EH) Spaces.

In order to resume the whole picture concerning expectation values, it can be said that, quantum mechanics, admits as a fact generic computational forms, as the integral (1). When using this formal structure, the particular examples (5) and (6), represent an expectation value, like in theoretical statistics. Nevertheless, at the same time, when gradient operators appear into the computational scenario, the expectation value integral has to be modified, adopting a form as in equation (3). This kind of integral expression transforms into equation (1) only in the case

---

* A brief digression about the quantum mechanical postulates may be worthwhile now. Proposed since the formulation of quantum theory, the presence of quantum mechanical postulates in the literature is characterised by quite a large choice of variants. This can be evidenced by perusal of any textbook contained in the limited collection provided in references [3,58,61-72], but looking towards earlier times the situation has not changed since then [4,5]. One can find there, from no postulate description at all [3], up to quite large lists of them [67]. Even the suggestion can be found that quantum mechanical postulates should be substituted by adequate definitions instead [6].

where the operator, Ω, do not depends on the momentum as a variable. Equation (1) looses sense, for instance, when kinetic energy laplacian operator is to be computed, and integral (3) necessarily emerges. On the contrary, when the involved operator is a function of the position only, then both integrals are equivalent. Thus, one could take the decision to accept the form given in the integral (3), as the adequate quantum mechanical expression of the expectation values to be always adopted. However, when doing so, the presence of the density function role is paradoxically lost if Appendix B, Algorithm 1 definition is adopted.

The question may be formulated as whether it is possible to find out a coherent computational way to obtain a statistically meaningful expression for expectation values in any observable operator case. Irrespective of the system's observables being made either of momentum or position functions. Moreover, if it is possible to find out such a general way, in the expectation value general expression, the DF must be explicitly present and featuring the customary role of probability distributions as in theoretical statistics.

A possible way to solve the problem will be shortly described in terms of the points discussed up to now, although the possible solution of the dilemma will be postponed until Section 6. Suppose that the original Hilbert space, $\mathscr{H}(\mathbf{C})$, where wavefunctions belong, is extended into another one, $\mathscr{H}^{(\nabla)}(\mathbf{C})$, which contains ***both wavefunctions and their first derivatives***, the quantum mechanical momentum representation accompanying the wavefunction, that is:

$$\forall \Psi \in \mathscr{H}(\mathbf{C}) \Rightarrow \Psi \in \mathscr{H}^{(\nabla)}(\mathbf{C}) \wedge \exists \nabla(\Psi) \in \mathscr{H}^{(\nabla)}(\mathbf{C}).$$

Such a possible feature can be found, as an example, within a typical set of solutions of the Schrödinger equation. The harmonic oscillator provides an obvious particular case of such an EH space. It is well known that harmonic oscillator solutions constitute the set of Hermite polynomials [73], weighted by a gaussian function [65]. These polynomials can be considered related to the GTO basis functions most widely used in contemporary Quantum Chemistry. First derivatives of Hermite polynomials are always well defined, producing another polynomial of the same kind.

Following this line of though, it can be said that, besides the properties, customarily attached to wavefunctions [58], there can be stressed a need for an additional condition. It might consist in that the same properties of wavefunctions must be fulfilled by their first derivatives. This has not to be taken as an oddity, but it has been clearly noticed in the quantum mechanical analysis of wavefunctions. See, for instance, the work of Messiah [58] or Bohm [5] and the

Hilbert space properties provided by Löwdin [74], where it is said that the norms of both wavefunction and its gradient must be finite. See, to enlarge this point of view, the extensive discussions of the references [4, 75, 76]. Along these studies, it is repeated many times the necessity that both wavefunctions and their first derivatives possess the same mathematical characteristics.

3.3.Considerations on EH functions.

Then, considering the attached VSS, $\mathscr{H}(\mathbf{R}^+)$, where the DF belong, one can also accept that:

$$\forall \rho = |\Psi|^2 \in \mathscr{H}(\mathbf{R}^+) \Rightarrow \exists \kappa = |\nabla \Psi|^2 \in \mathscr{H}(\mathbf{R}^+)$$

to every DF, ρ, there exists in this way a momentum DF. Perhaps, in order to distinguish one DF from another, one can call, in a better descriptive way, this kind, κ, of first derivative distribution: KE DF, in the same way as March [63] refers to it. The KE DF belongs to a Hilbert VSS, and integrated provides the expectation value of the associated QO KE. The following sequence, developing details appearing in equation (9), will shed light over the proposed question:

$$\begin{aligned} 2K &= \int \kappa dV = \int |\nabla \Psi|^2 dV = \int (\nabla \Psi)^* \cdot (\nabla \Psi) dV = \\ &- \int \Psi^* \nabla^2 \Psi \, dV = -\langle \nabla^2 \rangle \equiv -\int \Psi^* \Delta \Psi \, dV = -\Delta , \end{aligned} \tag{10}$$

where the negative sign appears as a consequence of Green's first identity [60], as has been commented when equation (9) was discussed. KE DF can be supposed normalised, in the same way as eDF can be normalised too. In this case the norm of KE DF is twice the system's KE.

It can be concluded that KE can be considered related to the norm of the QO wavefunctions gradient. As a consequence it could be interesting, to obtain KE DF, κ, maps or images in the same way as they are customarily obtained for the eDF, ρ [9]. A complementary information to eDF will surely be obtained from these representations. Similar shapes of both functions at large distances from the molecular nuclei shall be expected, but having very different behaviour near the nuclei.

A related discussion can be found in Bohm treatise [5], when diverse possible time-dependent DF forms in a relativistic framework are presented. For non-stationary relativistic states, a function made of a combination of eDF and KE

DF is proposed and rejected afterwards, due to the variant character of such a function. However, for stationary states and in a non-relativistic, classical quantum mechanical environment such a proposal may become interesting and could be related to Bader [13] analysis. The term KE DF, as it was commented before, can be considered here borrowed from March volume on DFT [63]. In this study, KE DF is widely used connected with the DFT of exchange and potential contributions.

As pointed out in Section 2.3 above, being both DF, ρ and κ, elements of a VSS, then nothing opposes to perform a convex linear combination as:

$$\lambda(\mathbf{r}) = \alpha\rho(\mathbf{r}) + (1-\alpha)\kappa(\mathbf{r}),$$

where the scalar coefficient $\alpha \in [0,1]$, acts as a weight balancing both density distributions. The combined DF still will bear a structure of probability distribution whenever the KE DF is adequately normalised. The KE DF normalisation factor can be trivially deduced from equation (10) to be: $(2K)^{-1}$, but in the present study, the same can be achieved whenever ASA approach is used with every term present in the linear combination normalised.

Figures 1 and **2** show two examples of such a mixed possible representation. **Figure 1** provides a set of pictures for L-Leucine, taken as a typical organic structure with biological implications. On the other hand, **figure 2** constitutes a similar characteristic molecule, with its structure borrowed from the Mezey book [9a)], for comparative purposes. In this second set of pictures, β-Alanine is presented in an internal hydrogen bond configuration, because in this atomic geometry presents a toroidal shaped surface.

Figure 1. Mixtures of ASA DF and KE DF over the L-leucine molecule

Funcion Value	α 1.0	0.8	0.6	0.5	0.4	0.2	0.0
$1 \cdot 10^{-3}$							
$2 \cdot 10^{-3}$							
$3 \cdot 10^{-3}$							
$7 \cdot 10^{-3}$							
$1 \cdot 10^{-2}$							

Figure 2. Mixtures of ASA DF and KE DF over the β-alanine molecule

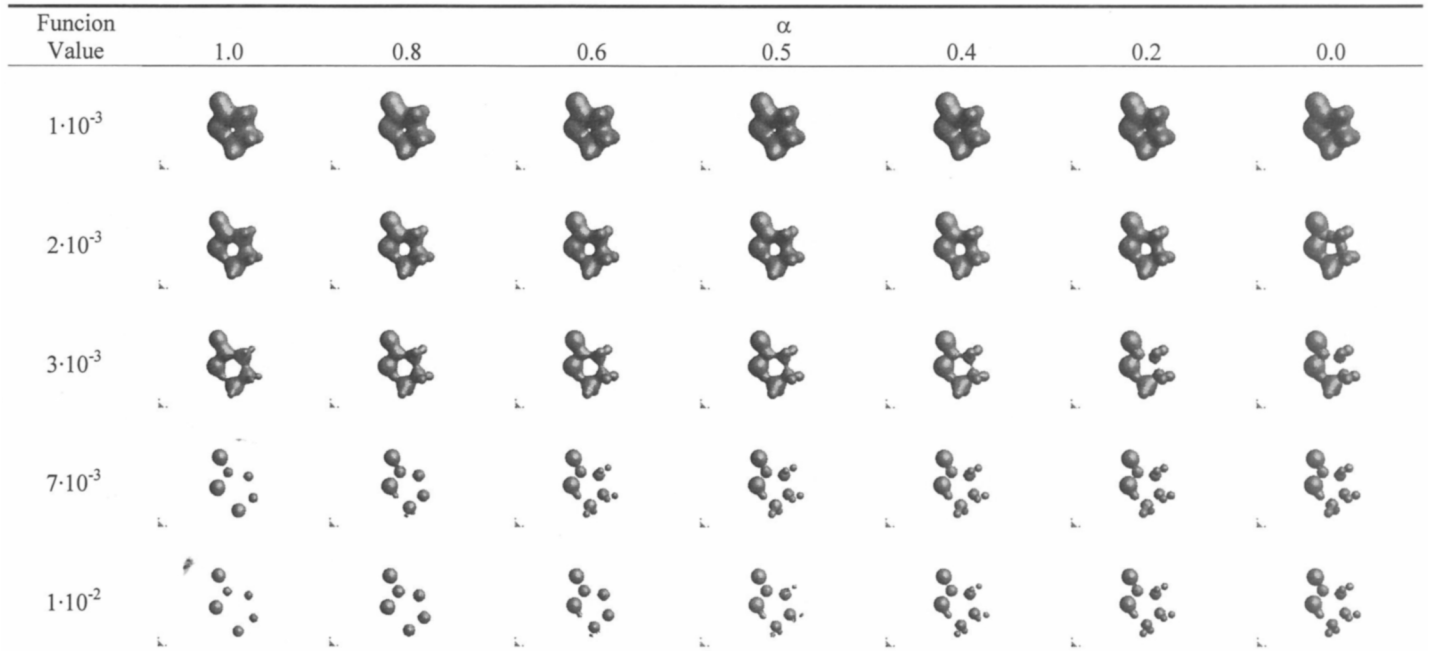

3.4. Generating Rules in EH Spaces.

It seems plausible to summarise the features of this discussion. To obtain a coherent picture, with KE occupying a sound place, among other quantum mechanical structures, then the EH VS, $\mathscr{H}^{(\nabla)}(\mathbf{C})$, could be defined not only containing wavefunctions but their first derivatives too. This allows to construct the associated DF VSS, $\mathscr{H}^{(\nabla)}(\mathbf{R}^{+})$, as containing not only eDF but also KE DF. The elements of this peculiar EH VS, where both wavefunctions and their gradients are contained, can be ordered in the form of column vectors, like:

$$\Phi = |\Psi;\nabla\Psi\rangle \in \mathscr{H}^{(\nabla)}(\mathbf{C}),$$

this form could be attached to some scalar-to-vector transformation using a vectorial operator, involving the gradient, such as:

$$|1;\nabla|[\Psi] = |\Psi;\nabla\Psi\rangle = |\Phi\rangle. \tag{11}$$

In the case of one particle QO, the necessary quadrivector structure, which must adopt the extended wavefunctions, acquire a qualitative similarity to relativistic spinors [77]. In order to obtain mathematical coherence, even non-relativistic Quantum Mechanics seems that can be easily attached to a vector-like wavefunction representation, originated due to the presence of momentum and thus of KE differential operators. An idea of Levy-Leblond [78], recently quoted by Karbowski [79] can be related to this feature.

An appropriate *generating rule* defined within the extended wavefunction domain, can now be written as:

$$\mathscr{R}(\Phi \rightarrow \rho;\kappa) = \left\{ \begin{array}{l} \forall\ \Phi = |\Psi;\nabla\Psi\rangle \in \mathscr{H}^{(\nabla)}(\mathbf{C}) \rightarrow \\ \exists\rho = \Psi^{*}\Psi = \Psi^{2} \wedge \exists\kappa = (\nabla\Psi)^{*}(\nabla\Psi) \\ = \nabla\Psi^{2} \Rightarrow \rho;\kappa \in \mathscr{H}^{(\nabla)}(\mathbf{R}^{+}) \end{array} \right\}. \tag{12}$$

3.5. Energy Scaling in EH spaces.

As discussed before, the eDF ρ can be considered normalised, according to equation (A-2). The KE DF κ, can be normalised too, the gradient density norms being in absolute value twice the kinetic energy expectation value, K.

This amounts the same as to consider normalised the total extended wavefunction, $|\Phi$:

$$\Phi|\Phi = 1 + 2K \quad . \tag{13}$$

This is a consequence of the characteristics of the spaces containing both, the wavefunction and their gradient, whose elements, then, should be considered square summable functions. The normalisation of the extended wavefunction Φ , may produce an energy scaling as interesting as the squared particle number scale factors, as analysed elsewhere [49]. However, the property that really matters from the variational point of view, as well as from the quantum mechanical basic formulation, is the normalisability of the generating scalar wavefunction $|\Psi$.

The effect of such an electronic energy scaling may be easily analysed. Taking into account that the electronic energy can be expressed as a sum of expectation values of kinetic and potential energies, respectively :

$$\mathscr{E} = K + V .$$

The corresponding energy scaled form can be readily written as:

$$\mathscr{E} = \left(1 + 2K\right)^{-1}\left(K + V\right),$$

which can be easily transformed into:

$$\mathscr{E} = \left(1 + \left(2K\right)^{-1}\right)^{-1}\left(\frac{1}{2} - \eta\right),$$

being the virial coefficient defined as:

$$\eta = -\left(2K\right)^{-1} V .$$

Considering that for systems where the number of particles becomes very large, the following simplification can be made:

$$1 + \left(2K\right)^{-1} \approx 1,$$

then:

$$\mathscr{E}_N \approx \frac{1}{2} - \eta .$$

In the case that: $\eta \approx 1$, the scaled energy becomes:

$$\mathscr{E}_N \approx -\frac{1}{2},$$

which is nothing more than the ground state energy of the H atom in a.u. . This kind of atomic energy behaviour upon scaling can be numerically checked by

transforming the energies arising from any set of accurate atomic calculations, for example the ones present in Clementi and Roetti [50] collection.

3.6.Extended Wavefunction Projectors.

The projectors, associated to the extended quantum mechanical wavefunctions Φ, will possess a matrix structure, which can be written as:

$$\Phi\Phi^{\dagger} = \begin{pmatrix} |\Psi|^2 & \Psi^*(\nabla\Psi) \\ (\nabla\Psi)^*\Psi & (\nabla\Psi)^* \otimes (\nabla\Psi) \end{pmatrix} = P, \tag{14}$$

then, using the symmetrisation: $Q = \frac{1}{2}(P^{\dagger} + P)$, the new projector could be rewritten as the matrix:

$$Q = \begin{pmatrix} \rho & \mathbf{j} \\ \mathbf{j}^{\dagger} & \mathbf{K} \end{pmatrix}$$

where $\mathbf{K}$ bears a certain resemblance to the hessian matrix of the eDF. Then, defining:

$$\kappa = Tr(\mathbf{K}):\ Tr(Q) = Tr(P) = \rho + \kappa,$$

and the off-diagonal elements can be related to the current density, see for example [5,58,70], except for an imaginary constant factor:

$$\mathbf{j}^{\dagger} = \frac{1}{2}\left(\Psi^*(\nabla\Psi) + (\nabla\Psi)^*\Psi\right).$$

4.Extended Density Functions.

The previous discussion leading to the concept of KE DF can be used to obtain the pertinent ASA DF counterpart, as well as this experience may be actually employed to construct other kinds of extended DF. In the present section several breeds of DF, arising from the consideration of EH spaces will be presented.

4.1.ASA Kinetic Energy DF.

ASA DF formalism could be easily manipulated by means of the KE DF formulation. In this case, as ASA eDF can be supposed constructed by the general MO eDF form, as in equation (A-1), then the MO KE DF may be written accordingly as:

$$\kappa(\mathbf{r}) = \sum_i \omega_i |\nabla \varphi_i(\mathbf{r})|^2. \tag{15}$$

Because in ASA the basis functions $\{\varphi_i(\mathbf{r})\}$ are assumed to be normalised 1s GTO functions, with centre at the position $\mathbf{R}_\mathbf{I}$, one can write the gradient vector as:

$$\nabla \varphi_i(\mathbf{r}) = \nabla\left(N(\alpha_i)\exp\left(-\alpha_i |\mathbf{r} - \mathbf{R}_\mathbf{I}|^2\right)\right) = -2\alpha_i(\mathbf{r} - \mathbf{R}_\mathbf{I})\varphi_i(\mathbf{r}), \tag{16}$$

and after this, one can obtain straightforwardly the ASA KE DF expression:

$$\kappa(\mathbf{r}) = 4\sum_i \gamma_i |\mathbf{r} - \mathbf{R}_\mathbf{I}|^2 |\varphi_i(\mathbf{r})|^2,$$

using: $\gamma_i = \omega_i \alpha_i^2$. This result, in the above framework, tells that ASA KE DF basis functions acquire a functional structure as a 2s GTO.

4.2.Quadrupole DF.

Another obvious set of ket elements in EH spaces can be constructed. It can be made with the vector wavefunction part multiplied by the position vector, as: $|\chi\rangle = |\Psi;\mathbf{r}\Psi\rangle$. The new extended functions are the quantum mechanical position companions of the formerly described momentum ones: $\Phi_i = |\Psi;\nabla\Psi\rangle_i$. In the same manner as it has been done before for the functions $|\Phi\rangle_i$, a density and a projector can be described for the extended ket $|\chi\rangle_i$. Thus, a Quadrupole DF (QDF) can be defined as:

$$q(\mathbf{r}) = |\mathbf{r}|^2 \rho(\mathbf{r}),$$

forming part of an alternative DF attached to this new collection of extended functions:

$$|\chi|^2 = \rho + |\mathbf{r}|^2 \rho = \left(1 + |\mathbf{r}|^2\right)\rho = \rho(\mathbf{r}) + q(\mathbf{r}).$$

The norm of the total density will be easily obtained as:

$$\int |\chi|^2 d\mathbf{r} = \int \rho \, d\mathbf{r} + \int |\mathbf{r}|^2 \rho \, d\mathbf{r} = 1 + \langle |\mathbf{r}|^2 \rangle .$$

Also, this new kind of extended DF can be obtained, in the same way as in equation (14) by computing the trace of the projector matrix:

$$|\chi\rangle\langle\chi| = \begin{pmatrix} 1 & |\mathbf{r}\rangle \\ \langle\mathbf{r}| & |\mathbf{r}\rangle\langle\mathbf{r}| \end{pmatrix} \rho = \begin{pmatrix} \rho & |\mu\rangle \\ \langle\mu| & \mathbf{Q} \end{pmatrix},$$

which corresponds to a matrix with dipole moment distributions in the off-diagonal elements and, moreover: $Tr|\mathbf{Q}| = q(\mathbf{r})$. QDF will obviously not be translationally invariant.

4.3. Angular Momentum DF.

Within the same reasoning context, it might be nice to see how angular momentum could be introduced in the EH wavefunction scheme. Defining the antisymmetric matrix:

$$\mathbf{e}(\mathbf{r}) = \begin{pmatrix} 0 & -z & y \\ z & 0 & -x \\ -y & x & 0 \end{pmatrix}$$

then it is easy to see that angular momentum can be obtained as [78]:

$$\mathbf{r} \times \nabla\Psi \equiv \mathbf{e}(\mathbf{r})\nabla\Psi = \mathbf{L}\Psi ,$$

where $\mathbf{L}$ is the angular momentum operator, except for an imaginary constant. Thus, the diagonal hypermatrix:

$$\mathbf{\Lambda} = Diag(1, \mathbf{e}(\mathbf{r})),$$

transforms the extended wavefunctions into angular momentum ones:

$$\Lambda|\Phi\rangle = \Lambda|\Psi, \nabla\Psi\rangle = |\Psi, \mathbf{r} \times \nabla\Psi\rangle .$$

At the same time, one can define angular momentum DF (AM DF) using the same arguments as before, taking the vector part of the resultant extended wavefunction:

$$\lambda(\mathbf{r}) = \left\| \mathbf{r} \times \nabla\Psi \right\|^2 = Tr(\mathbf{r} \otimes \mathbf{r}) Tr((\nabla\Psi) \otimes (\nabla\Psi)) - Tr(\mathbf{r} \otimes (\nabla\Psi))^2$$

which, when considering Ψ as an 1s GTO function, like in ASA environment, adopts the form:

$$\lambda(\mathbf{r}) = (4\alpha^2) \left\{ Tr(\mathbf{r} \otimes \mathbf{r}) Tr((\mathbf{r}-\mathbf{R}) \otimes (\mathbf{r}-\mathbf{R})) - Tr(\mathbf{r} \otimes (\mathbf{r}-\mathbf{R}))^2 \right\} \Psi^2 .$$

As in the previous QDF structure, the AM DF will not present translational invariance.

4.4.Mass Variation with Velocity DF.

When dealing with relativistic hamiltonians, a great amount of new operators appears because of several approximate procedures allowing the simplification of Dirac's equation. See, for example, the treatise of Bethe and Salpeter [81], as well as the Moss discussion [77 a)], the McWeeny's book [82], or a recent comprehensible brief résumé due to Almlöf and Gropen [83].

The also so-called mass-velocity term, is mainly related to the fourth power of momentum, and thus with the operator ∇^4. The adequate operator structure will be given by a diagonal operator: $\upsilon = Diag(1; -\nabla^2) = Diag(1; \Delta)$ acting on the extended wavefunctions, in this way, using Green's first theorem:

$$\nabla^4 = \Phi \upsilon \Phi = 1 - \int (\nabla\Psi)^* (\nabla^2)(\nabla\Psi) dV =$$
$$1 + \int (\nabla^2\Psi)^* (\nabla^2\Psi) dV = 1 + \int (\Delta\Psi)^* (\Delta\Psi) dV = 1 + \int \left\| \Delta\Psi \right\|^2 dV .$$

The three integrals appearing in the last sequence terms are the ones, which according to Bethe and Salpeter [81] must be used whenever mass-velocity integral terms have to be evaluated. So, the corresponding Mass-Velocity (MV) DF part may be written as:

$$\upsilon(\mathbf{r}) = \left\| \Delta\Psi \right\|^2 .$$

The corresponding ASA MV DF, form could be written knowing the ASA gradient as expressed in equation (16), the laplacian of a 1s GTO function located at the co-ordinates $\mathbf{R}_I$, as in equation (16), it is easily found to be:

$$\Delta\varphi_i(\mathbf{r}) = 2\alpha_i\left(2\alpha_i|\mathbf{r}-\mathbf{R}_I|^2 - 3\right)\varphi_i(\mathbf{r}).$$

Then the ASA MV DF could be expressed as the sum:

$$\upsilon(\mathbf{r}) = \sum_i \omega_i |\Delta\varphi_i(\mathbf{r})|^2 = 4\sum_i \gamma_i \left(2\alpha_i |\mathbf{r}-\mathbf{R}_I|^2 - 3\right)^2 \varphi_i(\mathbf{r})|^2,$$

where, as before in KE DF: $\gamma_i = \omega_i\alpha_i^2$. It can be easily seen that MV DF appears, according to the well-known properties of 1s GTO, as the square of a d_{z^2}-type function.

5. Visualisation Examples of DF.

The new set of varied DF found in the previous section can be studied in the same way as the well-known eDF maps are represented since the first plots used in Quantum Chemistry [53a)]. Here an alternative point of view, similar as the one used by Mezey [9a)], will be chosen. Three-dimensional maps of isodensity surfaces can be generated with available computational techniques [84]. This corresponds to follow several steps, some of them so trivial that appear to be irrelevant in a study as the present. The representation process starts with the evaluation of DF grids, enveloping the molecular co-ordinates, which can origin wireframe structures related with the isodensity values. After that, they can be rendered and rotated in space as virtual objects, until some adequate point of view is found. Finally, the chosen object snapshot can be manipulated, represented on a screen and, if necessary, printed into a paper surface. The processing detail, the computational techniques and the required programs and data are briefly commented in Appendix E. All the necessary items are available to the interested reader and permit to generate surfaces of his own [93-96].

A comparison of extended DF for some assorted molecular structures will be given below, just to present a quite limited sample of the available possibilities, at everyone's disposal, in order to show visually the many facets of molecular skin.

5.1. Visualisation examples of several molecular extended DF.

Here, several examples of molecular structures and DF, as discussed in the previous sections, will be given to illustrate the possibilities of such DF generalisation based on the structure and opportunities given by the EH spaces.

In all the examples given in the following sections, the plotted functions are generated under the ASA framework, using the function structures described in the previous sections starting at Section 3.6 and ending into Section 4.4. The conditions discussed in Section 2.3, are forced to hold for all the displayed DF in the next sections. That is, whichever DF, obtained by a convex superposition, must have the associated basis set made by normalised DF. This kind of fundamental property has been followed in all the cases shown below. Such examples contain a sample of the possible EH molecular DF, as described in the preceding sections, that is: ASA examples of eDF, KE, Q, AM and MV are provided. The molecular structures chosen are:

A) Diazepam (7-Chloro-1,3-dihydro-1-methyl-5-phenyl-2H-1,4-benzodiazepin-2-one).
B) Mescaline (Mescaline hydrochloride)(FFF).
C) Quinine (10-Hydroxy-10-methyl-10,11-dihydroquinine)
D) Lysergic acid (LSD or Lysergic acid diethylamide o-iodobenzoate monohydrate).

The corresponding molecular structures, used in the following pictures, have been extracted from experimental crystallographic data [97]. For each molecule, every isodensity surface is plotted at four isodensity levels.

5.1.1. *ASA eDF visualisation.*

The first example presented, along **Figures 3** to **6**, consists into the representation of the ASA eDF for the four molecular structures chosen.

Figure 3.- Graphical representation of ASA eDF calculated at four iso-density levels for the diazepam molecule.

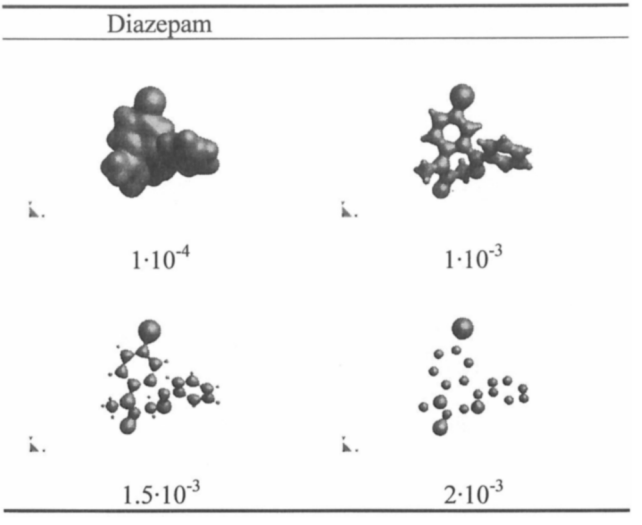

Figure 4.- Graphical representation of ASA eDF calculated at four iso-density levels for the mescaline molecule.

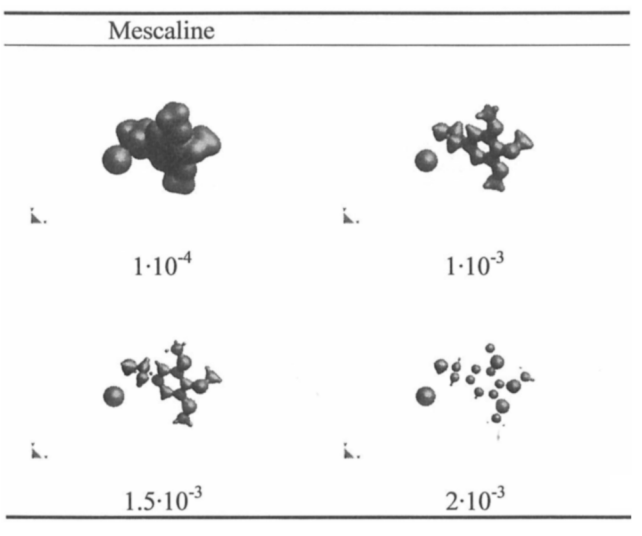

Figure 5.- Graphical representation of ASA eDF calculated at four iso-density levels for the quinine molecule.

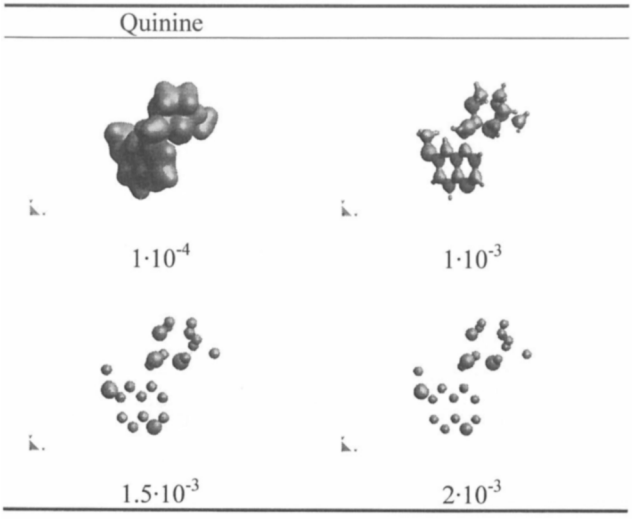

Figure 6.- Graphical representation of ASA eDF calculated at four iso-density levels for the LSD molecule.

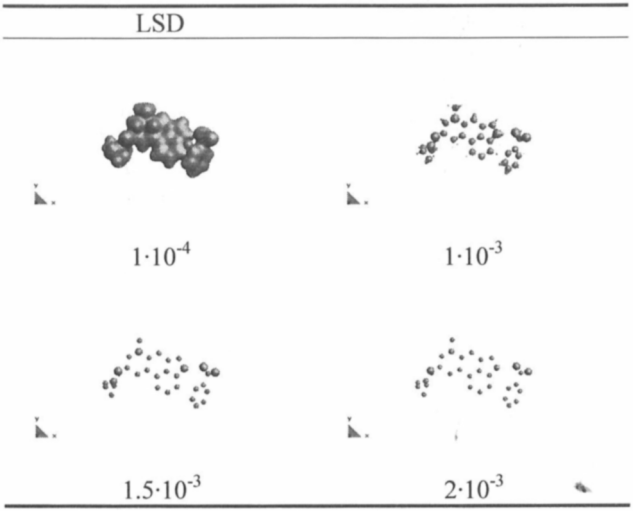

As it can be observed from the figures presented before, all systems are accurately described when low and high isodensity levels are considered, reaching a quality quite close to the obtained using ab initio procedures, see [9a)]. However, and due to the nature of the promolecular approach used, the description of the intermediate levels, which coincide with bond formation steps, are not so accurately described. Although, this inconvenience is omitted when working in QSM, the main user of ASA DF, because the density is greatly concentrated around atoms, and the contribution of bond density in similarity measures is negligible.

5.1.2 *ASA KE DF visualisation.*

The next presented example, corresponding to **Figures 7** up to **8**, involves the visualisation of KE DF. Similarly to the previous four ASA eDF surfaces, the representation is made over the same molecular set, and in the same manner, the corresponding isodensity surfaces are plotted at four levels.

Figure 7.- Graphical representation of ASA KE DF calculated at four iso-density levels for the diazepam molecule.

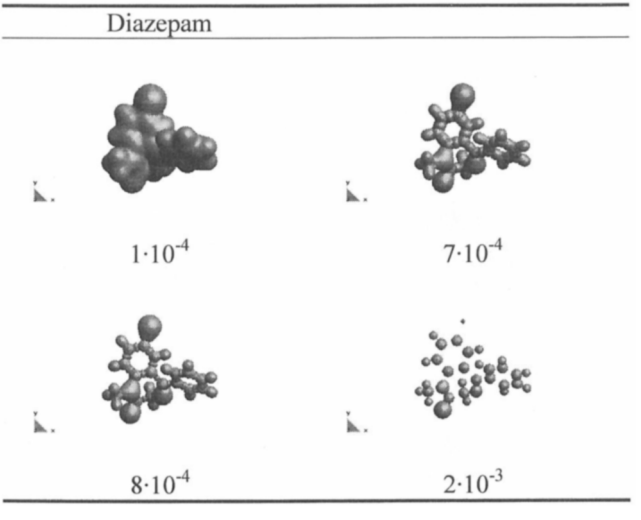

Figure 8.- Graphical representation of ASA KDF calculated at four iso-density levels for the mescaline molecule.

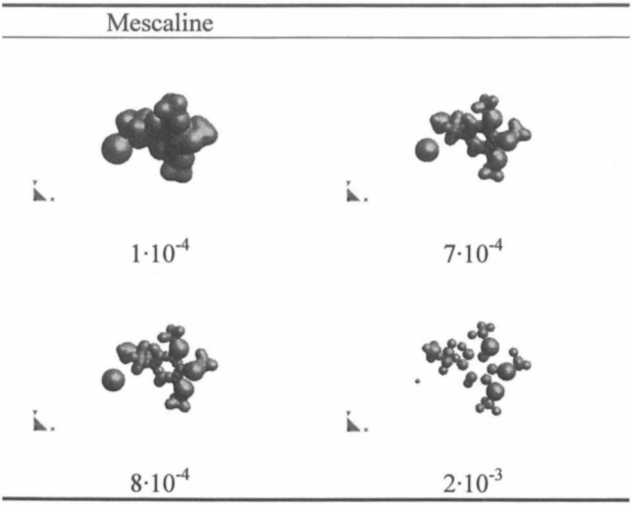

Figure 9.- Graphical representation of ASA KDF calculated at four iso-density levels for the quinine molecule.

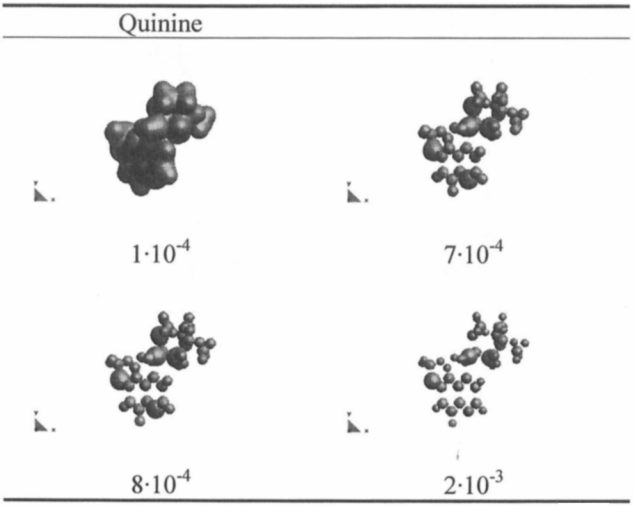

Figure 10.- Graphical representation of ASA KDF calculated at four iso-density levels for the LSD molecule.

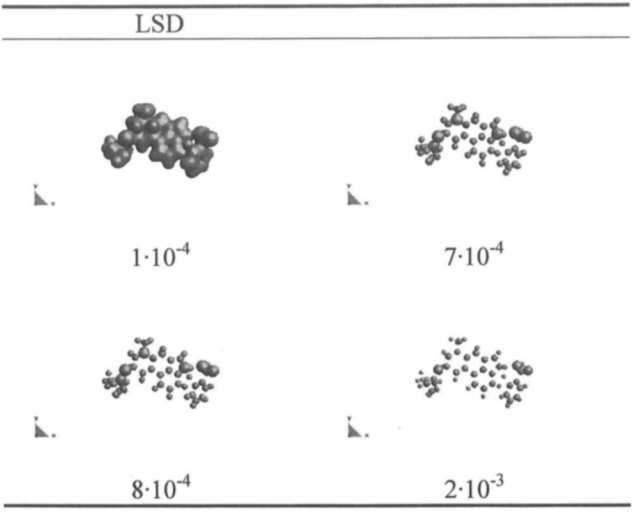

Taking the eDF as a comparison model, KE DF presents similar forms at low isodensity values, enveloping the molecular shape, and the same can be said at high function values, whereas only heavy atoms are represented. However, when the intermediate values are considered, an interesting difference arises, due to the decrease of eDF along the interatomic distance, KE DF increases creating a maximum between bonded atoms. At this point, it has to be pointed out the arbitrary change of sign carried out when deducing KE DF, done just for simplicity. It must be noted thus, that the change involving the maximum transforms it into a minimum, which coincides in turn with the position where electron velocity is lower. This situation is easy to understand, because the nearer any electron is to an atom, faster it will move, due to the increment of nuclear attraction.

Another remarkable difference, which is difficult to notice from the present Figures, is that, and according to ASA KE DF equation, the value of the function in the atomic co-ordinates is zero, just where eDF reaches a maximal value.

5.1.3. *ASA QDF visualisation.*

The next EH DF representation example presented, in **Figures 11** to **14**, involves the visualisation of QDF. Surface representation, similarly to the

previous figures, is based the same molecular set as before, plotted at four isodensity levels. Quadrupole moments provide a second-order approximation to the total electron distribution, and indeed, to the molecular shape, as they are the second order derivatives of the energy with respect to an applied electric field. Quadrupole-like DF arises from this idea and provides a new vision of the molecular shape from the point of view of a pre-established centre. In the presented examples, for each structure, all molecular co-ordinates have been translated at their centre of charges, in order to provide a sound reference for reproducibility purposes, as QDF is not invariant upon translation.

Figure 11.- Graphical representation of ASA QDF calculated at four iso-density levels for the diazepam molecule.

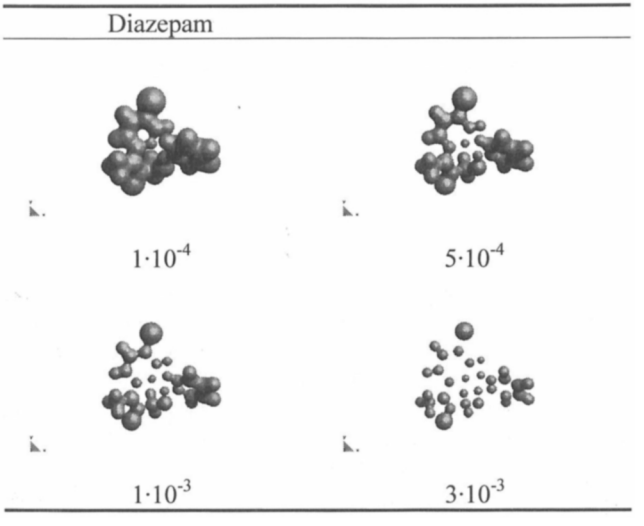

Figure 12.- Graphical representation of ASA QDF calculated at four iso-density levels for the mescaline molecule.

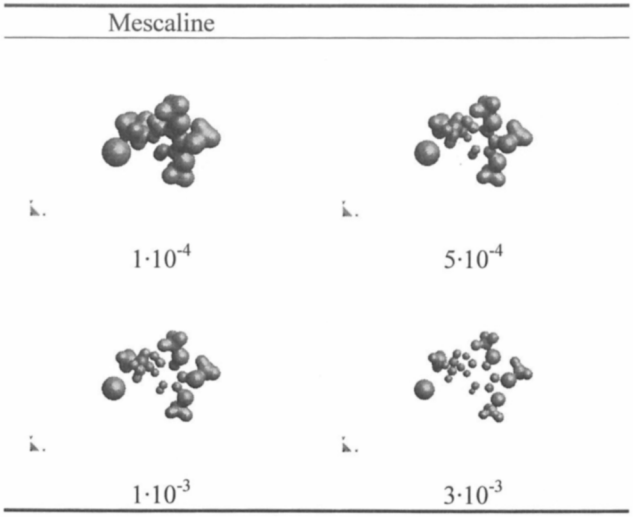

Figure 13.- Graphical representation of ASA QDF calculated at four iso-density levels for the quinine molecule.

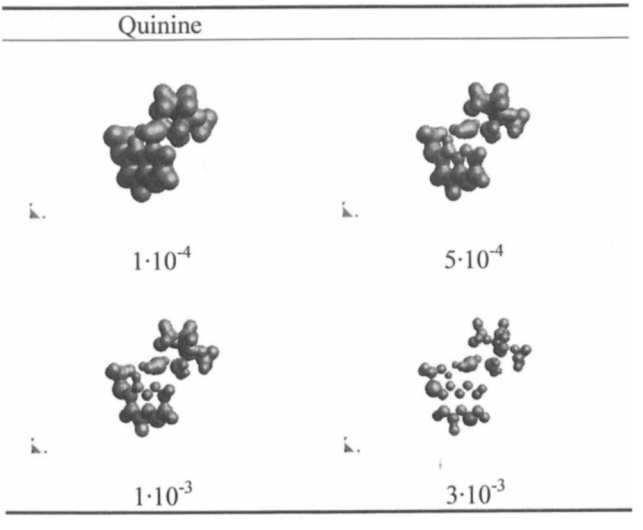

Figure 14.- Graphical representation of ASA QDF calculated at four iso-density levels for the LSD molecule.

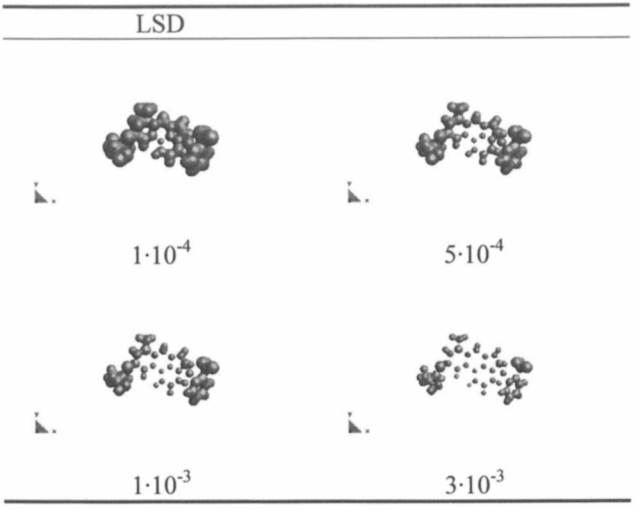

From the inspection of the figures above, it can be seen how at high values of QDF the regular molecular shape is split from the chosen molecular centre of charges. The function begins to have a structured form around the heavy atoms, present surrounding centre of charges. At low values of QDF, the shape becomes as regular as the eDF forms.

5.1.4 *ASA AM DF visualisation.*

The following example presented, in **Figures 15** up to **18**, corresponds to the visualisation of AM DF. Similarly to the examples above, the representation consists in the visualisation of the same set of molecules as before, plotted also at four iso density levels.

Figure 15.- Graphical representation of ASA AM DF calculated at four iso-density levels for the diazepam molecule.

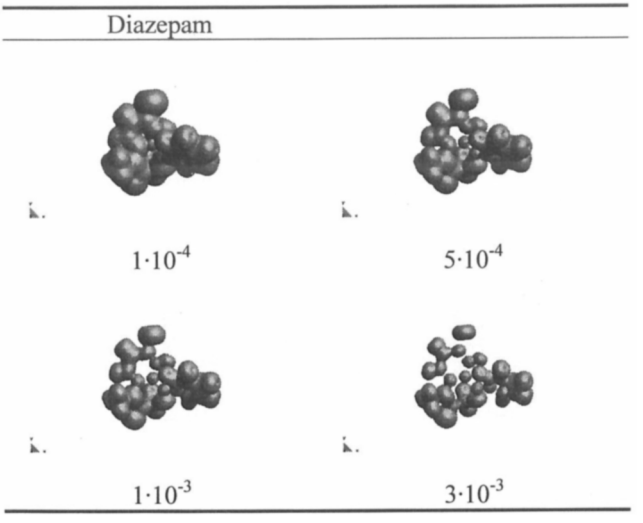

Figure 16.- Graphical representation of ASA AM DF calculated at four iso-density levels for the mescaline molecule.

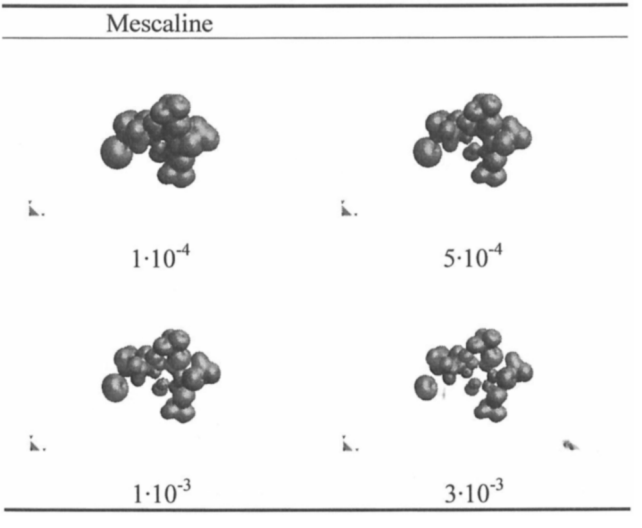

Figure 17.- Graphical representation of ASA AM DF calculated at four iso-density levels for the quinine molecule.

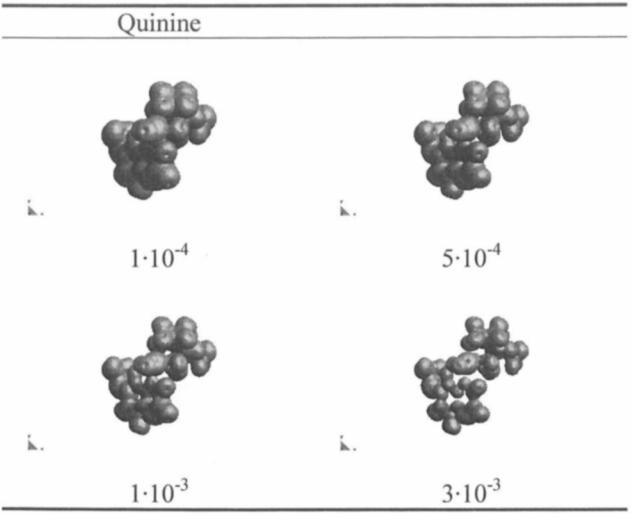

Figure 18.- Graphical representation of ASA AM DF calculated at four iso-density levels for the LSD molecule.

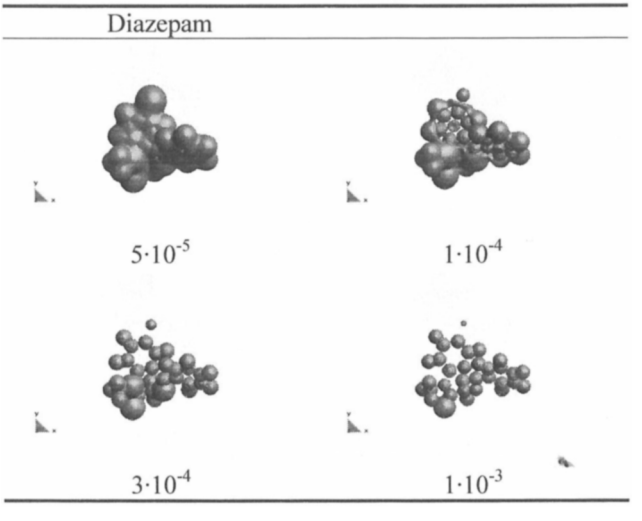

In order to understand the physical interpretation of this new kind of DF, a remind of what one can interpret by molecular AM must be discussed. AM corresponds to the momentum, associated with the rotational motion of a molecular object, and the greater the AM, stronger the braking force needed to bring it to rest. Combining this concept with the existence of molecular inertial axis, it can be seen how the major part of AM DF is gathered around the edges of the axis involving less mass translations. This point of view appears more obvious when high values of AM DF surfaces are observed. When low AM DF values are analysed, it is easy to grasp that the shape of the AM DF becomes uniformly distributed, as the contributions from the rest of the axis are added, adopting finally an eDF-like shape.

As in the QDF cases, the AM DF is not invariant upon translations, and the present images have been obtained upon translation of every molecular atomic co-ordinate set into the centre of charges.

5.1.5 *ASA VMV DF visualisation.*

The last example presented, in from **Figures 19** up to **22**, consists in the representation of MV DF. The figures involve the same set of molecules and molecular surfaces have been also plotted at four levels.

Figure 19.- Graphical representation of ASA MV DF calculated at four iso-density levels for the diazepam molecule.

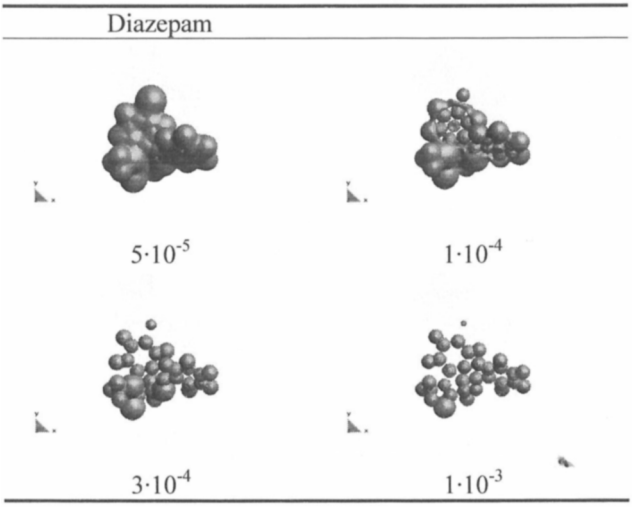

Figure 20.- Graphical representation of ASA MV DF calculated at four iso-density levels for the mescaline molecule.

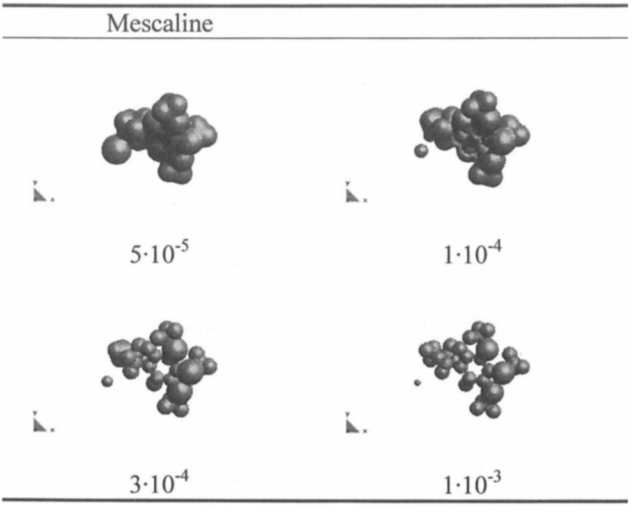

Figure 21.- Graphical representation of ASA MV DF calculated at four iso-density levels for the quinine molecule.

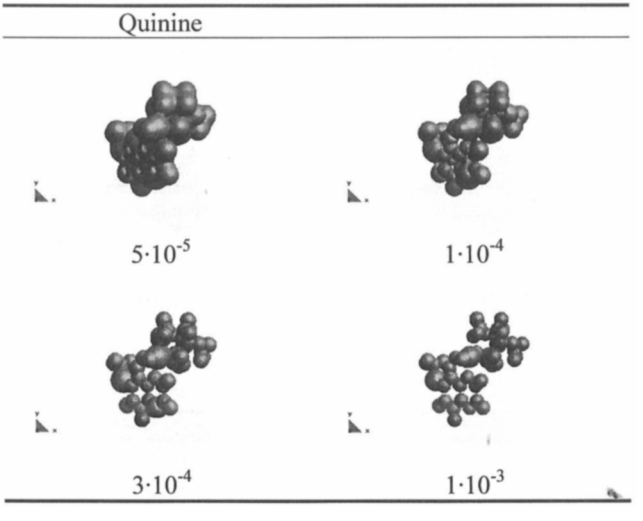

Figure 22.- Graphical representation of ASA MV DF calculated at four iso-density levels for the LSD molecule.

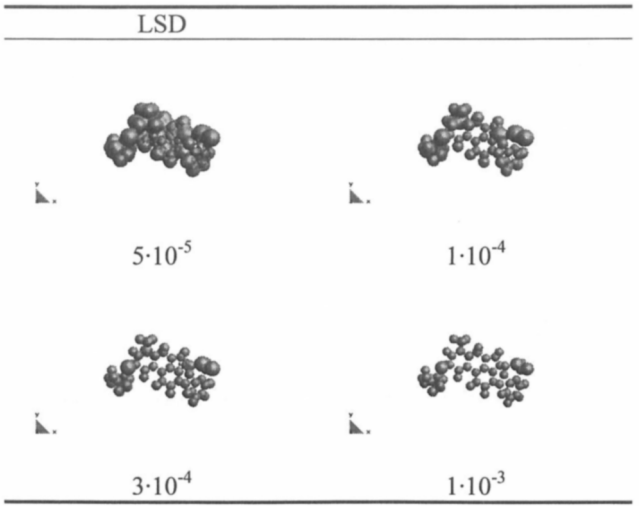

This new kind of DF arises, using the relativistic idea of the effect of MV DF. Once the definition of the KE DF is understood, it is assumed that the zones on the molecule where the electrons achieve more KE, or more velocity, are the ones located around the atoms. The next ones are the bond regions, with a minimum located at the middle of the bond. Finally, the zones with less KE are the most external ones.

According to the relativistic Breit Hamiltonian, the EH MV DF values are more accused as the velocity of the involved object, in this case an electron, increases. In this way, the zones where KE increases will present a high value of MV variation, which will be mostly localised surrounding the atoms of the molecule. Away from atomic centres, the value of MV DF decreases, and it turns most similar to eDF due to the KE in these points is low and more homogeneous in space.

5.2 Comparative Visualisation of several molecular extended DF

In this section, it is intended to graphically show all molecular extended DF presented into the preceeding sections. In this way, it is possible to follow the variations of all DF and the inherent differences between them. The molecular example, along **Figures 23** to **25**, has been α-D-Ribulose, a monosaccharide, which is found in the photosynthetic carbon cycle of all green plants [98]. The molecular geometry has been optimised using the AM1 Hamiltonian within the Ampac program [99]. The plots are presented from three different points of views, at seven isodensity levels in order to provide with a complete example of the surface visualisation.

In the three tables shown the subtle differences between the structure of the diverse DF surfaces can be appreciated.

6.Alternative Diagonal Representation of Extended Wavefunctions.

After the previous discussion and following the presence of various DF visualisation sets, still remains to be analysed the role of EH spaces in the possible construction of a unique expression for the expectation value formalism. This section will be devoted to develop this task and to present some of the consequences of the underlying theory.

6.1.Energy.

There still is a point to be discussed: the calculation of energy expectation values, within the EH space framework. This can be done, in practice, using Born-Oppenheimer approximation, defining in this context an electronic Hamilton operator, adopting some diagonal matrix structure and, in addition, supposing the original scalar wavefunction $|\Psi)$ normalised:

$$\mathbf{H} = Diag(V; \tfrac{1}{2}\mathbf{I}) \wedge (\Psi\ \Psi) = 1 \Rightarrow \mathscr{E} = (\Phi|\mathbf{H}|\Phi) = (\Psi V|\Psi) + \tfrac{1}{2}(\nabla\Psi|\nabla\Psi) \equiv (V) + (K). \tag{17}$$

In the diagonal Hamilton operator definition, V is the potential part and **I**, a unit

Figure 23.- Comparative analysis of extended density functions over the Ribulose molecule (front view) for several isodensity values.

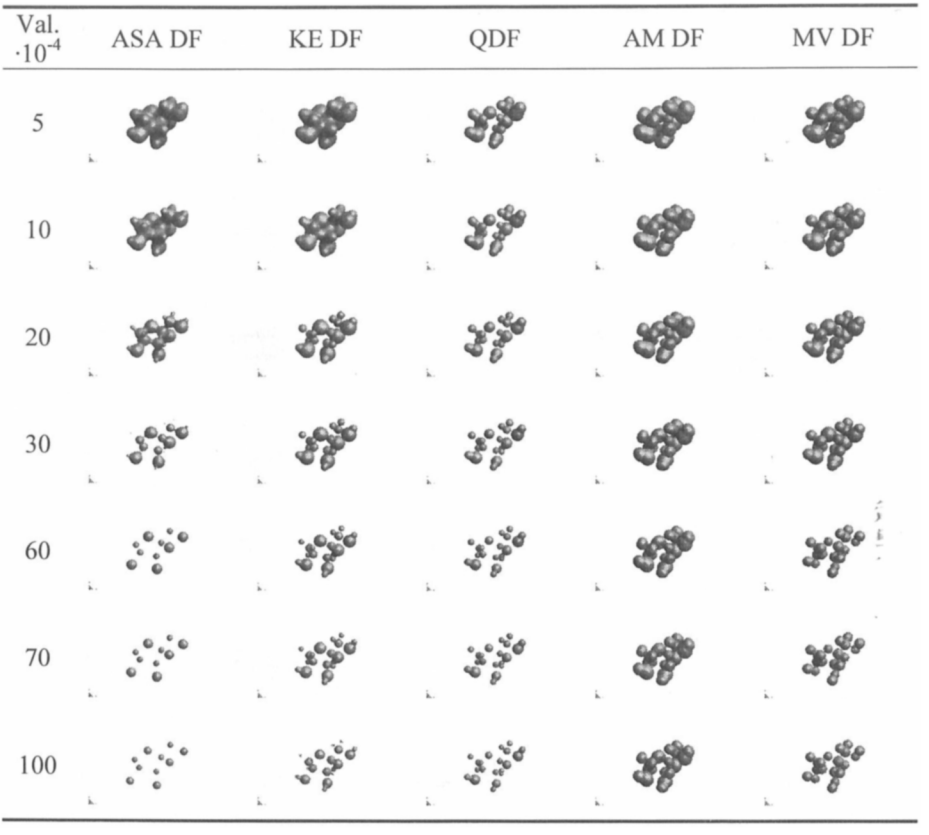

Figure 24.- Comparative analysis of extended density functions over the Ribulose molecule (intermediate view) for several isodensity values.

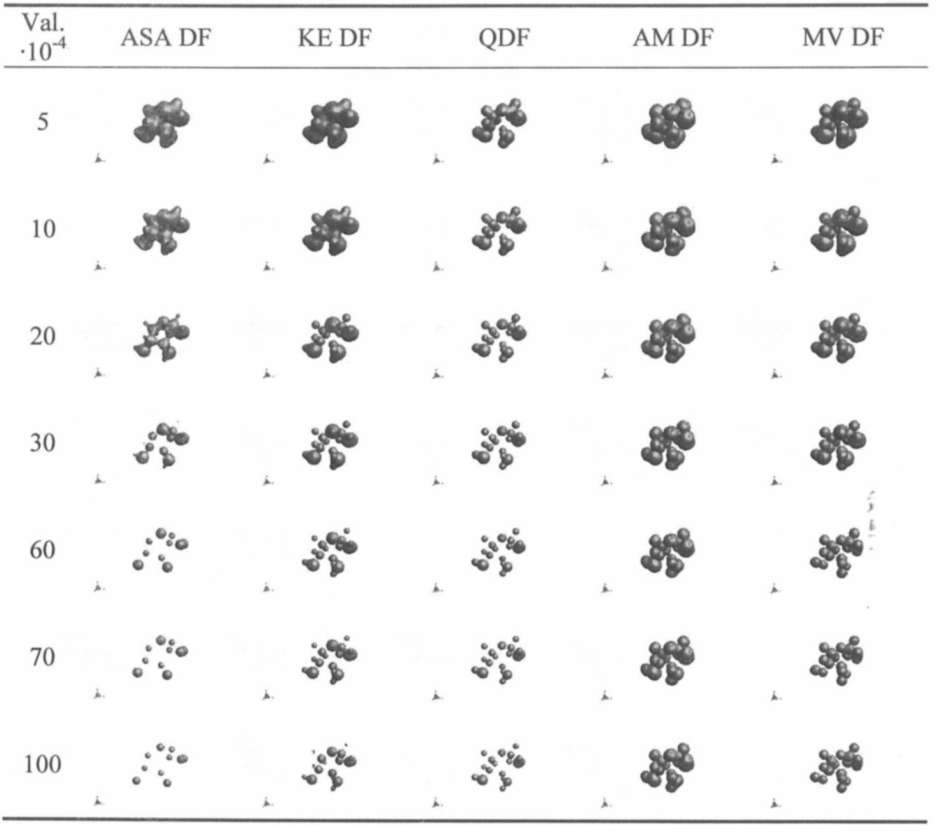

Figure 25.- Comparative analysis of extended density functions over the Ribulose molecule (side view) for several isodensity values.

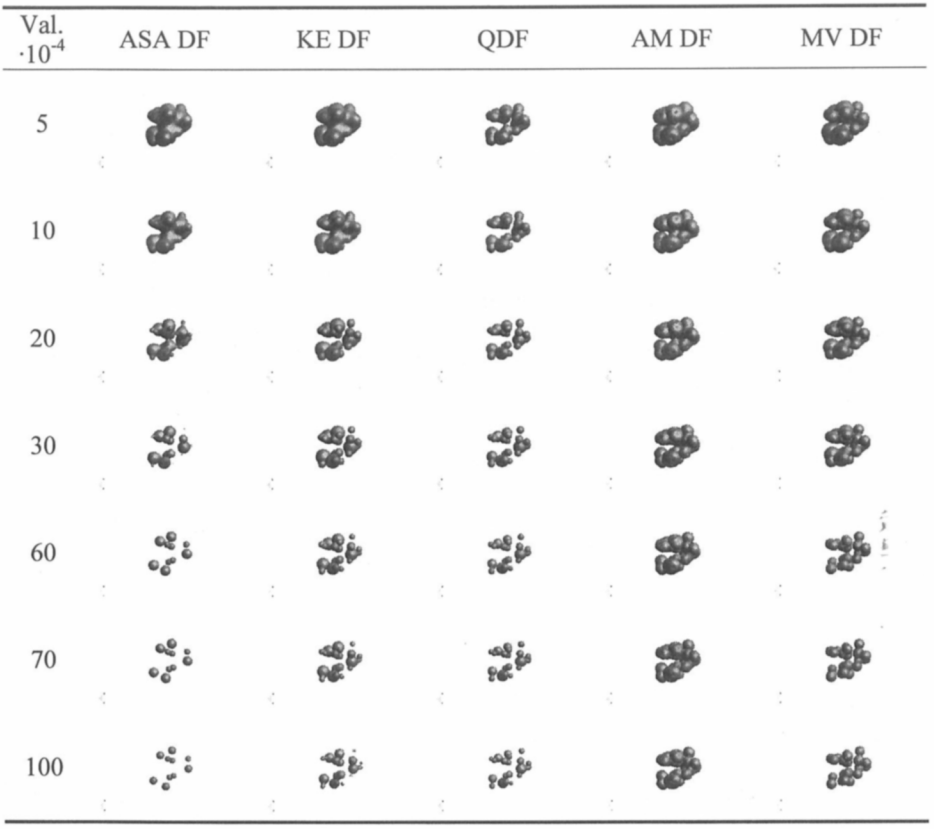

matrix with the appropriate dimension. In any case, the KE inverse mass factors if needed, could be supposed implicitly inserted into the gradient symbols *. This result shows that the possible use of standard variational procedures is allowed, even in the EH space $\mathscr{H}^{(V)}(\mathbf{C})$ formalism.

However, this picture still has the problem discussed in Section 3.2: corresponds to an integral of type (4), instead of having the statistical structure of equation (1). In order to arrive to a coherent statistical picture, associated to every expectation value expression it is needed to work in an environment involving diagonal matrices, used for both operators and wavefunctions.

There can be seen that, not only the Hamilton operator could be written as a diagonal matrix, but the elements of the EH space too. It is only necessary to take into account the isomorphism between the extended wavefunction form and a diagonal structure, which can be defined employing a diagonal operator instead of the vector one used in writing equation (11):

$$\mathbf{\Phi} = \mathbf{\Psi}, \nabla\mathbf{\Psi} \Leftrightarrow Diag(1;\nabla)\mathbf{\Psi} = Diag(\mathbf{\Psi};\nabla\mathbf{\Psi}).$$

Accordingly, the system energy in equation (17) can be also written from this alternative point of view as a trace of a diagonal matrix:

$$\mathscr{E} = \mathbf{\Phi}\,\mathbf{H}\,\mathbf{\Phi} = Diag\left(\Psi | V | \Psi \; ; \tfrac{1}{2} \nabla\Psi \; \nabla\Psi \right),$$

where the symbol $\mathbf{A}$, short for symbolising the diagonal matrix trace, is constructed employing the more general Definition 6 of Appendix A.

However, within this diagonal matrix formalism the statistical form of expectation values is preserved in any circumstance, at least when system's energy is sought. Indeed, if the extended function diagonal form is chosen, then the following sequence of integral expressions can be easily written:

---

* Both, gradient and hamiltonian unit submatrix can be organised in various coherent ways. If the gradient is presented as a sum of one-electron gradient terms, as usual, then the unit matrix is (3×3) dimensional. If, on the other hand, the gradient is organised as some n-dimensional vector, whose elements are made by one-electron gradients, then, the unit matrix appearing in the Hamilton operator shall be (n×n).

$$\mathscr{E} = \Phi\,\mathbf{H}|\Phi = \int Diag\left(\Psi^*;(\nabla\Psi)^*\right)Diag(V;\tfrac{1}{2}\mathbf{I})Diag(\Psi;(\nabla\Psi))\;d\mathbf{r} =$$

$$\int Diag(V;\tfrac{1}{2}\mathbf{I})Diag\left(\Psi^*;(\nabla\Psi)^*\right)Diag(\Psi;(\nabla\Psi))\;d\mathbf{r} =$$

$$\int Diag(V;\tfrac{1}{2}\mathbf{I})Diag\left(\Psi^{2};\nabla\Psi^{2}\right)\;d\mathbf{r} = \int Diag(V;\tfrac{1}{2}\mathbf{I})Diag(\rho;\kappa)\;d\mathbf{r} =$$

$$\int \mathbf{H}\tau\,d\mathbf{r} \equiv \int Diag(V\rho;\tfrac{1}{2}\kappa)\;d\mathbf{r} = Diag\left(\int V\rho\,d\mathbf{r};\tfrac{1}{2}\int\kappa\,d\mathbf{r}\right)$$

$$Diag\left(V;\tfrac{1}{2}\kappa\right) = V + K\ .$$

Where, there has been used the commutative property of the diagonal matrices product. A total density function has been represented by the symbol $\boldsymbol{\tau} = Diag(\rho;\boldsymbol{\kappa})$. Formally, the KE part, $\boldsymbol{\kappa}$, must be considered a diagonal matrix, where the components of the square gradient elements are located, for instance:

$$\nabla\Psi_i^{\,2} \equiv \boldsymbol{\kappa} = Diag\left(\frac{\partial\,|\Psi|^2}{\partial\,x_i}\right).$$

In this manner, the KE DF, as defined in section 3.2 above, can be generated as a trace of the matrix $\boldsymbol{\kappa}$.

Such a coherent statistical picture is possible in the context of EH spaces, due that the Hamilton operator no longer has the gradient in it, but the corresponding momentum operator is embedded into the EH space wavefunction. This interesting mathematical form may be related to the particular circumstances, involving quantum mechanical position and momentum observables.

It can be concluded, if the DF role must be preserved, that the statistical formalism of expectation values, represented by equation (1), has to be used in classical quantum mechanics for stationary states, in every circumstance. Furthermore, the following conditions must hold:

a) A computational environment shall be chosen. That is: The Schrödinger equation has to be transformed into the corresponding variational Rayleigh quotient.

b) A diagonal form of both observable operators and EH space wavefunctions must be adopted.

6.2. Virial Operators.

After the previous discussion, a virial related diagonal operator, **T**, can be defined without problems, using the same procedure followed in the energy expression. If the virial is fulfilled, then, the trace, η, of the resulting diagonal matrix product will be zero:

$$\mathbf{T} = Diag(-V;\mathbf{I}) \Rightarrow \langle \Phi | \mathbf{T} | \Phi \rangle =$$
$$Diag(-\langle \Psi | V | \Psi \rangle; \langle \nabla\Psi | \nabla\Psi \rangle) =$$
$$Diag(-\langle V \rangle; 2\langle K \rangle) = -\langle V \rangle + 2\langle K \rangle = \eta .$$

This last result, the diagonal form of virial operator and its possible use cannot be surprising, as both virial and energy variational procedures can be used to produce optimised wavefunctions, see for a recent review reference [85].

Similar situations, involving diagonal matrix algebra, are encountered when molecular discrete n-dimensional MO LCAO spaces and operator representations are studied. The formalism for these cases is discussed elsewhere [49].

6.3. Momentum and Extended Norm Operator.

One of the items, deliberately left not completely discussed in the present work, consists in the structure of momentum operators at the light of EH spaces. For finding out a computational energy expression it is not necessary that momentum bear the customary imaginary factor, as can be seen from the discussion in sections 3.1 to 3.3, and in section 6.1 above. Usually, in order that momentum gradient operator, in atomic units, becomes hermitian it must be multiplied by a factor, $\pm i = \pm \sqrt{-1}$. This peculiarity, omitting a mass factor, appearing in the literature in the form: $\pm i\nabla$ or $\pm i^{-1}\nabla$. That such an operator is certainly hermitian, but not hermitian conjugate, has been elegantly proved by Bohm [5]. In the present formalism, momentum operators may have a diagonal representation. They can be formally written as a diagonal matrix: $\partial = Diag(1;\nabla)$, or as in the column vector form of section 3 above, if needed.

How to reconcile this diagonal or vector form without the presence of the imaginary unit with the hermitian nature of momentum is a matter of mathematical formalism. In the EH space framework, it is sufficient to consider extended momentum operators, ∂, as elements of a Minkowsky space of signature (1,3) [78]. Admitting this space structure, then the property: $\partial^2 = 1 - \nabla^2$ is automatically fulfilled. Also, it is easy to consider the extended momentum operator as a linear transformation:

$$\partial : \mathscr{H} \to \mathscr{H}^{(\nabla)},$$

as :

$$\forall \Psi \in \mathscr{H} \Rightarrow \exists |\Phi\rangle = \partial\Psi = Diag(\Psi;\nabla\Psi) \in \mathscr{H}^{(\nabla)}.$$

This last expression ensures the extended wavefunction norm as defined in equation (13). The same relationships as in equation (10), can be obtained with the following sequence, employing once more Green's theorem:

$$\begin{aligned} \langle \partial^2 \rangle &= \langle \Psi | \partial^2 | \Psi \rangle = \langle \Psi | 1 - \nabla^2 | \Psi \rangle = \\ &\langle \Psi | \Psi \rangle - \langle \Psi | \nabla^2 | \Psi \rangle = 1 + \langle \nabla\Psi | \nabla\Psi \rangle = \\ &1 + 2\langle K \rangle. \end{aligned}$$

One can consider in this way that the imaginary factor in front of the gradient operator, which represents momentum in Quantum Mechanics, could

correspond to an equivalent extended operator. In turn, such operator is constructed by an element belonging to some four-dimensional Minkowsky space-time, defined over the real field, $\mathbf{M}_4(\mathbf{R})$. Choosing the canonical basis set of the appropriate dimension: $\{\mathbf{e}_k; k = 0,3\}$, as the columns of a (4×4) unit matrix, then the extended momentum operator can be written under this convention in $\mathbf{M}_4(\mathbf{R})$, as:

$$\partial = \mathbf{e}_0 + i\sum_{k=1}^{3} \mathbf{e}_k \frac{\partial}{\partial x_k} .$$

So, it is easy to show, that within these circumstances:

$$\partial^2 = 1 - \sum_{k=1}^{3}\sum_{l=1}^{3} \delta_{kl} \frac{\partial^2}{\partial x_k \partial x_l} = 1 - \sum_{k=1}^{3} \frac{\partial^2}{\partial x_k^2} = 1 - \nabla^2 .$$

6.4. Dirac Equation in EH Space.

It has already been noted the resemblance of the classical Schrödinger equation wavefunctions, when expressed in EH spaces, with relativistic spinors. Dirac equation can be found in many sources, see for example references [5,58,69,70,77,79,81-83]. It is well know how Dirac equation can be transformed as well as the problems appearing when trying to solve it for large atomic and molecular systems. Among all the possible transformations Dirac equation can suffer, the one described in Messiah's treatise [58] conforms the best to the EH space formalism here discussed. Indeed, whenever the relativistic spinors, $|\psi$, are expressed as made of large, $|\phi$, and small, $|\chi$, components: $|\psi = \phi, \chi$, then Dirac's equation may be transformed into a new expression, rigorously equivalent to the original one, which appears to be like:

$$\left[(\sigma \cdot \pi)\left(\frac{1}{2M}\right)(\sigma \cdot \pi) + V\right]|\phi = W|\phi \wedge |\chi = \left(\frac{1}{2M}\right)(\sigma \cdot \pi)\phi$$

where the following auxiliary definitions are needed:

$$M = \tfrac{1}{2}(m + \mu) \wedge \mu = E - V \wedge W = E - m,$$

where m is the rest mass, σ the Pauli matrix vector and π the momentum.

The transformed equation has the appropriate structure to be further transformed and manipulated into EH spaces. For this purpose, it is only necessary to construct an extended wavefunction like:

$$|\Psi\rangle = |\phi, (\sigma \cdot \pi)\phi\rangle \equiv |1, (\sigma \cdot \pi)\rangle\,|\phi\rangle, \tag{18}$$

jointly with a Hamilton operator bearing the diagonal form:

$$H = Diag\left(V, \frac{1}{2M}\mathbf{I}\right).$$

The self-evident resemblance to classical extended formalism is quite interesting. Total relativistic wavefunctions can be obtained by using a diagonal formalism. For this purpose, it must be used the diagonal operator:

$$S = Diag\left(1, \frac{1}{2M}\mathbf{I}\right),$$

over the EH space wavefunction $|\Psi\rangle$, defined in equation (18).

7.Conclusions.

The extended Hilbert space wavefunction formalism discussed in this work becomes a rich source of new concepts. Among others, it can be mentioned the deduction of KE DF and several alternative DF, like the functions constructed using Quadrupole or Angular Momentum operators. Such new DF forms are based upon EH spaces, where initially the wavefunction and its gradient are taken simultaneously into account. The new DF can be described and visualised too, producing useful suggestive pictures of the molecular structure environment. It is set in this manner a new source of DF able to be used in QO definition and, thus, in QSM studies.

Moreover, the presented simple formalism leads towards a diagonal matrix formulation of the energy and other expectation values in computational Quantum Mechanics. The usual quantum mechanical formalism is not at all lost, but

enhanced by this new point of view. Momentum and KE operators and its possible manipulations appear as a natural consequence of the theory even at the relativistic level. The eDF and KE DF became described within the same theoretical level. Interesting computational and pedagogical benefits could appear from this alternative point of view.

Appendix A. Definitions leading to Quantum Similarity measures.

Definition 1: Tagged Sets.

Let us suppose known a given set , the Object Set, $\mathscr{S}$, and another set, made of some chosen mathematical elements, which will be hereafter called tags, forming a Tag Set, $\mathscr{T}$. A *Tagged Set*, $\mathscr{Z}$, can be constructed by the ordered product : $\mathscr{Z} = \mathscr{S} \times \mathscr{T}$:

$$\mathscr{Z} = \left\{ \forall \theta \in \mathscr{Z} \middle| \exists s \in \mathscr{S} \wedge \exists t \in \mathscr{T} \rightarrow \theta = (s,t) \right\} . \square$$

Definition 2: Quantum Object.

A Quantum Object can be defined as an element of a Tagged Set: Quantum Systems in well-defined states are taken as the Object Set part and the corresponding Density Functions constitute the Tag Set part. ❐

A collection of Quantum Objects can be called a Quantum Object Set (QOS).

Definition 3: Vector Semispace.

A Vector Semispace (VSS) over the PD real field $\mathbf{R}^+$, is a Vector Space (VS) with the vector sum part provided by a structure of abelian *semigroup*. ❐

By an additive semigroup [86] it is understood here, an additive group without the presence of reciprocal elements. All VSS elements can be seen as directed towards the region of the positive axis hyperquadrant. It will also be accepted that *null elements* are both included in the scalar field as well as in the VSS structure.

Definition 4: First Order eDF.

The ASA eDF could be trivially related with the first-order eDF form, as expressed within MO theory, because the first-order MO eDF structure can be defined by means of the linear combination:

$$\rho(\mathbf{r}) = \sum_i \mathrm{w}_i |\varphi_i(\mathbf{r})|^2 . \qquad \text{(A-1)}$$

This MO eDF can be written in a general way, as a double sum of products of function pairs, coupled with a set of matrix coefficients [87]. However, a simple matrix diagonalization, followed by a unitary MO basis set transformation, can revert DF to the formal expression in equation (A-1), [54a),88]. The coefficient set: $\mathbf{W} = \{\mathrm{w}_i\} \subset \mathbf{R}^+$, interpreted as MO occupation indices, corresponds to a collection of positive real numbers. A unit norm convention has been adopted:

$$\int |\varphi_i|^2 dr = 1; \forall i \;\Rightarrow\; \int \rho(\mathbf{r}) d\mathbf{r} = \sum_i \mathrm{w}_i \int |\varphi_i|^2 d\mathbf{r} = \sum_i \mathrm{w}_i = 1, \qquad \text{(A-2)}$$

and this results in considering the coefficient set $\mathbf{W}=\{ \mathrm{w}_i \}$, as a discrete probability distribution.

Definition 5: Convex Conditions.

By the term Convex Conditions it is understood:

$$\mathscr{K}_n(\mathbf{w}) \equiv \left\{ \mathbf{w} \in \mathscr{V}_n(\mathbf{R}^+) \wedge < \mathbf{w} >= \sum_i \mathrm{w}_i = 1 \right\} \qquad \text{(A-3)}$$

The set of the vector elements, $\mathbf{w} = \{\mathrm{w}_i\}$, can be used instead in the convex conditions symbol, that is:

$$\mathscr{K}_n(\{\mathrm{w}_i\}) \equiv \left\{ \forall \mathrm{i} : \mathrm{w}_i \in \mathbf{R}^+ \wedge \sum_i \mathrm{w}_i = 1 \right\} \qquad \text{(A-4)}$$

Equations (A-3)and (A-4) can be considered the discrete counterparts of the continuous convex conditions, defining a convex DF:

$$\mathscr{I}_{\infty}(\rho) \equiv \left\{ \rho \in \mathscr{H}\left(\mathbf{R}^{+}\right) \wedge \int \rho(\mathbf{r}) d\mathbf{r} = 1 \right\} . \ \square \qquad \text{(A-5)}$$

Convex sets [89] play a leading role in optimisation problems. They have been introduced to deal with some chemical problems [9a]. Elementary Jacobi Rotations (EJR) [90] can be applied over a generating vector to obtain optimal coefficients, while preserving convex conditions [39e,41,49, 91].

Definition 6: Element sum of a (m×n) matrix A.

Known a (m×n) matrix $\mathbf{A} = \{a_{ij}\}$ by the symbol $\mathbf{A}$ it is meant:

$$\mathbf{A} = \sum_{i=1}^{m} \sum_{j=1}^{n} a_{ij} . \square$$

This symbol acts as a linear functional over matrix spaces.

Definition 7: General QSM.

A General QSM, G(Ω), can be considered a PD multiple scalar product defined by a contracted ν-direct product of a QOS, $\mathscr{I}$:

$$\mathrm{G}(\mathbf{\Omega}) : \bigotimes_{K=1}^{\nu} \mathscr{I} \rightarrow \mathbf{R}^{+} . \square$$

This allows to mix ν DF: $\{\rho_I(\mathbf{r}), I = 1, \nu\}$ of the QOS with ω PD operators, collected into a set: $\mathbf{\Omega} = \{\Omega_K(\mathbf{r}), K = 1, \omega\}$, belonging to the same VSS, for example:

$$\mathrm{G}(\mathbf{\Omega}) = \int \left[\prod_{K=1}^{\omega} \Omega_K(\mathbf{r}) \right] \left[\prod_{I=1}^{\nu} \rho_I(\mathbf{r}) \right] d\mathbf{r} , \qquad \text{(A-6)}$$

where the co-ordinate vector, **r**, shall be taken here as a general position vector. Thus, equations (1),(5), and (6) can be all of them considered as diverse forms of QSM.

Equation (A-6), can be interpreted as a general way to define generalised expectation values. A general picture of QSM was already given and studied in references [31,41].

Definition 8: Tagged Ensemble.

A Tagged Ensemble is a Tagged Set whose Object Set elements are Tagged Sets. ❐

QSPR studies could be described as the way in which a relationship is to be found between Objects and Tags defining the Tagged Ensemble.

Appendix B: Algorithms and Generating Rules.

Algorithm 1: Classical Quantum Mechanics.

1) Construction of the Hamilton operator, $\mathscr{H}$.
2) Computation of the state energy-wavefunction pairs, $\{\mathscr{E},\Psi\}$, by solving Schrödinger equation: $\mathscr{H}\Psi=\mathscr{E}\Psi$.
3) Evaluation of the state DF, $\rho=|\Psi|^2$. ❐

Definition 9: Continuous Generating Rule.

A generating rule can easily be written, summarising the three steps of quantum mechanical Algorithm 1:

$$\mathscr{R}(\Psi\rightarrow\rho)=\left\{\begin{matrix}\forall\Psi\in\mathscr{H}(\mathbf{C})\rightarrow\\ \exists\rho=\Psi^{*}\Psi=|\Psi|^{2}\in\mathscr{H}(\mathbf{R}^{+})\end{matrix}\right\}. \qquad \text{(B-1)}$$

In equation (B-1) are given explicitly the wavefunction Hilbert VS [75], $\mathscr{H}(\mathbf{C})$, and the DF Vector Semispace (VSS), $\mathscr{H}(\mathbf{R}^{+})$, see also Definition 3 in the appendix A.

Definition 10: Discrete Generating Rule.

Being **W** a PD real numerical set, it can be generated using a complex coefficient set: $\mathbf{X}=\{x_i\}\subset\mathbf{C}$. A new set of coefficients can be obtained as: $w_i=|x_i|^2;\forall i$. Supposing defined a column vector with the elements of **X**: $\mathbf{x}=\{x_i\}$, then the norm: $\langle\mathbf{x}|\mathbf{x}\rangle=\mathbf{x}^{+}\mathbf{x}=1$, corresponds to the last condition in equation (A-2). For this purpose the following *discrete generating rule* can be described, after collecting the elements of the set **W** into a column

vector **w**:

$$\mathscr{R}(\mathbf{x}\rightarrow\mathbf{w})=\left\{\begin{array}{l}\forall\mathbf{x}\in\mathscr{V}_n(\mathbf{C})\rightarrow\exists\mathbf{w}=\left\{w_i=x_i^*x_i=|x_i|^2\right\}\in\mathscr{V}_n(\mathbf{R}^+)\\ \wedge\,\mathbf{x}^+\mathbf{x}=\sum_i x_i^*x_i=\sum_i|x_i|^2=1\rightarrow|\mathbf{w}|=\sum_i w_i=1\end{array}\right\}. \qquad \text{(B-2)}$$

Appendix C: Algebra of Diagonal Vector Spaces.

Compared with the Dirac's bra-ket formalism, diagonal vector spaces, except for the possibility to have their elements conjugated, lack of the dual space distinction as bra-ket or row-column vectors have. A possible way to overcome this situation is to construct bra-ket diagonal matrices with the aid of a set of auxiliary matrices adopting the appropriate dimension. The following definition will be useful.

Definition 11: Unity matrices.

A unity matrix, **1**, is a (n×m) matrix whose elements are entirely made of the scalar unit element: $[\mathbf{1}]_{ij}=1;\forall i,j$.

Unity row or column n-dimensional vectors will be expressed by the symbols: $\langle\mathbf{1}|$ and $|\mathbf{1}\rangle$ respectively. ❐

Then, a bra-ket structure in diagonal spaces can be generated by multiplying a given diagonal matrix by a unity matrix by the right or the left respectively. To see this, it is only necessary to see, for example, that if $\mathbf{D}=Diag(d_i)$, then the matrix product: $\mathbf{1D}$, generates the matrix: $(d_i\langle\mathbf{1}|)$, while $\mathbf{D1}\equiv(d_i|\mathbf{1}\rangle)$.

A tensorial product of two diagonal matrices can be obtained using the unity matrix of the adequate dimension: $\mathbf{D}\otimes\mathbf{D}=\mathbf{D1D}=\{d_id_j\}$.

Appendix D: Inward matrix Product.

A new simple matrix product can be defined, which appears very useful in various matrix manipulations [92].

Definition 12: *Inward Matrix Product.*

Consider any arbitrary (m × n)-dimensional matrix space over a field: $\boldsymbol{M}_{(m \times n)}$. Let $\mathbf{A}, \mathbf{B} \in \boldsymbol{M}_{(m \times n)}$. An inward product of the matrix pair is a closed operation, resulting in a new matrix $\mathbf{P} \in \boldsymbol{M}_{(m \times n)}$, and symbolised by: $\mathbf{P} = \mathbf{A} * \mathbf{B}$, whose elements are defined by the algorithm:

$$\forall i, j : p_{ij} = a_{ij} b_{ij} . \square$$

It is a straightforward matter to generalise the inward product for applications within hyper-matrix spaces.

The interest in defining such a matrix product stems from the possibility to attach to it the most usual features of a multiplication composition rule. The following properties can be attached to the inward product:

Let be: $\mathbf{A}, \mathbf{B}, \mathbf{C}, \ldots \in \boldsymbol{M}_{(m \times n)}$. Inward products defined over them are:

1) Distributive with respect matrix sum:
$$\mathbf{A} * (\mathbf{B} + \mathbf{C}) = \mathbf{A} * \mathbf{B} + \mathbf{A} * \mathbf{C} .$$

2) Associative:
$$\mathbf{A} * \mathbf{B} * \mathbf{C} = \mathbf{A} * (\mathbf{B} * \mathbf{C}) = (\mathbf{A} * \mathbf{B}) * \mathbf{C} .$$

3) Commutative:
$$\mathbf{A} * \mathbf{B} = \mathbf{B} * \mathbf{A} .$$

4) An Inward Unit Element exists, the ***unity*** matrix, **1**, such that:
$$\mathbf{1} * \mathbf{A} = \mathbf{A} * \mathbf{1} = \mathbf{A} .$$
A unity matrix can be defined as in Definition 11 of Appendix C.

5) Existence of an Inward Inverse:
Iff $\mathbf{A} = \{a_{ij}\} \wedge \forall i,j : a_{ij} \neq 0$; then **A** can be called inwardly inversible or regular. A new matrix defines the inward inverse of a matrix **A**: $\mathbf{A}^{[-1]} = \left\{a_{ij}^{[-1]}\right\}$, with elements, which are computed as follows: $\forall i, j : a_{ij}^{[-1]} = \left(a_{ij}\right)^{-1}$. This definition produces the sequence of equalities:
$$\mathbf{A} * \mathbf{A}^{[-1]} = \mathbf{A}^{[-1]} * \mathbf{A} = \mathbf{1} .$$

Appendix E: DF Surface Visualisation Details.

A) Computational Details.

After a molecule has been chosen, and its atomic co-ordinates have been determined, the corresponding density function is constructed according to the promolecular ASA approach. This procedure involves fitting each atom with 1S gaussian functions [93] to the respective ab initio density function. Here, the density functions of the presented molecules have been built using 7 functions to fit hydrogen atoms, 8 functions to fit carbon and 9 functions to fit nitrogen and oxygen.

B) Image Construction.

When the density function of the involved molecule is known, the surface representation is made by the following steps: a) A grid, large enough to envelop the molecule, is defined. At each grid point the value of the desired DF representation is calculated and stored. b) When all grid points are calculated, after choosing the desired isodensity value, the wireframe model of the surface is created, by using the Marching Cubes Algorithm, described below. c) The resulting output file is then imported by GiD program [94], which is able to plot and render the model.

C) Marching Cubes Algorithm (MCA).

MCA is used to render isosurfaces in volumetric data [95,96]. The basic MCA notion consists in defining a *voxel*. A voxel is considered as the set made by the sequence of pixel values found at the eight cube vertices. If one or more pixels of a cube have values less than a user-specified isovalue, and one or more have values greater than this value, it is considered that the voxel must contribute to an isosurface component. By determining which edges of the cube are intersected by the isosurface, triangular patches can be created. Such triangles divide the cube between regions within the isosurface and regions outside. By connecting the patches from all cubes on the isosurface boundary, a surface representation is obtained. A Fortran 90 program version of MCA is available, it can be downloaded from a www site [100].

Acknowledgements

This work has been partially financed by a CICYT Research Project: #SAF 96-0158 and sponsored by a COMET contract: #ENV4-CT97-0508. Partial founding from the Fundació Maria Francisca de Roviralta is greatly acknowledged. Thanks are due to Mr. Ll. Amat for discussions, comments and test calculations related to the subject of this paper. One of us (R.C.-D.) wants to thank Prof. K. Hirao for his hospitality while a stage at the Department of Industrial Chemistry, Faculty of Engineering, of the University of Tokyo, where the present work has been partially elaborated.

References

1. E. Wigner, Phys. Rew. 40, 749 (1932).
2. D. Leibfried, T. Pfau and C. Monroe, Physics Today April, 22 (1998).
3. P.A.M.Dirac, in "The Principles of Quantum Mechanics", (Clarendon Press, Oxford 1958).
4. J. Von Neumann, in "Mathematical Foundations of Quantum Mechanics", (Princeton University Press, Princeton (N.J.) 1955). [This is a translation of the: *Matematische Grundlagen der Quanten-mechanik.* (Verlag Julius-Springer, Berlin 1932)]
5. D. Bohm, in "Quantum Theory", (Dover Publications, Inc., New York, (1989).[This is a reprint of the original edition of (Prentice Hall 1951)]
6. J.S.Bell, in "Speakable and Unspeakable in Quantum Mechanics", (Cambridge University Press, Cambridge 1993).
7. A. Einstein, B. Podolsky and N. Rosen, Phys. Rev. 47, 777 (1935).
8. See, for a recent review: S. Goldstein, Physics Today March, 42 (1998) and April, 38 (1998).
9. See for example:
    a) P.G. Mezey, in "Shape in Chemistry: an Introduction to Molecular Shape and Topology"(VCH, New York, 1993).
    b) P. G. Mezey, in "Molecular Similarity I", Topics in Current Chemistry, Vol. 173, 63 (Ed. K.Sen, Springer Verlag, Berlin, 1995).
10. See, for example:
    a) P.G. Mezey, Structural Chem. 6, 261 (1995).
    b) P.D. Walker and P.G. Mezey, J. Am. Chem. Soc. 115, 12423 (1993).
    c) P.D. Walker and P.G. Mezey, J. Am. Chem. Soc. 116, 12022 (1994).
    d) P.D. Walker and P.G. Mezey, Can. J. Chem. 72, 2531 (1994).
    e) P.D. Walker and P.G. Mezey, J. Math. Chem. 17, 203 (1995).
    f) P.G. Mezey, J. Math. Chem. 18, 141 (1995).

g) P.G. Mezey, Int. J. Quantum Chem. 63, 39 (1997).
h) P.G. Mezey, Pharm. News 4, 29 (1997).
i) P.G. Mezey, Z. Zimpel, P. Warburton, P.D. Walker, D.G. Irvine, X.-D. Huang, D.G. Dixon and B.M. Greenberg, Environ. Toxicol. Chem. 17, 1207 (1998).
j) P.G. Mezey, K. Fukui, S. Arimoto and K. Taylor, Int. J. Quantum Chem. 66, 99 (1998).
k) P.G. Mezey, Advances in Molecular Structure Research, Vol. 4 (4), 115 (1998).

11. See, for example:
a) P.G. Mezey, Int. J. Quantum Chem. Quant. Biol. Symp. 12, 113 (1986).
b) P.G. Mezey, Comput. Chem. 8, 462 (1987).
c) P.G. Mezey, Int. J. Quantum Chem. Quant. Biol. Symp. 14, 127 (1986).
d) P.G. Mezey, J. Math. Chem. 2, 325 (1988).
e) G.A. Arteca and P.G. Mezey Int. J. Quantum Chem. Symp. 24, 1 (1990).
f) P.G. Mezey, J. Math. Chem. 7, 39 (1991).
g) P.G. Mezey, J. Math. Chem. 11, 27 (1992).
h) P.G. Mezey, J. Chem. Inf. Comput. Sci. 32, 650 (1992).
i) X. Luo, G.A. Arteca and P.G. Mezey, Int. J. Quantum Chem. 42, 459 (1992).
j) P.G. Mezey, J. Math. Chem. 12, 365 (1993).
k) P.G. Mezey, J. Chem. Inf. Comput. Sci. 34, 244 (1994).
l) P.G. Mezey, Int. J. Quantum Chem. 51, 255 (1994).
m) P.D. Walker and P.G. Mezey, J. Comput. Chem. 16, 1238 (1995).
n) P.D. Walker, G.M. Maggiora, M.A. Johnson, J.D. Petke and P.G. Mezey, J. Chem. Inf. Comput. Sci. 25, 568 (1995).
o) P.D. Walker, P.G. Mezey, G.M. Maggiora, M.A. Johnson and J.D. Petke, J. Comput. Chem. 16, 1474 (1995).
p) Z. Zimpel and P.G. Mezey, Int J. Quantum Chem. 59, 379 (1996).
q) P.G. Mezey, J. Chem. Inf. Comput. Sci. 36, 1076 (1996).
r) G.A. Heal, P.D. Walker, M. Ramek and P.G. Mezey, Can. J. Chem. 74, 1660 (1996).
s) D.J. Klein and P.G. Mezey, Theor. Chim. Acta 94, 177 (1996).
t) P.G. Mezey, Z. Zimpel, P. Wartburton, P.D. Walker, D.G. Irvine, D.G. Dixon and B. Greenberg, J. Chem. Inf. Comput. Sci. 36, 602 (1997).
u) P.G. Mezey, Int. J. Quantum Chem. 63, 105 (1997).
v) Z. Zimpel and P.G. Mezey, Int. J. Quantum Chem. 64, 669 (1997).
w) P.G. Mezey, Int. Rev. Phys. Chem. 16, 361 (1997).
x) F. Harary and P.G. Mezey, Int. J. Quantum Chem. 62, 353 (1997).

12. a)P.G.Mezey. J. Math. Chem. 23, 65 (1998).
b) P.G. Mezey, Mol. Phys, 96, 169 (1999).

13. R.F.W. Bader, in "Atoms in Molecules, a Quantum Theory" (Clarendon Press, Oxford 1990).

14. See, for example:
    a) R.F.W. Bader, P.L.A. Popelier and T.A. Keith, Intl. Ed., Eng. 33, 620 (1994).
    b) R.F.W. Bader, Phys. Rev., B49, 13348 (1994).
    c) P.L.A. Popelier and R.F.W. Bader, J. Phys. Chem. 98 , 4473 (1994).
    d) P.F. Zou and R.F.W. Bader, Acta Cryst. A50 714 (1994).
    e) R.F.W. Bader and T. A. Keith, J. Chem. Phys. 99, 3683 (1993).
    f) T.A. Keith and R.F.W. Bader, J. Chem. Phys. 99, 3669 (1993).
    g) R.F.W. Bader, K.M. Gough, K.E. Laidig, T. A. Keith, Mol. Phys. 75 (1992) 1167.
    h) C. Chang and R.F.W. Bader, J. Phys. Chem. 96, 1654 (1992).
    i) K.B. Wiberg, R.F.W. Bader and C.D.H. Lau, J. Am. Chem. Soc. 109, 985 (1987).
15. P. Hohenberg and W. Kohn, Phys. Rev. 136, B864 (1964).
16. R. Carbó, M. Arnau and L. Leyda, Int. J. Quant. Chem. 17, 1185 (1980).
17. See for example:
    a) E. E. Hodgkin and W. G. Richards, Int. J. Quant. Chem. 14, 105 (1987).
    b) C. Burt, W. G. Richards and Ph. Huxley, J. Comp. Chem. 11, 1139 (1990).
    c) A. C. Good, E. E. Hodgkin and W. G. Richards, J. Chem. Inf. Comp. Sci. 32, 188 (1992).
    d) A. C. Good, Sung-Sau So and W.G. Richards, J. Math. Chem. 36, 433 (1993).
    e) A. C. Good and W. G. Richards, J. Chem. Inf. Comp. Sci. 33, 112 (1993).
    f) W.G.Richards and D.D.Robinson, in "Advances in Molecular Similarity" Vol. 2, 73 (Eds. R. Carbó-Dorca and P. G. Mezey, JAI Press Inc., Greenwich (Conn.) 1998).
18. See for example:
    a) D. L. Cooper and N. L. Allan, J. Comp. Aid. Mol. Des. 3, 253 (1989).
    b) D. L. Cooper and N. L. Allan, J. Am. Chem. Soc. 114, 4773 (1992).
    c) D. L. Cooper, K. A. Mort, N. L. Allan, D. Kinchington and Ch. McGuidan, J. Am. Chem. Soc. 115, 12615 (1993).
    d) N. L. Allan and D. L. Cooper, Topics in Current Chemistry 173, 85 (1995).
    e) N.L.Allan and D.L. Cooper, J. Math. Chem. 23, 51 (1998)
19. See for example:
    a) J. Cioslowski and E. D. Fleishmann, J. Am. Chem. Soc. 113, 64 (1991).
    b) J. B. Ortiz and J. Cioslowski, Chem. Phys. Lett. 185, 270 (1991).
    c) J. Cioslowski and M. Challacombe, Int. J. Quant. Chem. S25, 81 (1991).

d) J. Cioslowski and S. T. Mixon, Can. J. Chem. 70, 443 (1992).
e) J. Cioslowski and A. Nanayakkara, J. Am. Chem. Soc. 115, 11213 (1993).
f) J. Cioslowski, B. B. Stefanov and P. Constans, J. Comp. Chem. 17, 1352 (1996).

20. See for example:
a) R. Ponec and M. Strnad, Collect. Czech. Chem. Commun. 55, 896 (1990).
b) R. Ponec and M. Strnad, Collect. Czech. Chem. Commun. 55, 2583 (1990).
c) R. Ponec and M. Strnad, J. Phys. Org. Chem. 4, 701 (1991).
d) R. Ponec and M. Strnad, J. Math. Chem. 8, 103 (1991).
e) R. Ponec and M. Strnad, Int. J. Quant. Chem. 42, 501 (1992).
f) R. Ponec, J. Chem. Inf. Comp. Sci. 33, 805 (1993).
c) R. Ponec, in "Overlap Determinant Method in the Theory of Pericyclic Reactions", Lecture notes in Chemistry, 65 (Springer Verlag, Berlin 1995).

21. Ch. Lee and Sh. Smithline, J. Phys. Chem. 98, 1135 (1994).
22. C. Amovilli and R. McWeeny, J. Mol. Struct. (Theochem) 227, 1 (1991).
23. A. C. Good, J. Mol. Graph. 10, 144 (1992).
24. R. Benigni, M. Cotta-Ramusino, F. Giorgi and Gr. Gallo, J. Med. Chem. 38, 629 (1995).
25. J. D. Petke, J. Comp. Chem. 14, 928 (1993).
26. A. Riera, J. Mol. Struct. (Theochem) 259, 83 (1992).
27. See for example:
a) F. Fratev, O. E. Polansky, A. Mehlhorn and V. Monev, J. Mol. Struct. 56, 245 (1979).
b) F. Fratev, V. Monev, A. Mehlhorn, O. and E. Polansky, J. Mol. Struct. 56, 255 (1979).
28. See for example:
a) M. A. Johnson and G. Maggiora (Editors), in "Concepts and Applications of Molecular Similarity", (John Wiley & Sons Inc., New York 1990).
b) R. Carbó (Editor), in "Molecular Similarity and Reactivity: From Quantum Chemical to Phenomenological Approaches, Understanding Chemical Reactivity", Vol. 14, (Kluwer Academic Publishers, Dordrecht 1995).
c) K. Sen (Editor), in "Molecular Similarity. Topics in Current Chemistry", Vols. 173 & 174, (Springer Verlag, Berlin 1995).
d) P. M. Dean (Editor), in "Molecular Similarity in Drug Design", (Blackie Academic & Professional, London 1995).
e) R. Carbó-Dorca and P. G. Mezey (Editors), in "Advances in Molecular Similarity", Vol. 1, (JAI Press Inc., Greenwich (Conn.) 1996).

f) R. Carbó-Dorca and P. G. Mezey (Editors), in "Advances in Molecular Similarity", Vol. 2, (JAI Press Inc., Greenwich (Conn.) 1998).
29. R. Carbó and Ll. Domingo, Int. J. Quant. Chem. 23, 517 (1987).
30. See for example:
    a) R. Carbó and B. Calabuig, Comp. Phys. Commun. 55, 117 (1989).
    b) R. Carbó and B. Calabuig, J. Mol. Struct. (Theochem) 254, 517 (1992).
    c) R. Carbó and B. Calabuig, in "Computational Chemistry: Structure, Interactions and Reactivity", Vol. A, 300 (Ed. S. Fraga, Elsevier, Amsterdam 1992).
31. R. Carbó, B. Calabuig, L. Vera and E. Besalú, Adv. Quantum Chem. 25, 253 (1994).
32. R. Carbó and B. Calabuig, Int. J. Quant. Chem. 42, 1681 (1992).
33. R. Carbó and E. Besalú, in "Molecular Similarity and Reactivity: From Quantum Chemistry to Phenomenological Approaches", 3 (Ed. R. Carbó, Kluwer Academic Publishers, Dordrecht 1995).
34. R. Carbó and B. Calabuig, J. Chem. Inf. Comp. Sci. 32, 600 (1992).
35. R. Carbó-Dorca, E. Besalú, Ll. Amat and X. Fradera, in "Advances in Molecular Similarity", Vol 1, 1 (Eds. R. Carbó-Dorca and P. G. Mezey, JAI Press Inc., Greenwich (Conn.) 1996).
36. R. Carbó, E. Besalú, Ll. Amat and X. Fradera, J. Math. Chem. 18, 237 (1995).
37. See for more details:
    a) R. Carbó, E. Besalú, Ll. Amat and X. Fradera, J. Math. Chem. 19, 47 (1996).
    b) D.Robert, R.Carbó-Dorca, J. Chem. Inf. Comput. Sci. 38, 469 (1998).
38. R. Carbó, B. Calabuig, E. Besalú and A. Martínez, Molecular Engineering 2, 43 (1992).
39. See for example:
    a) J. Mestres, M. Solà, M. Duran and R. Carbó, J. Comp.Chem. 15, 1113 (1994).
    b) P. Constans and R. Carbó, J. Chem. Inf. Comput. Sci. 35, 1046 (1995).
    c) P. Constans, Ll. Amat, X. Fradera and R. Carbó-Dorca, in "Advances in Molecular Similarity", Vol 1, 187 (Eds. R. Carbó-Dorca and P. G. Mezey, JAI Press Inc. Greenwich (Conn.), 1996).
    d) Ll. Amat, R. Carbó and P. Constans, Scientia Gerundensis 22, 109 (1996).
    e) Ll. Amat and R. Carbó-Dorca, J.Comp.Chem. 18, 2023 (1997).
    f) Ll. Amat and R. Carbó-Dorca, Institute of Computational Chemistry Technical Report: IT-IQC-98-34. (1998) Also: J. Comp. Chem (in press)
40. P. Constans, Ll. Amat and R. Carbó-Dorca, J. Comp. Chem. 18, 826 (1997).
41. R. Carbó-Dorca, Ll. Amat, E. Besalú, X. Gironés and D. Robert; "The Quantum Mechanical Origin of QSAR: Theory and Applications". Institute of Computational Chemistry Technical Report: IT-IQC-99-01.(1999).
42. See for example:

a) D. Robert and R. Carbó-Dorca, J. Math. Chem. 23, 327 (1998).
b) D. Robert and R. Carbó-Dorca, Nuovo Cimento A111, 1311 (1998).
43. R. Carbó and E. Besalú, J. Math. Chem. 20, 247 (1996).
44. E. Besalú, R. Carbó, J. Mestres and M. Solà, in "Molecular Similarity I", Vol. 173, 31 (Ed. K. Sen, Topics in Current Chemistry, Springer Verlag, Berlin, 1995).
45. R. Carbó-Dorca, in "Advances in Molecular Similarity", Vol. 2, 43 (Eds. R. Carbó-Dorca and P. G. Mezey, JAI Press Inc., Greenwich (Conn.) 1998).
46. R.Carbó-Dorca and E.Besalú, J.Mol.Struct. (Theochem) 451, 11 (1998).
47. R. Carbó-Dorca, J.Math. Chem. 22, 143 (1997).
48. R. Carbó-Dorca, J. Math. Chem. 23, 353 (1998).
49. R. Carbó-Dorca, J.Math.Chem. 23, 365 (1998).
50. E. Clementi and C. Roetti, Atomic Data and Nuclear Data Tables 14, 177 (1974).
51. See for example:
    a) X. Fradera, Ll. Amat, E. Besalú and R. Carbó-Dorca, Quant. Struct.-Act. Relat. 16, 25 (1997)
    b) M. Lobato, Ll. Amat, E. Besalú and R. Carbó-Dorca, Scientia Gerundensis, 23, 17 (1998).
    c) M. Lobato, Ll. Amat, E. Besalú and R. Carbó-Dorca, Quant. Struct.-Act.Relat. 16, 465 (1997).
    d) D. Robert and R. Carbó-Dorca, J. Chem. Inf. Comp. Sci. 38, 620 (1998).
    e) L.Amat,D.Robert,E.Besalú and R.Carbó-Dorca, J. Chem. Inf. Comp. Sci. 38, 624 (1998).
    f) R.Ponec,L.Amat and R.Carbó-Dorca, J. Comput.-Aided Mol. Des., 13, 259 (1999).
    g) L.Amat, R.Carbó-Dorca and R.Ponec, J. Comp. Chem. 19, 1575 (1998).
    h) R,Ponec, L.Amat and R.Carbó-Dorca, "Similarity Approach to LFER : Substituent and solvent effects on the acidities of carboxylic acids". Institute of Computational Chemistry Technical Report: IT-IQC-98-14.(1998). See also: J. Phys. Org. (in press).
    i) P.G.Mezey, R.Ponec, L.Amat and R.Carbó-Dorca, "Quantum Similarity approach to the characterization of molecular chiratlity". Institute of Computational Chemistry Technical Report: IT-IQC-98-16. (1998)
    j) D. Robert, L. Amat and R. Carbó-Dorca, 3D QSAR from tuned molecular quantum similarity measures: Prediction of the CBG binding affinity for a steroids family. Institute of Computational Chemistry Technical Report: IT-IQC-98-17.(1998). See also: J. Chem. Inf. Comput. Sci. (in press).

52. K.D.Sen, E. Besalú and R. Carbó-Dorca, "A naïve look on the Hohenberg-Kohn theorem", Institute of Computational Chemistry Technical Report: IT-IQC-98-38. (1998)

53. See, for example:
    a) R. Bonaccorsi, E. Scrocco and J. Tomasi, J. Chem. Phys. 52, 5270 (1970).
    b) For an actualised lively review see: J. S. Murray and K. Sen (Eds.), in "Molecular Electrostatic Potentials: Concepts and Applications", Vol. 3, (Theoretical and Computational Chemistry, Elsevier, Amsterdam 1996).
54. See for example:
    a) P. O. Löwdin, Phys. Rew. 97, 1474 (1955).
    b) R. McWeeny, Revs. Mod. Phys. 32, 335 (1960).
55. R. Carbó and E. Besalú, J. Math. Chem. 18, 37 (1995).
56. R.McWeeny, Proc.Roy.Soc. A,253, 242 (1959).
57. E.R.Davidson, in "Reduced Density Matrices in Quantum Chemistry" (Academic Press, New York 1976).
58. A.Messiah, in " Mécanique Quantique" (Dunod, Paris 1959).
59. R. Shankar, in "Principles of Quantum mechanics", (Plenum Press, New York 1994).
60. A. Jeffrey, in "Handbook of mathematical Formulas and Integrals", (Academic Press, New York 1995).
61. V. R. Saunders, NATO Advanced Study Institute Series, 15, 347 (1975).
62. P. Hohenberg and W. Kohn, Phys. Rev., 136, B864 (1964).
63. N. H. March, in "Electron Density Theory of Atoms and Molecules", (Academic Press, London 1992).
64. P.W. Atkins and R. S. Friedman, in "Molecular Quantum Mechanics", (Oxford University Press, Oxford 1997).
65. H. Eyring, J. Walter and G.E. Kimball, in "Quantum Chemistry", (John Wiley, New York 1944).
66. F.L. Pilar, in "Elementary Quantum Chemistry", (McGraw-Hill Pub. Co., Princeton 1990).
67. H. Clark, in "Quantum Mechanics", (Van Nostrand Reinhold Co. Ldt., New York 1982).
68. L. Pauling and E.B. Wilson Jr., in "Introduction to Quantum mechanics", (Dover, New York 1985).
69. A.S. Davydov, in "Quantum Mechanics", (Pergamon Press, New York 1965).
70. H.A. Bethe and R. Jackiw, in "Intermediate Quantum Mechanics", (Benjamin, Menlo Park 1986).
71. C. Cohen-Tannoudji, B. Diu and F. Laloë, in "Mécanique Quantique", (Hermann, Paris 1992).
72. E.E. Dykstra, in "Introduction to Quantum Chemistry", (Prentice Hall, Englewood Cliffs, New Jersey 1991).

73. M. Abramowitz and I.A. Stegun, in "Handbook of Mathematical Functions", (Dover, New York 1972).
74. P.O. Löwdin, in "Linear Algebra for Quantum Theory", (Wiley-Interscience, New York, 1998).
75. S.K. Berberian, in "Introducción al Espacio de Hilbert", (Editorial Teide, Barcelona, 1970).
76. A. Bohm and M. Gadella, in "Dirac Kets, Gamov Vectors and Gel'Fand Triplets", (Springer Verlag, Berlin 1989).
77. See for example:
    a) R.E.Moss, in "Advanced Molecular Quantum Mechanics", (Chapman and Hall, London 1973).
    b) E.Cartan, in "The theory of spinors", (Dover Pub.Inc. New York 1966).
78. J.M. Levy-Leblond, Commun. Math. Phys. 6, 286 (1997).
79. J. Karwowski, G. Pestka and M. Stanke, Adv. In Quantum Chem. 24, 1 (1998).
80. K. Gürlebeck and W. Sprössig, in "Quaternionic and Clifford Calculus for Physicists and Engineers", (J Wiley & Sons, New York 1997).
81. H.A. Bethe and E.E. Salpeter, in "Quantum Mechanics of One- and Two-electron Systems", (Springer Verlag, Berlin 1957).
82. R. McWeeny, in "Methods of Molecular Quantum Mechanics, Academic Press, London (1978).
83. J. Almlöf and O. Gropen, Revs. In Comp. Chem., 8, 203 (1996).
84. X. Gironés, Ll. Amat, R. Carbó-Dorca, "A Comparative Study of Isodensity Surfaces Using *Ab Initio* and ASA Density Functions". Institute of Computational Chemistry Technical Report: IT-IQC-98-30 (1998). See also: J. Molec. Graph (in press).
85. M. Lehd and F. Jensen, J. Comp. Chem. 9, 1089 (1991).
86. In "Encyclopaedia of Mathematics", Vol. 8, 249 (Ed. I.M. Vinigradov and Reidel-Kluwer Academic Publishers, Dordrecht 1987).
87. E.V. Ludeña, in "Química Teórica, Nuevas Tendencias" Vol. 4, 117 (Ed. S. Fraga, Consejo Superior de Investigaciones Científicas, Madrid 1987).
88. I. Shavitt, in "Methods of Electronic Structure Theory, Modern Theoretical Chemistry", vol. 3, 188 (Ed. H. F. Schaefer III , Plenum Press, New York 1977).
89. See for example:
    a) J. Stoer and Ch. Witzgall, in "Convexity and Optimization in Finite Dimensions", (Die Grundlehren der matematischen Wissenchaften in Einzeldarstellungen, Band 163, Springer Verlag, Berlin, 1970).
    b) P.M.Gruber and J.M.Wills (Editors), in "Handbook of Convex Geometry", (North-Holland, Amsterdam, 1993).
90. C.G.J. Jacobi, J. Reine Angew. Math. 30, 51 (1846).
91. R. Carbó-Dorca, Ll. Amat, E. Besalú, and M. Lobato, in "Advances in Molecular Similarity", Vol. 2, 1 (Eds. R. Carbó-Dorca and P. G. Mezey, JAI Press Inc., Greenwich (Conn.) 1998).

92. K.D.Sen and R.Carbó-Dorca, "Inward Matrix Products, Generalised Density Functions and Rayleigh-Schrödinger Perturbation Theory", Institute of Computational Chemistry Technical Report: IT-IQC-98-42. (1998)
93. ASA coefficients and exponents information for a sample of several atoms can be seen and downloaded from the Institute of Computational Chemistry WWW site: http://iqc.udg.es/cat/similarity/ASA/funcset.html
94. GiD, Geometry and Data, a pre/postprocessor graphical interface. An academic version can be downloaded at the WWW site: http://gatxan.upc.es International Center for Numerical Methods in Engineering (CIMNE), 1998, Barcelona, e-mail: cimne@etseccpb.upc.es
95. W.E. Lorensen and H.E. Cline, Computer Graphics 21, 163 (1987).
96. A. Watt and M.Watt, in "Advanced Animation and Rendering Techniques", (Addison-Wesley, Reading, Massachusetts 1992).
97. F.H. Allen and O. Kennard, Chemical Design Automation News, 8, 31 (1993).
98. J.B. Harborne, H. Baxter and G.P. Moss (Eds), in "Phytochemical Dictionary", 7 (Taylor and Francis Ltd, London 1999).
99. Ampac 6.0, Semichem, 7128 Summit, Shawnee, KS 6621DA (1994).
100. A Fortran 90 Procedure implementing the MCA can be downloaded from the web site: http://iqc.udg.es/cat/similarity/ASA/mca.html. In the same site, details on MCA can be found.

Theory of extended two-particle Green's functions

Joachim Brand and Lorenz S. Cederbaum
Theoretische Chemie, Universität Heidelberg,
Im Neuenheimer Feld 229, D-69120 Heidelberg, Germany
(August 17, 1999)

A general theory of extended two-particle Green's functions constructed from orthonormal extended states is presented. Three types of fermionic propagators are considered that allow the description of a wide range of two-particle processes in non-relativistic many-body systems: the extended particle-hole, particle-particle, and hole-hole Green's functions. Each member of the considered class of two-particle propagators fulfils a Dyson equation and defines a well-behaved two-particle self energy in analogy to the single-particle Green's function of traditional many-body theory. Besides presenting a general formalism for the unified treatment of the different extended two-particle Green's functions we discuss several formal properties on the example of the extended particle-hole Green's function. Particular emphasis is also given to the significance of the static part of the two-particle self energies because it carries the leading terms in perturbation theoretic approximations. A physical interpretation of the static part of the particle-particle self energy, which serves as an exact optical potential for two-particle scattering, is given for the example of Coulomb-interacting fermions. In analogy the particle-hole self energy can be understood as a scattering potential for particle-hole projectiles.

Contents

ADVANCES IN QUANTUM CHEMISTRY, VOLUME 38

0065-3276/01 $35.00

I. INTRODUCTION

Effective or *optical potentials* have proven to be a powerful tool for investigating excitations of single-particle nature in many-body systems. These include ionisation (or knockout reactions), attachment, and single-particle scattering. Besides the phenomenological approaches there have been numerous theoretical derivations of physically equivalent, yet mathematically distinct single-particle potentials. The basic, unifying idea behind all optical potentials is that in a many-body system with a great number of degrees of freedom the motion of a single (or very few) particles can be described by a single- (or few-) particle Schrödinger equation while an effective or optical potential takes account of influences by the motion of the remaining particles. Especially the potential derived by Feshbach projection [1–3], on the one hand, in contrast to the self energy or mass operator of the single-particle Green's function [4–6], on the other hand, have seen wide applications in the fields of nuclear, atomic, and molecular physics. There have also been comparative investigations of the properties of these and other possible approaches from the practical [7] and the more formal point of view [8,9], respectively. The advantages of the Green's functions approach over the other competitors in the field are manifold. We want to mention especially the fact, that the single-particle Green's function can be seen as the resolvent of an effective Hamiltonian in the complete single-particle Hilbert space, regardless whether the many-body system is fully correlated or not. This is important since it allows a perturbation theoretical expansion of the effective Hamiltonian which is constituted by the single-particle kinetic energy and the self energy. Effective Hamiltonians of the Feshbach type, however, may only be defined restricted to subspaces of the single-particle Hilbert space in the case of non or only partially interacting systems and are thus not directly amenable to a perturbation theoretical treatment [8].

Looking at two-particle type excitations, some features of the theory of single-particle processes remain the same whereas others change. By two-particle type excitations we mean double-attachment and scattering by compound projectiles, on the one hand, but also particle-number conserving (neutral) excitations of the particle-hole type like excitons and collective vibrations of nuclei, on the other hand. Also two-particle removal processes can be treated by a similar formalism. One of the difficulties that arise in the theoretical description is that the fundamental two-particle Green's functions do not fulfil Dyson's equation but instead are governed by the much more complicated Bethe-Salpeter equation. Thus there is no direct access to an optical potential in the usual sense and using the Bethe-Salpeter kernel instead gives rise to many problems since it depends on three independent time or energy variables.

Recently, however, we succeeded in defining an extended particle-particle Green's function that fulfils a Dyson equation [10]. We could also show that the extended propagator possesses a well-behaved self energy that serves as an optical potential for scattering with two-particle projectiles. In the present work we will present a more general ansatz that leads to a manifold of effective two-particle Hamiltonians and corresponding Green's functions. The formal ansatz we use will also show clearly the underlying concepts that lead to a well-behaved Dyson equation. We will develop a theoretical framework that allows to treat three different types of extended Green's functions on the same footing, which will allow for the description of two-particle, two-hole, and particle-hole type excitations. It is interesting to note, that the suggested extended particle-hole Green's functions contain the (standard) polarisation propagator [11] and thus it is possible to derive the well-known random-phase approximation (RPA) as a special approximation to the particle-hole self energy. In general, however, approximations to the extended Green's functions lead to non-standard schemes. The same is also true for the extended two-particle and two-hole Green's functions, which contain the common particle-particle propagator [11].

We also want to mention that a Dyson-equation approach for propagators like the polarisation and the particle-particle propagator has been formulated and used to derive a self-consistent extension of the RPA, also called cluster-Hartree-Fock approximation, that has been applied in the fields of plasma and nuclear physics [12–14]. This formalism, however, has similar problems like Feshbach's theory and does not yield a universal, well-behaved optical potential because the two-particle space has to be restricted in order to make the approach well-defined [14].

The main goal of this paper is the construction of two-particle propagators that fulfil a Dyson equation in the unrestricted two-particle space. The reasons for being interested in a Dyson equation are manifold:

- First of all the Dyson equation defines an optical potential and the concept of an optical potential as a physical entity is an intuitively appealing concept. We already mentioned the advantages of Green's function optical potentials over Feshbach-type optical potentials. One major technical advantage of using optical potentials in numerical calculations is that the scattering problem can be separated from the many-body problem and the latter can be treated using bound-state techniques. However, also in purely bound state applications like the calculation of ionisation or excitation energies, the concept of an optical potential remains advantageous. When the self energy is approximated within a given scheme and then the Dyson equation utilised to construct the propagator, the "scattering problem" is solved exactly and the only approximation has been made

in the potential. Speaking in terms of perturbation theory, this idea manifests itself in the fact that Dyson's equation produces diagrams of infinite order for the propagator even if the self energy is only approximated to finite order. When instead also the "scattering problem" is solved only to a given order, an additional error is introduced. And it is a well-known fact in atomic and molecular physics that Møller-Plesset perturbation theory [15] performs very badly on excited states although it is the most direct (even size-consistent) way to approximate excitation energies in a perturbation theoretic framework. It has even been shown that the Møller-Plesset perturbation series may diverge in numerical calculations on single-determinant dominated atomic and molecular systems if extended basis sets are used [16].

- Also the case of one-particle Hamiltonians deserves particular attention. When the Hamiltonian of the system is a one-particle operator, i. e. no two-body forces are present but only external or mean fields, the self energy of the single-particle Green's function becomes an energy independent, first order quantity [11,10] (We will show that the same is true for the extended two-particle Green's function we are going to construct). Thus the first order approximation to the self energy is already the exact solution. Approximating instead the propagator directly, i. e. without using Dyson's equation, the perturbation expansion extends to infinite order (unless, of course, a diagonalising single-particle basis is chosen).

- Another point that we derive from experience in numerical calculations is that the static diagrams in the Feynman-Dyson series for the single-particle Green's function [11] generally do not give a well-converging perturbation series. They have to be renormalised. A much better approximation for the static self energy results by calculating it from the dynamic part of the self energy as described, e. g., in Ref. [17]. When approximating the particle propagator directly, this way of renormalising the static diagrams is not accessible. Using well-adapted algorithms [18], also the numerical evaluation of the self energy is not slower than the direct approximation of the propagator, since the same number of matrix elements has to be calculated. None the less, successful approximation schemes for bound state properties to the one-particle Green's function that avoid Dyson's equation have been reported in the literature (see, e. g. [19,20] and references cited therein).

- In a recent publication [21], we have shown that already the simplest approximation to the self energy of the extended particle-hole propagator yields a well-behaved, hermitian approximation scheme that removes

drawbacks of the RPA, which derives from the traditional polarisation propagator. A perturbation theoretical analysis as well as a simple model case could show that higher order corrections to the excitation energies deriving from ground state correlation are consistently taken into account in the first order self energy in contrast to non-Dyson approximations like the Tamm-Dancoff approximation (TDA) [11] or the RPA.

This paper is organised as follows: A rigorous and formal introduction into the basic formalism used throughout this paper is given in Chapter II. The reader who is not so much interested in the formal aspects of the theory may skip this Chapter in first reading. In the rest of the paper many of the concepts are explained in a less rigorous fashion and references to the formal definitions are given. In Chapter III we define the three different types of extended two-particle Green's functions. We derive Dyson's equation and define the self energies for these propagators in an analogous way to Ref. [10], but in a generalised formalism. Chapter IV is devoted to the formal properties of the extended propagators, focusing on the example of the extended particle-hole Green's function. We will mainly be concerned with the consequences of the introduction of "unphysical" components in the extended Green's functions necessary to fulfil Dyson's equation (Sec. IV A–IV B). In Sec. IV C the general analytic structure of the extended particle-hole Green's function for complex arguments is discussed before defining the extended Green's functions for real arguments in Sec. IV D. Properties of the self energy are discussed in Chapter V. We show two simple approximations for the particle-hole self energy that lead to approximation schemes for excitation energies and transition moments of finite Fermi systems. In Chapter VI we adopt a different point of view by viewing the static self energy as a scattering potential in a system of fermions interacting by Coulomb force. For the sake of comparison, we briefly review the Green's function's and Feshbach's optical potentials for single-particle scattering in Sec. VI A before looking at the explicit expressions for the static two-particle and particle-hole self energy (Sec. VI B and VI C). Appendix A gives a definition of an abstract Hilbert space introduced in Chapter II and the two Appendices B and C contain formulas for the static self energy discussed in Chapter VI.

II. BASIC FORMALISM

Many of the algebraic properties of the single-particle Green's function, in particular Dyson's equation, are transferable to two-particle propagators if they are constructed starting from an orthonormal set of "primary" states. In this paper we will construct propagators $\mathcal{G}(\omega)$ with the help of the "extended

states" $|\, A, B)$ defined in this Section. The peculiar property of these states is that they are "orthonormal" if A and B are chosen canonical particle creation or destruction operators. The extended Green's functions can then be defined in the following way:

$$\mathcal{G}(\omega) = (A, B\, |\frac{1}{\omega - \breve{H}}|\, A', B').$$

The round brackets indicate the so-called μ-product which is a generalisation of the usual Hilbert space inner product with an indefinite metric. The "extended operator" $\breve{H}$ takes the role of an excitation energy operator which lives, like the extended states $|\, A, B)$, in an "extended Hilbert space" Y. These objects will be defined rigorously in this chapter in a very formal manner. In first reading these formal definitions may well be skipped.

The abstract formalism introduced in this chapter builds the fundament of the theory of extended two-particle Green's functions. Our approach is very general in order to allow for a unified treatment of the different species of extended Green's functions discussed in the main part of this paper. Since the discussed propagators can be applied to a wide variety of physical situations, the emphasis of this chapter lies on the unifying mathematical structure. The formalism is developed simultaneously for (projectile) particles of fermionic and bosonic character. We will define the general extended states which serve to define the primary or "model" space of the extended Green's functions. We also define the μ-product under which the previously defined extended states fulfil peculiar orthonormality conditions. Finally we introduce a canonical extension of common Fock-space operators and super-operators to the space of the extended states.

A. Extended States

Definition Let $|\psi\rangle$ and $|\varphi\rangle$ be normalised many-particle states, i. e. elements of the physical Fock space with $\langle\psi|\psi\rangle = \langle\varphi|\varphi\rangle = 1$, and let $Q = 1 - |\psi\rangle\langle\psi|$ denote the orthogonal projector onto the complement of $\{\, |\psi\rangle\}$. For linear Fock-space operators A and B we define the **extended state** $|\, A, B)$ by the vector

$$|\, A, B) = \begin{pmatrix} QAB\,|\psi\rangle \\ \langle\psi|\, ABQ \\ \langle\varphi|\, A \otimes \langle\psi|\, B \mp \langle\varphi|\, B \otimes \langle\psi|\, A \\ A\,|\varphi\rangle \otimes \langle\psi|\, B \mp B\,|\varphi\rangle \otimes \langle\psi|\, A \end{pmatrix}, \tag{1}$$

where the upper sign is appropriate for operators A and B with fermionic character and the lower sign for operators of bosonic character.

Properties

- The extended state $|\,A,B)$ is linear in A and B.
- If the operators A and B anti-commute (commute) the extended state $|\,A,B)$ is anti-symmetric (symmetric) under permutation of A and B:

$$|\,A,B) = \mp|\,B,A) \qquad \text{if} \quad [A,B]_{\pm} = 0. \tag{2}$$

  The square bracket $[.\,,.]_{\pm}$ denotes the usual anti-commutator (commutator). Again, the upper (lower) sign applies in the fermionic (bosonic) case.

- An inner product for extended states can be constructed by the following rules which are the canonic rules for direct sums and tensor product states [22] (c. f. Ref. [10]). For a direct sum the inner products of the components add:

$$\left\langle \begin{pmatrix} |A\rangle \\ \langle B| \end{pmatrix}, \begin{pmatrix} |C\rangle \\ \langle D| \end{pmatrix} \right\rangle = \langle A|C\rangle + \langle D|B\rangle. \tag{3}$$

  Here, the second component was chosen a "bra" state. This is understood as the particular element of the dual space to the corresponding space for "kets" according to the Riesz theorem [22].

  For tensor product states the inner products of the components multiply:

$$(\,|A\rangle \otimes |B\rangle\,,\ |C\rangle \otimes |D\rangle) = \langle A|C\rangle\langle B|D\rangle. \tag{4}$$

  Examples involving the extended states (1) will be given later [Eq. (10)].

- The extended states $|\,A,B)$ are elements of a Hilbert space denoted by Y that is constructed by direct sums and tensor products from the component spaces and possesses the inner product introduced above. Strictly speaking, the extended states $|\,A,B)$ can be elements of a Hilbert space only if all components have finite norm, like usual in quantum mechanics. In the following example we define the Hilbert space Y relevant for the extended particle-hole Green's function. For the other propagators, the appropriate space Y can be constructed in a completely analogous manner. A convenient formal definition of Y for the general case is given in App. A. It is important to realise that the space Y is in general *not* isomorphic to any subspace of the fermion or boson Fock-space. This is because the tensor products in the third and fourth component in (1) do not fulfil the symmetry requirements of the Pauli principle.

Example Choosing both reference states $|\psi\rangle$ and $|\varphi\rangle$ equal to the N particle ground state $|\Psi_0^N\rangle$ of a fermionic system, the definition of the so-called extended particle-hole states becomes

$$|\, a_r^\dagger, a_s) = \begin{pmatrix} Q a_r^\dagger a_s \,|\Psi_0^N\rangle \\ \langle\Psi_0^N|\, a_r^\dagger a_s Q \\ \langle\Psi_0^N|\, a_r^\dagger \otimes \langle\Psi_0^N|\, a_s - \langle\Psi_0^N|\, a_s \otimes \langle\Psi_0^N|\, a_r^\dagger \\ a_r^\dagger\,|\Psi_0^N\rangle \otimes \langle\Psi_0^N|\, a_s - a_s\,|\Psi_0^N\rangle \otimes \langle\Psi_0^N|\, a_r^\dagger \end{pmatrix}. \tag{5}$$

These are elements of a Hilbert space Y which is the direct sum of four subspaces related to the four entries of the above defined column vector. The first component $Q a_r^\dagger a_s\,|\Psi_0^N\rangle$ is element of of the physical N fermion Hilbert space H^N (excluding the ground state due to Q) and can be understood as an approximate particle-hole type excitation. The second entry $\langle\Psi_0^N|\, a_r^\dagger a_s Q$ is a "bra" state and thus an element of the dual space H^{N*} of the N particle space. This second entry can also be seen as an approximate excited state but the "hole" and "particle" role of the indices r and s has interchanged. Each of the remaining two entries is the direct sum of tensor product states of "bras" or "kets" in the $N-1$ and $N+1$ particle Hilbert spaces, e. g. $\langle\Psi_0^N|\, a_r^\dagger \otimes \langle\Psi_0^N|\, a_s \in \mathsf{H}^{(N-1)^*} \otimes \mathsf{H}^{(N+1)^*}$. For the present example, the full composite space Y is consequently described by

$$\begin{aligned} \mathsf{Y} = \mathsf{H}^N \oplus \mathsf{H}^{N^*} \oplus \mathsf{H}^{(N-1)^*} \otimes \mathsf{H}^{(N+1)^*} \oplus \mathsf{H}^{(N+1)^*} \otimes \mathsf{H}^{(N-1)^*} \\ \oplus \mathsf{H}^{(N+1)} \otimes \mathsf{H}^{(N+1)^*} \oplus \mathsf{H}^{(N-1)} \otimes \mathsf{H}^{(N-1)^*}. \end{aligned} \tag{6}$$

The construction of a basis of this space by sums and products of Slater determinantal basis sets of the component spaces is trivial. Obviously the dimension of the composite Hilbert space Y is considerably enlarged in comparison with the physical N particle space H^N, which contains all particle-number conserving excitations. The expression (6), however, only allows a rather rough estimate of the actual dimension of the relevant space for which it gives an upper bound. The minimal space needed is certainly smaller because symmetries may reduce the relevant spaces drastically. E. g. the fact that both reference states were chosen equal in Eq. (5) allows to replace the third component of the extended states by $\sqrt{2}\langle\Psi_0^N|\, a_r^\dagger \otimes \langle\Psi_0^N|\, a_s$, which spares the component $\mathsf{H}^{(N+1)^*} \otimes \mathsf{H}^{(N-1)^*}$ from the direct sum constituting the space Y in Eq. (6). Also symmetries of the physical system may lead to a reduced dimensionality. For an exact but non-constructive definition of the minimal space needed, we again refer the reader to App. A.

A possible way to construct a basis for the Hilbert space Y may also be the definition of operator sets $\mathcal{A}$ and $\mathcal{B}$, such that the set of states $\{|\, A, B) \,|\, A \in \mathcal{A}, B \in \mathcal{B}\}$ span the Hilbert space Y. In the context of traditional one- and two-particle propagators of many-body theory, such complete operator manifolds have been found [23] and used for deriving approximation schemes (see e. g. [24] and references cited therein). In the present context, however, such a construction seems difficult because of the complicated nature of the extended states $|\, A, B)$. It is certainly an interesting open question whether a convenient construction can be found.

- *Linear operators on the space* Y are, in general, 4×4 matrices of operators. In this paper, however, we will restrict ourselves to diagonal matrix operators that do not mix the different components of the space Y. Such a diagonal matrix operator O is determined by specifying the operators O_i that act in the different component spaces of Y. We denote

$$O = \mathrm{diag}(O_1, O_2, O_3, O_4). \tag{7}$$

In a dual space the operator acts "from the right". E. g. for the second component we have

$$\big[O|\, A, B)\big]_2 = \langle \psi |\, ABQO_2. \tag{8}$$

Note that there is no canonic way to define the application of a general Fock-space operator to an element of the space Y. We will see later how to construct so-called extended operators that operate in the space Y from Fock-space operators.

B. The μ-product

The *inner product* (scalar product) $\langle .\,, .\rangle$ in the Hilbert space Y follows from the canonical rules for inner products of direct sums and tensor products of Hilbert spaces like mentioned above. We use common Dirac notation for matrix elements $\langle Y|\, O\,|Z\rangle$ of an operator O and vectors $|Y\rangle$ and $|Z\rangle$ in the Hilbert space Y.

Definition The **μ-product** between two states $|Y\rangle, |Z\rangle \in$ Y is given by the matrix element $\langle Y|\, \mu\,|Z\rangle$ where $\mu = \mathrm{diag}(1, -1, 1, \pm 1)$ is called the metric operator. Again, here and in the following, the upper sign refers to the fermionic case and the lower to the bosonic case. For extended states of the form (1) we introduce the following shorthand notation for the μ-product:

$$(A, B \,|\, C, D) = \Big\langle |\, A, B)\,,\, \mu |\, C, D) \Big\rangle. \tag{9}$$

Properties

- Note that the metric operator μ commutes with all diagonal operators in the space Y.
- The "metric" induced by the μ-product is indefinite which means that $\langle Y|\,\mu\,|Y\rangle$ need not be positive but can also be negative or zero even if $|Y\rangle$ is not the null-vector.
- The μ-product of the extended states $|\,A, B)$ and $|\,C, D)$ evaluates (by the canonic rules discussed above) to

$$\begin{aligned}(A, B \,|\, C, D) = {} & \langle\psi|\,[B^\dagger A^\dagger, CD]_-\,|\psi\rangle \\ & + \langle\varphi|\,[C, A^\dagger]_\pm\,|\varphi\rangle\langle\psi|\,DB^\dagger\,|\psi\rangle + \langle\varphi|\,[D, B^\dagger]_\pm\,|\varphi\rangle\langle\psi|\,CA^\dagger\,|\psi\rangle \\ & + \langle\varphi|\,[C, B^\dagger]_\pm\,|\varphi\rangle\langle\psi|\,DA^\dagger\,|\psi\rangle + \langle\varphi|\,[D, A^\dagger]_\pm\,|\varphi\rangle\langle\psi|\,CB^\dagger\,|\psi\rangle. \end{aligned} \tag{10}$$

  This expression simplifies further in the case when the anti-commutators (commutators) of any pair of the operators $A^\dagger$, $B^\dagger$, C, and D simply are complex numbers:

$$(A, B \,|\, C, D) = [A^\dagger, C]_\pm [B^\dagger, D]_\pm \mp [A^\dagger, D]_\pm [B^\dagger, C]_\pm. \tag{11}$$

  Note that this result is independent of the states $|\psi\rangle$ and $|\varphi\rangle$.

Example Let $a_r^\dagger$ (a_r) denote the creation (destruction) operator for a single fermion and let the canonical anti-commutation relations be fulfilled ($[a_r^\dagger, a_s]_+ = \delta_{rs}$, etc.). We then find that the extended states $|\,a_r^\dagger, a_s)$ are "normalised" and "orthogonal" with respect to the μ-product:

$$(a_r^\dagger, a_s \,|\, a_{r'}^\dagger, a_{s'}) = \delta_{rr'}\delta_{ss'}. \tag{12}$$

Definition A set of states $\{\,|Y_I\rangle\}_I \subset \mathsf{Y}$ is called **μ-orthonormal** if

$$\langle Y_I|\,\mu\,|Y_J\rangle = \pm\delta_{IJ}, \tag{13}$$

where the sign is left indeterminate (in the fermionic as well as in the bosonic case).

Notes

- A μ-orthonormal set of states is necessarily linear independent.

- A countable set of linearly independent states $\{|\tilde{Y}_I\rangle\}_I$ with μ-norm other than zero can in general be μ-orthonormalised following the Gram-Schmidt construction procedure.

- Throughout the paper we are using both the μ-product notation indicated by round brackets and common Dirac notation of the inner product indicated by angular brackets like usual. While the μ-product notation in particular allows for an elegant handling of super-operator expansions, the foremost advantage of the Dirac notation is to stress the Hilbert space nature of the formalism which allows for an intuitive understanding of basis set expansions and matrix representations.

C. Super-operators

The specification "super-operator" is common in quantum chemical and physical literature for linear mappings of Fock-space operators. It is very helpful to transfer this concept to the extended states $|A,B)$ and define the application of super-operators by the action on the operators A and B. We will see later how this definition helps for a compact notation of iterated equations of motion and perturbation expansions. In certain cases, however, the action of a super-operator is fully equivalent to the action of an operator in the Hilbert space Y. The alternative concept of Y-space operators allows to introduce approximations by finite basis set representations of operators in a well-defined and lucid way.

We will only use super-operators constructed in the following way:

Definition Given a Fock-space operator U, we define $\hat{U}$ by the linear mapping of an operator A onto the commutator of U with A:

$$\hat{U}(A) = [U, A]_-. \tag{14}$$

We call $\hat{U}$ the **super-operator associated with the operator** U. The application of the super-operator $\hat{U}$ to the extended state $|A,B)$ (for arbitrary operators A and B) is defined as follows:

$$\begin{aligned} \hat{U}|A,B) &= |\hat{U}(A),B) + |A,\hat{U}(B)) \\ &= |[U,A]_-,B) + |A,[U,B]_-). \end{aligned} \tag{15}$$

Example Let $a_r^{(\dagger)}$ be a fermionic operator as above and let $v = \sum_{ij} v_{ij} a_i^\dagger a_j$ be a one-particle operator. Then

$$(a_r^\dagger, a_s\,|\hat{v}|\,a_{r'}^\dagger, a_{s'}) = v_{rr'}\delta_{ss'} - v_{s's}\delta_{rr'} \tag{16}$$

describes a matrix element that is determined only by the operator v and the single-particle basis while it is independent of the states $|\psi\rangle$ and $|\varphi\rangle$.

Properties If the states $|\psi\rangle$ and $|\varphi\rangle$ are eigenstates of the self-adjoint operator U with respective eigenvalues u_ψ and u_φ then applying the super-operator $\hat{U}$ is equivalent to applying the diagonal operator

$$\check{U} = \mathrm{diag}(U - u_\psi, u_\psi - U, u_\varphi - U \otimes 1 + u_\psi - 1 \otimes U, U \otimes 1 - u_\varphi + u_\psi - 1 \otimes U). \tag{17}$$

We illustrate the statement $\hat{U}|A,B) = \check{U}|A,B)$ by looking at the second component where

$$\begin{aligned}\left[\check{U}|A,B)\right]_2 &= \langle\psi|ABQ(u_\psi - U) = \langle\psi|UABQ - \langle\psi|ABQU \\ &= \langle\psi|[U,AB]Q = \left[\hat{U}|A,B)\right]_2 \end{aligned} \tag{18}$$

holds because Q commutes with U.

Definition We call $\check{U}$ the **extended operator associated with the** self-adjoint (Fock-space) **operator** U.

Notes

- The symbols $\hat{}$ and $\check{}$ are understood as operations that map a Fock-space operator onto the corresponding super-operator and Y-space operator, respectively.
- A Y-space operator corresponding to the super-operator $\hat{U}$ generally exists only if $|\psi\rangle$ and $|\varphi\rangle$ are eigenstates of the operator U and not for operators without this property.
- The operations $\hat{}$ and $\check{}$ are linear in the sense that if the operator U is a linear combination of Fock-space operators V and W

$$U = aV + bW \tag{19}$$

with complex numbers a and b then

$$\hat{U} = a\hat{V} + b\hat{W} \tag{20}$$

holds for the associated super-operators. If further $|\psi\rangle$ and $|\varphi\rangle$ are eigenstates of V and W then also

$$\check{U} = a\check{V} + b\check{W} \tag{21}$$

holds for the associated extended operators.

- It is easily seen that the extended operator $\breve{U}$ associated with a self-adjoint operator U is also self-adjoint:

$$\Big\langle |\, A, B), \mu\breve{U} |\, C, D) \Big\rangle = \Big\langle \breve{U} |\, A, B), \mu |\, C, D) \Big\rangle. \tag{22}$$

The same "holds" for the super-operator associated with a self-adjoint operator.

III. EFFECTIVE TWO-PARTICLE DESCRIPTION WITH ORTHONORMAL STATES

In the preceding section a self-contained introduction to the abstract formalism related to the extended states and the μ-product with rigorous definitions has been given but many properties will also be explained in the text. In this chapter we will show how a Dyson equation can be derived and a self energy defined upon the extended two-particle Green's functions. This derivation has already been shown in Ref. [10] for the example of the extended particle-particle Green's function. It is repeated here for the sake of self-containedness and also because the present formalism is more general including different types of fermionic two-particle Green's functions as well as bosonic two-particle Green's functions. Reviewing the derivation of Dyson's equation in the abstract formalism also shows clearly the underlying concepts.

A. Extended two-particle Green's functions

The particular choice of the operators A and B used for constructing the extended states $|\, A, B)$ define the nature of the propagator while the choice of the Hamiltonian and the reference state $|\psi\rangle$ contained in the definition (1), define the physical system under investigation. In the following we will discuss three cases of Green's functions which are very similar from the formal point of view but allow for the description of different physical situations.

(a) The **extended particle-hole Green's function** is defined by

$$\mathcal{G}^{(ph)}_{rs,r's'}(\omega) = (a^\dagger_r, a_s \,|\, \frac{1}{\omega - \breve{H}} \,|\, a^\dagger_{r'}, a_{s'}), \tag{23}$$

and contains information related to particle-number conserving excitations and linear response properties. It is constructed with the states $|Y^{(ph)}_{rs}\rangle = |\, a^\dagger_r, a_s)$ which we call **extended particle-hole states**.

(b) The **extended particle-particle Green's function** is defined by

$$\mathcal{G}^{(pp)}_{rs,r's'}(\omega) = (a^\dagger_r, a^\dagger_s \,|\, \frac{1}{\omega - \breve{H}} \,|\, a^\dagger_{r'}, a^\dagger_{s'}), \tag{24}$$

and may be used for describing two-particle attachment or scattering processes. It is constructed using the **extended particle-particle states** $|Y^{(pp)}_{rs}\rangle = |\, a^\dagger_r, a^\dagger_s)$.

(c) The **extended hole-hole Green's function** is defined by

$$\mathcal{G}^{(hh)}_{rs,r's'}(\omega) = (a_r, a_s \,|\, \frac{1}{\omega - \breve{H}} \,|\, a_{r'}, a_{s'}), \tag{25}$$

and allows the description of two-particle removal processes like atomic or molecular Auger decay. The corresponding **extended hole-hole states** are $|Y^{(hh)}_{rs}\rangle = |\, a_r, a_s)$.

Here, the operators $a^\dagger_r$ and a_r denote canonical fermionic single-particle creation and destruction operators, respectively. We are not going to dicuss bosonic two-particle Green's functions here further but most of the discussion in this chapter applies to bosons as well.

A preliminary justification for the classification given for the Green's functions and extended states is provided by the fact that the first or **physical component** of the defining vector of the extended state $|\, A, B)$ is related to the state $AB\,|\psi\rangle$ [see definition (1)]. In this paper we will choose the reference state $|\psi\rangle$ to describe the exact ground state $|\Psi^N_0\rangle$ of an interacting N-fermion system. The physical component of the extended states $|Y^{(ph)}_{rs}\rangle$, $|Y^{(pp)}_{rs}\rangle$, and $|Y^{(hh)}_{rs}\rangle$ therefore describes states with N, $N+2$, and $N-2$ particles, respectively. The remaining components of the extended state $|\, A, B)$ relate to different physical situations and we will classify them as **unphysical components**. They should be regarded as useful additives for achieving the particular algebraic properties presented in the following. Their nature and their importance upon approximate solutions will be discussed in later chapters.

The set of states $\{|Y_{rs}\rangle\}$, where the indices r and s are both taken from the full set of single-particle indices, will be called **primary set of states** which spans the so-called **model space**. For each of the three choices this set of states is μ-orthonormal (in the sense of Sec. II B) since the following orthonormality relations hold:

$$(a^\dagger_r, a_s \,|\, a^\dagger_{r'}, a_{s'}) = \delta_{rr'}\delta_{ss'}, \tag{26}$$

$$(a^\dagger_r, a^\dagger_s \,|\, a^\dagger_{r'}, a^\dagger_{s'}) = (a_r, a_s \,|\, a_{r'}, a_{s'}) = \delta_{rr'}\delta_{ss'} - \delta_{rs'}\delta_{sr'}. \tag{27}$$

These relations follow directly from the formal property (11) of the extended states $|\,A,B)$.

Note that these equations can also be written without resuming to the μ-product notation indicated by the round brackets. Instead one can use common Dirac notation of the inner product in the Hilbert space Y which is indicated by the use of angular brackets like usual. In this case the metric operator μ (defined in Sec. II B) appears explicitly and, e.g., Eq. (26) becomes

$$\langle Y^{(ph)}_{rs}|\mu|Y^{(ph)}_{r's'}\rangle = \delta_{rr'}\delta_{ss'}. \tag{28}$$

In the following we will use both notations because each has its own advantages.

In the orthonormality relations (26) and (27), a difference occurs between the particle-hole case (a), on the one hand, and the cases of two-particle attachment (b) or removal (c), on the other hand. In the latter case Eq. (27) shows antisymmetry upon interchanging the single-particle indices r and s or r' and s'. The antisymmetry with respect to the interchange of single-particle labels applies to the extended states $|Y^{(pp)}_{rs}\rangle$ and $|Y^{(hh)}_{rs}\rangle$ as well (as shown in Sec. II A). As a consequence, the primary set of states $\{|Y_{rs}\rangle\}$ for the choices (b) and (c) spans a model space which is isomorphous to the antisymmetrised Hilbert space of two indistinguishable fermions. In the particle-hole case (a), however, the symmetry is broken and the primary set $\{|Y^{(ph)}_{rs}\rangle\}$ now spans a model space which is isomorphous to the physical space of two distinguishable particles.

The primary states $|Y_{rs}\rangle$ as defined above are elements of an extended Hilbert space Y. This point has been discussed in Sec. II where special attention is given to the choice (a) as an example. Within the space Y, the role of a generalised **excitation energy operator** is taken by the extended operator $\breve{H}$ associated with the common Fock-space Hamiltonian H of the system as defined in Sec. II C. Indeed, Eq. (17) shows that the operator $\breve{H}$ acts on the physical component of the states $|Y_{rs}\rangle$ as $H - E_0^N$, where E_0^N is the energy eigenvalue of the N-particle ground state $|\Psi_0^N\rangle$ of the system. Therefore $\breve{H}$ can be said to measure the energy of the system relative to the N-particle ground state energy.

The extended two-particle propagators can now be understood as projections of the resolvent of the excitation energy operator $\breve{H}$ onto the primary states $|Y_{rs}\rangle$. Without specifying the particular choice [(a), (b), or (c)] we may define the general **extended two-particle Green's function** $\underline{\underline{\mathcal{G}}}(\omega)$ as a function of the frequency variable ω and a matrix with two-particle indices (rs) by the matrix elements

$$\mathcal{G}_{rs,r's'}(\omega) = \langle Y_{rs}|\frac{\mu}{\omega - \breve{H}}|Y_{r's'}\rangle. \tag{29}$$

This definition has before been written in the equivalent notation involving the μ-product for each case separately.

B. Dyson equation and self energy

We will now derive a Dyson equation by expressing the inverse matrix of the extended two-particle Green's function $\mathcal{G}_{rs,r's'}(\omega)$ by a matrix representation of the extended operator $\breve{H}$. We already mentioned that the primary set of states $\{|Y_{rs}\rangle\}$ spans a subspace (the model space) of the Hilbert space Y. Since the states $\{|Y_{rs}\rangle\}$ are μ-orthonormal they are also linearly independent and thus form a basis of this subspace. Here and in the following the set of pairs of single-particle indices (r, s) has to be restricted to $r > s$ for the pp and hh cases (b) and (c) where the states $|Y_{rs}\rangle$ are antisymmetric under permutation of r and s. No restriction applies in the ph case (a). The primary set of states $\{|Y_{rs}\rangle\}$ can now be extended to a complete basis $\{|Q_J\rangle\} \supset \{|Y_{rs}\rangle\}$ of the Hilbert space Y. We may further demand that the states $|Q_J\rangle$ are μ-orthonormal:

$$\langle Q_I|\,\mu\,|Q_J\rangle = \pm\delta_{IJ}. \tag{30}$$

As a consequence of the indefinite nature of the metric μ, basis states with negative norm appear. We now define the diagonal overlap matrix $\underline{\underline{\mu}}$ by

$$\left[\underline{\underline{\mu}}\right]_{IJ} := \langle Q_I|\,\mu\,|Q_J\rangle, \tag{31}$$

and the basis set representation $\underline{\underline{H}}$ of the extended operator $\breve{H}$ with the matrix elements

$$\left[\underline{\underline{H}}\right]_{IJ} := \langle Q_I|\,\mu\breve{H}\,|Q_J\rangle. \tag{32}$$

A block structure is imposed onto $\underline{\underline{H}}$ by the division of the basis $\{|Q_J\rangle\}$ into the primary set of states $\{|Y_{rs}\rangle\}$ and the rest:

$$\underline{\underline{H}} = \begin{pmatrix} \underline{\underline{H}}_{aa} & \underline{\underline{H}}_{ab} \\ \underline{\underline{H}}_{ba} & \underline{\underline{H}}_{bb} \end{pmatrix}. \tag{33}$$

The primary block $\underline{\underline{H}}_{aa}$, in particular, is just the part of the matrix representation of the operator $\breve{H}$ that corresponds to the states $\{|Y_{rs}\rangle\}$:

$$\left[\underline{\underline{H}}_{aa}\right]_{rs,r's'} = \langle Y_{rs}|\mu\breve{H}|Y_{r's'}\rangle. \tag{34}$$

Now the extended Green's function $\underline{\underline{\mathcal{G}}}(\omega)$ can be expressed as the "upper left corner" of an inverse matrix:

$$\underline{\underline{G}}(\omega) = \left[\frac{1}{\omega\mu - \underline{\underline{H}}}\right]_{aa}. \tag{35}$$

This equation expresses the fact that the extended Green's function $\underline{\underline{G}}(\omega)$ is the projection of an operator resolvent onto a set of μ-orthonormal states [10]. Note that the matrix $\underline{\underline{H}}$ is hermitian if the Hamiltonian H of the many-body system is hermitian (which is assumed throughout this paper). By matrix partitioning we can write for the inverse of the Green's function

$$\left[\underline{\underline{G}}(\omega)\right]^{-1} = \omega\underline{\underline{1}} - \underline{\underline{H}}_{aa} - \underline{\underline{H}}_{ab}\frac{1}{\omega\underline{\underline{\mu}}_{bb} - \underline{\underline{H}}_{bb}}\underline{\underline{H}}_{ba}. \tag{36}$$

This equation is the main result of the present considerations. In order to define the two-particle self energy $\underline{\underline{S}}(\omega)$ and for establishing the connection to the familiar form of Dyson's equation we adopt a perturbation theoretical view where a convenient single-particle description (e. g. the Hartree-Fock approximation) defines the zeroth order. We will see later that the coupling blocks $\underline{\underline{H}}_{ab}$ and $\underline{\underline{H}}_{ba}$ vanish in a single-particle approximation. Consequently the extended Green's function is the proper resolvent of the zeroth order primary block $\underline{\underline{H}}^{(0)}_{aa}$ which can be understood as an operator in the physical two-particle space:

$$\underline{\underline{G}}^{(0)}(\omega) = \frac{1}{\omega\underline{\underline{1}} - \underline{\underline{H}}^{(0)}_{aa}}. \tag{37}$$

Introducing the **two-particle self energy**

$$\underline{\underline{S}}(\omega) = \underline{\underline{H}}_{aa} - \underline{\underline{H}}^{(0)}_{aa} + \underline{\underline{H}}_{ab}\frac{1}{\omega\underline{\underline{\mu}}_{bb} - \underline{\underline{H}}_{bb}}\underline{\underline{H}}_{ba}, \tag{38}$$

Eq. (36) can be rewritten into

$$\underline{\underline{G}}(\omega) = \frac{1}{\omega\underline{\underline{1}} - \underline{\underline{H}}^{(0)}_{aa} - \underline{\underline{S}}(\omega)}. \tag{39}$$

Rearranged it takes on the familiar form of a **Dyson equation**:

$$\underline{\underline{G}}(\omega) = \underline{\underline{G}}^{(0)}(\omega) + \underline{\underline{G}}^{(0)}(\omega)\underline{\underline{S}}(\omega)\underline{\underline{G}}(\omega). \tag{40}$$

C. Static and dynamic self energy

The self energy $\underline{\underline{S}}(\omega)$ has a similar analytic structure to the common self energy [25,26] of the single-particle Green's function [11] in having single poles

and branch cuts on the real axis corresponding to the eigenvalue spectrum of the block $\underline{\underline{H}}_{bb}$. For high energies ω (far outside the eigenvalue spectrum of the Hamiltonian) the self energy $\underline{\underline{\mathcal{S}}}(\omega)$ has a finite limit. It is called the **static self energy** $\underline{\underline{\mathcal{S}}}(\infty)$ and consists of the higher-order contributions to the primary block $\underline{\underline{H}}_{aa}$:

$$\underline{\underline{\mathcal{S}}}(\infty) = \underline{\underline{H}}_{aa} - \underline{\underline{H}}^{(0)}_{aa}. \tag{41}$$

This equation yields a closed expression for the static self energy. The physical significance is to account for interactions and exchange phenomena between the two test particles (or holes) and the (static) particle density of isolated N-particle system. Also the additional (unphysical) components of the extended states take some effect here as well. The discussion of the static self energy and its physical significance will be the main objective of the rest of this paper.

The remaining ω-dependent part of the self energy is called **dynamic self energy** $\underline{\underline{\mathcal{M}}}(\omega)$:

$$\underline{\underline{\mathcal{M}}}(\omega) = \underline{\underline{\mathcal{S}}}(\omega) - \underline{\underline{\mathcal{S}}}(\infty) = \underline{\underline{H}}_{ab} \frac{1}{\omega \underline{\underline{\mu}}_{bb} - \underline{\underline{H}}_{bb}} \underline{\underline{H}}_{ba}. \tag{42}$$

This part takes account for dynamic correlation between the test particles and the finite system and is necessary for the complete description of two particle excitation processes. Of course, also here the unphysical components of the extended states enter.

Adopting the three choices for the extended states $|Y_{rs}\rangle$ from the beginning of this Chapter, we get three different types of two-particle self energies. Before we will concentrate on discussing in how far these self energies are useful for an effective two-particle description of diverse many-body phenomena in the remaining Chapters of this paper, we will briefly touch an alternative formal approach.

D. Super-operator expansions

So far we have used the picture of operators like $\breve{H}$ and μ, acting on states like $|Y_{rs}\rangle$ and $|Q_I\rangle$ in the Hilbert space Y. For developing perturbation theoretic expansions, however, it is useful to use the complementary concept of super-operators acting on Fock-space operators as defined in Sec. II C. Using the super-operator $\hat{H}$, the definition for the extended particle-hole Green's function of Eq. (23) can be written as

$$\mathcal{G}^{(ph)}_{rs,r's'}(\omega) = (a^\dagger_r, a_s \,|\, \frac{1}{\omega - \hat{H}} \,|\, a^\dagger_{r'}, a_{s'}). \tag{43}$$

The "superoperator resolvent" $\frac{1}{\omega-\hat{H}}$ is defined by the usual series expansion and the application of $\hat{H}$ on the extended states $|\, a^\dagger_{r'}, a_{s'})$ has been defined by Eq. (15). Perturbation expansions of the super-operator resolvent in combination with perturbation expansions of the reference states give easy access to perturbation expansions of the Green's function and the self energy. In the case of the single-particle Green's function this has been carried out explicitly by Kutzelnigg and Mukherjee [27]. They could show that the common Feynman-Dyson perturbation expansion can be obtained in this manner without using Wick's theorem. They also gave appropriate perturbation expansions for multi-determinantal zeroth order reference states. Their techniques can be applied to the extended Green's functions in an analogous manner. The justification for the expansions cannot be given in the same way as in Ref. [27] because the mathematical concepts they use for the eigenvalue spectra of super-operators cannot be directly transferred to the extended two particle Green's functions. Instead one would have to use the equivalence between the super-operator $\hat{H}$ and the extended operator $\breve{H}$ (see Sec. II C). Here we do not want to elaborate this point further because the main goal of this paper does not lie in the development of perturbation theoretic expansions.

We will now continue with discussing some properties including the pole structure and a first order approximation to the self energy for the case of the extended particle-hole Green's function. Previously we have treated the particle-particle Green's function for which the self energy is an exact optical potential of elastic two-particle scattering [10]. In the last Chapter of this paper we will then concentrate on the physical interpretation of the static self energy as a scattering potential in the particle-particle and the particle-hole case.

IV. FORMAL PROPERTIES OF THE EXTENDED PROPAGATORS

We now want to discuss several formal properties of the extended states, the Green's functions, and the self energies that were defined in the preceding section by Eqs. (23) – (25) and (38). In particular, we consider the meaning of the components of the extended states and the consequences the extensions have for degeneracies of the extended states and the analytic structure of the Green's functions. We also discuss two simple first-order approximations to the self energy. In order to be definite, we restrict ourselves to the particle-hole case [choice (a) of Sec. III] in this chapter although most of the features considered appear in an analogous fashion for the other cases as well. Several properties of the extended particle-particle Green's function and its self energy have already been discussed in Ref. [10].

We consider a fairly general system of indistinguishable fermions interacting by two-body forces and possibly with static external fields. In order to allow perturbation theory, we split the Hamiltonian H into two parts as usual: $H = H_o + H_1$. The one-particle operator $H_o = \sum_i \varepsilon_i a_i^\dagger a_i$ defines the zeroth order of perturbation theory and is characterised by the diagonalising single-particle basis $\{|\varphi_i\rangle\}$ and single-particle energies $\{\varepsilon_i\}$. The residual interaction $H_1 = v + V$ generally contains contributions of a one-particle operator v and the two-body interaction V:

$$v = \sum_{i,j} v_{ij}\, a_i^\dagger a_j, \tag{44}$$

$$V = \frac{1}{2} \sum_{i,j,k,l} V_{ijkl}\, a_i^\dagger a_j^\dagger a_l a_k. \tag{45}$$

When using the Møller-Plesset partitioning of the Hamiltonian, the zeroth order Hamiltonian H_o is defined by the Hartree-Fock approximation. For a nondegenerate ground state the matrix elements v_{ij} of the one-particle part of the interaction in Eq. (44) are then given by

$$v_{ij}^{HF} = -\sum_k n_k V_{ik[jk]}. \tag{46}$$

Here $V_{rs[r's']} = V_{rsr's'} - V_{rss'r'}$ denotes the anti-symmetrised matrix element of the two-body interaction and n_r is the occupation number of the orbital $|\varphi_r\rangle$ in the zeroth order ground state Slater determinant $|\Phi_0^N\rangle$.

A. Extended particle-hole states

The extended states $|Y_{rs}^{(ph)}\rangle$ that appear in the definition of the extended particle-hole Green's function $\mathcal{G}_{rs,r's'}^{(ph)}(\omega)$ of Eq. (23) are given by

$$|Y_{rs}^{(ph)}\rangle = |\, a_r^\dagger, a_s) = \begin{pmatrix} Q a_r^\dagger a_s\, |\Psi_0^N\rangle \\ \langle \Psi_0^N |\, a_r^\dagger a_s Q \\ \langle\varphi|\, a_r^\dagger \otimes \langle\Psi_0^N|\, a_s - \langle\varphi|\, a_s \otimes \langle\Psi_0^N|\, a_r^\dagger \\ a_r^\dagger\, |\varphi\rangle \otimes \langle\Psi_0^N|\, a_s - a_s\, |\varphi\rangle \otimes \langle\Psi_0^N|\, a_r^\dagger \end{pmatrix}, \tag{47}$$

where the choice of the Fock-space vector $|\varphi\rangle$ is arbitrary for the general algebra of the last section. For the following discussion of formal properties it is not very important either. We will discuss the freedom of choice for the secondary reference states $|\varphi\rangle$ in Sec. VI B. The operator Q is a projector that projects onto the orthogonal complement of the primary reference state $|\Psi_0^N\rangle$.

The first component $Q a_r^\dagger a_s\, |\Psi_0^N\rangle$ of the extended particle-hole state $|Y_{rs}^{(ph)}\rangle$ determines the physical situations that we want to describe namely particle

number conserving excitations of the system. The other components are only necessary to fulfil the orthonormality relation (26) that was crucial for the derivation of Dyson's equation in Sec. III B. The μ-orthonormality of the extended states is peculiar in two respects: firstly, because it extends over the full index space of two independent single-particle indices and secondly because it holds completely independent of the reference states $|\Psi_0^N\rangle$ and $|\varphi\rangle$. Thus the orthonormality persists through all orders of perturbation theory.

In order to understand how orthonormality is achieved it is useful to take a look at the zeroth order of the extended particle-hole states where the role of the single components can easily be understood:

$$|Y_{rs}^{(ph)}\rangle^{(0)} = \begin{pmatrix} Q^{(0)} a_r^\dagger a_s \,|\Phi_0^N\rangle & \leftarrow ph \\ \langle\Phi_0^N|\, a_r^\dagger a_s Q^{(0)} & \leftarrow hp \\ \langle\Phi_0^N|\, a_r^\dagger \otimes \langle\Phi_0^N|\, a_s - \langle\Phi_0^N|\, a_s \otimes \langle\Phi_0^N|\, a_r^\dagger & \leftarrow hp \\ a_r^\dagger\,|\Phi_0^N\rangle \otimes \langle\Phi_0^N|\, a_s - a_s\,|\Phi_0^N\rangle \otimes \langle\Phi_0^N|\, a_r^\dagger & \leftarrow pp, hh \end{pmatrix} . \tag{48}$$

On the right a classification of the contributing entries is given which refers to the character of the single particle indices. We classify an index r as a particle index (p) if it refers to a single particle orbital $\varphi_r(x)$ which is vacant (virtual) in the Slater determinant $|\Phi_0^N\rangle$. Conversely a hole index (h) labels an occupied orbital in $|\Phi_0^N\rangle$. Accordingly the first component of $|Y_{rs}^{(ph)}\rangle^{(0)}$ in Eq. (48) is classified ph because it contributes only if r is a particle and s is a hole index. Correspondingly the second and third component vanish if the index pair (r, s) is of another type than hp, and so on.

We can now interpret the role of the components of the extended state $|Y_{rs}^{(ph)}\rangle$ in the following way: According to the orthonormality relation (28), the extended states have always the μ-norm 1. Since the first (and physical) component contributes in zeroth order only for ph index pairs, the other components (the extensions) have to take over in the remaining cases. The second component of the extended state of Eq. (47) or Eq. (48) is a kind of symmetric partner of the first component (which is also present in the polarisation propagator of traditional many-body theory). On its own, it leads to a negative contribution to the μ-product $\langle Y_{rs}^{(ph)}|\mu|Y_{r's'}^{(ph)}\rangle$ because the metric μ introduces a minus sign for the second component:

$$\mu = \begin{pmatrix} 1 & 0 & 0 & 0 \\ 0 & -1 & 0 & 0 \\ 0 & 0 & 1 & 0 \\ 0 & 0 & 0 & 1 \end{pmatrix} . \tag{49}$$

The third component of the extended state $|Y_{rs}^{(ph)}\rangle$ then takes the part of overcompensating this contribution, securing a positive "μ-norm". This means

that two components contribute for *hp* index pairs. Consequently there exist also linear independent partners to the Y-states $|Y_{rs}^{(ph)}\rangle$ with negative μ-norm. We will see later that these states, which we call K-states, are in zeroth-order degenerate to the Y-states and contribute to the dynamic part of the self energy. The fourth component of the primary states $|Y_{rs}^{(ph)}\rangle$ contributes in the remaining cases of *pp* and *hh* index pairs and contains tensor product states like the third component does.

At first sight it may seem strange to have an indefinite metric, on the one hand, and overcompensation of the negative contributions by the third component, on the other hand. The reason for this peculiar mechanism to achieve the orthonormality relation (28) independent of the reference states is that the contribution of the first component of the extended state $|Y_{rs}^{(ph)}\rangle$ to the μ-product $\langle Y_{rs}^{(ph)}|\mu|Y_{r's'}^{(ph)}\rangle$ contains a two-particle density of the ground state

$$\langle\Psi_0^N|\, a_s^\dagger a_r Q a_{r'}^\dagger a_{s'}\,|\Psi_0^N\rangle = \langle\Psi_0^N|\, a_s^\dagger a_r a_{r'}^\dagger a_{s'}\,|\Psi_0^N\rangle - \langle\Psi_0^N|\, a_s^\dagger a_r\,|\Psi_0^N\rangle\langle\Psi_0^N|\, a_{r'}^\dagger a_{s'}\,|\Psi_0^N\rangle. \tag{50}$$

The second component gives rise to another two-particle density that is subtracted due to the minus sign in the metric, yielding the commutator $[a_s^\dagger a_r\,,\, a_{r'}^\dagger a_{s'}] = a_{s'} a_s^\dagger \delta_{rr'} + a_r a_{r'}^\dagger \delta_{ss'}$. Thus the two-particle densities are reduced to single-particle densities that are compensated for by the third and fourth component.

B. The generalised excitation energy operator $\breve{H}$

The operator $\breve{H}$ appears in the definitions of the extended Green's functions $\mathcal{G}_{rs,r's'}(\omega)$ in Eq. (29) and the matrix $\underline{\underline{H}}$ in Eq. (32) that builds the self energy $\underline{\underline{\Sigma}}(\omega)$. For a simple single-component propagator, its place is usually taken by the difference of the common (Fock-space) Hamiltonian H of the system with the ground state energy E_0^N. This operator measures the excitation energy with respect to the N-particle ground state $|\Psi_0^N\rangle$. The operator $\breve{H}$, which will be called the extended operator associated to H or generalised excitation energy operator, presents a suitable generalisation for the extended Green's functions. Since the extended Green's functions derive from the four-component states $|Y_{rs}\rangle$, the operator $\breve{H}$ is a 4×4 matrix. For the particle-hole Green's function, the proper choice is, according to Eq. (17), given by

$$\breve{H} = \begin{pmatrix} H - E_0^N & 0 & 0 & 0 \\ 0 & E_0^N - H & 0 & 0 \\ 0 & 0 & A & 0 \\ 0 & 0 & 0 & B \end{pmatrix}, \tag{51}$$

with

$$A = E_\varphi - H \otimes 1 + E_0^N - 1 \otimes H, \tag{52}$$

$$B = H \otimes 1 - E_\varphi + E_0^N - 1 \otimes H. \tag{53}$$

Here, E_φ is the eigenvalue of the Hamiltonian H that belongs to the reference state $|\varphi\rangle$. We will characterise the operator $\breve{H}$ explicitly by its eigenstates and eigenvalues at the end of this subsection.

The matrix element of $\breve{H}$ that acts on the first and physical component of the extended states $|Y_{rs}\rangle$ indeed measures the excitation energy. The particular choice of the other components can best be motivated by the derivation via the super-operator $\hat{H}$ of Sec. II C. The super-operator associated to the Hamiltonian operator H is denoted by $\hat{H}$ and acts on the extended states by giving the commutator of the Hamiltonian with the canonic operators $a_r^\dagger$ and a_s:

$$\hat{H}|\, a_r^\dagger, a_s) = |\, [H\,,\, a_r^\dagger]_-, a_s) + |\, a_r^\dagger, [H\,,\, a_s]_-). \tag{54}$$

Under the condition that the reference state $|\varphi\rangle$ is an eigenstate of the Hamiltonian H, the super-operator $\hat{H}$ can be replaced by the associated extended operator denoted by $\breve{H}$ and given by Eq. (51):

$$\breve{H}|\, a_r^\dagger, a_s) = \hat{H}|\, a_r^\dagger, a_s). \tag{55}$$

While the concept of the (Hilbert space) operator $\breve{H}$ has the advantage of giving the possibility to interpret $\underline{\underline{H}}$ of Eq. (32) as a matrix representation of a common operator, the equivalent formulation with the super-operator $\hat{H}$ is an appealing alternative concept. Not only does it present a simple and unified way to define a generalisation of excitation energy operator for all families of extended Green's functions covered in this paper, but it also simplifies perturbation theoretic expansions. Super-operator expansions have also been a popular tool for deriving approximation schemes in traditional propagator theory for many decades [28,29]. The practical advantage emerges in the present context when the Hamiltonian is split into zeroth order and interaction parts

$$\hat{H}|\, a_r^\dagger, a_s) = \hat{H}_0|\, a_r^\dagger, a_s) + \hat{H}_1|\, a_r^\dagger, a_s), \tag{56}$$

because the first term is very simple to evaluate regardless of approximations or particular choices for the reference states $|\Psi_0^N\rangle$ and $|\varphi\rangle$ in Eq. (47):

$$\hat{H}_0|\, a_r^\dagger, a_s) = (\varepsilon_r - \varepsilon_s)\,|\, a_r^\dagger, a_s). \tag{57}$$

The difference of single particle energies $\varepsilon_r - \varepsilon_s$ appears here as a kind of "eigenvalue". As a first step towards a physical interpretation of the states $|Y_{rs}^{(ph)}\rangle = |\,a_r^\dagger, a_s)$ one can thus say that the index r has something to do with a test particle and s with a test hole that are probing the system. Without interaction the test particles move freely and are correctly characterised by the difference of single-particle energies $\varepsilon_r - \varepsilon_s$.

Equation (57) holds for arbitrary reference states but becomes a proper eigenvalue equation when taking the Slater determinant $|\Phi_0^N\rangle$ as the reference state in Eq. (47), which means that the extended state $|Y_{rs}^{(ph)}\rangle = |\,a_r^\dagger, a_s)$ is replaced by its zeroth order $|Y_{rs}^{(ph)}\rangle^{(0)}$ of Eq. (48). In this case the super-operator $\hat{H}_0$ can be replaced by its corresponding extended operator $\breve{H}^{(0)}$ (c. f. Sec. II C) which is the zeroth order of the operator $\breve{H}$:

$$\breve{H}^{(0)}|Y_{rs}^{(ph)}\rangle^{(0)} = (\varepsilon_r - \varepsilon_s)|Y_{rs}^{(ph)}\rangle^{(0)}. \tag{58}$$

In fact, the zeroth order extended states are eigenstates of the zeroth order excitation energy operator. Note that in contrast to the super-operator $\hat{H}$, the perturbation expansion of the extended operator $\breve{H}$ contributes in all orders because the ground state energy E_0^N is a general function of the interaction strength.

Finally we want to give the explicit diagonal representation of the extended operator $\breve{H}$ in the form

$$\breve{H} = \sum_q \omega_q \,|q\rangle\langle q|\,, \tag{59}$$

thereby characterising its eigenvectors $|q\rangle$ and eigenvalues ω_q. Assuming no degeneracies between the physically distinct component spaces, the eigenvectors of $\breve{H}$ are single-component states in the 4-component Y-space, as can be seen from Eqs. (51) to (53). Thus the projectors $|q\rangle\langle q|$ onto the eigenstates are proportional to the 4×4 projection matrices $\underline{\underline{P}}_i$ where all elements are zero except for the element in the ith row and the ith column, which is one. For example

$$\underline{\underline{P}}_3 = \begin{pmatrix} 0 & 0 & 0 & 0 \\ 0 & 0 & 0 & 0 \\ 0 & 0 & 1 & 0 \\ 0 & 0 & 0 & 0 \end{pmatrix}. \tag{60}$$

Choosing for the secondary reference state $|\varphi\rangle = |\Psi_0^N\rangle$, we can now write Eq. (59) explicitly as

$$\breve{H} = \sum_\nu (E_\nu^N - E_0^N)\Big(\;\overleftarrow{|\Psi_\nu^N\rangle}\;\Big)\Big(\;\overrightarrow{\langle\Psi_\nu^N|}\;\Big)\underline{\underline{P}}_1$$

$$
\begin{aligned}
&+\sum_{\nu}(E_0^N - E_\nu^N)\Big(\overleftarrow{\langle\Psi_\nu^N|}\Big)\Big(\overrightarrow{|\Psi_\nu^N\rangle}\Big)\underline{\underline{P}}_2 \\
&+\sum_{\kappa,\mu}(2E_0^N - E_\kappa^{N-1} - E_\mu^{N+1})\Big(\overleftarrow{\langle\Psi_\kappa^{N-1}| \otimes \langle\Psi_\mu^{N+1}|}\Big)\Big(\overrightarrow{|\Psi_\kappa^{N-1}\rangle \otimes |\Psi_\mu^{N+1}\rangle}\Big)\underline{\underline{P}}_3 \\
&+\Bigg\{\sum_{\mu,\lambda}(E_\mu^{N+1} - E_\lambda^{N+1})\Big(\overleftarrow{|\Psi_\mu^{N+1}\rangle \otimes \langle\Psi_\lambda^{N+1}|}\Big)\Big(\overrightarrow{\langle\Psi_\mu^{N+1}| \otimes |\Psi_\lambda^{N+1}\rangle}\Big) \\
&+\sum_{\kappa,\sigma}(E_\kappa^{N-1} - E_\sigma^{N-1})\Big(\overleftarrow{|\Psi_\kappa^{N-1}\rangle \otimes \langle\Psi_\sigma^{N-1}|}\Big)\Big(\overrightarrow{\langle\Psi_\kappa^{N-1}| \otimes |\Psi_\sigma^{N-1}\rangle}\Big)\Bigg\}\underline{\underline{P}}_4 \quad (61)
\end{aligned}
$$

Here, we generalised the notation $|q\rangle\langle q|$ for a projection operator onto the "ket" state $|q\rangle$ to $\Big(\overleftarrow{|q\rangle}\Big)\Big(\overrightarrow{\langle q|}\Big)$ because not all of the eigenstates of $\breve{H}$ are ket vectors but some are bra vectors $\langle p|$ or tensor product states $\langle p| \otimes \langle q|$. Of course, it is also possible to project onto tensor product states like $\langle p| \otimes \langle q|$. We use arrows in our notation for this projection operator

$$\mathcal{P} = \Big(\overleftarrow{\langle p| \otimes \langle q|}\Big)\Big(\overrightarrow{|p\rangle \otimes |q\rangle}\Big),$$

in order to indicate the relevant directions for forming inner products. In the present example, operating $\mathcal{P}$ on a product state $\langle a| \otimes \langle b|$ yields

$$\mathcal{P}(\langle a| \otimes \langle b|) = \langle a|p\rangle\langle b|q\rangle(\langle p| \otimes \langle q|),$$

which is again a product state proportional to $\langle p| \otimes \langle q|$. The inner products $\langle a|p\rangle\langle b|q\rangle$ here form the proportionality constant.

The sums in Eq. (61) always run over the complete sets of eigenvectors of the corresponding Hilbert spaces. The sums over ν, in particular, run over all exact states with N particles, μ and λ lable the $N+1$, and κ and σ the $N-1$ particle states. As already mentioned in the discussion of the Hilbert space Y of Eq. (6), symmetry considerations may reduce the number of states that actually couple to the primary states. Along with a reduced Hilbert space Y, then also less terms are needed in the diagonal representation (61) of the extended operator $\breve{H}$.

The eigenvalue spectrum of the extended operator $\breve{H}$ contained in Eq. (61) determines the pole structure of the extended Green's function and will be discussed in the following paragraph.

C. The analytic structure of the extended particle-hole Green's function

The analytic structure of the particle-hole Green's function $\underline{\underline{\mathcal{G}}}^{(ph)}(\omega)$ as a function of the complex variable ω is governed by single poles and branch cuts

at the eigenvalue spectrum of the generalised excitation energy operator $\breve{H}$. This can be seen easily by inserting the (Y-space) complete set of eigenvectors $|q\rangle$ of this operator with eigenvalues ω_q into the definition of $\underline{\underline{G}}^{(ph)}(\omega)$ [Eq. (29) or (23)]:

$$G^{(ph)}_{rs,r's'}(\omega) = \sum_q \frac{\langle Y^{(ph)}_{rs}|q\rangle m_q \langle q|Y^{(ph)}_{r's'}\rangle}{\omega - \omega_q}. \tag{62}$$

Here, $m_q = \pm 1$ are the eigenvalues of the metric operator μ.

The eigenvectors $|q\rangle$ and eigenvalues ω_q corresponding to the four components of the Hilbert space Y have already been listed explicitly in Eq. (61) for $|\varphi\rangle = |\Psi^N_0\rangle$ and assuming finite basis Hilbert spaces. In general, the eigenvalue spectrum ω_q leads by Eq. (62) to single poles and branch cuts of the extended Green's function. The overlaps $\langle q|Y^{(ph)}_{r's'}\rangle$ may vanish, however, when due to symmetry properties the components of $|Y^{(ph)}_{rs}\rangle$ decouple from classes of excitations of a given particle number. In this case the corresponding eigenvalues do not appear in the pole structure of the Green's function.

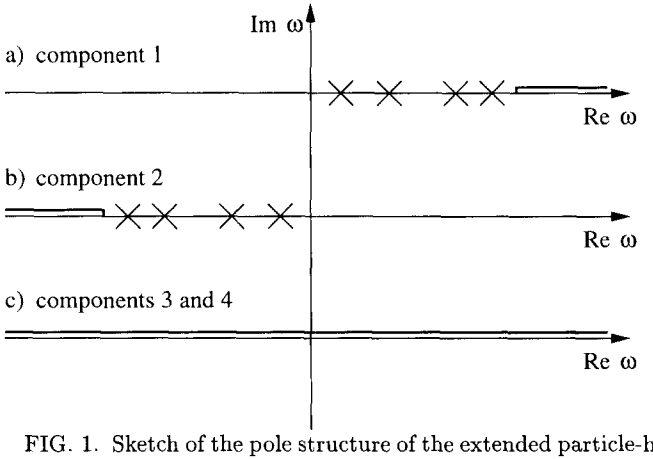

FIG. 1. Sketch of the pole structure of the extended particle-hole Green's function $\underline{\underline{G}}(\omega)$ in the complex omega plane. Crosses correspond to single poles and thick lines to branch cuts. Part a) shows the poles corresponding to the first component of the extended states $|Y^{(ph)}_{rs}\rangle$, which are given by the physical excitation energies of the system. Since excitations from the ground state are considered, all energies are non-negative. The start of the branch cut marks the threshold for ionisation of a particle. Part b) shows the poles and cuts that are introduced by the second component. They are the same as for the first component, mirrored at the imaginary axis. The contributions of the third and fourth component are shown in part c). In general they yield a cut along the whole real axis.

Figure 1 shows a schematic plot of the eigenvalue spectrum of $\breve{H}$ and therefore the pole structure of $\mathcal{G}^{(ph)}(\omega)$ for the first, second, and the additional components. The eigenvalues ω_q that derive from the physical, first component of $\breve{H}$ are the exact (discrete and continuous) excitation energies $E_q^N - E_0^N$ of the N particle system under study. Since E_0^N is the ground state energy, these energies are positive or possibly zero in the case of a degenerate ground state. There are usually some discrete eigenvalues corresponding to bound excited states but above the threshold energy for ionisation of one particle, the excitation spectrum is continuous. The second component of $\breve{H}$ mirrors the excitation spectrum of the first component to negative values. The parts of the spectrum that are contributed by the additional third and fourth component of the extended operator $\breve{H}$ are more difficult to interpret. Through these components, the eigenvalue spectrum of the $N+1$ and the $N-1$ particle system are introduced as can be seen from Eq. (61). In particular the 4th component of $\breve{H}$ introduces the energy differences $(E_\mu^{N+1} - E_\lambda^{N+1})$ and $(E_\kappa^{N-1} - E_\sigma^{N-1})$. Since the spectrum of the Hamiltonian H in $N \pm 1$-particle systems will generally be unbounded from above showing a continuous spectrum at the top end, we may conclude that the spectrum of the last component of the generalised excitation energy operator $\breve{H}$ comprises the full real axis. This can already be seen in zeroth order where the primary states $|Y_{rs}^{(ph)}\rangle^{(0)}$ have the eigenvalues $\varepsilon_r - \varepsilon_s$. Since r and s can be chosen to denote virtual or scattering orbitals with arbitrary, positive energy, the difference $\varepsilon_r - \varepsilon_s$ can adopt any real value.

D. The extended Green's function for real arguments

In order to define the extended Green's function $\underline{\underline{\mathcal{G}}}(\omega)$ for real arguments, the branch cuts introduced by the eigenvalue spectrum of $\breve{H}$ have to be moved away from the real axis. Commonly this is achieved by introducing a positive infinitesimal η with the option of performing the limit $\eta \to 0^+$ after all formal manipulations. In this way a **retarded** or **advanced extended Green's function** may be defined by $\underline{\underline{\mathcal{G}}}(E \pm i\eta)$ where E now serves as a real energy variable. The concept of retarded or advanced Green's functions is traditionally associated with the properties of the Fourier transforms into time space representation. The Fourier transform from the variable E to t can be performed by using the residue theorem and yields a time space function which contributes only for $t > 0$ or $t < 0$ according to the sign of $i\eta$ [11].

The formal definition (29) of the extended Green's function implies a sum of propagators according to the different components of the extended state's vector. The terms introduced by the product states can be transformed into convolutions of single-particle propagators if we resort to real energies. For

the retarded version of the extended particle-hole Green's function $\mathcal{G}^{(ph)}_{rs,r's'}(\omega)$ defined by Eq. (23) we get:

$$\begin{aligned}
&\mathcal{G}^{(ph)}_{rs,r's'}(E+i\eta) = \Pi^{ph}_{rs,r's'}(E+i\eta) - \Pi^{hp}_{rs,r's'}(E+i\eta) \\
&+\frac{1}{i}\Big\{\langle\varphi|\, a^\dagger_{r'}\frac{1}{E-E_\varphi+H+i\eta}a_r\,|\varphi\rangle * \langle\Psi^N_0|\, a_{s'}\frac{1}{E-E_o+H+i\eta}a^\dagger_s\,|\Psi^N_0\rangle \\
&+\langle\Psi^N_0|\, a^\dagger_{r'}\frac{1}{E-E_o+H+i\eta}a_r\,|\Psi^N_0\rangle * \langle\varphi|\, a_{s'}\frac{1}{E-E_\varphi+H+i\eta}a^\dagger_s\,|\varphi\rangle \\
&+\langle\varphi|\, a_r\frac{1}{E-H+E_\varphi+i\eta}a^\dagger_{r'}\,|\varphi\rangle * \langle\Psi^N_0|\, a_{s'}\frac{1}{E-E_o+H+i\eta}a^\dagger_s\,|\Psi^N_0\rangle \\
&+\langle\Psi^N_0|\, a^\dagger_{r'}\frac{1}{E-E_o+H+i\eta}a_r\,|\Psi^N_0\rangle * \langle\varphi|\, a^\dagger_s\frac{1}{E-H+E_\varphi+i\eta}a_{s'}\,|\varphi\rangle\Big\}. \qquad (63)
\end{aligned}$$

The asterisk $*$ denotes convolution with respect to E defined by

$$f(E) * g(E) = \frac{1}{2\pi}\int_{-\infty}^{\infty} dE' f(E')g(E-E'). \qquad (64)$$

The particle-hole part $\Pi^{ph}_{rs,r's'}(\omega)$ and the hole-particle part $\Pi^{hp}_{rs,r's'}(\omega)$ of the well-known polarisation propagator [11] are defined by

$$\Pi^{ph}_{rs,r's'}(\omega) = \langle\Psi^N_0|\, a^\dagger_s a_r\frac{Q}{\omega-H+E^N_0}a^\dagger_{r'}a_{s'}\,|\Psi^N_0\rangle, \qquad (65)$$

$$\Pi^{hp}_{rs,r's'}(\omega) = \langle\Psi^N_0|\, a^\dagger_{r'}a_{s'}\frac{Q}{\omega-E^N_0+H}a^\dagger_s a_r\,|\Psi^N_0\rangle. \qquad (66)$$

Another possibility for defining the Green's functions for real energies is to distribute different $i\eta$'s or different signs for $i\eta$ among the components of the propagator. This is, e. g., the case for the so-called time-ordered Green's functions of traditional many-body theory [11]. In our formalism, this can be achieved by adding $i\eta$s with the chosen sign to each component of the generalised excitation energy operator $\breve{H}$ of Eq. (51). This has the effect that the eigenvalue spectrum of the different components of this operator is shifted into the complex plane and consequently the argument ω of the extended Green's function may be chosen real. In the extended particle-particle Green's function of reference [10], e. g., we have chosen the signs of $i\eta$ such that the physical (in this case *pp*) component carries a positive sign while all others carry negative signs. For the Fourier transformed time space function this has the consequence that for positive times only the physical component contributes which allows the correct description of scattering processes.

So far we have discussed the pole structure of the extended particle-hole Green's function, which is given by the eigenvalue spectrum of the generalised

excitation energy operator $\breve{H}$. The self energy formally has a similar analytic structure to the extended Green's function but poles and cuts appear at different energies. The connection between the pole structure of the Green's function and its self energy is, of course, established by Dyson's equation (39). Before discussing the energy dependence of the self energy, however, we first want to consider the lowest order approximation to the self energy in which it represents a static, energy independent quantity.

V. PROPERTIES OF THE SELF ENERGY

According to Eq. (42) the extended self energy can be written as the sum of a uniquely determined static, energy independent part $\underline{\underline{\mathcal{S}}}(\infty)$ and the so-called dynamic part $\underline{\underline{\mathcal{M}}}(\omega)$:

$$\underline{\underline{\mathcal{S}}}(\omega) = \underline{\underline{\mathcal{S}}}(\infty) + \underline{\underline{\mathcal{M}}}(\omega). \tag{67}$$

While the dynamic part is of second order, the static self energy $\underline{\underline{\mathcal{S}}}(\infty)$ contributes in first order. For brevity we will discuss only the particle-hole self energy in this chapter. In contrast to the single-particle Green's function where the first order of the self energy upon Hartree-Fock vanishes, the first order of the particle-hole self energy yields an interesting, nontrivial model for the extended particle-hole Green's function.

After looking at the static self energy part and its special role for one-particle potentials, we will briefly touch upon the meaning and the structure of the dynamic particle-hole self energy part. In the following we will then discuss the first order of the static part as the simplest non-trivial approximation to the particle-hole self energy in more detail. The rest of this chapter is devoted to another simple approximation of the self energy where additionally to the first order of the static self energy, also part of the dynamic self energy is taken into account, which leads to the RPA approximation.

A. The static part

According to Eqs. (41) and (34) the static self energy $\underline{\underline{\mathcal{S}}}(\infty)$ is given by the primary block $\underline{\underline{H}}_{aa}$ of the matrix $\underline{\underline{H}}$ of Eq. (33) minus its zeroth order part. An explicit expression can be found with the help of the super-operator formalism and using the definition of the extended states (47):

$$\begin{aligned}\left[\underline{\underline{H}}_{aa}\right]_{rs,r's'} &= (a_r^\dagger, a_s \,|\hat{H}|\, a_{r'}^\dagger, a_{s'}') \\ &= \langle \Psi_0^N | \left[a_s^\dagger a_r \,,\, \left[H \,,\, a_{r'}^\dagger a_{s'}\right]\right] | \Psi_0^N \rangle\end{aligned}$$

$$
\begin{aligned}
&+\langle\varphi|\left\{\left[H\,,\,a_{r'}^{\dagger}\right]\,,\,a_r\right\}|\varphi\rangle\langle\Psi_0^N|\,a_{s'}a_s^{\dagger}\,|\Psi_0^N\rangle \\
&+\delta_{rr'}\langle\Psi_0^N|\,[H\,,\,a_{s'}]\,a_s^{\dagger}\,|\Psi_0^N\rangle \\
&+\langle\Psi_0^N|\left[H\,,\,a_{r'}^{\dagger}\right]a_r\,|\Psi_0^N\rangle\delta_{ss'} \\
&+\langle\Psi_0^N|\,a_r a_{r'}^{\dagger}\,|\Psi_0^N\rangle\langle\varphi|\left\{[H\,,\,a_{s'}]\,,\,a_s^{\dagger}\right\}|\varphi\rangle. \qquad (68)
\end{aligned}
$$

For the one-particle part $H_0 + v$ of the Hamiltonian $H = H_0 + v + V$ this expression yields a very simple result:

$$
(a_r^{\dagger}, a_s\,|\hat{H}_0 + \hat{v}|\,a_{r'}^{\dagger}, a_s') = \delta_{rr'}\delta_{ss'}(\varepsilon_r - \varepsilon_s) + v_{rr'}\delta_{ss'} - v_{s's}\delta_{rr'}. \qquad (69)
$$

In the special case of systems without real two-body potentials V, where only interactions with external potentials or mean fields are considered, this is the exact solution for the primary block $\underline{\underline{H}}_{aa}$, which determines the self energy. Since the dynamic self energy vanishes in this case, as will be shown shortly, the self energy is energy independent and given by

$$
\mathcal{S}_{rsr's'} = v_{rr'}\delta_{ss'} - v_{s's}\delta_{rr'}. \qquad (70)
$$

Note that this exact solution for the self energy is of first order and completely independent of the many-body system's ground state $|\Psi_0^N\rangle$ or the secondary reference state $|\varphi\rangle$. The matrix $\underline{\underline{H}}_{aa}$ of Eq. (69) can obviously be diagonalised by an appropriate choice of single-particle orbitals and then takes the form of the zeroth order part $\delta_{rr'}\delta_{ss'}(\varepsilon_r - \varepsilon_s)$. Thus the self energy of Eq. (70) describes particle-hole excitations in a system of independent particles. The unphysical components present in the extended states $|Y_{rs}^{(ph)}\rangle$ here serve to circumvent Pauli's exclusion principle because Eqs. (69) and (70) allow excitations from any orbital to any other orbital, regardless of their occupation in the many-body state $|\Psi_0^N\rangle$. The same behaviour with respect to one-particle Hamiltonians of the self energy becoming an energy-independent, first-order quantity and the lifting of the Pauli principle is also shown by the other extended two-particle Green's functions and the traditional single-particle Green's function.[1] The reason for this behaviour can be traced back to two features of the present theory: the construction from orthonormal states and the fact that the excitation energy operator $\breve{H}$ is equivalent to the super-operator $\hat{H}$, which leads to commutators. This can be seen when considering that the associated super-operator $\hat{A}$ to a general single-particle operator $A = \sum_{ij} a_i^{\dagger}a_j A_{ij}$ maps the primary states $|Y_{rs}^{(ph)}\rangle$ onto linear combinations of primary states:

---

[1]The case of the extended particle-particle Green's function in comparison with the single-particle Green's function has already been discussed in Ref. [10]

$$\hat{A}|Y_{rs}^{(ph)}\rangle = |\,[A\,,\,a_r^\dagger]_-,a_s) + |\,a_r^\dagger,[A\,,\,a_s]_-) \\ = \sum_{kl}(A_{rk}\delta_{sl} - A_{ls}\delta_{rk})|Y_{kl}^{(ph)}\rangle. \tag{71}$$

Thus, the overlaps with basis states of the orthogonal complement of the primary set $|Q_I\rangle \in \{|Y_{rs}^{(ph)}\rangle\}^\perp$ vanish:

$$\langle Q_I|\,\mu\hat{A}|Y_{rs}^{(ph)}\rangle = 0, \tag{72}$$

and so do the off-diagonal blocks $\underline{\underline{H}}_{ab}$ and $\underline{\underline{H}}_{ba}$. In the case of a single-particle Hamiltonian, thus, the self energy indeed is purely static and yields the exact energy eigenvalues of particle-hole type excitations while higher excitation classes like two-particle-two-hole excitations decouple completely.

In the more general case of a correlated system, the dynamic self energy does not vanish and thus the eigenvalues of the primary block $\underline{\underline{H}}_{aa}$ are generally not the exact excitation energies.

B. The dynamic particle-hole self energy

The dynamic self energy $\underline{\underline{\mathcal{M}}}(\omega)$ as a function of the complex energy variable ω has an analytic structure which is very similar to that of the extended Green's function $\underline{\underline{\mathcal{G}}}(\omega)$ discussed earlier (Sec. IV C). We have defined the self energy by matrix partitioning of the matrix $\underline{\underline{H}}$ of Eq. (33) which yields the expression (42) for the dynamic part. From this formula it can be seen that the dynamic self energy has single poles or branch cuts where the denominator of (42) becomes singular:

$$\det(\omega\underline{\underline{\mu}}_{bb} - \underline{\underline{H}}_{bb}) = 0. \tag{73}$$

By introducing a similarity transformation which simultaneously diagonalises the matrices $\underline{\underline{\mu}}_{bb}$ and $\underline{\underline{H}}_{bb}$, Eq. (42) can be cast into the form of Eq. (62). The difference is that the poles and cuts of the Green's function $\underline{\underline{\mathcal{G}}}(\omega)$ appear at the generalised eigenvalues of the whole matrix $\underline{\underline{H}}$ while the pole structure of the self energy is given by the generalised eigenvalues of the block $\underline{\underline{H}}_{bb}$ only. The relation to the eigenvalue spectra of the block $\underline{\underline{H}}_{bb}$ and the full matrix $\underline{\underline{H}}$ depends much on the coupling blocks $\underline{\underline{H}}_{ab}$ and $\underline{\underline{H}}_{ba} = \underline{\underline{H}}_{ab}^\dagger$.

In the limiting case of vanishing coupling $\underline{\underline{H}}_{ab} = 0$, the eigenvalue spectrum of $\underline{\underline{H}}_{bb}$ is a subset of the spectrum of $\underline{\underline{H}}$. At the same time, however, the dynamic self energy part vanishes and the self energy becomes ω-independent. This happens, e. g. if the Hamiltonian is a single-particle operator and does not contain true two-particle forces but only external forces or mean fields as discussed in the last paragraph.

In the more general case of a fully correlated system all higher excitations couple. If the coupling is weak enough, however, the diagonal zeroth order of the matrix $\underline{\underline{H}}$ may give a good guess for the poles of the self energy. Of course, the coupling affects the poles by eventually lifting degeneracies and shifting the poles like discussed in the case of the single-particle Green's function in reference [25]. Similar to the full extended Green's function $\underline{\underline{\mathcal{G}}}(\omega)$, physical as well as unphysical poles appear. Like before, the physical poles caused by excited states of the system appear at positive energies. They lie above a threshold energy where double excitation ($2p$-$2h$) becomes possible. Another threshold for double excitation into the continuum indicates the lower border of the physical branch cut of the dynamic self energy. The dynamic self energy also contains diverse poles and cuts originating in the unphysical component of the extended state vectors (47). In particular the so-called K-states that will be discussed in the next paragraph give rise to poles of the dynamic self energy which are in zeroth order degenerate to eigenvalues of the primary block $\underline{\underline{H}}_{aa}$. This, however, concerns only the negative energy part of the spectrum. The existence of the degenerate K-states can be traced back to the degeneracy of the second and third component – both unphysical – of the extended states $|Y_{rs}^{(ph)}\rangle$ in Eq. (48). I. e., these two degenerate unphysical components are mixed in the zeroth order Y-states. Taking the K-states into account additionally to the primary Y-states, leads to a minimal extension of the primary block $\underline{\underline{H}}_{aa}$ which allows the degenerate components to decouple. Interestingly the first order Hartree-Fock based approximation to this extended primary block $\underline{\underline{H}}_{aa}^{\mathrm{ext}\,(1)}$ yields the well known RPA. We will show this by presenting a universal unitary transformation which transforms the extended eigenvalue problem to the RPA after discussing the first-order approximation to the static self energy.

At this point we would briefly like to mention that the self energy $\underline{\underline{\mathcal{S}}}(\omega)$ of Eq. (38) is fully specified by the Dyson equation (39) or (40) only for energies ω where the Green's function $\underline{\underline{\mathcal{G}}}(\omega)$ can be inverted. Capuzzi and Mahaux have shown for the case of the single-particle Green's function that the self energy can be modified at isolated zeros of the Green's function and still satisfy the Dyson equation [9]. These modifications may be used to tailor dispersion relations for the self energy parts, however, they do not have physical implications. The arguments of Ref. [9] apply also to the extended two-particle Green's functions.

C. The zeroth-order degenerate states $|K_{an}^{(ph)}\rangle$

We are now going to discuss one example of states that lie outside the model space of the primary Y-states. These states, called K-states, play a special

role because they are in zeroth order degenerate with states of the primary space and also couple to the primary space in first order. The remaining states outside the primary space are generally not degenerate to the Y-states although accidental degeneracies may still occur.

We already remarked earlier that for a particular index pair (r,s) only certain components of the zeroth order states $|Y_{rs}^{(ph)}\rangle^{(0)}$ of Eq. (48) contribute according to the classification of the indices as p or h. For hp indices two components of the extended states contribute at the same time and naturally have the same (zeroth order) energies because the extended states are zeroth order eigenstates of the excitation energy operator. Therefore a linear independent, degenerate combination of the two components exits. A suitable choice for these states is given by

$$|K_{\alpha n}^{(ph)}\rangle = \begin{pmatrix} 0 \\ \sqrt{2}\langle\Phi_0^N|\, a_\alpha^\dagger a_n \\ \frac{1}{\sqrt{2}}\left(\langle\Phi_0^N|\, a_\alpha^\dagger \otimes \langle\Phi_0^N|\, a_n - \langle\Phi_0^N|\, a_n \otimes \langle\Phi_0^N|\, a_\alpha^\dagger\right) \\ 0 \end{pmatrix}, \tag{74}$$

where the indices α and n stand for occupied (h) and virtual (p) orbitals, respectively. It is readily verified that the states $|K_{\alpha n}^{(ph)}\rangle$ fulfil the following orthonormality relations (with α, α' occupied, n, n' virtual, and r and s arbitrary):

$$\langle K_{\alpha n}^{(ph)}|\, \mu |Y_{rs}^{(ph)}\rangle^{(0)} = \langle Y_{rs}^{(ph)}|^{(0)} \mu\, |K_{\alpha n}^{(ph)}\rangle = 0, \tag{75}$$

$$\langle K_{\alpha n}^{(ph)}|\, \mu\, |K_{\alpha' n'}^{(ph)}\rangle = -\delta_{\alpha\alpha'}\delta_{nn'}. \tag{76}$$

The states $|K_{\alpha n}^{(ph)}\rangle$ are obviously elements of the composite Hilbert space Y but they lie outside of the (zeroth order) primary space spanned by the states $\{|Y_{rs}^{(ph)}\rangle^{(0)}\}$. Thus the "degenerate states" $\{|K_{\alpha n}^{(ph)}\rangle\}$ (which we also call K-states) contribute to the dynamic, ω-dependent part $\underline{\underline{\mathcal{M}}}(\omega)$ of the self energy $\underline{\underline{\mathcal{S}}}(\omega)$ of Eq. (42) whereas the primary states $\{|Y_{rs}^{(ph)}\rangle\}$ define the static self energy part $\underline{\underline{\mathcal{S}}}(\infty)$.

The zeroth order degeneracy of K and Y-states is lifted in the spectral representation of the fully interacting Green's function. The exact eigenstates decouple to yield N-particle states in the second component and tensor products of $N-1$ and $N+1$-particle states in the third component. We will come back to discuss the meaning of the degenerate states $|K_{\alpha n}^{(ph)}\rangle$ in connection with the lowest order of the static self energy $\underline{\underline{\mathcal{S}}}(\infty)$ in Sec. V.

Apart from the K-states there are other zeroth-order states outside the primary space that couple to Y-states. These are made up from higher excitations of the components of the zeroth-order Y-states of Eq. (48). E. g., there are states with a two-particle–two-hole configuration $a_n^\dagger a_{n'}^\dagger a_{\alpha'} a_\alpha |\Phi_0^N\rangle$ in

the first or in the second component, states with a tensor product of a two-hole–one-particle with a particle configuration in the third component, etc. All these states contribute in second order to the dynamic self energy and higher excitations contribute in higher orders to the self energy, like it is the case for the single-particle Green's function.

For completeness we would like to remark that the K-states can also be written as extended states of the form $|\, A, B)$ according to definition (1). For convenience we introduce the particle number operator $N^{\mathrm{Op}} = \sum_i a_i^\dagger a_i$ and define $m = (N^{\mathrm{Op}} - N)^2 + 1$, where N is the number of particles in the state $|\Psi_0^N\rangle$. Then the K-states can be written as $|K_{\alpha n}^{(ph)}\rangle = \sqrt{2}\,|\, a_\alpha^\dagger, a_n m^{-1})^{(0)}$.

D. First order self energy

The first order of the particle-hole self energy is readily obtained from the expression (68) by replacing the reference states $|\Psi_0^N\rangle$ and $|\varphi\rangle$ by their zeroth orders $|\Phi_0^N\rangle$ and $|\varphi^{(0)}\rangle$, respectively, and by considering the interaction part $\hat{H}_1$ of the associated super-operator $\hat{H}$. We obtain

$$\left[\underline{\underline{H}}_{aa}^{(1)}\right]_{rs,r's'} = (a_r^\dagger, a_s\,|\hat{H}_1|\,a_{r'}^\dagger, a_s')\Big|_{\substack{|\Psi_0^N\rangle \to |\Phi_0^N\rangle \\ |\varphi\rangle \to |\varphi^{(0)}\rangle}}. \tag{77}$$

In a recent publication we have investigated this first order approximation to the particle-hole self energy for the choice $|\varphi\rangle = |\Psi_0^N\rangle$ for the reference state $|\varphi\rangle$ and starting from a Hartree-Fock zeroth order [21]. This particular approximation to the particle-hole self energy is referred to as **First Order Static Excitation Potential (FOSEP)**. In terms of the matrix elements of the Hamiltonian the FOSEP approximation of the primary block $\underline{\underline{H}}_{aa}$ reads

$$\begin{aligned}\left[\underline{\underline{H}}_{aa}^{\mathrm{FOSEP}}\right]_{rs,r's'} &= (\varepsilon_r - \varepsilon_s)\,\delta_{rr'}\delta_{ss'} \\ &\quad + V_{rs'[sr']}\,(\overline{n}_r n_s - n_r \overline{n}_s)(\overline{n}_{r'} n_{s'} - n_{r'} \overline{n}_{s'}).\end{aligned} \tag{78}$$

Here, n_r denotes the occupation number of the orbital with index r in the ground state Slater determinant $|\Phi_0^N\rangle$, while $\overline{n}_r = 1 - n_r$ is the anti-occupation number. The eigenvalues of this hermitian matrix yield approximations for the excitation energies of the system under study while the eigenvectors can be used to approximate transition moments. Since the FOSEP approximation has been studied in detail in reference [21], we will only summarise the most important properties in this paragraph.

The matrix that has to be diagonalised $\underline{\underline{H}}_{aa}^{\mathrm{FOSEP}}$ has the dimension of the primary space like discussed in Chapter III. It is labelled by pairs of indices which comprise the full set of single-particle orbitals each. Like it has been

done before, the index pairs can be classified as *hh*, *ph*, *hp*, and *pp* with respect to the occupation of the orbitals in the ground state Slater determinant $|\Phi_0^N\rangle$. This classification superposes a four by four block structure to the matrix $\underline{\underline{H}}^{\mathrm{FOSEP}}_{aa}$. It can be seen easily from Eq. (78) that the *hh*-*hh* and the *pp*-*pp* blocks are diagonal and decouple form the rest:

$$\left[\underline{\underline{H}}^{\mathrm{FOSEP}}_{aa}\right] = \begin{pmatrix} * & 0 & 0 & 0 \\ 0 & * & * & 0 \\ 0 & * & * & 0 \\ 0 & 0 & 0 & * \end{pmatrix} \begin{matrix} \leftarrow hh \\ \leftarrow ph \\ \leftarrow hp \\ \leftarrow pp \end{matrix} . \tag{79}$$

Since the zeroth order extended states $|a_r^\dagger, a_s\rangle^{(0)}$ of Eq. (48) that are used as basis give physical contributions only in the *ph* part of the index space, the decoupled *hh* and *pp* blocks do not have to be considered and a matrix eigenvalue problem comprising the *ph* and *hp* blocks remains:

$$\underline{\underline{M}}^{\mathrm{FOSEP}}\,\underline{x} = \omega\,\underline{x}, \tag{80}$$

$$\text{with} \qquad \underline{\underline{M}}^{\mathrm{FOSEP}} = \underline{\underline{H}}^{\mathrm{FOSEP}}_{aa}\Big|_{ph \text{ and } hp \text{ blocks}} . \tag{81}$$

The resulting eigenvectors have to be classified into so-called **physical** and **unphysical eigenvectors** according to the association with the zeroth order *ph* or *hp* states. Usually the physical eigenvalues are positive and well separated from the negative, unphysical ones.

The FOSEP approximation has to be compared with two other well-known first order approximation schemes, the Tamm-Dancoff approximation (TDA) [11,30] and the random phase approximation (RPA) [31,32,11,30]. The TDA leads to a hermitian eigenvalue problem of half the dimension of FOSEP. In fact the upper left (*ph*-*ph*) block of the FOSEP matrix $\underline{\underline{M}}^{\mathrm{FOSEP}}$ coincides with the matrix that is diagonalised in the TDA. In this respect FOSEP can be seen as an extension of the TDA. The same holds for the RPA which has the same matrix size as FOSEP but poses a non-hermitian eigenvalue problem. Thus instabilities, which are avoided in FOSEP, can occur in the RPA and lead to complex eigenvalues.

The TDA for excitation energies yields the difference between the energies of the Hartree-Fock ground state and excited states which are correlated by single-excitation configuration interaction (SCI). A perturbation theoretical analysis shows that the TDA energies are consistent in first order with Rayleigh-Schrödinger perturbation theory and contain part of the second order correlation of the excited states [33]. FOSEP also shows these features and additionally takes into account part of the second order ground state correlation while the RPA proves inconsistent by containing second order ground state

correlation with the wrong sign. From the second order analysis it can thus be concluded that the FOSEP energies will generally lie above the TDA energies due to consideration of ground state correlation while the RPA energies will be lower.

These findings are also supported by the results of a simple, exactly solvable model (Hubbard model for H_2) where the ground state is correlated while the singly excited states are not [21]. For this model, the RPA yields bad results collapsing to complex eigenvalues for certain choices of the model parameters while the FOSEP approximation even gives the exact excitation energies.

Some numerical tests on small molecules have been performed by F. Tarantelli [34], which also support the perturbation theoretical results. While in most cases FOSEP yields comparable results to the RPA, there are examples, like the lowest (triplet) excitation energy of Ethylene (C_2H_4), where the RPA fails by one order of magnitude while FOSEP yields a reasonable approximation of the experimental value improving considerably upon the TDA. This situation resembles the results on the earlier mentioned Hubbard model of H_2.

The FOSEP method can also be used to calculate approximate transition moments. For a given transition operator T, the transition moment $\langle \Psi_m | T | \Psi_0^N \rangle$ is defined by the matrix element of T between the exact excited state $|\Psi_m\rangle$ and the ground state $|\Psi_0^N\rangle$. Analysing this approximation by perturbation theory shows that the FOSEP approximation yields a consistent first-order description. So does the RPA while the TDA transition moments only describe the zeroth order correctly. One point that is often brought up in favour of the RPA is that it exactly preserves the equivalence of the length and the velocity forms of the transition moments of the dipole operator. It is indeed an unusual feature for a perturbation theory based approximation scheme to preserve this equivalence because it is not fulfilled in the Hartree-Fock approximation, which defines the zeroth order. Introducing the usual perturbation parameter in the Hamiltonian by $H = H_0 + \lambda H_1$, we see that the perturbation expansion for the difference Δ_m between the length and the velocity forms does not vanish identically as a function of λ but only disappears for $\lambda = 1$. The FOSEP approximation consistently describes this behaviour through first order and a discrepancy to the exact function $\Delta_m(\lambda)$ of second order remains. The RPA to the function $\Delta_m(\lambda)$ is in principle of the same first order quality but possesses the peculiar property to vanish exactly for $\lambda = 1$ when the transition moments are computed using a complete single-particle basis [35]. This property can be regarded unique to the RPA. Indeed, Hansen and Bouman [36] have shown that the RPA equations with their special non-hermitian structure may be derived from a configuration interaction representation of the ground and excited state wave function, requiring conditions which are a straightforward generalisation of the equivalence of the

length and the velocity forms.

E. First order extended eigenvalue problem and RPA

We consider the same first order approximation to the primary block $\underline{\underline{H}}_{aa}$ which defines the FOSEP approximation taking additionally into account the coupling to the K-states defined by Eq. (74). Considering the states $|K^{(ph)}_{\alpha n}\rangle$ as a minimal extension of the primary set of extended states $\{|Y^{(ph)}_{rs}\rangle\}$ we get additionally the block $\underline{\underline{H}}_{bb}$ and the coupling blocks $\underline{\underline{H}}_{ab}$ and $\underline{\underline{H}}_{ba}$. The matrix elements up to first order are given by

$$\left[\underline{\underline{H}}_{ba}\right]^{(1)}_{\alpha m,rs} = \langle K^{(ph)}_{\alpha m}|\,\mu\hat{H}|Y^{(ph)}_{rs}\rangle^{(0)} = -\sqrt{2}V_{\alpha s[rm]}(n_r - n_s), \tag{82}$$

$$\left[\underline{\underline{H}}_{bb}\right]^{(0)+(1)}_{\alpha m,\alpha' m'} = -\delta_{\alpha\alpha'}\delta_{mm'}(\varepsilon_\alpha - \varepsilon_m) - 2V_{\alpha m'[\alpha' m]}. \tag{83}$$

Taking into account the block structure of the $\underline{\underline{H}}_{aa}$ block which is approximated by $\underline{\underline{H}}^{\mathrm{FOSEP}}$ of Eqs. (78) and (79), it can be seen that the *pp-pp* and the *hh-hh* blocks of the primary part do not couple to the K-states. Thus the structure of the present approximation to the matrix $\underline{\underline{H}}$ is as follows:

$$\underline{\underline{H}}^{\mathrm{ext}} = \begin{pmatrix} * & 0 & 0 & 0 & 0 \\ 0 & * & * & 0 & * \\ 0 & * & * & 0 & * \\ 0 & 0 & 0 & * & 0 \\ 0 & * & * & 0 & * \end{pmatrix} \begin{matrix} \leftarrow hh \\ \leftarrow ph \\ \leftarrow hp \\ \leftarrow pp \\ \leftarrow K(hp) \end{matrix} . \tag{84}$$

Dropping the non-coupling *hh* and *pp* rows and columns we are left with a 3×3 matrix of square blocks of the same dimension which can be written in the following way:

$$\underline{\underline{M}}^{\mathrm{ext}} = \begin{pmatrix} \underline{\underline{\varepsilon}}^{ph} + \underline{\underline{V}} & \underline{\underline{W}} & \sqrt{2}\underline{\underline{W}} \\ \underline{\underline{W}} & -\underline{\underline{\varepsilon}}^{ph} + \underline{\underline{V}} & \sqrt{2}\underline{\underline{V}} \\ \sqrt{2}\underline{\underline{W}} & \sqrt{2}\underline{\underline{V}} & \underline{\underline{\varepsilon}}^{ph} + 2\underline{\underline{V}} \end{pmatrix} \begin{matrix} \leftarrow ph \\ \leftarrow hp \\ \leftarrow K(hp) \end{matrix} . \tag{85}$$

Here the zeroth order matrix $\underline{\underline{\varepsilon}}^{ph}$ and the first order coupling blocks $\underline{\underline{V}}$, $\underline{\underline{W}}$ are defined by their matrix elements:

$$\left[\underline{\underline{\varepsilon}}^{ph}\right]_{n\alpha,m\beta} = \delta_{nm}\delta_{\alpha\beta}(\varepsilon_n - \varepsilon_\alpha), \tag{86}$$

$$\left[\underline{\underline{V}}\right]_{n\alpha,m\beta} = V_{n\beta[\alpha m]}, \tag{87}$$

$$\left[\underline{\underline{W}}\right]_{n\alpha,m\beta} = -V_{nm[\alpha\beta]}. \tag{88}$$

The representation (85) of the extended FOSEP matrix follows directly from Eqs. (78), (82), and (83) by renumbering the rows and columns of the blocks in the hp and the $K(hp)$ row and under the assumption that the matrix elements of the two-body interaction V_{ijkl} are real and thus $V_{ijkl} = V_{klij}$.

The corresponding eigenvalue problem for the matrix $\underline{\underline{M}}^{\text{ext}}$ that remains reads

$$\underline{\underline{M}}^{\text{ext}}\underline{x} = \omega\underline{\underline{S}}\,\underline{x}, \tag{89}$$

where the diagonal overlap matrix $\underline{\underline{S}}$ is given by the proper part of the matrix $\underline{\underline{\mu}}$ of Eq. (31) which reads in block matrix notation

$$\underline{\underline{S}} = \begin{pmatrix} \underline{\underline{1}} & 0 & 0 \\ 0 & \underline{\underline{1}} & 0 \\ 0 & 0 & -\underline{\underline{1}} \end{pmatrix} \begin{matrix} \leftarrow ph \\ \leftarrow hp \\ \leftarrow K(hp) \end{matrix}. \tag{90}$$

The eigenvalue problem (89) can be transformed without changing the eigenvalues with the help of an orthonormal transformation with respect to the metric $\underline{\underline{S}}$:

$$\underline{\underline{T}}^{\dagger}\underline{\underline{S}}\,\underline{\underline{T}} = \underline{\underline{S}}. \tag{91}$$

With the help of the inverse matrix

$$\underline{\underline{T}}^{-1} = \underline{\underline{S}}^{-1}\underline{\underline{T}}^{\dagger}\underline{\underline{S}}, \tag{92}$$

Eq. (89) can be reformulated to yield

$$\underline{\underline{T}}^{\dagger}\underline{\underline{M}}^{\text{ext}}\underline{\underline{T}}\,\underline{\underline{T}}^{-1}\underline{x} = \omega\underline{\underline{T}}^{\dagger}\underline{\underline{S}}\,\underline{\underline{T}}\,\underline{\underline{T}}^{-1}\underline{x}. \tag{93}$$

Introducing

$$\underline{\underline{M}}' = \underline{\underline{T}}^{\dagger}\underline{\underline{M}}^{\text{ext}}\underline{\underline{T}}, \tag{94}$$

$$\underline{x}' = \underline{\underline{T}}^{-1}\underline{x}, \tag{95}$$

we obtain the transformed equation

$$\underline{\underline{M}}'\underline{x}' = \omega\underline{\underline{S}}\,\underline{x}'. \tag{96}$$

The particular choice

$$\underline{\underline{T}} = \begin{pmatrix} \underline{\underline{1}} & 0 & 0 \\ 0 & \sqrt{2}\underline{\underline{1}} & \underline{\underline{1}} \\ 0 & \underline{\underline{1}} & -\sqrt{2}\underline{\underline{1}} \end{pmatrix} \begin{matrix} \leftarrow ph \\ \leftarrow hp \\ \leftarrow K(hp) \end{matrix} \tag{97}$$

of the transformation matrix applied to the eigenvalue problem (89) leads to a further decoupling in the secular matrix

$$\underline{\underline{M}}^{\text{ext}} = \begin{pmatrix} \underline{\underline{\varepsilon}}^{ph} + \underline{\underline{V}} & 0 & -\underline{\underline{W}} \\ 0 & -\underline{\underline{\varepsilon}}^{ph} & 0 \\ -\underline{\underline{W}} & 0 & \underline{\underline{\varepsilon}}^{ph} + \underline{\underline{V}} \end{pmatrix}. \tag{98}$$

Dropping the decoupled central row and column, the following 2×2 block matrix eigenvalue problem remains:

$$\begin{pmatrix} \underline{\underline{\varepsilon}}^{ph} + \underline{\underline{V}} & -\underline{\underline{W}} \\ -\underline{\underline{W}} & \underline{\underline{\varepsilon}}^{ph} + \underline{\underline{V}} \end{pmatrix} \underline{x}'' = \omega \begin{pmatrix} \underline{\underline{1}} & 0 \\ 0 & -\underline{\underline{1}} \end{pmatrix} \underline{x}''. \tag{99}$$

This is identical to the RPA eigenvalue problem which has been presented in similar notation in Refs. [21] and [37]. A thorough comparison to the FOSEP approximation has been made in Ref. [21].

Concluding, we have shown that the present approximation $\underline{\underline{H}}^{\text{ext}}_{aa}$ to the matrix $\underline{\underline{H}}$ leads to the RPA. In terms of the self energy, the present approach consists of a first order static part of the self energy like in the FOSEP approximation and additionally to that part of the dynamic self energy comprising the K-states which are in zeroth order degenerate to parts of the primary (static) block.

It can also be shown that an approximation of the transition moments with the physical solutions of the $\underline{\underline{H}}^{\text{ext}}$ eigenvalue problem yields the RPA for the transition moments. The transition moments thus have all the RPA properties like, e. g., the exact equivalence of length and velocity form.

VI. STATIC SCATTERING POTENTIALS

In this chapter we will further discuss the static self energy of the extended two-particle Green's function. We have shown in a previous paper that the self energy of this propagator is an optical potential for elastic scattering of two-particle projectiles [10]. It is a well known fact that optical potentials are non-unique [8]. Thus it is useful to investigate the properties of a given optical potential critically from the formal, practical, and intuitive point of view. In the following we will try to illuminate the physical significance of the static self energy by viewing it as a static scattering potential. A strong analogy can here be drawn from the well established Green's function optical potential for single-particle scattering, which we will start with. We also compare with the alternative description by Feshbach's optical potential. The discussion of single-particle optical potentials then helps us to identify terms of the particle-particle self energy. Considering Coulomb-interacting particles and presenting

the static self energy in position space allows us to motivate the important terms in the static part of the optical potentials. Finally, the interpretation of the static self energy in the light of a scattering potential will also be transferred to the particle-hole self energy.

A. Optical potentials for single-particle scattering

We begin with the physical situation of scattering a single particle off an N-particle target in its ground state $|\Psi_0^N\rangle$. All particles are indistinguishable fermions and we only consider the elastic scattering channel where the out-asymptotes leave the target in its ground state. The influences of the interaction of the projectile particle with the many-body target can be accounted for by a so-called optical potential [3] that is a potential in the single-particle space and allows one to solve single-particle scattering equations that still give the exact results with all many-body effects included. This optical potential has to be non-local in order to describe exchange phenomena and has to depend on the energy of the incident particles in order to correctly describe the many-body interactions which can lead to resonances. Furthermore the optical potential is in general a non-hermitian operator in order to take account of the loss of scattering amplitude into inelastic channels.

1. Green's function optical potential

It has been shown by Bell and Squires [4] that the self energy $\underline{\underline{\Sigma}}(\omega)$ of the single-particle Green's function represents an exact optical potential for elastic single-particle scattering. In an analogous way to Sec. III, the usual Dyson equation defining the single-particle self energy can be derived by a projection onto the span of the orthonormal primary set of states [26,9]

$$|Y_p^{(G)}\rangle = \begin{pmatrix} a_p^\dagger |\Psi_0^N\rangle \\ \langle \Psi_0^N | a_p \end{pmatrix}. \tag{100}$$

The formal analogy between the derivation of Dyson's equation for the single-particle Green's function and the extended two-particle Green's functions has been the original motivation for the construction of the present two-particle formalism and is discussed in detail in Ref. [10]. Here we only want to mention that the definition of the Green's function (29) and the expressions for the inverse Green's function (36) and the self energy (38) hold as well for the single-particle Green's function $G_{pq}(\omega)$ and self energy $\Sigma_{pq}(\omega)$ when the states $|Y_p^{(G)}\rangle$ replace the extended states $|Y_{rs}\rangle$ and the metric μ is replaced by unity.

Thus, the single-particle Green's function $\underline{\underline{G}}(\omega)$ can be written as the resolvent of an energy-dependent effective Hamiltonian:

$$\underline{\underline{G}}(\omega) = \frac{1}{\omega \underline{\underline{1}} - \underline{\underline{H}}_{aa}^{(G)(0)} - \underline{\underline{\Sigma}}(\omega)}. \tag{101}$$

We will now take a closer look at the static part of the Green's function optical Hamiltonian

$$\mathcal{R}_{pq}^{(G)} := \left[\underline{\underline{H}}_{aa}^{(G)(0)}\right]_{pq} + \Sigma_{pq}(\infty) = \langle \Psi_0^N | \left[a_p \left[H\,,\, a_q^\dagger\right]_-\right]_+ | \Psi_0^N \rangle. \tag{102}$$

The commutators of the creation and destruction operators with the Hamiltonian H are readily evaluated and we are left with the expression

$$\mathcal{R}_{pq}^{(G)} = \varepsilon_p \delta_{pq} + v_{pq} + \mathcal{V}_{pq}^{(G)} \tag{103}$$

for the static part of the Green's function optical Hamiltonian. The first two terms on the right hand side are easily interpreted as the influence of the single-particle part of the Hamiltonian like the kinetic energy and external forces on the projectile particle. The third term

$$\begin{aligned} \mathcal{V}_{pq}^{(G)} &= \langle \Psi_0^N | \left[a_p \left[V\,,\, a_q^\dagger\right]_-\right]_+ | \Psi_0^N \rangle \\ &= \sum_{kl} V_{pk[ql]}\, \rho_{lk} \end{aligned} \tag{104}$$

accounts for two-body interactions between the projectile and the target particles. The single-particle density ρ_{ij} is defined by

$$\rho_{ij} = \langle \Psi_0^N | \, a_j^\dagger a_i \, | \Psi_0^N \rangle. \tag{105}$$

This two-body interaction part of the static self energy becomes even more intuitive, when we consider a local interaction potential and transform the formulas into position space. Take, e. g., Coulomb interacting electrons where the matrix elements read

$$V_{r_1 r_2 r_1' r_2'} = \frac{\delta_{r_1 r_1'} \delta_{r_2 r_2'}}{|\mathbf{r}_1 - \mathbf{r}_2|} \tag{106}$$

in position-space representation. The indices $r = (\mathbf{r}, \sigma)$ are composed of the spatial part $\mathbf{r}$ and spin part σ and adequately the delta function becomes $\delta_{rr'} := \delta(\mathbf{r} - \mathbf{r}')\, \delta_{\sigma\sigma'}$.

In position space the interaction part of the static Green's function optical Hamiltonian (or the static self energy) reads

$$\mathcal{V}^{(G)}_{rr'} = \delta_{rr'} \int dr_1 \frac{\rho_{r_1}}{|\mathbf{r} - \mathbf{r}_1|} - \frac{\rho_{rr'}}{|\mathbf{r} - \mathbf{r}'|}, \tag{107}$$

where the integration is taken to run over the three-dimensional coordinate space and to additionally include summation over the spin part. $\rho_r = \rho_{rr}$ denotes the diagonal part of the single-particle density. Of course, the spin part is easily accounted for in the case of a singlet ground state and a purely spatial interaction part remains [38]:

$$\mathcal{V}^{(G)}(\mathbf{r}, \mathbf{r}') = \delta(\mathbf{r} - \mathbf{r}') \int d\mathbf{r}_1 \frac{\rho(\mathbf{r}_1)}{|\mathbf{r} - \mathbf{r}_1|} - \frac{\rho(\mathbf{r}, \mathbf{r}')}{|\mathbf{r} - \mathbf{r}'|}. \tag{108}$$

It becomes evident that the static self energy describes the Coulomb repulsion of the projectile electron by the static charge density of the target, the effect of which is diminished by the possibility of exchange of the projectile particle with one of the target particles described by the second term. If the target is approximated by a Slater determinant, the static entity $\underline{\underline{\mathcal{R}}}^{(G)}$ approximates the projectile-target interaction on the so called **static exchange** level. Taking $\underline{\underline{\mathcal{R}}}^{(G)}$ with a correlated ground state density instead is known as the **correlated static exchange** approximation [39–41]. Of course, these approximations cannot account for effects due to the response of the target's wavefunction to the incident projectile particle. These effects are called dynamic effects and are described by the dynamic part of the self energy.

2. Feshbach's optical potential

The optical model potential of Feshbach [2] was the first, rigorously derived optical potential. There exist, however, an infinite number of physically equivalent yet mathematically distinct optical potentials. A thorough examination of the mathematical properties of various kinds of single-particle optical potentials has been given by Capuzzi and Mahaux [8]. An equivalent reformulation of the original effective Hamiltonian used by Feshbach including the single-particle kinetic energy and optical potential reads in matrix notation

$$\underline{\underline{h}}^{(\mathrm{F})}(E) = [\underline{\underline{\mathcal{R}}}^{(\mathrm{F})} + \underline{\underline{\mathcal{D}}}(E)]\underline{\underline{\sigma}}^{-1}. \tag{109}$$

The connection to the original formulas of Feshbach [2] is established in Ref. [8]. The matrix $\underline{\underline{\sigma}}$ is the difference between the unit matrix and the single-particle ground state density with the matrix elements

$$\begin{aligned} \sigma_{pq} &= \langle \Psi_0^N | \, a_p a_q^\dagger \, | \Psi_0^N \rangle \\ &= \delta_{pq} - \rho_{pq}. \end{aligned} \tag{110}$$

Note that the eigenvalues of this matrix are just one minus the natural occupations of the target's ground state. If the target does contain an uncorrelated hard core, the matrix $\underline{\underline{\sigma}}$ cannot be inverted in the full space of single-particle indices. Rather one has to exclude the hard core explicitly from the accessible space for the projectile's wave function. In the important special case where the target wave function is a Slater determinant, the matrix $\underline{\underline{\sigma}}$ becomes a projector onto the virtual orbital space.

The matrix $\underline{\underline{\mathcal{R}}}^{(\mathrm{F})}$ is what we call the static part of the Feshbach Hamiltonian. It is defined by the matrix elements

$$\mathcal{R}^{(\mathrm{F})}_{pq} = \langle \Psi^N_0 |\, a_p \,[H\,,\, a^\dagger_q]_- \,| \Psi^N_0 \rangle. \tag{111}$$

The dynamic part $\underline{\underline{D}}(E)$, which can be found in the literature [8], possesses poles related to resonances of two-particle–hole and higher excitations and a branch cut above the ionisation threshold. It has an analytic structure similar to the dynamic self energy (42) from the formal point of view. This is not surprising since the projection method for deriving the Feshbach Hamiltonian is formally similar to the derivation of Dyson's equation of Sec. III or in Refs. [26,9]. There, a partitioning was performed yielding a projection to the primary space spanned by the orthonormal Y-states while Feshbach, on the other hand, projected onto the space spanned by the non-orthonormal states $a^\dagger_r \,|\Psi^N_0\rangle$.

Like we have done for the Green's function optical potential we can also evaluate the static part $\mathcal{R}^{(\mathrm{F})}_{pq}$ of Feshbach's optical Hamiltonian:

$$\mathcal{R}^{(\mathrm{F})}_{pq} = \varepsilon_p \sigma_{pq} + \sum_j v_{pj}\sigma_{jq} + \mathcal{V}^{(\mathrm{F})}_{pq}, \tag{112}$$

with

$$\mathcal{V}^{(\mathrm{F})}_{pq} = \langle \Psi^N_0 |\, [a_p\,,\, V]_-\, a^\dagger_q \,| \Psi^N_0 \rangle. \tag{113}$$

First we note that the $\underline{\underline{\sigma}}$ matrices cancel with their inverse in Eq. (109), leaving the same single-particle part as for the Green's function optical potential. The interaction part $\mathcal{V}^{(\mathrm{F})}_{pq}$, however, differs from its Green's function analogue $\mathcal{V}^{(G)}_{pq}$ of Eq. (107) by involving the two-particle density

$$\gamma_{ijkl} = \langle \Psi^N_0 |\, a^\dagger_l a^\dagger_k a_i a_j \,| \Psi^N_0 \rangle \tag{114}$$

of the target's ground state. The two-particle density comes into play because the expectation value $\langle \Psi^N_0 |\, [a_p\,,\, V]_-\, a^\dagger_q \,| \Psi^N_0 \rangle$ contains products of three creation and three destruction operators. While one of each is cancelled by the commutator, a two-particle density remains. Considering the fact that the two-particle density of Slater determinants factorise into single-particle densities according to

$$\gamma^{\mathrm{Sd}}_{ijkl} = \rho_{ik}\rho_{jl} - \rho_{il}\rho_{jk}, \tag{115}$$

we may introduce the reminiscent two-particle density

$$\tilde{\gamma}_{ijkl} = \gamma_{ijkl} - \gamma^{\mathrm{Sd}}_{ijkl}. \tag{116}$$

This allows to further simplify $\mathcal{R}^{(\mathrm{F})}_{pq}$ to yield

$$\mathcal{R}^{(\mathrm{F})}_{pq} = \sum_i \mathcal{R}^{(G)}_{pi}\sigma_{iq} + \sum_{jkl} \tilde{\gamma}_{plji} V_{ijlq}. \tag{117}$$

In the case of an uncorrelated (Slater determinantal) target, the static part of the Feshbach Hamiltonian (109) thus reduces to the well-known static exchange approximation. For correlated targets, however, there remains a term due to the non-factorising part of the two-particle density $\tilde{\gamma}_{plji}$ which is not easily interpretable by intuition. We therefore conclude that the Green's function optical potential, which is well defined in the full single-particle space also for hard-core potentials, provides the simpler to compute and more intuitive static part than the Feshbach optical potential. For completeness we would like to mention that the Feshbach approach also has more difficulties with the dynamic part in showing a more complicated energy dependence and nonlocality in studies of nuclear matter, at least at low energy [8,42].

B. Two-particle scattering

We have shown in Ref. [10] that the self energy of the extended particle-particle Green's function $\underline{\underline{G}}^{(pp)}(\omega)$ serves as an exact optical potential for elastic scattering of two particle-projectiles by a many-body target. In a situation where both projectile particles are asymptotically free, one may choose the kinetic energy as the zeroth order Hamiltonian H_0. The effective Hamiltonian in the two-particle space then is given as usual as a sum of the zeroth order part $\underline{\underline{H}}^{(pp)(0)}_{aa}$, which is now the kinetic energy for the projectile particles, and the self energy $\underline{\underline{S}}^{(pp)}(E)$ taking account for the full interaction. Interaction now occurs between the projectile particles, between the projectile and the target particles, within the target and with external fields. The static part of the optical Hamiltonian is given by

$$\mathcal{R}^{(pp)}_{rs,r's'} = \left[\underline{\underline{H}}^{(pp)}_{aa}\right]_{rs,r's'} = (a^\dagger_r, a^\dagger_s \,|\hat{H}|\, a^\dagger_{r'}, a^\dagger_{s'}). \tag{118}$$

Again, the contributions of the single-particle part of the Hamiltonian H may be split off easily due to the linearity $\hat{H} = \hat{H}_0 + \hat{v} + \hat{V}$ of the super-operators:

$$\mathcal{R}^{(pp)}_{rs,r's'} = (\varepsilon_r + \varepsilon_s)(\delta_{rr'}\delta_{ss'} - \delta_{rs'}\delta_{sr'}) + \mathcal{S}_{rs,r's'}(\infty), \tag{119}$$

with

$$\mathcal{S}^{(pp)}_{rs,r's'}(\infty) = v_{rr'}\delta_{ss'} + \delta_{rr'}v_{ss'} - v_{rs'}\delta_{rs'} - \delta_{rs'}v_{rs'} + \mathcal{V}^{(pp)}_{rs,r's'}. \tag{120}$$

Thus the kinetic energy and the influence of external forces is already described exactly by the static part of the optical Hamiltonian and independent of approximations for the target wavefunction. Note that the possibility for two particles labelled by r and s to exchange can be seen explicitely in the kinetic energy and external field parts of Eqs. (119) and (120) by the terms that antisymmetrise the matrix with respect to interchange of these labels. An expression for the interaction part $\mathcal{V}^{(pp)}_{rs,r's'}$ contained in the static self energy is gained by applying the definitions of Sec. II:

$$\begin{aligned}
\mathcal{V}^{(pp)}_{rs,r's'} &= (a_r^\dagger, a_s^\dagger\,|\hat{V}|\,a_{r'}^\dagger, a_{s'}^\dagger) \\
&= \langle\Psi_0^N|\left[a_s a_r\,,\,\left[V\,,\,a_{r'}^\dagger a_{s'}^\dagger\right]_-\right]_-|\Psi_0^N\rangle + \\
&\quad \Big\{\langle\varphi|\left[\left[V\,,\,a_{r'}^\dagger\right]_-\,,\,a_r\right]_+|\varphi\rangle\langle\Psi_0^N|\,a_{s'}^\dagger a_s\,|\Psi_0^N\rangle + \\
&\qquad \delta_{ss'}\langle\Psi_0^N|\left[V\,,\,a_{r'}^\dagger\right]_+ a_r\,|\Psi_0^N\rangle\Big\} - \\
&\quad \Big\{r \leftrightarrow s\Big\} - \Big\{r' \leftrightarrow s'\Big\} + \Big\{r \leftrightarrow s\ \&\ r' \leftrightarrow s'\Big\},
\end{aligned} \tag{121}$$

where the term in braces reappears three more times with interchanged indices as indicated in the last line of Eq. (121). When we again consider the case of Coulomb-interacting electrons and transform Eq. (121) into position space, we get a large number of terms due to the many possibilities of the two electrons to exchange with each other and with the target particles. All terms are written down in App. B. Here we will only motivate some important ones.

Firstly, one certainly expects terms describing the direct repulsion of the two projectile particles as well as the Coulomb interaction of both particles with the static charge density of the target. These terms also arise if the projectile particles are distinguishable from the target, e.g. for positrons. In order to isolate these terms we introduce positronic creation and destruction operators $c_r^\dagger$ and c_r which commute with the electronic operators $a_r^\dagger$ and a_r. Including the Coulomb interactions of the positrons using the interaction operator $V_{\text{composite}}$ for the composite electron-positron system (taken from Ref. [43]), we obtain the following expression for the interaction part of the static self energy of the extended two-positron Green's function:

$$\mathcal{V}^{(\text{positrons})}_{rs,r's'} = (c_r^\dagger, c_s^\dagger\,|\hat{V}_{\text{composite}}|\,c_{r'}^\dagger, c_{s'}^\dagger)$$

$$= (\delta_{rr'}\delta_{ss'} - \delta_{rs'}\delta_{rs'})\left(\frac{1}{|\mathbf{r}-\mathbf{s}|} - \int d\mathbf{r}_1 \frac{\rho_{r_1}}{|\mathbf{r}_1-\mathbf{r}|} - \int d\mathbf{r}_1 \frac{\rho_{r_1}}{|\mathbf{r}_1-\mathbf{s}|}\right). \quad (122)$$

This is a very intuitive result showing that the static particle-particle self energy incorporates the full two-body interaction between both projectile particles as well as the Coulomb interaction with the static charge density of the target. The possibility of exchange between the projectile particles is explicitely present in Eq. (122) through the antisymmetric delta functions.

Returning to the problem of scattering projectile particles that are indistinguishable from the target particles, we can expect additional exchange terms. These terms do indeed occur and a straightforward evaluation of Eq. (121) yields nine different terms:

$$(a_r^\dagger, a_s^\dagger |\hat{V}| a_{r'}^\dagger a_{s'}^\dagger) = A + B + C + D + E + F + G + I + J - (r \leftrightarrow s) - (r' \leftrightarrow s') + (r \leftrightarrow s \,\&\, r' \leftrightarrow s'). \quad (123)$$

As mentioned before, all terms are written down in App. B. Note that outside of the target, i. e. when the positions r, r', s, and s' of the projectile particle are such that the target's particle densities vanish, only the terms A and B with their antisymmetric combinations survive. These terms exactly reproduce Eq. (122) except for the obvious change of sign of the projectile-target Coulomb interaction.

Of the remaining terms, $C = -\delta_{ss'}\frac{\rho_{rr'}}{|\mathbf{r}-\mathbf{r}'|}$ is most easily identified as the kind of exchange interaction of a single projectile particle with the target that already appeared in the case of single-particle scattering in Eq. (107). All the other terms have to be attributed either to the possibility of simultaneous projectile-projectile Coulomb interaction with projectile-target exchange (D - G) or projectile-target exchange occurring along with the projectile-target Coulomb interaction (I and J). The occurrence of two-particle densities in terms F and I appears quite natural in this context although the intuitive interpretation of these mixed or simultaneous exchange terms remains obscure.

Note that the terms G and J are proportional to the single-particle density $\rho_{ij}^{\varphi} = \langle\varphi| a_j^\dagger a_i |\varphi\rangle$ of the secondary reference state $|\varphi\rangle$ that was introduced in the definition (1) of the extended states $|A, B)$. The choice of this reference wavefunction is arbitrary for the algebraic properties of the extended wavefunction and, in particular, for the derivation of the Dyson equation. Here it obviously introduces differences and the freedom of choice can be used to change the static self energy. The only condition that $|\varphi\rangle$ has to comply with in order to have the full formalism at hand, is to be an eigenfunction of the Fock-space Hamiltonian H (c. f. Sec. II C). The two obvious choices for $|\varphi\rangle$

are the target state $|\Psi_0^N\rangle$ and the Fock-space vacuum $|\mathrm{vac}\rangle$. Choosing the vacuum, the terms G and J vanish because the particle density in the vacuum is zero. This choice was used in Ref. [10]. Choosing instead the target's ground state $|\Psi_0^N\rangle$, the terms G and J look similar to terms F and I, respectively, which involve two-particle densities appearing with a different sign.

Like in the case of single-particle scattering, there are other possibilities of defining optical potentials. Without going into detail we want to mention that an analogous expression to the Feshbach effective Hamiltonian (109) can be derived for two-particle scattering. The static part $\underline{\underline{\mathcal{R}}}^{(\mathrm{F})}$ has now the matrix elements $\mathcal{R}^{(\mathrm{F})}_{rsr's'} = \langle\Psi_0^N|\, a_s a_r\, [H\,,\, a_{r'}^\dagger a_{s'}^\dagger]_-\, |\Psi_0^N\rangle$. For positrons as projectile particles (i. e. distinguishable particles from the target) the same result as Eq. (122) is found. In this special case the static particle-particle self energy and the static part of Feshbach's potential are identical. If all particles are indistinguishable fermions, however, $\underline{\underline{\mathcal{R}}}^{(\mathrm{F})}$ involves three-particle densities that are cumbersome to evaluate and even more difficult to interpret.

C. Particle-hole scattering

In the preceding section we have discussed the static part of the particle-particle self energy as a scattering potential for two-particle scattering by a correlated many-body target. This point of view is justified by the fact that the particle-particle self energy is in fact an exact optical potential for two-particle scattering [10]. Earlier in this paper we have presented a unified formalism comprising three different types of two-particle Green's functions: the extended particle-particle, particle-hole and hole-hole Green's functions. The strong formal analogy between the three cases already hints towards carrying this analogy to the discussion of scattering potentials. Especially the particle-hole case deserves more attention since we know that in extended electronic systems, particles and holes attract each other and may form bound states known as excitons. The excitons then may act as projectiles and scatter off defects, other kinds of interaction centres, or simply because of the presence of electronic correlation.

Looking at the expression for the static part of the effective particle-hole Hamiltonian [which can be evaluated from Eq. (68)] we notice that the kinetic energy part describes two distinguishable particles with masses of opposite sign:[2]

---

[2]Choosing H_0 to be the kinetic energy operator for electrons, the single particle indices p, q in this equation should be read as the momentum space representation

$$(a_p^\dagger, a_q \,|\hat{H}|\, a_{p'}^\dagger, a_{q'}) = \delta_{pp'}\delta_{qq'}(\varepsilon_p - \varepsilon_q) + \mathcal{S}^{(ph)}_{pqp'q'}(\infty). \tag{124}$$

The interaction with external (one particle) potentials is contained in the static self energy and also shows different signs like for particles carrying opposite charges:

$$\mathcal{S}^{(ph)}_{pqp'q'}(\infty) = v_{pp'}\delta_{qq'} - \delta_{pp'}v_{q'q} + (a_p^\dagger, a_q \,|\hat{V}|\, a_{p'}^\dagger, a_{q'}). \tag{125}$$

The interaction potential $(a_p^\dagger, a_q \,|\hat{V}|\, a_p'^\dagger, a_q')$ describes the two-particle interactions and may again be simplified by switching to position-space representation. The full expression, however, is still fairly complicated and can be found in App. C. Note that this interaction part of the static self energy simplifies very much when the projectile particles are outside of the target, i. e. where the particle density has dropped to zero. In this "outer" region we are left with the Coulomb interaction of two oppositely charged particles with the target's charge density:

$$(a_r^\dagger, a_s \,|\hat{V}|\, a_{r'}^\dagger, a_{s'})\Big|_{\text{outer region}} = \delta_{rr'}\delta_{ss'}\int d\mathbf{r}_1 \frac{\rho_{r_1}}{|\mathbf{r}_1 - \mathbf{r}|} - \delta_{rr'}\delta_{ss'}\int d\mathbf{r}_1 \frac{\rho_{r_1}}{|\mathbf{r}_1 - \mathbf{s}|}. \tag{126}$$

In the outer region there is no direct coupling between the particle and the hole. However, there are no formal restrictions that prohibit a hole from being outside the target. In regions of vanishing particle density, holes move with negative mass interacting by opposite charge with external potentials and the target's charge density. Inside the target interactions between the particle and the hole arise. This is best seen when the interaction potential is further simplified by assuming that all two particle densities in Eq. (C1) factorise, which is the case if the target's ground state can be described by a Slater determinant. Choosing further the secondary reference state $|\varphi\rangle$ to be the target's wavefunction we arrive at the following expression:

$$\begin{aligned}(a_r^\dagger, a_s \,|\hat{V}|\, a_{r'}^\dagger, a_{s'})\Big|_{\text{factorised}} = {} & \delta_{rr'}\delta_{ss'}\int d\mathbf{r}_1 \frac{\rho_{r_1}}{|\mathbf{r}_1 - \mathbf{r}|} - \delta_{ss'}\frac{\rho_{rr'}}{|\mathbf{r} - \mathbf{r}'|} \\ & -\delta_{rr'}\delta_{ss'}\int d\mathbf{r}_1 \frac{\rho_{r_1}}{|\mathbf{r}_1 - \mathbf{s}|} + \delta_{rr'}\frac{\rho_{s's}}{|\mathbf{s} - \mathbf{s}'|} \\ & -\delta_{rr'}\int d\mathbf{r}_1 \frac{\rho_{s'r_1}\rho_{r_1 s}}{|\mathbf{r}_1 - \mathbf{r}|}\end{aligned}$$

---

where the kinetic energy is diagonal. Later we will again switch to position space representation (with indices r and s) where the local Coulomb force simplifies.

$$
\begin{aligned}
&-\delta_{ss'} \int d\mathbf{r}_1 \frac{\rho_{rr_1}\rho_{r_1r'}}{|\mathbf{r}_1 - \mathbf{s}|} \\
&+\rho_{rr'}\rho_{s's} \left(\frac{1}{|\mathbf{r} - \mathbf{s}'|} + \frac{1}{|\mathbf{r}' - \mathbf{s}|} \right) \\
&+\mathcal{V}^A_{rs,r's'}. \qquad (127)
\end{aligned}
$$

Additionally to the terms of Eq. (126) we now have the usual exchange terms (2nd term on the r.h.s) for the particle and an analogous exchange term (4th term) for the hole. The following two terms (5th and 6th) describe attractive forces between the particle and the hole, mediated through the target. In particular if the one-particle densities are almost diagonal this becomes obvious. The next (7th) term has to be interpreted as an exchange correction to the preceding Coulombic terms. The last term is called the "annihilation potential" $\mathcal{V}^A_{rs,r's'}$ and is given by

$$
\mathcal{V}^A_{rs,r's'} = \rho_{rs}\rho_{s'r'} \left(\frac{1}{|\mathbf{r} - \mathbf{r}'|} + \frac{1}{|\mathbf{s} - \mathbf{s}'|} - \frac{1}{|\mathbf{r} - \mathbf{s}'|} - \frac{1}{|\mathbf{r}' - \mathbf{s}|} \right). \qquad (128)
$$

It plays a special role since the single-particle densities involved mix particle (r, r') and hole (s, s') indices. This term thus originates from the possibility of particle-hole excitations to annihilate. Note also that this term vanishes for a target in a singlet state if the particle-hole pair forms a triplet excitation, e.g., if the spins are opposite [$r = (\underline{r}, \uparrow)$, and $s = (\underline{s}, \downarrow)$].

VII. CONCLUSIONS

In this paper we have presented a general theory of extended two-particle Green's functions and discussed a number of formal properties as well as the physical interpretation of the corresponding static self energies. We have developed a general formalism and used it to define fermionic extended two-particle Green's functions of three categories: particle-hole, particle-particle, and hole-hole functions. An important property of the treated class of Green's functions is that they obey a Dyson equation in analogy to the well-known single-particle Green's function of traditional many-body theory. Many properties of the extended two-particle Green's functions can be explained by this analogy. Dyson's equation defines well-behaved self energies that are amenable to a perturbation theoretical treatment. A further analogy to the single-particle Green's function lies in the property of the two-particle self energy to serve as an optical potential for elastic scattering of two-particle projectiles by a many-body target.

The fundamental construction principle for fulfilling Dyson's equation is to define the Green's function upon an orthonormal set of primary states. In order to achieve this orthonormality property, the physical two-particle states have to be extended by additional, "unphysical" components. The new components introduce additional poles and branch cuts in the analytic structure of the extended Green's functions. When defining the Green's function for real arguments, however, one can still manipulate the singularities by shifting them off the real axis or choosing principle value singularities. Another consequence of the extensions is the occurrence of zeroth-order degenerate states.

In this contribution we have given particular attention to the two-particle self energies. In the special case of a many-particle system without proper inter-particle forces, where the particles only interact with external potentials or by mean fields, the two-particle self energies take on a particularly simple, energy-independent form. The first order of perturbation theory already solves the full problem in strict analogy to the self energy of the single-particle Green's function.

Also for a truly correlated many-body system it turned out that already the first-order static approximation of the self energy yields a well-behaved approximation as we discussed for the particle-hole case. We have compared the resulting FOSEP approximation for excitation energies and transitions moments with two other well-known first order approximation schemes, the RPA and the TDA. It turned out that the FOSEP approximation is not only consistent in first order but also includes parts of the higher order correlation in a consistent manner without showing the instabilities of the RPA. The RPA, on the contrary, treats higher-order ground state correlation in the excitation energies inconsistently while the TDA fails to yield consistent transition moments. Interestingly both the TDA as well as the RPA can be won as specific approximations to our extended particle-hole self energy. The TDA results by exclusion of the zeroth-order unphysical states and the RPA is gained by inclusion of a class of zeroth-order degenerate states.

The static self energy was also examined from a less formal and more physical perspective by viewing it as a static scattering potential. On the example of Coulomb-interacting fermions we interpreted various terms of the static part of the particle-particle self energy by comparison with the Green's function's and Feshbach's optical potentials for single-particle scattering. We could also draw an analogy to the static self energy of the extended particle-hole Green's function. Apart from describing the static projectile-target interactions, also intra-projectile forces mediated by the target are present. One thinkable application of particle-hole optical potentials is the scattering of excitons in extended systems but room is left for physical imagination.

The development of approximations to the two-particle self energies be-

yond the leading order is certainly a challenging task for the future. In this context, additional insight into the structure and meaning of the dynamic self energy parts is needed. The underlying concepts of the presented formalism, in particular the orthonormal primary set of states, which is invariant under a change of the single-particle basis, form a sound basis for developing powerful approximation schemes. These may go beyond single-determinant based perturbation theory because the choice of the primary reference state $|\Psi_0^N\rangle$ in the definition of the extended Green's functions is not restricted in this way. Multi-configuration, coupled-cluster, or density-functional based approximate wave functions may be employed here. The arbitrariness of the secondary reference state $|\varphi\rangle$, on the other hand, may be used to tailor approximation schemes with particular properties.

ACKNOWLEDGEMENTS

Valuable comments and a critical reading of the manuscript by E. Pahl are gratefully acknowledged. We also wish to thank F. Tarantelli for unpublished numerical results.

APPENDIX A: FORMAL DEFINITION OF THE HILBERT SPACE Y

The following formal definition of the space Y refers to a given choice of reference states $|\psi\rangle$ and $|\varphi\rangle$ [as in Eq. (1)] that are proper eigenstates of a given Fock-space Hamiltonian H. The mathematical concepts used in this formal chapter can be found in common textbooks on functional analysis, e. g. Ref. [22].

Definition Given a set of primary states $\mathcal{P} = \{|\, A, B) \,|\, A \in \mathcal{A}, B \in \mathcal{B}\}$ defined by sets of Fock-space operators $\mathcal{A}$ and $\mathcal{B}$, we define the space Y as the smallest closed linear space containing $\mathcal{P}$ as a subset $\mathcal{P} \subset \mathsf{Y}$ that is closed under action of the extended operator $\breve{H}$, i. e.

$$|y\rangle \in \mathsf{Y} \quad \Rightarrow \quad \breve{H}\,|y\rangle \in \mathsf{Y}. \tag{A1}$$

Notes

- The "smallest" space satisfying the demanded conditions is defined, like usual, as the intersection of all spaces that fulfil the conditions.
- It should become clear that this definition of a minimal space Y is appropriate because the extended propagators will be defined by matrix elements of the resolvent of $\breve{H}$ between primary states. Thus all states that "couple" to the primary states via $\breve{H}$ are relevant.

Proposition Together with the canonical inner product of Sec. II A, the space Y is a Hilbert space.

This can be shown as follows: An arbitrary element $|p\rangle$ of $\mathcal{P}$ is defined [by definition (1)] by directs sums and products of component states $|\phi_i\rangle$:

$$|p\rangle = |\phi_1\rangle \oplus |\phi_2\rangle \oplus |\phi_3\rangle \otimes |\phi_4\rangle \oplus |\phi_5\rangle \otimes |\phi_6\rangle \oplus |\phi_7\rangle \otimes |\phi_8\rangle \oplus |\phi_9\rangle \otimes |\phi_{10}\rangle. \tag{A2}$$

The component states $|\phi_i\rangle$ are elements of physical Hilbert spaces H_i with given particle number (if the operator sets $\mathcal{A}$ and $\mathcal{B}$ allow). The extended state $|p\rangle$ is thus an element of a composite space C, given by the following direct sum of tensor product spaces:

$$\mathsf{C} = \mathsf{H}_1 \oplus \mathsf{H}_2 \oplus \mathsf{H}_3 \otimes \mathsf{H}_4 \oplus \mathsf{H}_5 \otimes \mathsf{H}_6 \oplus \mathsf{H}_7 \otimes \mathsf{H}_8 \oplus \mathsf{H}_9 \otimes \mathsf{H}_{10}. \tag{A3}$$

Due to its definition by direct sums and tensor products, the space C, with the canonical inner product for sums and products of Hilbert spaces, is a Hilbert space itself. Since the Hamiltonian H is a particle number conserving operator (we only consider non-relativistic systems), the application of H to the component state $|\phi_i\rangle$ will not lead out of the corresponding component space H_i. It is easily seen that also the application of $\breve{H}$ to the extended state $|p\rangle$ then does not lead out of the space C. Thus the above defined linear space Y is a subspace of C. A closed subspace of a Hilbert space, however, is a Hilbert space itself. This concludes the proof of the proposition.

Obviously the given definition of a minimal space Y is not constructive. For most means, however, it is not really necessary to have the minimal space and the space C can be taken instead. A basis of C can be easily constructed from Slater determinantal bases of the component spaces H_i.

APPENDIX B: STATIC PARTICLE-PARTICLE SELF ENERGY FOR ELECTRONS

Here we present all terms of the static particle-particle self energy for Coulomb-interacting electrons. As usual the static self energy is given by

$$\begin{aligned}\mathcal{S}^{(pp)}_{rsr's'}(\infty) &= (a_r^\dagger, a_s^\dagger\,|\hat{H}_1|\,a_{r'}^\dagger, a_{s'}^\dagger) \\ &= \delta_{rr'}v_{ss'} - \delta_{sr'}v_{rs'} - \delta_{rs'}v_{sr'} + \delta_{ss'}v_{rr'} \\ &\quad + (a_r^\dagger, a_s^\dagger\,|\hat{V}|\,a_{r'}^\dagger, a_{s'}^\dagger).\end{aligned} \tag{B1}$$

Evaluating the two-particle interaction part $(a_r^\dagger, a_s^\dagger\,|\hat{V}|\,a_{r'}^\dagger, a_{s'}^\dagger)$ from Eq. (121), we arrive at nine different terms:

$$(a_r^\dagger, a_s^\dagger \,|\hat{V}|\, a_{r'}^\dagger, a_{s'}^\dagger) = A + B + C + D + E + F + G + I + J \\ - (r \leftrightarrow s) - (r' \leftrightarrow s') + (r \leftrightarrow s \,\&\, r' \leftrightarrow s'). \tag{B2}$$

Each of the nine terms also appears with interchanged single-particle indices, which is indicated by the second line of Eq. (B2). The static self energy thereby becomes antisymmetric with respect to interchange within the first or second pair of single particle indices. This antisymmetry is due to the indistinguishable nature of the projectile particles. In the position space notation already used in Sec. VI the nine terms read:

$$A = \frac{\delta_{rr'}\delta_{ss'}}{2|\mathbf{r}-\mathbf{s}|}, \tag{B3}$$

$$B = \delta_{rr'}\delta_{ss'} \int d\mathbf{r}_1 \frac{\rho_{r_1}}{|\mathbf{r}_1-\mathbf{r}|}, \tag{B4}$$

$$C = -\delta_{ss'}\frac{\rho_{rr'}}{|\mathbf{r}-\mathbf{r}'|}, \tag{B5}$$

$$D = -\delta_{ss'}\frac{\rho_{rr'}}{|\mathbf{r}-\mathbf{s}|}, \tag{B6}$$

$$E = -\delta_{ss'}\frac{\rho_{rr'}}{|\mathbf{r}'-\mathbf{s}|}, \tag{B7}$$

$$F = \frac{\gamma_{rsr's'}}{|\mathbf{r}-\mathbf{r}'|}, \tag{B8}$$

$$G = -\rho_{ss'}\frac{\rho^{\varphi}_{rr'}}{|\mathbf{r}-\mathbf{r}'|}, \tag{B9}$$

$$I = -\delta_{ss'} \int d\mathbf{r}_1 \frac{\gamma_{rr_1r'r_1}}{|\mathbf{r}_1-\mathbf{s}|}, \tag{B10}$$

$$J = \delta_{ss'}\rho_{rr'} \int d\mathbf{r}_1 \frac{\rho^{\varphi}_{r_1}}{|\mathbf{r}_1-\mathbf{s}|}. \tag{B11}$$

Here, ρ_r and $\rho_{rr'}$ denote the diagonal and full single-particle density with respect to the target's ground state $|\Psi_0^N\rangle$ as usual. The superscript φ indicates that the density $\rho^{\varphi}_{rr'} = \langle\varphi|\, a_{r'}^\dagger a_r \,|\varphi\rangle$ is taken with respect to the secondary reference wavefunction $|\varphi\rangle$ [see also the definition of the extended states (1)]. For the choice $|\varphi\rangle = |\Psi_0^N\rangle$ it is identical to the common single-particle density and for $|\varphi\rangle = |\text{vac}\rangle$ these terms vanish. The latter choice was taken for the extended particle-particle Green's function of Ref. [10]. The two particle density γ_{ijkl} is defined in Eq. (114).

APPENDIX C: STATIC PARTICLE-HOLE SELF ENERGY FOR ELECTRONS

In this appendix we present the interaction part $(a_p^\dagger, a_q \,|\hat{V}|\, a_{p'}^\dagger, a_{q'})$ of the static particle-hole self energy discussed in Sec. VI C. We assume Coulomb interacting electrons with the usual position space representation (106) of the two-body interaction V. The expression for the interaction part of the static self particle-hole self energy can then be readily evaluated, either from the definitions of the extended states (1) or from Eq. (68):

$$\begin{aligned}
(a_r^\dagger, a_s \,|\hat{V}|\, a_{r'}^\dagger, a_{s'}) = {} & \delta_{rr'}\delta_{ss'} \int d\mathbf{r}_1 \frac{\rho^\varphi_{r_1}}{|\mathbf{r}_1 - \mathbf{r}|} - \delta_{ss'} \frac{\rho^\varphi_{rr'}}{|\mathbf{r} - \mathbf{r}'|} \\
& - \delta_{rr'}\delta_{ss'} \int d\mathbf{r}_1 \frac{\rho_{r_1}}{|\mathbf{r}_1 - \mathbf{s}|} + \delta_{rr'} \frac{\rho_{s's}}{|\mathbf{s} - \mathbf{s}'|} \\
& + \delta_{ss'} \int d\mathbf{r}_1 \frac{\gamma_{rr_1r'r_1}}{|\mathbf{r}_1 - \mathbf{s}|} - \delta_{ss'}\rho_{rr'} \int d\mathbf{r}_1 \frac{\rho^\varphi_{r_1}}{|\mathbf{r}_1 - \mathbf{s}|} \\
& + \delta_{rr'} \int d\mathbf{r}_1 \frac{\gamma_{s'r_1sr_1}}{|\mathbf{r}_1 - \mathbf{r}|} - \delta_{rr'}\rho_{s's} \int d\mathbf{r}_1 \frac{\rho^\varphi_{r_1}}{|\mathbf{r}_1 - \mathbf{r}|} \\
& - \frac{\gamma_{rs'r's}}{|\mathbf{r} - \mathbf{r}'|} + \frac{\rho^\varphi_{rr'}\rho_{s's}}{|\mathbf{r} - \mathbf{r}'|} \\
& - \frac{\gamma_{rs'r's}}{|\mathbf{s} - \mathbf{s}'|} + \frac{\rho^\varphi_{s's}\rho_{rr'}}{|\mathbf{s} - \mathbf{s}'|} \\
& + \frac{\gamma_{rs'r's}}{|\mathbf{r} - \mathbf{s}'|} + \frac{\gamma_{rs'r's}}{|\mathbf{r}' - \mathbf{s}|}.
\end{aligned} \tag{C1}$$

The same nomenclature as in App. B and Sec. VI is used.

---

[1] H. Feshbach, Ann. Phys. (N.Y.) **5**, 357 (1958).
[2] H. Feshbach, Ann. Phys. (N.Y.) **19**, 287 (1962).
[3] H. Feshbach, *Theoretical Nuclear Physics: Nuclear Reactions* (Wiley, New York, 1992).
[4] J. S. Bell and E. J. Squires, Phys. Rev. Lett. **3**, 96 (1959).
[5] M. Namiki, Prog. Theor. Phys. **23**, 629 (1960).
[6] G. Y. Csanak, H. S. Taylor, and R. Yaris, Adv. At. Mol. Phys. **7**, 287 (1971).
[7] H.-D. Meyer, Phys. Rev. A **40**, 5605 (1989).
[8] F. Capuzzi and C. Mahaux, Ann. Phys. (N.Y.) **239**, 57 (1995).
[9] F. Capuzzi and C. Mahaux, Ann. Phys. (N.Y.) **245**, 147 (1996).
[10] J. Brand and L. S. Cederbaum, Ann. Phys. (N.Y.) **252**, 276 (1996).

[11] A. L. Fetter and J. D. Walecka, *Quantum Theory of Many-Particle Systems*, 1st ed. (McGraw-Hill, New York, 1971).
[12] G. Röpke, Ann. Physik **3**, 145 (1994).
[13] G. Röpke, Z. Phys. B **99**, 83 (1995).
[14] J. Dukelsky, G. Röpke, and P. Schuck, Nucl. Phys. A **628**, 17 (1998).
[15] C. Møller and M. S. Plesset, Phys. Rev. **46**, 618 (1934).
[16] O. Christiansen *et al.*, Chem. Phys. Lett. **261**, 369 (1996).
[17] J. Schirmer, L. S. Cederbaum, and O. Walter, Phys. Rev. A **28**, 1237 (1983).
[18] H.-G. Weikert, H.-D. Meyer, L. S. Cederbaum, and F. Tarantelli, J. Chem. Phys. **104**, 7122 (1996).
[19] M. Nooijen and J. G. Snijders, Int. J. Quantum Chem. Symp. **26**, 55 (1992).
[20] J. Schirmer, A. B. Trofimov, and G. Stelter, J. Chem. Phys. **109**, 4734 (1998).
[21] J. Brand and L. S. Cederbaum, Phys. Rev. A **57**, 4311 (1998).
[22] M. Reed and B. Simon, *Functional Analysis*, No. 1 in *Methods of Modern Mathematical Physics* (Academic Press, New York, 1980).
[23] E. Dalgaard, Int. J. Quantum Chem. **15**, 169 (1979).
[24] M. F. Herman, K. F. Freed, and D. L. Yeager, Adv. Chem. Phys. **48**, 1 (1981).
[25] L. S. Cederbaum and W. Domcke, Adv. Chem. Phys. **36**, 205 (1977).
[26] A. Tarantelli and L. S. Cederbaum, Phys. Rev. A **45**, 2790 (1992).
[27] W. Kutzelnigg and D. Mukherjee, J. Chem. Phys. **90**, 5578 (1989).
[28] P. O. Löwdin, Phys. Rev. **139**, 357 (1965).
[29] B. T. Pickup and O. Goscinski, Mol. Phys. **26**, 1013 (1973).
[30] P. Ring and P. Schuck, *The Nuclear Many-Body Problem* (Springer, New York, 1980), p. 623 ff.
[31] D. J. Thouless, Nucl. Phys. **22**, 78 (1961).
[32] D. J. Rowe, Rev. Mod. Phys. **40**, 153 (1968).
[33] J. Schirmer, Phys. Rev. A **26**, 2395 (1982).
[34] F. Tarantelli, private communication.
[35] R. A. Harris, J. Chem. Phys. **50**, 3947 (1969).
[36] A. E. Hansen and T. D. Bouman, Mol. Phys. **37**, 1713 (1979).
[37] J. Schirmer and F. Mertins, J. Phys. B **29**, 3559 (1996).
[38] H.-G. Weikert and L. S. Cederbaum, Few-Body Syst. **2**, 33 (1987).
[39] J. R. Rumble, W. J. Stevens, and D. Truhlar, J. Phys. B **17**, 3151 (1984).
[40] C. A. Weatherford, F. B. Brown, and A. Temkin, Phys. Rev. A **35**, 4561 (1987).
[41] H.-D. Meyer, S. Pal, and U. V. Riss, Phys. Rev. A **46**, 186 (1992).
[42] C. Mahaux and R. Sartor, Nucl. Phys. A **530**, 303 (1991).
[43] M. Müller and L. S. Cederbaum, Phys. Rev. A **42**, 170 (1990).

The Density Matrix Renormalization Group Method: Application to the Low-lying Electronic States in Conjugated Polymers

S. Ramasesha[1] and *Swapan K. Pati*[2]
Solid State and Structural Chemistry Unit
Indian Institute of Science, Bangalore 560 012, India.

Z. Shuai and *J. L. Brédas*
Service de Chimie des Matériaux Nouveaux
Centre de Recherche Electronique et Photonique Moléculaires
Université de Mons-Hainaut, Place u Parc 20, B-7000 Mons, Belgium.

Contents

[1]Also at Jawaharlal Nehru Center for Advanced Scientific Research, Jakkur Campus, Bangalore 560064, India; e-mail: ramasesh@sscu.iisc.ernet.in

[2]Present address: Department of Chemistry, Northwestern University, Illinois 60208; e-mail: pati@chem.nwu.edu

ADVANCES IN QUANTUM CHEMISTRY, VOLUME 38

0065-3276/01 $35.00

1 Introduction

Conjugated organic systems have occupied the centre stage of activity in chemistry over much of this century. This is because of their unique properties such as high reactivity, unusually large anisotropic diamagnetic susceptibility and long wavelength electronic absorption [1, 2]. Theoretical interest in these systems has been fueled by the fascinating resonance structure first proposed by Kekule for the canonical conjugated molecule, benzene. Soon after the advent of quantum mechanics, one of the earliest applications of the quantum chemical techniques was to the study of conjugated molecules [3, 4]. In fact, the model for explaining the increase in wavelength of the optical absorption in conjugated molecules with increasing chain length was the pedagogical particle-in-a-box description. Another focus of interest in the study of conjugated molecules was the equilibrium geometry of infinite polyenes. It is well known that benzene has equal C-C bond lengths while 1,3,5-hexatriene has alternating short and long C-C bonds. A fascinating question that was raised in the context of infinite polyenes was whether the system would behave like benzene or like 1,3,5-hexatriene. Interestingly, while this question was answered by Peierls [5] in the specific case of tight-binding models, the exact answer to this problem in more realistic cases is still being pursued.

In recent years, it has been observed that many conjugated systems can be doped to high electrical conductivities and/or intrinsically possess large luminescence, electroluminescence, and nonlinear optical responses, as well as, in some cases, the ability to lase when optically or electrically pumped [6]. These properties point to the distinct possibility of their role in molecular electronics as well as optoelectronics or photonics devices. In fact, the operation of conjugated polymer-based light emitting diode via a polymer field-effect transistor has already been demonstrated [7]. The large nonlinear optical response could lead to applications in optical limiters and in storage devices which, *e.g.*, use two-photon absorption or the photorefractive effect for read-write operations [8, 9]. Optical switches can be designed using the large nonlinear optical response of conjugated polymers that could lead to applications in optical computing. These interesting possibilities have resulted in an enduring interest

in conjugated polymers and oligomers.

All these properties involve the low-lying π electronic states of these molecules, that thus need to be properly characterized. This review deals with reliable methods of studying the low-lying electronic states and the linear and nonlinear optical responses of conjugated systems.

With the recent advances in quantum chemical techniques, it would appear that dealing with the electronic states of conjugated polymers is but a straightforward application of the methods. Unfortunately, these systems still prove quite elusive for such applications of the standard methods for many reasons. The standard quantum chemical techniques such as the Hartree-Fock and density functional methods are best suited for the study of the ground state properties of molecules. However, most of the interesting properties exhibited by conjugated polymers involve excited states. Furthermore, the conjugated polymers show evidence for the presence of strong electron-electron repulsions. This implies that we have to carry out fairly extensive configuration interaction (CI) calculations for obtaining reliable excited states. If all the valence orbitals of the polymers are included in a quantum chemical calculation, then the space of configuration functions would increase beyond manageable limits even for small polyenes. Yet, restricting the configuration space to just singly or doubly excited configurations would imply absence of size consistency. Since the longest oligomers experimentally studied are often longer than those that can be handled by quantum chemical techniques, one often resorts to extrapolating properties computed for short oligomers. The absence of size consistency then would lead to unreliable extrapolation of the properties even for the low-lying excitations.

There do exist recent quantum chemical techniques which are size consistent. Among them, the Random Phase Approximation (RPA), its variants such as the Second-Order Polarization Propagator Approximation (SOPPA) [10], and the Coupled Cluster Approximation (CCA) [11] are the most prominent and being widely used. In the SOPPA method, electron correlation effects are included in the two-particle polarization propagator to second order. The coupled cluster method uses an exponential *ansatz* through which higher-order exci-

tations are included as multiples of singles, doubles and a few higher-order excitations. These methods can be viewed as approximations to the full CI in molecular orbital formulation. For relatively strong correlated systems, these methods fail to describe properly the electronic properties, especially for the electronic and optical excitations [12]. In principle, one can increase the number of excitations going beyond double, triple, and quadruple excitations, yet the numerical performance does limit such expansions, in addition to the algebraic complexity.

The problem of obtaining size consistent and reliable excited states in large oligomers of conjugated molecules can be overcome to some extent by using several strategies. Firstly, we know that the "action" in conjugated polymers is mainly confined to the π electrons. Thus, it would be sufficient to deal with the π system, albeit as accurately as possible. To deal with the large π systems with great accuracy, we need to devise techniques that go beyond the conventional quantum chemical methods which usually have their origin in either a restricted variational CI method or a many-body perturbation method. In the next two sections, we give a brief introduction to the model Hamiltonians that have been largely employed for the study of conjugated molecules. In section 4, we describe an innovative way for solving the model Hamiltonians, which goes beyond the conventional techniques and is based on the Density Matrix Renormalization Group (DMRG) theory. Various applications of DMRG to the electronic structure of π-conjugated chains are described in the following sections.

2 Model Many-Body Hamiltonians for π Conjugated Systems

The valence orbitals of the conjugated systems can be classified into two categories: the σ orbitals and the π-orbitals. The σ orbitals have very strong overlaps leading to a large covalent splitting of the molecular orbitals (MOs). The bonding MOs are usually fully occupied and the antibonding MOs are well separated from these on the energy scale. The π-orbitals on the other hand have weaker overlaps and hence the bonding and antibonding MOs of the π system are

located closer to the zero of energy defined by the fully dissociated system. Thus, chemists have long focussed on the π molecular orbitals for studying properties of conjugated molecular systems. The validity of the σ - π separability was a topic of intense study and it is generally found to be valid for low-energy excitations in extended systems wherein the energy scales of the σ and π MOs are well separated. This review deals with the electronic structure and properties of the systems where π-electrons play the leading role. Hence, our discussion will be restricted to π-electron Hamiltonians.

The second quantized Hamiltonian for the π-electron system of a conjugated molecule can be written in the form [2]

$$\hat{H}_\pi = \hat{H}_{One-electron} + \hat{H}_{Two-electron} \tag{1}$$

The one-electron part is approximated by assuming that the π-electrons move in an effective field of the nuclear attraction and the electron repulsion of all the remaining electrons. The two-electron part corresponds to the electron-electron repulsion experienced by the π-electrons amongst themselves [13]. The one-electron part is further assumed to be represented by a Hamiltonian matrix $h_{\mu\nu}$. The two-electron part, for the present is assumed to consist of all possible repulsion integrals. With this, the above Hamiltonian can be written as:

$$H_\pi = \sum_{\mu\nu} h_{\mu\nu}\hat{E}_{\mu\nu}$$
$$+1/2 \sum_{\mu\nu\mu'\nu'} [\mu\nu|\mu'\nu'](\hat{E}_{\mu\nu}\hat{E}_{\mu'\nu'} - \delta_{\nu\mu'}\hat{E}_{\mu\nu'}) \tag{2}$$

$$\hat{E}_{\mu\nu} = \sum_\sigma \hat{a}^\dagger_{\mu,\sigma}\hat{a}_{\nu,\sigma} \tag{3}$$

where $\hat{a}^\dagger_{\mu,\sigma}(\hat{a}_{\mu,\sigma})$ corresponds to creation (annihilation) of an electron with spin σ in the μ^{th} π-orbital and the two-electron integrals $[\mu\nu|\mu'\nu']$ are given in the charge cloud notation.

2.1 The Hückel Model

The Hückel model [3] was the earliest π-electron model. Here, the two-electron integrals are completely neglected. Furthermore, the

Hamiltonian matrix of the one-electron part is assumed to have nonzero elements only along the diagonal and for the pair of π-orbitals μ, ν, which are on neighboring carbon atoms. To simplify further, these integrals are treated as phenomenological parameters. Thus, in the case of benzene, the nonzero off-diagonal elements are all assumed to correspond to a parameter β known as the resonance (or transfer) integral and the diagonal elements are assumed to be another parameter α, known variously as the orbital energy, site energy, and Coulomb integral. Since in benzene, all carbon atoms are in identical environments, the site energy can be set to zero without losing any physical content in the model. The second quantized form of the Hückel Hamiltonian is given by:

$$\hat{H}_{Huckel} = \sum_{\mu\sigma} \alpha_\mu \hat{a}^\dagger_{\mu\sigma} \hat{a}_{\mu\sigma} + \sum_{<\mu\nu>\sigma} t_{\mu\nu} (\hat{E}_{\mu\nu} + h.c.) \qquad (4)$$

where α_μ is the orbital energy (Coulomb integral) at site μ and $t_{\mu\nu}$ is the resonance (transfer) integral between bonded sites, *h.c.* stands for Hermitian conjugate and the summation, $< \mu\nu >$, is over all bonded sites. The Hückel Hamiltonian has been widely used because of its simplicity and the physical insight it can often provide[14, 4]. The early major successes of this model have been that (i) it provides the theoretical basis for the $(4n + 2)$ rule of aromaticity in conjugated ring systems; and (ii) it explains the *red-shifts* in the optical spectra of conjugated systems with increase of conjugation length. However, the Hückel model also suffers from a lot of drawbacks as it fails to explain many of the qualitative and quantitative features of conjugated systems [15].

The Hückel model as applied to polyenes possesses a symmetry known as alternancy symmetry, since the polyene system can be subdivided into two sublattices such that the Hückel resonance integral involves sites on different sublattices. In such systems, the Hamiltonian remains invariant when the creation and annihilation operators at each site are interchanged with a phase of +1 for sites on one sublattice and a phase of -1 on sites of the other. Even in interacting models this symmetry exists when the system is half-filled. The alternancy symmetry is known variously as electron-hole symmetry or charge-conjugation symmetry [16].

The existence of alternancy symmetry leads to very strong predictions concerning the electronic properties of the system. For instance, it imposes that the lowest energy excitation is dipole allowed. However, in long polyenes, there is unambiguous experimental evidence for states below the lowest dipole-allowed excited state [17]. The alternancy symmetry also predicts that in polyene radicals (with an odd number of carbon atoms), the spin density should reside on only one sublattice and that the spin density on the other sublattice be strictly zero. However, electron spin resonance experiments indicate the presence of spin density on both sublattices, with the spin projections on the sites of one sublattice being opposite in direction to those of the sites belonging to the other sublattice [18].

Besides these qualitative differences, there also exist quantitative discrepancies between the Hückel model for polyenes and the experimental observations. The Hückel theory predicts an order of magnitude larger oscillator strength in the absorption to the lowest dipole allowed state [4]. The bond length alternation required to fit the optical gap in polyenes within a Hückel model is twice the experimentally observed bond alternation. Thus, the Hückel model is mainly of pedagogical interest and one needs to go beyond it for dealing accurately with realistic conjugated systems.

2.2 The Hubbard Model

While the Hubbard model can be derived from the Hamiltonian in eqn.(2), the model was invented in an entirely different context, independently by Kanamori [19], Gutzwiller [20] and Hubbard [21]. It was first introduced to explain ferromagnetism in metals. While the simple Hubbard model is now known not to have a ferromagnetic ground state (except in some pathological cases [22]), it has become one of the most widely studied models in the context of metal-insulator transitions [23, 24].

The Hubbard model can be derived from eqn.(2) by: (i) making a zero differential overlap (ZDO) approximation; and (ii) by assuming the range of Coulomb interactions to be truncated to just on-site repulsion by virtue of strong shielding of the interactions by the conduction electrons in metals. The ZDO approximation [25] restricts the nonzero electron repulsion integrals to those of the form

$[\mu\mu|\nu\nu]$. That is to say, the two-electron integrals are nonzero only when charge density of one electron resides completely in an orbital μ and that of the other in orbital ν. As the Hubbard model further restricts the nonvanishing two-electron integrals to the type $[\mu\mu|\mu\mu]$, it can therefore be written as:

$$\hat{H}_{Hubbard} = \hat{H}_{Huckel} + \frac{U}{2}\sum_{\mu}\hat{n}_{\mu}(\hat{n}_{\mu} - 1) \tag{5}$$

where $\hat{n}_{\mu}$ is the number operator at site μ and U is the on-site electron repulsion integral which is phenomenologically taken as the absolute difference of ionization potential and electron affinity of the atom. In its simplest form, the Hubbard model is a one-parameter model involving U since all the energies can be scaled in units of the uniform transfer (resonance) integral t. As can be seen from this model, the electrons try to reduce their kinetic energy *via* delocalization through the transfer term (first term) while in the process they pay an energy overhead U, whenever a doubly occupied site results. Thus, this model incorporates electron repulsion at the crudest level and has been used to study metal-insulator transitions.

The model has been exactly solved in one-dimension [26] for arbitrary band-filling. The results indicate that the ground state for a half-filled Hubbard band is insulating for any nonzero U. The ground state is found to be a spin singlet. The lowest triplet state is degenerate with the singlet state in the limit of infinite chain length. However, there is a finite optical gap (the energy difference between the ground state and the lowest dipole- coupled state), which is given as a function of U as:

$$\Delta E = U - 4t - 8t\sum_{n=1}^{\infty}(-1)^n[(1 + \frac{1}{4}n^2U^2)^{\frac{1}{2}} - \frac{1}{2}nU] \tag{6}$$

The Hubbard model, being the simplest model which incorporates the essence of electron correlations, has been intensively studied for more than three decades [27]. However, even in the one-dimensional case, our understanding of the model is far from complete.

2.3 The Pariser-Parr-Pople (PPP) Model

The Hamiltonian that can be obtained from eqn.(2) by employing the ZDO approximation was derived independently by Pariser and Parr

[28] and by Pople [29] almost a decade before the Hubbard model. This model has been the standard model for a serious study of the electronic states of conjugated systems. It is also appropriate to use a site chemical potential in the intersite interaction part such that all the carbon sites remain electrically neutral when singly occupied. This is achieved by setting z_μ to 1 in the Hamiltonian given below:

$$\hat{H}_{PPP} = \hat{H}_{Hubbard} + \sum_{\mu>\nu} V_{\mu\nu}(\hat{n}_\mu - z_\mu)(\hat{n}_\nu - z_\nu) \tag{7}$$

In keeping with the spirit of phenomenology associated with the PPP Hamiltonian, the off-site electron repulsion integrals, $V_{\mu\nu}$, are interpolated smoothly between U for zero intersite separation and e^2/r_{12} for the intersite separation tending to infinity, and explicit evaluation of the repulsion integrals is thus bypassed. There are two widely used interpolation formulae given by Ohno and Klopman [30] and by Mataga and Nishimoto [31]. In the Ohno interpolation scheme, the intersite electron repulsion integrals, $V_{\mu\nu}$, are given by:

$$V_{\mu\nu} = 14.397[\frac{28.794}{(U_\mu + U_\nu)^2} + r_{\mu\nu}^2]^{-1/2} \tag{8}$$

where $r_{\mu\nu}$ is the distance between site μ and ν. The Mataga-Nishimoto interpolation formula gives:

$$V_{\mu\nu} = [\frac{2}{(U_\mu + U_\nu)} + r_{\mu\nu}]^{-1} \tag{9}$$

In both cases, it is assumed that $r_{\mu\nu}$ is in $\AA$ and U and V are in eV.

The repulsion potential given by Ohno decays more rapidly than that of Mataga-Nishimoto. Unlike the Hubbard model, the PPP model has not been solved analytically, in any limit. Even numerically exact solutions of the model are restricted to systems with about sixteen orbitals at half-filling. The parameters of the model for systems with carbon and nitrogen atoms in conjugation are fairly well standardized. The model has been successfully used in studying the low-energy excitation spectrum of a large number of interesting conjugated systems [32, 33]. The model is found to be capable

of providing quantitative results which are in good agreement with experiments.

There exist a few studies of models in which the ZDO approximation is not fully implemented. In these models, terms of the type $[\mu\nu|\mu'\nu']$ and $[\mu\mu|\mu'\nu']$ where the pairs $\mu\nu$ and $\mu'\nu'$ correspond to nearest neighbours have been included. These terms are known as bond-bond repulsions and charge-bond repulsions respectively. However, these models lack the generality to be considered as basic models of conjugated systems.

2.4 The "U-V" Model

In the physics literature, the model invented to go beyond the severely truncated electron-repulsion range of the Hubbard model has been the extended Hubbard Hamiltonian or the "U-V" model. Here, the intersite interactions are introduced between bonded sites through another independent phenomenological interaction parameter V [26] from which the model derives its name. The Hamiltonian is given by:

$$\hat{H}_{UV} = \hat{H}_{Hubbard} + \sum_{<\mu\nu>} V(\hat{n}_\mu - z_\mu)(\hat{n}_\nu - z_\nu) \qquad (10)$$

This model, first proposed in the context of organic semiconductors, has the advantage of retaining the range of the interaction at the same level even as the system size is increased [34]. In the PPP model, an increase in system size leads to new longer range interactions appearing in the Hamiltonian, thereby making a systematic study with increasing system size less reliable.

The "U-V" Hamiltonian contains the essential physics necessary to model insulators and semiconductors [35]. For a half-filled band, this model makes some qualitatively new predictions [36, 37]. In the parameter range, $0 \leq V < U/2$, for any given U, antiferromagnetic correlations dominate and the ground state is described by a spin-density wave (SDW) state. However, for $V > U/2$, charge correlations dominate and the ground state is described by a charge density wave (CDW) state, namely, opposite charge resides on the neighbor site (favoring V term) stabilizes the ground state. It is, however, not clear whether the transition between SDW and CDW phases is first-order or second-order for $U = 2V$. The lowest energy

optical excitation occurs at an energy $(U - V)$ in the limit $U \longrightarrow \infty$ and the nature of this excitation is qualitatively different from that in the Hubbard model. In the "U-V" model, this excitation consists of an electron and a hole residing on nearest neighbour sites and is called an exciton. In fact, the "U-V" model is the minimal model which allows a bound electron-hole pair in real space with its energy lower than the band edge of the one-electron and one-hole continuum. The edge of the continuum lies at energy U and the continuum consists of band-like optical excitations [38] for which the electron and the hole are separate free carriers.

2.5 The Heisenberg Model

In the limit of very large U of the Hubbard model at half-filling, we can expect all the sites to be singly occupied. Furthermore, the energy of all such states in which the sites are singly occupied is the same. When the transfer term is introduced as a perturbation, the degeneracy of the ground state is not lifted in first order since the transfer term does not connect states with same site occupancies. However, in second order, the degeneracy is lifted by terms involving virtual transfer of electron between the covalent ground state manifold and the singly ionic excited state manifold. The matrix encountered in the second-order degenerate perturbation theory for the case of the one-dimensional Hubbard chain is found to be identical to the matrix representation of a spin Hamiltonian given by:

$$H_{Heisenberg} = \sum_{<\mu\nu>} J_{\mu\nu}(\mathbf{S}_\mu \cdot \mathbf{S}_\nu - 1/4) \qquad (11)$$

with $J = 4t^2/U$. This spin Hamiltonian is the familiar Dirac-Heisenberg Hamiltonian [39]. The Heisenberg Hamiltonian does not allow for a simple analytic solution but the ground and a few elementary excitations can be obtained using the approach of Bethe which has now come to be known as the Bethe *ansatz* [40] in the special case of one site per unit cell. The ground state is a singlet state with energy per site $(-ln2 + 1/4)$ in units of J [41]. The higher spin excited states have zero gap to the ground state in the thermodynamic limit [42].

Neither the Hubbard model nor the Heisenberg model have analytic solutions even for the ground state in higher than one dimension

or for that matter, even when the restriction to one site per unit cell is removed in one dimension.

3 Methods for Solving Model Many-Body Hamiltonians

The study of model Hamiltonians of correlated electrons is a very difficult problem. There does not exist any well-controlled analytical technique to analyze them reliably, except in limiting cases such as in the weak correlation limit or the very narrow band limit. Mean-field and variational calculations can often lead to unphysical solutions and fare very poorly while describing excited states of the system. These difficulties have led numerous groups worldwide to develop reliable nonperturbative numerical methods. It is now clear that considerable progress can be made towards the goal with the help of computers at least in the study of quasi-one- dimensional correlated electron systems. In this section, we will discuss the diagrammatic valence bond (VB) method which has been widely used for exactly solving small conjugated systems and briefly touch upon the Quantum Monte Carlo method which has been used extensively in recent times in the study of Hubbard and "U-V" models mainly in two-dimensions. Other conventional techniques such as restricted CI, perturbation and coupled cluster techniques will not be discussed here.

The Fock space dimensionality is finite when one deals with finite model systems. Thus, it appears that we can solve the model Hamiltonians exactly for finite systems and from the finite system properties, infer the behaviour of the system in the thermodynamic limit by suitable scaling techniques. However, the dimensionality increases as $(2S+1)^N$ for a spin-S chain and as 4^N for fermions, where N is the number of sites. Thus, it is very difficult to carry out brute force numerical computations on a large system and the exact diagonalization studies are primarily restricted to quasi-one-dimensional systems with very few sites per unit cell.

Even in the simplest cases, to be able to extrapolate properties to the thermodynamic limit, we need to extend the exact diagonalization technique to the very limit. This involves exploiting all the

symmetries of the model Hamiltonians discussed in the previous section in order to reduce the Hilbert space dimensionalities (as against the Fock space dimensionality) in each of the subspaces, for a given system size. For example, the Hamiltonians discussed above conserve S_{tot} (total spin of the system), S^z_{tot} (z-component of the total spin), while the Fermion models also conserve the total number of particles, M. Thus, one can choose a particular subspace, labelled by these quantum numbers and work in a Hilbert space of smaller dimensions. The general numerical approach for the exact solution of a finite many-body Hamiltonian involves choosing an appropriate many-body basis set and setting up the Hamiltonian matrix in the desired subspace within that basis.

3.1 Diagrammatic Valence Bond Method

An exact diagonalization scheme that has been employed widely is the valence bond (VB) method and the implementation of the method in the form described below, was first carried out by Soos and Ramasesha [43] in 1983. In this method, the Hamiltonian matrix is set-up in the VB basis. The VB method bypasses the cumbersome ways of constructing spin-adapted basis functions such as the symmetric group method and the unitary group method. The VB functions are, however, non-orthogonal although complete and linearly independent. In general, this leads to a nonsymmetric representation of the Hamiltonian matrix [44]. The nonsymmetric form of the Hamiltonian matrix is not particularly disadvantageous as will become evident in the forthcoming discussion.

Given the number of sites, N, the number of electrons, M, S (total spin) and M_s (z-component of the total spin), it is straightforward to construct a VB basis. It involves explicit spin pairing of electrons which have opposite spins. This process, however, in general leads to an overcomplete basis since the number of explicit spin pairs clearly exceeds the dimensionality of the Hilbert space for a given N, M, S and M_s set as given by the Weyl dimensional formula. The overcompleteness can be avoided easily, by using the Rumer-Pauling rules [45, 46] the details of which can be found in [44]. It is possible to exploit the spatial symmetries of the system in VB theory [47]. Besides spatial and spin symmetries, certain systems can be considered

as bipartite lattices. For such systems, at half-filling, we can also exploit the alternancy symmetry of the Hamiltonian. This symmetry divides the Hilbert space into *ionic* and *covalent* spaces. The ionic space *does not* contain VB diagrams in which every site occupancy is exactly one while the covalent space contains all such diagrams besides the ionic diagrams in appropriate linear combinations.

The VB basis (as also a constant M_s basis) states are represented as integers on a computer. For the fermionic models, we associate each fermionic site with two bits. In our notation, "11"represents a site which is doubly occupied, "00" denotes an empty site. "10" corresponds to the beginning of a singlet line or a site which contains an unpaired up spin while "01" represents the ending of a singlet line or an unpaired down spin. The Rumer-Pauling rules lead to an unique association between a 2N bit integer and the VB diagram corresponding to an S, M_s and M value. For spin Hamiltonians, just one bit per site is sufficient to represent a VB diagram as there do not exist empty or doubly occupied sites. The bit representation allows extremely rapid generation of the integers associated with VB diagrams. These integers are generated in an ascending order to facilitate the binary search, which allows for rapid setting up of the Hamiltonian matrix. The Hamiltonian matrix is constructed by sequentially operating with the Hamiltonian on each state of the VB basis. The resulting Hamiltonian matrix is usually very sparse and exploiting the sparseness reduces both the CPU times and the storage requirement in obtaining a few low-lying eigenstates.

As we are dealing with a non-orthogonal basis set, we obtain a non-symmetric Hamiltonian matrix. To solve for the eigenvalues of this non-symmetric matrix, Rettrup's modification of Davidson's algorithm for nonsymmetric matrices is used to obtain a few low-lying eigenvalues and corresponding eigenvectors of the system [48].

The major problem with exact diagonalization methods is the exponential increase in dimensionality of the Hilbert space with the increase in the system size. Thus, the study of larger systems becomes not only CPU intensive but also memory intensive as the number of nonzero elements of the matrix also increases with system size. With increasing power of the computers, slightly larger problems have been solved every few years. To illustrate this trend, we consider the case

of the spin-1 Heisenberg chain. In 1973, ten years before the Haldane conjecture, De Neef [49] used the exact diagonalization procedure to solve a 8-site chain. In 1977, Blote [50] diagonalized the Hamiltonian of a chain of 10 sites. In 1982, Botet and Jullien [51] increased this to 12 sites. In 1984, Parkinson and Bonner [52] solved the 14-site spin-1 problem. In the same year, Moreo [53] solved the 16-site spin-1 chain. In 1990, Takahashi [54] pushed this up to 18 sites. And in 1994, Golinelli *et al.* [55] have solved for the low-lying states of a 22-site spin-1 chain. The growth in chain length of the longest spin-1 chain solved is almost linear with time, roughly increasing by 2 sites in every three years. Just to remind ourselves, the Fock space dimensionality increases as 3^N with chain length N. The size of the matrix also increases similary and the CPU and storage scale quadratically in the size of the matrix, if we are targeting only a few eigenstates. Currently, a sixteen-carbon polyene can be studied within a PPP model using the VB technique to obtain a few exact low-lying states of the Hamiltonian in different subspaces. The singlet space of this system is spanned by about 35 million VB states. In fact, a similar number of VB states span the singlet subspace of the 32-spin Heisenberg system.

The exact diagonalization method has been widely exploited in the study of polyenes as well as small conjugated molecules. It has also been employed in studying spin systems and systems with interacting fermions and spins such as Kondo lattices. These studies have been mainly confined to low- dimensions. The exact diagonalization techniques also allow bench-marking various approximate many-body techniques for model quantum cell Hamiltonians.

3.2 Quantum Monte Carlo Methods

Another technique which has gained prominence in recent years is the Quantum Monte Carlo (QMC) technique. This technique maps a d-dimensional quantum model onto a $d+1$ dimensional classical model via a Trotter decomposition of the partition function or the ground state projection operator [56, 57]. The quantum model is then studied by performing a Monte Carlo sampling procedure on the classical model in higher dimension. For fermions, the mapping of the interacting quantum model system to the classical system could

be effected via a discrete Hubbard-Stratanovich tranformation which replaces each interaction term in the Hamiltonian by a noninteracting term in the presence of a fluctuating Bosonic field provided by a S=1/2 Ising spin [58]. The size of the classical lattice that is simulated thus depends upon the number of interactions present in the Hamiltonian as well as the temperature of simulation. For obtaining ground- state properties, the simulation needs to be carried out at very low temperatures. Thus, the number of discrete steps along the Trotter axis increases as the temperature is lowered. For the Hubbard model, the number of Ising-fields per interaction is one while for every intersite interaction the number of Ising-fields encountered is four. Thus, the QMC method is best suited for Hubbard models. The QMC technique is basically a ground-state technique. While it is possible to obtain excited states of the systems by using symmetrized sampling procedures, it could turn out to be very CPU intensive [59]. Besides, away from half-filling, the QMC technique also suffers from the 'negative' sign problem. While the latter can be controlled to some extent by using schemes such as the constrained-path QMC simulations [60], the problem is endemic to fermion systems. The QMC method has been mainly employed in the simulation of higher dimensional Hubbard models and in some cases, "U-V" models for system sizes of $\sim 10^2$ sites [61].

4 DMRG Method

The method which held the promise of overcoming the difficulty of exploding dimensionalities is the renormalization-group technique in which one systematically throws out the degrees of freedom of a many-body system. While this technique found dramatic success in the Kondo problem [62], its straightforward extension to interacting lattice models was quite inaccurate [63].

Recently, the key problems associated with the failure of the old RG method have been identified and a different renormalization procedure based on the eigenvalues of the many-body density matrix of proper subsystems has been developed [64, 65]. This method has come to be known as the density matrix renormalization group (DMRG) method and has found dramatic success in dealing with

quasi-one-dimensional many-body Hamiltonians. Here, we will discuss first the standard real-space quantum RG method and then we will introduce the DMRG method.

4.1 Standard real-space quantum RG procedure

In this approach, one begins by subdividing the total system into several blocks A_n and proceeds to iteratively build effective blocks so that at each iteration, each effective block represents two or more blocks of the previous iteration, without increasing the Fock space dimensionality of the blocks from what existed at the previous iteration. Usually, one starts with each A_n consisting of a single site. Since the Hilbert space grows exponentially with the increase in system size, one truncates the number of states kept at each iteration. The quantum RG procedure proceeds as follows:

1. Choose p consecutive blocks $A_i^{(0)}$, $A_{i+1}^{(0)}$, $A_{i+2}^{(0)}$, ..., $A_{i+p-1}^{(0)}$ from the set $A_n^{(0)}$.

2. Construct the Hamiltonian matrices, $H_{A_i^{(0)},A_{i+1}^{(0)},A_{i+2}^{(0)},\ldots,A_{i+p-1}^{(0)}}$ from Hamiltonian matrices of the individual blocks, $A_i^{(0)}$, $A_{i+1}^{(0)}$, $A_{i+2}^{(0)}$, ..., $A_{i+p-1}^{(0)}$ and the matrices of relevant site operators appearing in the interblock terms in the Hamiltonian consisting of the chosen blocks i, $i+1$, $i+2$, ..., $i+p-1$.

3. Diagonalize the Hamiltonian, $H_{A_i^{(0)}A_{i+1}^{(0)}A_{i+2}^{(0)}\ldots,A_{i+p-1}^{(0)}}$ and obtain m eigenvectors corresponding to the m lowest energy states.

4. Take the new block $A_i^{(1)}$ to be represented by the diagonal matrix which has the m lowest energy eigenvalues on the diagonal.

5. Transform all the operators corresponding to the block such as the creation and annihilation operators, number operators, spin operators etc., to the basis of the m chosen eigenvectors.

6. Go to (1) and iterate until the energy/site converges.

The main reason for the failure of this method is the choice of the states retained at each stage of the iteration as discussed by White

and Noack [64]. It can be shown that retaining only the ground states or a few eigenstates of the Hamiltonian of p-blocks is not sufficient to construct the ground state of the full Hamiltonian. This problem can be overcome to some extent by choosing to retain eigenstates of the p-block Hamiltonian obtained from different boundary conditions imposed upon the block. This is, however, a cumbersome procedure for dealing with interacting model Hamiltonians [64].

4.2 Truncation scheme based on density matrix eigenvalues

S.R. White [65], in 1992, introduced a completely different truncation procedure than the one that was used in the old quantum RG procedures. White recognized that the weakness of the old RG procedure was in the truncation of the Fock space of a block based on the eigenvalues of the block Hamiltonian being renormalized. He replaced this choice by the eigenvalues of the reduced density matrix of the block constructed from the desired state of the full Hamiltonian. The truncated Fock space is now spanned by the m eigenvectors of the reduced density matrix of order $l \times l$ corresponding to the m *highest* eigenvalues of the reduced density matrix. The reason for choosing the eigenvalues of the reduced density matrix as a criterion for implementing a cut-off is that, the larger the density matrix eigenvalue, the larger is the weight of the eigenstate of the density matrix in the expectation value of any property of the system. This result becomes evident when all the dynamical operators are expressed as matrices in the basis of the eigenvectors of the density matrix. The expectation value of any operator $\hat{A}$ is simply:

$$< \hat{A} >= \sum_i A_{i,i}\rho_i / \sum_i \rho_i \tag{12}$$

where ρ_i is the density matrix eigenvalue and the larger ρ_i, the larger is its contribution to the expectation value.

The many-body density matrix of a part of the system can be easily constructed as follows. Let us begin with given state $|\psi >_S$ of S, which is called the *universe* or *superblock*, consisting of the system (which we call a block) A and its *environment* A'. Let us assume that the Fock space of A and A' are known, and can be labelled as $|i >_A$

and $|j>_{A'}$. The representation of $|\psi>_S$ in the product basis of A and A' can be written as:

$$|\psi>_S = \sum_{i,j} \psi_{i,j} |i>_A \times |j>_{A'} \tag{13}$$

where we assume the coefficients $\psi_{i,j}$ to be real, without loss of generality. Then the reduced many-body density matrix for block A, is defined as:

$$\rho_{k,l} = \sum_j \psi_{k,j} \psi_{l,j}$$

The eigenvalue, ρ_i of the density matrix ρ, gives the probability of finding the corresponding eigenstate $|\mu_i>_A$ in the projection of $|\psi>_S$ on block A. It therefore follows that the eigenvectors with highest eigenvalues of the density matrix of A, are the optimal or most probable states to be retained while the system is augmented.

In the early literature in quantum chemistry, the eigenvectors corresponding to large eigenvalues of one-particle density matrices were employed as the orbital basis for carrying out a configuration interaction (CI) calculation. The eigenvectors of the density matrix were called the 'natural' orbitals and it was observed that the CI procedure converged rapidly when the 'natural' orbitals were employed in setting up the Slater determinants [66].

The DMRG scheme differs from the 'natural' orbital scheme in two important respects: (i) the reduced density matrices are many-body density matrices and (ii) the size of the system in terms of the number of sites being studied at each iteration is usually augmented by two sites. However, the Hamiltonian matrix that one encounters from iteration to iteration, remains roughly of the same order while the matrix elements keep changing. In this sense, the procedure can be called a renormalization procedure. The coupling constants (the Hamiltonian matrix elements) keep changing while the system size increases, as in the RG procedure carried out within a blocking technique.

4.3 Implementation of the DMRG method

We now describe the procedure to carry out the computations. One starts the computation with a small size system, $2n$, which can be exactly solved, $1 \leq n \leq 4$, depending on the degree of freedom at each site. By exact diagonalization, one gets the desired eigenstate of that system. The density matrices of the left and right blocks, each consisting of n sites (in principle it is not necessary to have the same number of sites for the two blocks, although in practice this is what is most generally used), are obtained from the desired eigenstate. The density matrices are diagonalized and at the first iteration usually all the density matrix eigenvectors (DMEV) are retained. The Hamiltonian matrix of the left and right blocks (denoted A and A') obtained in any convenient basis are transformed into the density matrix eigenvector basis. So also are the matrices corresponding to the relevant site operators in both blocks. Now, the iterative procedure proceeds as follows:

1. Construct a superblock $S = A \bullet \bullet A'$, consisting of the block A, two additional sites σ and σ' and the block A'. Thus, at the first iteration, the system S has (2n+2) sites.

2. Set up the matrices for the total Hamiltonian of the superblock S in the direct product basis of the DMEV and the Fock space states of the new sites.

3. Diagonalize the superblock S to find the desired eigenstate $|\psi>$. At this point, expectation values of the various operators of interest can be evaluated.

4. Construct the reduced many-body density matrix, ρ, for the block $A\bullet$. If the system does not possess reflection symmetry, construct the density matrix, ρ', for the right block $\bullet A'$ as well.

5. Diagonalize the density matrix, ρ (and if necessary ρ'). Usually, the density matrix is block-diagonal in the number operator corresponding to the block and in the $z-$ component of the total spin of the block. Exploiting the block diagonal form of the density matrix while diagonalizing it proves to be computationally efficient. Construct a nonsquare matrix $\mathbf{O}$, with

m columns, each column being an eigenvector of the density matrix corresponding to one of the m largest eigenvalues. The number of rows in the matrix **O** corresponds to the order of the density matrix.

6. Construct the matrices corresponding to the Hamiltonian, $H_{A\bullet}$, of the new left block $A\bullet$, and the site creation operators of all the necessary sites. That of the annihilation operators are simply the adjoints of the creation operators. It is some times computationally efficient to store matrices of operators such as occupation number and site spin operators, although these can be computed from the matrices for the site creation operators.

7. Renormalize all the matrices corresponding to the block and site operators by using the RG transfomation matrix **O** [eg: $\tilde{H}_{A\bullet} = OH_{A\bullet}O^{\dagger}$]. The resulting renormalized matrices are of order $m \times m$ and the procedure amounts to simultaneous change of basis and truncation.

8. Replace the block A by $A\bullet$. If the system does not possess reflection symmetry, replace A' by $\tilde{A}'\bullet$.

9. Go to step 1.

Using the block-diagonal nature of the density matrix, besides reducing the requirement in CPU time, also allows one to label the DMEV by the appropriate particle number(n_e) and the $z-$ component of the total spin of the block ($M_{s,A}$). The Fock space of the individual sites that are added at each iteration are eigenstates of the site spin and number operators. This allows targeting a definite particle number (N_e) and a definite projected spin (M_s) state of the total system.

At this point it is useful to pause and describe the notation we have used for various states. A state of $A\bullet$ is given by the tensor product of a state of A with quantum number q and an index i, and a state σ of the additional site. Thus,

$$|q, i, \sigma >_{A\bullet} = |q, i >_A \times |\sigma > \qquad (14)$$

A state of a superblock $S = A \bullet \bullet A'$ is given by:

$$|q_A, \mu, \sigma; q_{A'}, \nu, \tau >= |q_A, \mu, \sigma >_{A\bullet} \times |q_{A'}, \nu, \tau >_{\bullet A'} \qquad (15)$$

The eigenstate of the Hamiltonian of the super-block can be written as:

$$|\psi >_S = \sum_{q_A, q_{A'}, \mu, \nu, \sigma, \tau} \psi_{\mu,\nu}^{q_A, q_{A'}, \sigma, \tau} |q_A, \mu, \sigma; q_{A'}, \nu, \tau >_S \qquad (16)$$

The density matrix for $A\bullet$ then will have a block structure and can be expressed as

$$\rho_{\mu,\nu}^{q_A,\sigma} = \sum_{q_{A'}, \mu', \tau} \psi_{\mu,\mu'}^{q_A, q_{A'}, \sigma, \tau} \psi_{\nu,\mu'}^{q_A, q_{A'}, \sigma, \tau} \qquad (17)$$

The above algorithm is called the infinite lattice DMRG algorithm because this procedure is best suited for the system in the thermodynamic limit, *i.e.*, when the properties of the system are extrapolated to the infinite system-size limit.

4.4 Finite lattice DMRG algorithm

If we are interested in accurate properties of the system at a chosen size, then it is possible to improve upon the accuracies obtainable from the infinite DMRG procedure. This involves recognizing that the reduced many-body density matrices at each iteration correspond to a different system size. For example, when we carry out the DMRG procedure to obtain the properties of a system of $2M$ sites, at an iteration corresponding to $2p$ sites ($n \leq p \leq M$), the reduced density matrix we construct is that of a block of p sites in a system of $2p$ sites. However, if our interest is in the $2M$-site system, we should employ the density matrix of the block of p sites in a $2M$-site system. It is possible to construct, iteratively, the p-site reduced density matrix of the $2M$-site system. This is achieved by the so called finite-size algorithm.

To obtain the $2M$-site result, we should perform the infinite lattice algorithm up to $l = (M - 1)$ sites first storing all operators in each iteration. Now the algorithm for finite lattices with reflection symmetry, proceeds as follows:

1. On reaching a system size of $2M$ sites, obtain the density matrix of the block of M sites.

2. Use the density matrix of M sites on the left and that of $(M-2)$ sites on the right, add two new sites as in the infinite DMRG procedure and obtain the desired eigenstate of the $2M$ system.

3. Now obtain the reduced density matrix of the $(M+1)$ sites from the eigenstate of the previous iteration obtained in the direct product basis of the DMEVs of the M-site, $(M-2)$-site density matrices, and the Fock space states of the individual sites.

4. Go back to step 2, replacing M by $(M+1)$ and $(M-2)$ by $(M-3)$ and iterate until a single site results on the right and $(2M-3)$ sites result on the left.

5. Since the system has reflection symmetry, use the density matrix of the $(2M-3)$ sites on the right and construct the $2M$ system as built-up from three individual sites on the left and $(2M-3)$ sites on the right. Obtain the desired eigenstate of the $2M$ system in this basis.

6. Now obtain the new 2-site density matrix on the left and $(2M-4)$ site density matrix on the right. Replace the single-site on the left by two sites and $(2M-3)$ sites on the right by $(2M-4)$ sites in step 5.

7. Repeat steps 5 and 6 until $(M-1)$ sites are obtained both on the left and right. The properties of the $2M$ system obtained from the eigenstates at this stage corresponds to the first iteration of the finite-size algorithm. We can now go back to step 1 and carry through the steps to obtain properties at later iterations of the finite-size DMRG algorithm.

In systems without reflection symmetry, the DMEVs of the right and left parts are not identical even if the sizes of the reduced systems are the same. The finite-DMRG algorithm in this case involves first constructing the density matrices of the left part for sizes greater than M and on reaching the density matrix of $(2M-3)$ sites, reducing

the size of the left-part and increasing that of the right, from one site to $(M-1)$. This will result in the refined density matrices of both the right and the left block of the total system, for block sizes of $(M-1)$. At this stage, we can compute all the properties and continue the reverse sweep until the right block is of size $(2M-3)$ and the left block is of size 1. The forward sweep that follows will increase the block size on the left and decrease that of the right. We would have completed the second iteration when the two block sizes are equal. The forward and reverse sweeps can be continued until we reach the desired convergence in the properties of the whole system.

The finite-size DMRG algorithm provides high-accuracy solutions even when the states of the full Hamiltonian have inhomogeneous (symmetry breaking) properties.

4.5 Periodic boundary conditions

While for systems with periodic (PBC) or antiperiodic (ABC) boundary conditions, the same algorithms described above can be used without modifications, by simply adding the additional bond between the open ends of the blocks A and A', the procedure turns out to be computationally inefficient. In such a procedure, the additional interaction involves taking direct product of two matrices corresponding to site operators which are both in the DMEV basis. These matrices in the DMEV basis are of order $(m \times m), m \approx O(10^2)$, and the direct products lead to a very large number of nonzero matrix elements in the Hamiltonian matrix of the full system. However, if one chooses to modify the algorithm such that one new site is added in the middle of the two blocks and another at the end of either of the two blocks (instead of adding both the new sites in the middle of the system), the Hamiltonian matrix would involve direct product of one matrix of order $q \times q$ (q is the Fock space dimensionality of a single site) and another of order $m \times m$, consequently the total Hamiltonian matrix would be more sparse [65]. However, it still remains true that the DMRG algorithm is more accurate for systems with open boundary conditions than the corresponding systems with closed boundary conditions.

4.6 Computation of properties

At the end of each iteration, one can calculate the properties of the targeted state [67]. The reduced many-body density matrix computed at each iteration can be used to calculate the static expectation values of any site operator or their products. Care should be taken to use the density matrices appropriate to the iteration. The expectation value of a site property corresponding to the operator $\hat{A}_i$ can be written as:

$$< A_i >= Tr\rho\mathbf{A}_i \tag{18}$$

ρ is the density matrix of the block in which the site i is situated and $\mathbf{A}_i$ is the matrix of the renormalized site operator at site i. For calculating correlation functions, one can use a similar equation. The correlation function between two site operators belonging to separate blocks can be written as:

$$< A_iA_j >= Tr\rho(\mathbf{A_i})(\mathbf{A_j}) \tag{19}$$

However, the accuracy of this procedure turns out be very poor if the sites i and j belong to the same block [65]. The reason is that a feature implicit in the above procedure is the resolution of identity by expansion in terms of the complete basis. Unfortunately, the basis in which the site operators are represented is incomplete and such an expansion is therefore error prone. To circumvent this difficulty, it has been suggested [65] that, one obtains the matrix representation of the products of the site operators from the first occurrence of the product pair $< ij >$ and, by renormalizing the product operator $\hat{A}_i\hat{A}_j$, at every subsequent iteration until the end of the RG procedure. Then, the correlation function between $\hat{A}_i$ and $\hat{A}_j$ (where i and j belong to the same block) can be evaluated as:

$$< A_iA_j >= Tr\rho(\mathbf{A_iA_j}) \tag{20}$$

This procedure is found to be reasonably accurate in most cases.

4.7 Comments on the implementation of the method

We have implemented the DMRG code in FORTRAN language. The only in-core algorithm we need to use is the matrix diagonalization

algorithm for the diagonalization of the density matrices and the diagonalization of the "small" matrices encountered in the Davidson algorithm for low-lying eigenstates of sparse symmetric systems.

All the matrices computed at each DMRG iteration are stored in compact sparse form. This leads to savings in storage as well as CPU by avoiding doing arithmetic with zeroes. The CPU requirement to calculate an eigenvalue and the associated eigenvector by the Davidson's algorithm then scales as the number of nonzero elements of the superblock Hamiltonian. It is possible to avoid storing the entire Hamiltonian matrix of the superblock and computing the necessary matrix elements of the superblock Hamiltonian from the matrices of the site operators and the block Hamiltonians, during every Davidson iteration. However, for the systems we have studied, we find this procedure to be slower than storing the superblock Hamiltonian matrix during Davidson iterations. Most of our calculations have been carried out on IBM RISC machines and DEC Alphas.

4.8 Accuracies and applications of the DMRG method

The overall accuracy of the DMRG method is exceptionally high for one-dimensional systems with only nearest neighbour interactions. For a spin-1/2 chain where exact Bethe-*ansatz* ground-state energy is available, the DMRG ground-state energy per site is found to be accurate to seven decimal places with a cut-off $m = 100$ [65]. The method is found to be almost as accurate for the one-dimensional Hubbard model, where again it is possible to compare the DMRG results with exact results obtained from the exact Bethe-*ansatz* solution [68]. The reason why the DMRG method for the spin-1/2 model is more accurate than that for the Hubbard model has its origin in the dimensionality of the individual site Fock space in the two cases. This dimensionality is 2 in the spin-1/2 case while it is 4 in the fermionic system. Thus, the truncation is more severe in the Hubbard model compared to the spin-1/2 Heisenberg model, for the same DMRG cut-off m.

The density matrix eigenvalues sum to unity and the *truncation error*, which is defined as the sum of the density matrix eigenvalues corresponding to the discarded DMEV, gives a qualitative estimate as to the accuracy of the calculation as well as providing a framework

for the extrapolation to the $m \to \infty$ limit. The accuracy of the results obtained in this way was unprecedented [69, 70]. The accuracy of the ground state energy per site for the spin-1 chain is limited by the precession of machine arithmetic, i.e., $e_0 = 1.401484038971(4)$. Similarly, the accuracy persists even while calculating for the Haldane gap, *e.g.*, the gap was evaluated to be 0.41050(2).

Extending the range of interactions to nearest and next-nearest neighbours does not significantly deteriorate the accuracy [71]. However, inclusion of cyclic boundary conditions reduces the accuracy of the method significantly, although in one-dimension, the DMRG method still would outperform any other method for the same system size. In the DMRG procedure, the most accurate quantity computed is the total energy. In dealing with other quantities such as correlation functions, caution must be exercised in interpreting the results.

Finite size algorithms have been used extensively to study the edge states and systems with impurities, where substantial improvement of the accuracy is needed to characterize the various properties of a finite system. The DMRG method has been applied to diverse problems in magnetism: study of spin chains with $s > 1/2$ [72], chains with dimerization and/or frustration [71, 73, 74], coupled spin chains [71, 75, 76], to list a few. The method has also been used to study models with itinerant fermions [77, 78], Kondo systems[79, 80, 81, 82], as well as coupled fermion chains [83, 84], including doping. Formulations for systems with a single impurity [85, 86] as well as randomly distributed impurities [87] and disorder [88] have also been reported. There has also been a study of the disordered bosonic Hubbard model in one dimension [89].

Highly accurate studies of the structure factor and string order parameter (topological long range order) [69] as well as edge states in Haldane phase systems [90] have been performed. Dynamical properties for both spin and fermionic systems with DMRG have also been reported within the Maximum Entropy Method [91] as well as continued fraction [92] and correction vector [93] approaches. Finally, DMRG has been successfully formulated to obtain low-temperature thermodynamic properties for various spin systems [94, 95] and the solution of models of spin chains dynamically coupled to dispersionless phonons [96].

Recently, we have developed a symmetrized DMRG (SDMRG) method to target the desired excited states very accurately [97]. This will find application in calculating various properties related to optical spectroscopic studies [98]. Furthermore, Nishino and Okunishi have derived two reformulations of DMRG, namely, the product wavefunction renormalization group (PWFRG) [99] and the corner transfer matrix renormalization group (CTMRG) [100] methods. These methods offer the means of calculating dynamical correlation functions in spin chains as well as highly accurate results for the 2-dimensional Ising model at criticality.

4.9 Remarks on the DMRG method

The DMRG method is currently the most accurate method for large quantum lattice models in one dimension. It can be applied to interacting bosonic, fermionic or spin models as well as to models which have interactions amongst them. Since higher dimensionality is tantamount to longer-range interactions within one dimension, the model also restricts the range of interactions in one dimension. It has been surmised that the number of DMEVs that should be retained in a calculation on higher dimensional systems, for accuracies comparable to accuracy in one dimension, scales exponentially with dimensionality. Thus, to obtain accuracy comparable to that obtained in a chain of L-sites for a cut-off m, in a $L \times L$ square lattice, the number of DMEVs needed to be retained for the corresponding 2-dimensional lattice is $\approx m^2$.

Another aspect of the DMRG technique worth noting is that the method is best suited for targeting one eigenstate at a time. However, it is possible to obtain reasonable results for a set of states by using an average many-body reduced density matrix constructed as a weighted sum of the density matrices corresponding to each of the states in question. One way of constructing the average density matrix is by using a statistical weight for the chosen set of states and the averaged density matrix in this instance is given by:

$$\rho_{\beta;k,l} = \sum_i (\sum_j \psi_{i;k,j}\psi_{i;l,j}) exp[-\beta\epsilon_i] / \sum_i exp[-\beta\epsilon_i] \qquad (21)$$

One can thus construct the averaged density matrix for $T \neq 0$ and

extend the method to finite temperatures.

5 Symmetrized DMRG for the Excited States

The Density Matrix Renormalization Group (DMRG) method [65, 101] has proved to be an accurate technique for obtaining a few low-lying states of interacting model Hamiltonians with short-range interactions in low-dimensions [69, 102, 103]. This technique would find wide applications in the electronic structure studies of conjugated polymers and donor-acceptor systems, if we can obtain excited eigenstates in different symmetry subspaces. However, the DMRG techniques reported in the literature for fermions can exploit only the conservation of the z-component of the total Spin (S^z_{tot}) and total number of particles (N_{tot}) in the system [104, 105, 83]. Using these symmetries one can obtain a few (about ten) low-lying states in different M_s and N sectors [101]. This is due to the limitation on the number of eigenstates that can be targetted effectively because of the large matrices that one encounters in the DMRG algorithm. Additionally, the Hamiltonians being spin conserving, the states with higher total spin repeat in many M_s sectors. For example, triplet states will be present in the $M_s = 0, +1$ and -1 sectors. Therefore, obtaining the second singlet state usually requires targetting the third state in the $M_s = 0$ sector and eliminating the $M_s = 0$ intruder triplet state. Besides, with increasing system size, the number of intruders also increases. Thus, the inclusion of just these symmetries is not sufficient to make detailed comparisons between theory and experiments that probe excited states.

In a system with spatial symmetries, the states important from the point of view of optical (one-photon) spectroscopies always lie in a spatial symmetry subspace different from the subspace in which the ground state is found. For example, in Hubbard chains, the ground state is in the A subspace while the dipole-allowed excited states are in the B subspace [106].

Hubbard chains at half-filling also possess electron-hole symmetry. This allows labelling of the states as either $'+'$, corresponding to *covalent* subspace, or $'-'$, corresponding to *ionic* subspace. The dipole-allowed excited states are found in the $'-'$ subspace while the

ground state is in the $'+'$ subspace. The number of higher energy states in the $'+'$ subspace intruding below the lowest $'-'$ subspace state increases as the strength of electron correlation U/t increases [107]. Hence, if this symmetry is not incorporated, many $'+'$ space states intrude below the lowest $'-'$ space state, rendering the optically allowed excited state difficult to access computationally.

5.1 Implementation of the symmetries within DMRG method

In the implementation of the symmetrized DMRG scheme, we use the group theoretic projection operators for projecting the direct product DMRG basis functions onto different symmetry subspaces. The symmetries we have incorporated are the electron-hole symmetry, $\hat{J}$, end-to-end interchange symmetry of chains, $\hat{C}_2$ and spin parity, $\hat{P}$. The latter two symmetries have been employed within the DMRG scheme for spin chains. While the full spin symmetry classification can be incorporated into the scheme using Clebsch-Gordon coefficients [108], for the present we have only included parity which bifurcates the space of spin eigenvectors into even (e) and odd (o) spin spaces.

The electron-hole symmetry operator interchanges, with a phase, the creation and annihilation operators at a site,

$$a_i^\dagger = (-1)^{\eta_i} b_i \tag{22}$$

where η_i is zero for sites on one sublattice and unity for sites on the other. Thus, the Fock space of a single site i, under electron-hole symmetry transforms as $\hat{J}_i|0>=|\uparrow\downarrow>$, $\hat{J}_i|\uparrow>=(-1)^i|\uparrow>$, $\hat{J}_i|\downarrow>=(-1)^i|\downarrow>$, $\hat{J}_i|\uparrow\downarrow>=(-1)|0>$. The full electron-hole symmetry operator, $\hat{J}$, is given by the direct product of the single site operators:

$$\hat{J} = \prod_i \hat{J}_i \tag{23}$$

The parity operator at a site i, $\hat{P}_i$, flips the electron spin at the site. Thus, $\hat{P}_i|0>=|0>$, $\hat{P}_i|\downarrow>=|\uparrow>$, $\hat{P}_i|\uparrow>=|\downarrow>$, $\hat{P}_i|\uparrow\downarrow>=(-1)|\uparrow\downarrow>$. The full parity operator for the system is also given by

the direct product of the single site parity operators:

$$\hat{P} = \prod_i \hat{P}_i \tag{24}$$

The $\hat{C}_2$ symmetry interchanges the states of the left and right halves of the system with a phase factor. Thus, $\hat{C}_2$ operating on the direct product state $|\mu, \sigma, \sigma', \mu' >$ gives:

$$\hat{C}_2|\mu, \sigma, \sigma', \mu' >= (-1)^\gamma |\mu', \sigma', \sigma, \mu >$$
$$\gamma = (n_\mu + n_\sigma)(n_{\mu'} + n_{\sigma'}) \tag{25}$$

where $\mu(\mu')$ refers to the $\mu^{th}(\mu'^{th})$ eigenvector of the left (right) density matrix while $\sigma(\sigma')$ refers to the Fock space state of the new left (right) site as in the standard DMRG procedure, and n_μ, $n_{\mu'}$, n_σ and $n_{\sigma'}$ are the occupancies in the states $|\mu >$, $|\mu' >$, $|\sigma >$ and $|\sigma' >$, respectively.

The operators $\hat{C}_2$, $\hat{J}$ and $\hat{P}$ commute amongst each other and the group formed by identity and these symmetries consists of eight elements with the remaining four elements resulting from the closure condition. This group being Abelian has eight irreducible representations which are labelled ${}^eA^+$, ${}^eA^-$, ${}^oA^+$, ${}^oA^-$, ${}^eB^+$, ${}^eB^-$, ${}^oB^+$, ${}^oB^-$.

The projection operator for a given irreducible representation, Γ, from standard group theory is given by:

$$\hat{\mathbf{P}}_\Gamma = \frac{1}{h} \sum_{\hat{R}} \chi_\Gamma(\hat{R}) \hat{R} \tag{26}$$

where $\hat{R}$'s are the symmetry operators, $\chi_\Gamma(\hat{R})$ is the character of $\hat{R}$ in Γ and h is the order of the group. The construction of the *symmetry adapted* direct product states consists in sequentially operating on each of the direct product states by the projection operator, $\hat{\mathbf{P}}$. However, the resulting basis is linearly dependent and these linear dependencies have to be eliminated to avoid working with an overcomplete basis. The number of linearly independent functions spanning the desired subspace is known *a priori* and is given by:

$$l_\Gamma = \frac{1}{h} \sum_{\hat{R}} \chi_\Gamma(\hat{R}) \chi_{red.}(\hat{R}) \tag{27}$$

where $\chi_{red.}(\hat{R})$ is the trace of the matrix of the symmetry element $\hat{R}$ in the DMRG representation. This allows terminating the Gram-Schmidt orthonormalization process when the number of orthonormal functions obtained is l_Γ. In practice, we first obtain the matrix representation of $\hat{P}_\Gamma$ in the direct product DMRG basis in a way which is analogous to the setting-up of the full Hamiltonian matrix from the blocks. The linear dependencies discussed above manifest as linearly dependent rows of the matrix of $\hat{P}_\Gamma$.

The computational procedure involves obtaining the matrix representation of the symmetry operators of the $(2n+2)$ site chain in the direct product basis. The matrix representation of both $\hat{J}$ and $\hat{P}$ for the new sites in the Fock space is known from their definitions. Similarly, the matrix representations of the operators $\hat{J}$ and $\hat{P}$ for the left (right) part of the system at the first iteration are also known in the basis of the corresponding Fock space states. These are then transformed to the density matrix eigenvectors basis. The matrix representation of the symmetry operators of the full system in the direct product space are obtained as the direct product of the corresponding matrices:

$$\begin{aligned} &< \mu, \sigma, \sigma', \mu' | \hat{R}_{2n+2} | \nu, \tau, \tau', \nu' > = \\ &< \mu | \hat{R}_n | \nu >< \sigma | \hat{R}_1 | \tau >< \sigma' | \hat{R}_1 | \tau' >< \mu' | \hat{R}_n | \nu' > \end{aligned} \tag{28}$$

At the next iteration, we require the matrix representation of the symmetry operators in the basis of the eigenvectors of the new density matrix. This is achieved by obtaining the matrix $\mathbf{R}$ as a direct product of $\mathbf{R}_n$ and $\mathbf{R}_1$ given by:

$$< \mu, \sigma | \hat{R}_{n+1} | \nu, \tau > = < \mu | \hat{R}_n | \nu >< \sigma | \hat{R}_1 | \tau > \tag{29}$$

This matrix is renormalized by the transformation

$$\tilde{\mathbf{R}}_{n+1} = \mathbf{O}^\dagger \mathbf{R}_{n+1} \mathbf{O} \tag{30}$$

where $\mathbf{O}$ is the matrix whose columns are the chosen eigenvectors of the density matrix.

The matrix representation of $\hat{C}_2$ is quite straightforward in that each state $|\mu, \sigma, \sigma', \mu' >$ is mapped into a state $|\mu', \sigma', \sigma, \mu >$ with a phase factor. Thus, each row in the matrix of $\hat{C}_2$ contains only one

element and the entire matrix can be represented by a correspondence vector. The matrices **J** and **P** are also rather sparse and can be stored in sparse form to avoid doing arithmetic with zeroes. This aspect of the computation turns out to be crucial for the implementation of the scheme since the dimensionality of the direct product space is usually very large (about 10^5 for a cut-off of m=150).

The coefficients of the direct product functions in the symmetrized basis form a matrix **S**. The Hamiltonian matrix in the direct product basis can be transformed to the Hamiltonian in the symmetrized basis by the transformation

$$\tilde{\mathbf{H}}_{2n+2,\Gamma} = \mathbf{S}_{\Gamma}^{\dagger}\tilde{\mathbf{H}}_{2n+2}\mathbf{S}_{\Gamma} \tag{31}$$

The size of the symmetrized Hamiltonian matrix is of the order 2000×2000 for a cut-off of $m = 100$. The low-lying eigenstates of this matrix can be obtained by Davidson's algorithm.

To proceed to the next iteration, the eigenvector obtained in the desired symmetry subspace is back transformed to the unsymmetrized basis by using the **S** matrix as follows:

$$\psi = \mathbf{S}\psi_{symm} \tag{32}$$

The resulting unsymmetrized eigenvector is used to obtain the density matrix of the half-blocks as in the standard DMRG algorithm. The symmetrization procedure is essentially restricted to obtaining the Hamiltonian matrix of the full system in a particular symmetry subspace. This process continues till the desired number of sites is reached (basis for the finite size algorithm) or till the energy per site converges (infinite size algorithm).

The symmetry adaptation scheme described above has been implemented both within the infinite chain DMRG algorithm and within the finite system algorithm. In the finite size algorithm, we encounter different fragments for the left and right parts of the system in each finite size iteration. Thus, we cannot incorporate the C_2 symmetry except when the left and right parts of the system are equivalent, *i.e.*, at the end of each finite size iteration. The matrices for all the other symmetry operators can be self-consistently built up to define the particular finite size fragment in each step of finite size algorithm. Incorporating the C_2 symmetry in the final step of each finite size

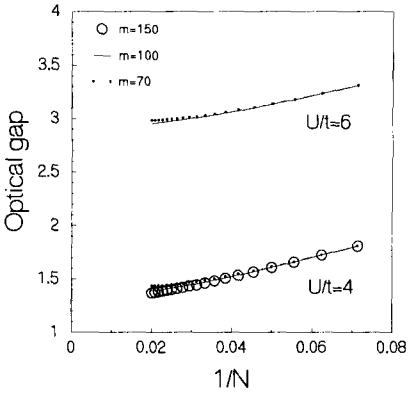

Figure 1: Optical gap (in unit of t) as a function of inverse chain length for Hubbard chains with $U = 4.0t$ and $U = 6.0t$; m corresponds to the number of density matrix eigenvectors retained in the DMRG procedure.

iteration ensures that the targetted state is in the desired symmetry subspace. Without iterating over the density matrices of the fragments (*i.e.*, within the infinite system algorithm), we find that the energy difference between a chain of length N with $N+1$ and $N-1$ electrons is equal to the Hubbard parameter U to an accuracy of $\approx 10^{-3}$. After three iterations of the finite system algorithm, the accuracy improves to $\approx 10^{-5}$, for a value of $U = 4t$.

5.2 Accuracy of the SDMRG method

As test of the above technique, we present results of DMRG calculations for uniform Hubbard chains at half-filling, for U/t of 4.0 and 6.0, with chain lengths of up to 50 sites. The exact optical gaps in both cases can be obtained from the Bethe *ansatz* solution for comparison with our technique. We have obtained the lowest energy states in all the eight subspaces (of $\hat{C}_2$, $\hat{J}$ and $\hat{P}$), keeping 70 to 150 eigenvectors of the density matrix. The extrapolated ground state energy per site of the infinite chain
for both values of U/t agrees with the exact values of $0.5737331t$ and

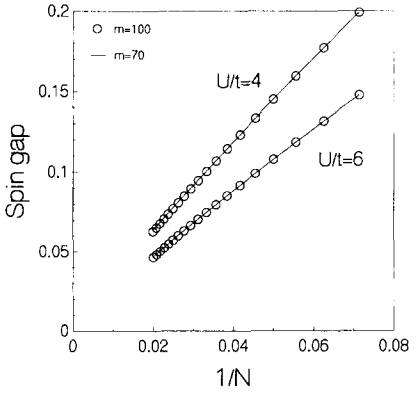

Figure 2: Spin gap (defined in the text, in unit of t) as a function of $1/N$ for Hubbard chains with $U = 4.0t$ and $U = 6.0t$; m corresponds to the DMRG cut-off. Model exact spin gaps vanish for infinite chains.

$0.4200125t$ respectively to 5 decimal places.

The energy of the one-photon transition from the ground state (lying in the ${}^eA^+$ subspace) to the lowest energy state in the ${}^eB^-$ subspace defines the optical gap of the chain. In Fig. 1, we show a plot of optical gap *vs.* inverse chain length (1/N) for $U/t = 4.0$ and 6.0 for different values of the cut-off m. The optical gaps for these values of U/t, from the Bethe *ansatz* solution for the infinite chain, are $1.2867t$ for $U/t = 4.0$ and $2.8926t$ for $U/t = 6.0$ [26]. The corresponding extrapolated values from a polynomial fit in powers of $1/N$ from DMRG are $1.278t$ and $2.895t$, obtained with a cut-off of $m = 150$ for $U/t = 4.0$ and m=100 for $U/t = 6.0$. We also find that the DMRG optical gap tends to saturate at shorter chain lengths as we decrease m. The fit of the optical gap to $1/N$ is a reasonably good straight line although the best fit is to a polynomial in this variable.

In Fig. 2, we plot the spin gap which we define as the energy gap between the lowest triplet state and the ground state singlet as a function of $1/N$. The Bethe *ansatz* solution yields a vanishing spin gap in the thermodynamic limit of the uniform Hubbard chain. Polynomial fits to our DMRG data are consistent with this.

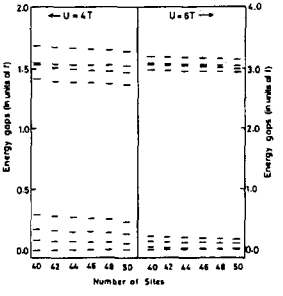

Figure 3: Energy gaps (measured from the ground state) of the lowest state in each subspace for chain length varying from 40 to 50, for two different values of U/t. The level ordering is $E_{e\,A+} < E_{o\,A+} < E_{o\,B+} < E_{e\,B+} < E_{e\,B-} < E_{e\,A-} < E_{o\,B-} < E_{o\,A-}$.

In Fig. 3, we present the energy gaps, relative to the ground state, obtained by solving for the lowest energy state in each of the eight subspaces, for Hubbard chains with 40 to 50 sites, for two values of U/t. The excitations clearly break up into two bands. The lower energy excitations correspond to states of different symmetry in the *covalent* subspace (*i.e.* predominantly spin-like excitations), while the higher energy excitations correspond to the *ionic* subspace (*i.e.* charge-like excitations). With increasing U/t the states in the *covalent* subspace are less dispersed and so are the states in the *ionic* subspace. However, with increase in U/t, the gap between the two bands increases. This feature is in agreement with the basic physics of the Hubbard models.

6 Dynamical Nonlinear Optical Coefficients from the SDMRG Method

The DMRG method [64, 65], as it was first introduced, is essentially a static technique for a few low-lying eigenstates. Extension of the method [97] to access higher energy excited states in chosen symmetry subspaces, as discussed in the previous section, allows detailed comparisons of these states with results from optical spectroscopic studies [2, 109, 110]. This is particularly useful in understanding the electronic structure of conjugated polymers as has been borne out by recent DMRG studies of poly-para-phenylenes (PPP) and poly-para-phenylene vinylenes (PPV) [67, 111].

One of the main properties of interest in the field of conjugated polymers is the study of their dynamic nonlinear optical (NLO) response [112, 113]. It is a major challenge to obtain reliable dynamics of interacting electron systems. While for short oligomers there exist reasonable approximations for computing these properties [114], for longer chains even within model Hamiltonian approximations, the dynamic NLO coefficients had proved elusive. Yet most interest lies in the longer chains since the dynamic NLO properties exhibit dominant finite-size effects.

The dynamic response functions of finite interacting systems have most commonly been obtained from an explicit computation of the eigenstates of the Hamiltonian and the matrix elements of the appropriate operators in the basis of these eigenstates [115]. This has been a widely used method particularly in the computation of the dynamic NLO coefficients of molecular systems and is known as the sum-over-states (SOS) method. In the case of model Hamiltonians, the technique that has been widely exploited to study dynamics is the Lanczos method [116]. The spectral intensity corresponding to an operator $\hat{O}$ is given by:

$$I(\omega) = -\frac{1}{\pi} Im[< G|\hat{O}^{\dagger} \frac{1}{(\omega + E_0 + i\epsilon - \hat{H})} \hat{O}|G >] \qquad (33)$$

where $|G >$ is the ground state eigenvector of the Hamiltonian $\hat{H}$, with eigenvalue E_0, ω is the frequency at which the response is sought, ϵ is the mean life time parameter. In the Lanczos method,

$I(\omega)$ is computed as a continued fraction,

$$I(\omega) = -\frac{1}{\pi} Im[\cfrac{< G|\hat{O}^\dagger \hat{O}|G >}{z - a_0 - \cfrac{b_1^2}{z - a_1 - \cfrac{b_2^2}{z - a_2 - \ldots}}}] \tag{34}$$

wherein the coefficients a_i and b_i are respectively the diagonal and the off-diagonal matrix elements in the tridiagonal matrix representation of the Hamiltonian obtained in the Lanczos procedure. Thus, this method relies exclusively on the tridiagonal form of the Hamiltonian matrix [116]. Besides, there is an implicit truncation of the Hilbert space due to the smaller size of the tridiagonal matrix compared with the total dimensionality of the space spanned by the Hamiltonian, which is quite akin to the truncation in the SOS method. Therefore, the dynamic quantities computed by this technique are approximate even though the ground state obtained is exact.

In the context of NLO properties of interacting models such as the Hubbard and extended Hubbard models, it was shown by Soos and Ramasesha that the model exact dynamical NLO coefficients could be obtained by solving for correction vectors [106]. If we define the correction vector $\phi^{(1)}(\omega)$ by the equation

$$(\hat{H} - E_0 - \omega - i\epsilon)\phi^{(1)}(\omega) = -\hat{O}|G > \tag{35}$$

then the spectral function, $I(\omega)$, can be expressed as:

$$I(\omega) = -\frac{1}{\pi} Im < G|\hat{O}^\dagger|\phi^{(1)}(\omega) > \tag{36}$$

The correction vector is solved for in the basis of the configuration functions, which is also the basis in which the Hamiltonian matrix is set-up for obtaining the ground state. Given the ground state and the correction vector, it is straightforward to compute the spectral function. This method is quite general and has been employed in the computations of dynamic NLO coefficients of a wide variety of Hamiltonians [117]. The inhomogeneous linear algebraic equations encountered in this method involve large sparse matrices. An iterative small matrix algorithm, which runs parallel to the Davidson

algorithm for eigenvalue problems, gives rapid convergence for the solution of the system of equations [118].

The correction vector method is not limited to tridiagonal matrices. Furthermore, by defining higher-order correction vectors, it is possible to compute nonlinear spectral functions as are encountered in the study of nonlinear optical properties. This technique provides a way of computing the dynamics which is exact for the chosen restricted configuration space, unlike other techniques which involve truncations over and above that imposed by the choice of the space of configurations. Although the dynamics of a spin chain [119] and also that of a spinless fermion system [91] have been reported in the literature using the DMRG technique, the first one employed the Lanczos algorithm which amounts to further truncation of the Hilbert space over and above the truncation involved in the DMRG procedure and the latter used the maximum entropy method which relies on analytic continuation and involves large uncertainties.

6.1 DMRG technique for dynamic NLO response

The computation of the dynamic NLO coefficients by the correction vector method requires the ground-state eigenfunction, the Hamiltonian matrix and the dipole displacement matrices [120]. The DMRG method as implemented, readily provides us with the ground state and the Hamiltonian matrix. The matrices of the dipole operators are constructed in the DMRG scheme by renormalizing the matrix representations of the dipole operator corresponding to the left and right parts of the system using the density matrix eigenvector basis in a way which is completely analogous to the corresponding Hamiltonian operators for the fragments. The matrix representation of the dipole operators for the full system are obtained as direct products of the fragment matrices analogous to the way by which the full Hamiltonian matrix is constructed. The matrices of the *dipole displacement* operators are then obtained by subtracting the corresponding components of the dipole moments in the ground state from the diagonal elements of the dipole matrices.

The two correction vectors $|\phi_i^{(1)}(\omega_1)>$ and $|\phi_{ij}^{(2)}(\omega_1,\omega_2)>$ encountered in the computation of first-order and third-order polariz-

abilities are obtained by solving the following linear equations:

$$(H - E_0 + \omega_1 + i\epsilon)|\phi_i^{(1)}(\omega_1) >= \tilde{\mu}_i|G > \tag{37}$$

$$(H - E_0 + \omega_2 + i\epsilon)|\phi_{ij}^{(2)}(\omega_1) >= \tilde{\mu}_j|\phi_i^{(1)}(\omega_1) > \tag{38}$$

where $\tilde{\mu}_i$'s are the dipole displacement operators, the indices i and j correspond to the Cartesian coordinates (x, y, z) of the physical system and other quantities are as defined in eqn.(33). In terms of these correction vectors, the components of the first polarizability, α_{ij}, and third-order polarizability, γ_{ijkl}, can be written as:

$$\alpha_{ij}(\omega) =< \phi_i^{(1)}(\omega)|\tilde{\mu}_j|G > + < \phi_j^{(1)}(-\omega)|\tilde{\mu}_i|G > \tag{39}$$

and

$$\gamma_{ijkl}(\omega_1, \omega_2, \omega_3) = \hat{P} < \phi_i^{(1)}(-\omega_1 - \omega_2 - \omega_3) \\ |\tilde{\mu}_j|\phi_{kl}^{(2)}(-\omega_1 - \omega_2, -\omega_1) > \tag{40}$$

where the operator $\hat{P}$ generates all the permutations: $(-\omega_\sigma, i), (\omega_1, j), (\omega_2, k)$ and (ω_3, l) leading to 24 terms for γ_{ijkl} with $\omega_\sigma = -\omega_1 - \omega_2 - \omega_3$. The tumbling averaged $\bar{\alpha}$ and $\bar{\gamma}$ defined as

$$\bar{\alpha} = \frac{1}{3}\sum_{i=1}^{3}\alpha_{ii} \tag{41}$$

and

$$\bar{\gamma} = \frac{1}{15}\sum_{i,j=1}^{3}(2\gamma_{iijj} + \gamma_{ijji}) \tag{42}$$

can also be computed to allow comparison of the calculated NLO response with experiments on systems containing molecules in random orientations [112].

While the extension of the DMRG scheme for obtaining the correction vectors appears to be straightforward, given the eigenstate and the matrices corresponding to the relevant operators, in the actual implementation there exist some severe problems. The correction vector lies in the symmetry subspace which is connected to the ground state by the electric dipole operator. For ω values corresponding to resonance between the ground state and eigenstates in

that particluar symmetry subspace, *lhs* of eqns. (37) and (38) become singular for $\epsilon = 0$ and present numerical difficulties even when solving them for reasonable nonzero ϵ values. However, if we do not exploit the symmetries of the Hamiltonian, we encounter singularities in eqns. (37) and (38) even for those ω values corresponding to eigenstates of the Hamiltonian found in other symmetry subspaces which are not connected to the ground state by the dipole operator. Therefore, numerically it would be impossible to obtain the correction vectors at these frequencies and thereby the associated response of the system. For example, in Hubbard chains at intermediate correlation strengths, a triplet excited state lies below the lowest singlet state in the *ionic* B subspace [107]. The resonances in polarizability are expected only at frequencies corresponding to the energy levels in the *ionic* B space, relative to the ground state. However, we can not solve for the correction vector using equation (37) at an excitation energy corresponding to the energy of the lowest triplet state. Thus, the technique of correction vectors will not be able to give the complete dispersion of the polarizabilities up to the first one-photon resonance, unless interferences due to spurious intruders such as the triplet states are eliminated by suitably block diagonalizing the Hamiltonian matrix. This problem of intruders becomes more severe with increasing system size due, as mentioned previously, to increasing number of intruder states lying below the frequency corresponding to the first *true* resonance.

We have thus exploited the electron-hole symmetry, the reflection symmetry of the polymers and spin parity to block-diagonalize the Hamiltonian [97]. Usually, DMRG method targets a single state at a time. However, in this case we need the ground state and the correction vectors to be determined simultaneously with comparable accuracy. In order to achieve this we have constructed an average density matrix using various target states, namely, i) one or more states in covalent subspace, ii) one or more states in ionic subspace and iii) ϕ >s at the chossen frequency. In the course of our test calculations, we have considered a single excitation frequency in all our calculations ($\omega = \omega_1 = \omega_2 = \omega_3$). We have exploited sparseness of all the matrices to improve upon the computational efficiency and have employed the finite size DMRG algorithm in some cases to check

the convergence of the DMRG results. In these cases, the spatial symmetry is exploited only at the end of the DMRG procedure when the left and the right density matrices correspond to fragments of the same size, *i.e.*, at the end of each finite size iteration.

6.2 Accuracy of the dynamic SDMRG method

In order to assess the accuracy of the dynamic SDMRG technique, we have performed a series of model calculations; we computed the dynamic linear polarizabilities ($\alpha(\omega)$) and third-order polarizabilities ($\gamma(\omega,\omega,\omega)$) corresponding to the third harmonic generation (THG), for the Hubbard and "$U-V$" polyene-like chains of up to 20 sites with and without dimerizations (note that the dimerization parameter δ reflects the degree of carbon-carbon bond-length alternation along the polyene chain; nonzero δ leads to alternating t and V values while zero δ means uniform t and V).

We have compared our results with the *model exact* α and γ values obtained from the correction vector method in the valence bond basis, for chains of up to 12 sites. The results compare well with a cut-off of $m = 100$, *i.e.*, by retaining the dominant 100 density matrix eigenvectors in the DMRG sceme. For the 8-site problem, DMRG with $m = 100$ is exact and the DMRG results compare with exact results to numerical accuracy. In the case of the 12-site chain, the largest relative error is less than 0.5% for $U/t = 4$ in the uniform Hubbard model. The exact $\bar{\alpha}$ is 5.343×10^{-24} *esu* while $\bar{\alpha}$ from DMRG is 5.317×10^{-24} *esu*. The corresponding exact $\bar{\gamma}$ and DMRG $\bar{\gamma}$ values are 5.983×10^{-34} *esu* and 5.911×10^{-34} *esu*. The dominant α and γ components (namely the longitudinal α_{xx} and γ_{xxxx} components) are in relative error of 0.05% and 0.1%, respectively. However, the data presented in what follows have been obtained with a much higher value of $m = 200$. In the model calculations, the simplified geometries of the Hubbard and "$U - V$" chains correspond to bond angles of 120° and average bond lengths of 1$\AA$ and model the $all - trans$ polyacetylene configuration.

Results for the Hubbard model: In Fig. 4, we display the dependence of $\bar{\alpha}$ on the chain length for different values of U/t, for uniform (Fig. 4a) and dimerized (Fig. 4b) Hubbard chains. The polarizability decreases with increasing correlation strength in both

the dimerized and uniform chains. For the same chain length, the uniform chains have, as expected [121], higher polarizability than the corresponding dimerized chain at every value of U/t we have studied. For the uniform chain, the average polarizability, $\bar{\alpha}$, for weak correlations exhibits a nice power law dependence on chain length with an exponent of 2.022 ± 0.001. However, for stronger correlations, the polarizability deviates from a power law and shows a size dependent variation at longer chain lengths leading to saturation. The chain length at which the change over from the power law behaviour occurs, systemetically reduces with increasing U/t. As the chain dimerizes, the range over which power law behaviour is observed decreases (Fig. 4b). Eventually, in the limit $\delta = 1.0$, where the chain breaks down to noninteracting dimers, we would observe only size-consistent dependence. In Fig. 5, we show the ln-ln plot of average third-order polarizabilty $\bar{\gamma}$ with chain length for chains of up to 20 sites without (Fig. 5a) and with (Fig. 5b) bond alternation. The variation of $\bar{\gamma}$ with chain length is similar to that found for $\bar{\alpha}$ both in the dimerized and undimerized cases. Nonzero δ leads to a decrease in the $\bar{\gamma}$ value and the decrease is smaller for higher U/t values. An exponent of 5.570 ± 0.001 is found for $\delta = 0.0$ and $U/t = 2.0$, while the exponent is 4.00 ± 0.01 for $\delta = 0.09$ and $U/t = 2.0$. In both cases, the power-law behaviour is observed up to the maximum chain length we have studied. It is interesting to note the strong dependence of the exponent on the dimerization parameter.

Results for the "$U - V$" Model: The polarizabilities show a behaviour similar to that found for the Hubbard model. However, the "$U - V$" model is more polarizable than the Hubbard model. While the dimerization, δ, decreases the polarizability of the chain, the nearest neighbour interaction, V, increases it.

In Fig. 6, we present the dependence of $\bar{\gamma}$ on chain length for various values of U/t for the uniform (Fig. 6a) and dimerized (Fig. 6b) chains. There are some very interesting differences between the Hubbard and the "$U - V$" chains. The behaviour of the "$U - V$" chains is similar to the behaviour of the Hubbard chains for $U > 2V$. In this regime, which is the SDW regime, the third-order polarizability of the "$U - V$" model is larger than that in the Hubbard model for corresponding chain lengths both with and without dimerization.

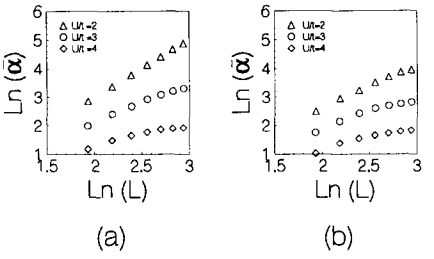

Figure 4: Ln-Ln plot of the average polarizability ($\bar{\alpha}$) in units of 10^{-24} *esu* versus chain length L in $\mathring{A}$ for Hubbard chains of up to 20 sites in $all - trans$ polyacetylene configuration for (a) $\delta = 0$ and (b) $\delta = 0.09$, for three different values of U/t.

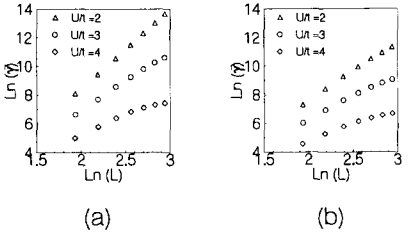

Figure 5: Plot of the ln of average third-order polarizability ($\bar{\gamma}$) in units of 10^{-36} *esu* versus log of the chain length L in $\mathring{A}$, for Hubbard chains, with three different values of U/t for (a) $\delta = 0$ and (b) $\delta = 0.09$.

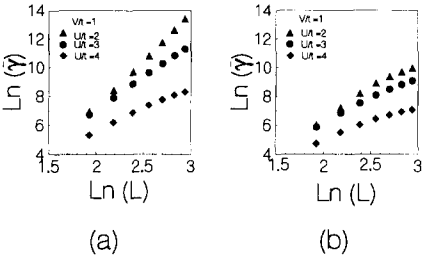

Figure 6: Ln-Ln plot of the average third-order polarizability ($\bar{\gamma}$) in units of 10^{-36} *esu* versus chain length L in $\mathring{A}$ for "$U - V$" chains for three values of U/t and for $V/t = 1$ for (a) $\delta = 0$ and (b) $\delta = 0.09$.

However, when $U = 2V$, which is the CDW/BOW (Bond Order Wave) transition point, we find that the Hubbard chains have higher third-order polarizability than their counterparts in the "$U - V$" model. This trend is observed only for $\bar{\gamma}$ and is not seen for the polarizability $\bar{\alpha}$.

To understand this behavior, we have studied the variation of the *lowest one − photon gap* (Fig. 7a) and the *lowest two − photon gap* (Fig. 7b) as a function of chain length in the Hubbard model and the "$U - V$" model at the SDW/CDW transition point. The gap to the lowest one-photon state in the former is higher than that in the latter at all chain lengths, independent of δ; therefore, since $\bar{\alpha}$ in a conjugated chain very much depends on the one-photon gap [121], the linear polarizabilities of the "$U - V$" model at the transition point are higher than that of the Hubbard model. The third-order polarizability, however, also has contributions from the two-photon states. The lowest two-photon state in the "$U - V$" model for these parameters is at a higher energy than in the Hubbard model for all the chain lengths and δ. Consequently, we can expect that the two-photon contribution to γ is higher for the Hubbard model than

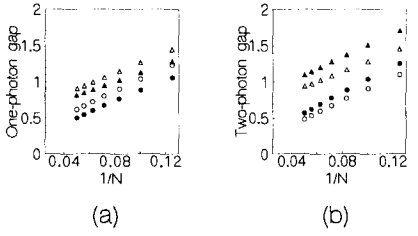

Figure 7: Dependence of (a) one-photon gap (ground state to $1^1B_u^-$) and (b) two-photon gap (ground state to $2^1A_g^+$) on $1/N$. N is the number of sites in the chain. The model parameters are $U = 2t, V = 0, \delta = 0$ (open circle), $U = 2t, V = t, \delta = 0$ (closed circle), $U = 2t, V = 0, \delta = 0.09$ (open triangle) and $U = 2t, V = t, \delta = 0.09$ (closed triangle). The gaps are given in units of t.

for the "$U - V$" model.

For values of $V > U/2$ (CDW regime), the optical gap reduces rapidly with chain length. At moderate chain length ($N \geq 10$), it is observed that the optical gap is small enough that the first three-photon resonance occurs below $\hbar\omega = 0.1t$ (optical gap E_g becomes $< 0.3t$); this is reflected in a change of sign in all components of γ. The behaviour of γ in the CDW phase is qualitatively different from what is observed in the SDW phase. In the latter, the optical gap remains finite and γ is expected to remain positive.

The dependence of $\bar{\gamma}$ on frequency is similar in both the "$U - V$" and Hubbard models for all chain lengths. We see clear indications of an $E_g/3$ resonance (Fig. 8) and a two-photon resonance. Below the first resonance, $\bar{\gamma}$ shows a larger increase for longer chains. This could be due to a sharp increase in the number of excited states with increase in chain length. Furthermore, from the excitation gaps in the 20-site Hubbard chain, we note that the one- and two-photon

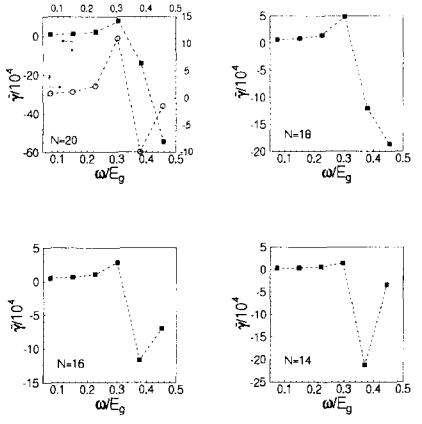

Figure 8: Dispersion curves of $\bar{\gamma}$ in units of 10^{-36} *esu* for different chain lengths, N (indicated in the boxes) for the dimerized $"U-V"$ model with $U = 3t$, $V = t$ and $\delta = 0.09$. E_g is the lowest one-photon gap for the corresponding model. For comparison, the dispersion curve of Hubbard chain ($V = 0$) for 20 sites is also shown by open circles.

resonances coalesce.

Static γ values cannot be computed from correction vector method as the equations for $\phi_{ij}^{(2)}(\omega_1, \omega_2)$ become singular for $\omega_2 = 0$. However, following Soos and Ramasesha [106], it is possible to obtain static γ values from the dynamic values at two different frequencies by a Taylor expansion. We have computed $\gamma_{xxxx}(0)$ using this method from THG coefficients at two different frequencies of $0.1t$ and $0.2t$, at the crossover region ($U = 2V$) between SDW and CDW phases. In Fig. 9, we present the ln-ln plot of $\gamma_{xxxx}(0)$ vs L for a dimerized chain ($\delta = 0.09$). The $\gamma_{xxxx}(0)$ value is positive and the thermodynamic limit of the CDW phase is not reached even at the maximum chain length (20-site chain) we have studied; $\gamma_{xxxx}(0)$ has a power law dependence on chain length L with an exponent of 3.94. This is very close to the value for Pariser-Parr-Pople models obtained from an earlier exact study of finite chains in the static limit [106].

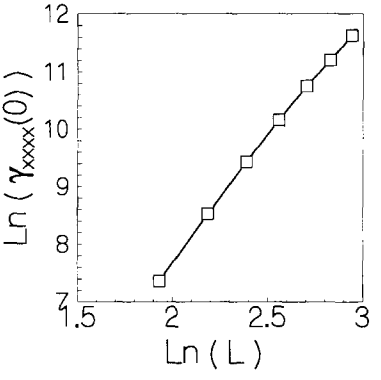

Figure 9: Ln-Ln plot of $\gamma_{xxxx}(0)$ with chain length for the parameters U=3t, V=1.5t and $\delta = 0.09$.

7 SDMRG Studies of Conjugated Polymers

The electronic structure theory of conjugated polymers for the most part has been confined to the study of polyenes and polyacetylene, which appear as the structurally most simple conjugated chains. The focus on these compounds was sharpened by the discovery of high electrical conductivity upon doping of trans-polyacetylene and the several interesting predictions of the Su-Schreiffer-Heeger model [1, 2]. There also followed a large number of experimental studies on these systems. Interestingly, polyenes are also best suited for interacting model studies because each unit cell consists of just two sites in the dimerized case and thus exact diagonalization studies could be carried out on systems with up to six unit cells. This allowed reliable extrapolations of several properties asociated with the polymers such as optical gaps and two-photon gaps of the system in the limit of infinite chain length.

However, there exist many properties of the polyenes that cannot be studied reliably from model exact studies of oligomers consisting of just six to eight monomers. These include studies of exciton binding energies, quantum confinement and finite-size effects of the electronic excitations as well as the equilibrium or relaxed geometries of the

polyene chains in excited states. The symmetrized DMRG method can be used to study long polyene chains with a degree of reliability unmatched by any of the earlier methods.

In recent years, the focus of study in conjugated polymers has shifted to conjugated polymers containing aromatic rings, which exhibit many fascinating properties. These polymers which have phenyl groups in conjugation consist of at least six carbon atoms per unit cell in conjugation. Thus, the exact diagonalization techniques which can at best deal with two unit cells fail to provide ground and excited state properties of these systems in the polymer limit. The symmetrized DMRG technique provides the most reliable tool yet for a proper study of these systems [67]. In this section, we review some of our recent symmetrized DMRG studies of conjugated polymers.

7.1 Linear and nonlinear optical sepctra of polyene molecules

Optical spectra of polyenes have been a major focus of investigation on conjugated organic systems. Theoretically, the major task is to understand the excited-state structures. Based on semiempirical CI calculations for short polyenes, Heflin *et al.* have suggested that one higher-lying A_g state plays an important role in NLO processes [122]; this state is strongly coupled to the lowest (and most active) optically allowed $1B_u$ state. More recently, based on a model for short polyenes solved by exact diagonalization, Mazumdar and co-workers have proposed an "essential states" mechanism which has enjoyed wide recognition; these authors have shown that in strongly correlated one-dimensional systems, the NLO processes are dominated by 4 essential states, namely, the ground state ($1A_g$), the lowest optically allowed $1B_u$ exciton state, the lowest ionic even parity mA_g exciton state, and the continuum band-edge nB_u state [123]. Except for the controversial nature of the continuum band edge, the roles played by the $1B_u$ and mA_g exciton states in transient o ptical processes have been highlighted.

In previous section, we proposed the Correction Vector method to calculate both linear and nonlinear polarizabilities. However, it is cumbersome to calculate the dispersion curve because one needs to iterate the CV equation at every input frequency. Thus, in this sub-

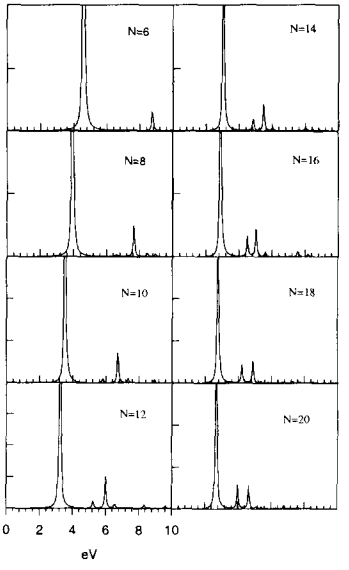

Figure 10: SDMRG linear optical absorption spectra (arbitrary units) for polyenes with 10-20 carbons.

section, we apply the common Sum-Over-States [114] approach to calculate the various excitation spectra, such as absorption, third-harmonic generation, and electro-absorption. Note that doing this requires a full diagonalization of the renormalized Hamiltonian in the symmetry adapted subspace. For instance, if we choose a DMRG cut-off $m = 120$, the Hamiltonian matrix dimension is in the order of 3000×3000. This is only doable if the cut-off $m < 150$ (while for correction vector, one can go beyond 200). In this approach, the ground state and the excited states are expressed in the same renormalized basis; thus, we construct the density matrix as the average of those for the $1A_g$ (ground state), $1B_u$, $2A_g$, and $2B_u$ states. We find that this procedure is even more numerically efficient than averaging $1A_g$, $\mu|1A_g>$ etc as suggested before [119].

Based on the "U-V" model, we first fit the experimental energies of the lowest-lying $1B_u$ and $2A_g$ states for short polyenes; we find that the optimal parameters for U and V are U=3t, V=1.2t (with

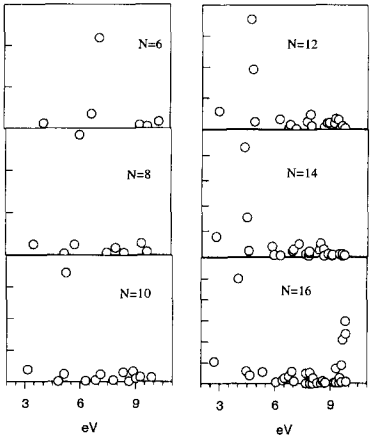

Figure 11: SDMRG two-photon absorption spectra (corresponding to the dipole transition moments from $1B_u$ to different A_g states) for N=6-16 (arbitrary units).

t=2.4 eV and alternation δ=0.07). All the optical spectra are calculated within this set of parameters.

We first turn to the discussion of linear absorption, see Fig. 10 for N=10 to 20. The highest peak always corresponds to the $1B_u$ transition. We observe that the second highest peak is usually the $3B_u$ state for short oligomers; however, as the chain length increases, the $2B_u$ transition becomes more intense. The general picture for optical absorption is that in addition to $1B_u$, there appears a small peak that would correspond to the continuum band edge threshold in very long chains. We find that the difference between $1B_u$ and $2B_u$ is 0.66 eV for N=40 (not shown in the figure). However, both from experiments and our theoretical calculations (see next subsection), the binding energy of the $1B_u$ exciton is about 0.1 eV in polyacetylene. This apparent discrepancy demonstrates that the chain length dependence of higher lying excited states is much more pronounced

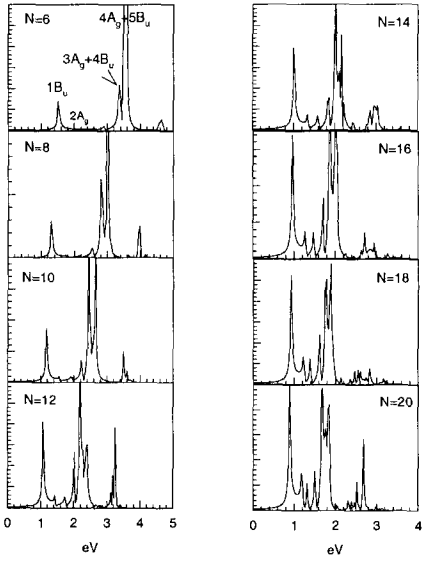

Figure 12: SDMRG theoretical third-harmonic generation (THG) spectra for polyenes with N=6-20. The units on the vertical axis are arbitrary and chosen in order to show the relative intensities of the resonance structures.

than that of the lowest lying excited state.

In Fig. 11, we depict the two-photon absorption spectra (represented by the dipole transition between the A_g excited states and the $1B_u$ state). Kohler and Terpougov have been able to measure the higher A_g states of trans-octatetraene by two-photon fluorescence excitation spectroscopy [124]. Our theoretical results for N=8 agree very well with experiment (which further justified our parameter set). There are four distinct features in Kohler and Terpougov's spectrum, located at 5.54 eV, 5.81 eV, 5.96 eV, and 6.18 eV, respectively; for a wide range of energy between 3.4 and 5.5 eV, the two-photon fluorescence excitation spectrum can only be ascribed to the $2A_g$ state and its vibronic bands. The theoretical spectrum in the high energy regime gives three features at 5.19 eV, 5.75 eV, and 6.00 eV; these three A_g states ($3A_g$, $4A_g$, and $5A_g$) are well separated from both

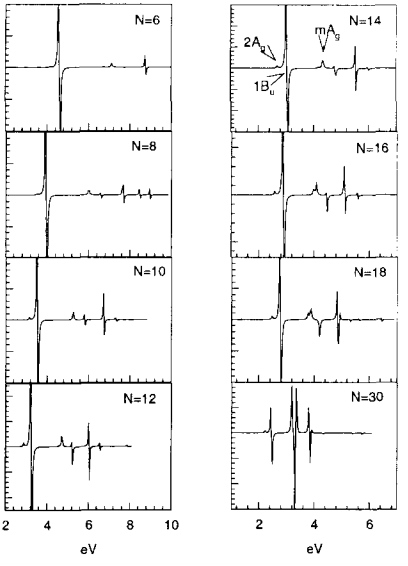

Figure 13: SDMRG theoretical electro-absorption (EA) spectra for polyenes with N=6-18 and N=30. The units on the vertical axis are arbitrary.

below and above. We believe that the middle two peaks in the experiment have the same electronic origin, namely, the $4A_g$ state and its vibronic band. Both the calculated relative intensities and positions are in good agreement with the experiment.

The third-harmonic generation (THG) and electro-absorption (EA) spectra are presented in Figs. 12 and 13, respectively. For THG, the first peak is due to a three-photon resonance to the $1B_u$ state, which is much less pronounced for short chains than longer chains. As pointed out previously, there always occurs a double resonance phenomenon in the higher energy regime, irrespective of the form of the electron interaction potential [125]. For instance, for N=6, at least two double resonances occur; namely $E(3A_g)/2$ is close to $E(4B_u)/3$ and $E(4A_g)/2$ is close to $E(5B_u)/3$. The double resonance makes the higher energy peak even more intense than that related to $1B_u$. This has been attributed to finite-size effects [126]; for very

long chains, the double resonance can disappear. For instance, in our THG calculation for N=20, the three-photon resonance to $1B_u$ becomes more intense than other peaks. Both for EA and THG, we note that the $2A_g$ state has a very weak intensity, which confirms the previous conclusion by Guo *et al.* [126]; such a small feature has been found in experiments for β-carotene [127]. We also note that the intensity of $1B_u$ relative to other peaks has a opposite tendency in EA with respect to THG when the chain length increases. In EA, for short chains, the $1B_u$ state is much more intense than the other peaks; for longer chains, the intensities of higher-lying states become increasingly important. The general EA profile for the B_u states has positive and negative parts similar to the first derivative of a Gaussian function. For the $1B_u$ state, the height of the positive part is equal to that of the negative part, which is due to the fact that $1B_u$ is well separated from any other state, so that its EA response is due to the electric-field induced exciton energy (Stark) shift (first-derivative behavior). However, for higher states, the inter-state energy spacing can be very small; the EA response is then also affected by wavefunction shifts in addition to energy shifts. Thus, in general, there can be appear asymmetry, as shown in several peak structures in Figure 13.

7.2 Binding Energy of the $1B_u$ Singlet Exciton

It has been shown that electron correlation affects strongly the polymer geometry (bond alternation) [128], excitation spectra [129, 130], and nonlinear optical response [47, 131] and it is generally accepted that an exciton is mainly responsible for the low-lying photoexcitations. However, the location of the conduction band edge and the exciton binding energy (E_b) are still imprecise both from experimental and theoretical standpoints. Early experimental estimates led to $E_b \sim 0.1$ eV [132]. Recently, in the context of investigations on the remarkable photocurrent and luminescence properties of poly(paraphenylene vinylene), PPV, the value of exciton binding energy has become a hotly debated issue. No less than four models of binding have been proposed: (i) very weak binding (semiconductor band model), $E_b \sim 0.025$ eV [133]; (ii) weak to intermediate binding, $E_b \sim 0.2$ eV [134]; (iii) intermediate binding $E_b \sim 0.4$ eV

[135, 136, 137]; and (iv) very strong binding, $E_b \sim 1$ eV, with a theoretical explanation based on the strong correlation picture [138]. Earlier quantum-chemical calculations show that the exciton binding energy is extremely sensitive to both the level of sophistication at which electron correlation effects are treated and the basis size, and usually provide too large a binding energy in comparison to experiment [139, 140].

We have applied the symmetrized density matrix renormalization group (SDMRG) theory to calculate the $1B_u$ singlet exciton energy and charge excitation band gap within a reasonable parameter space of the extended Hubbard-Peierls model, *i.e.*, the "U-V" model supplemented by the consideration of the δ dimerization term. To improve the accuracy of our results, we have used the finite-size symmetrized DMRG method in all our studies. The extent of improvement in accuarcy (ranging from 10^{-2} to 10^{-3} eV) by the finite DMRG algorithm depends on the parameters in the Hamiltonian. For instance, for more delocalized systems (small alternation δ or small Hubbard U), the improvement is larger than in the case of larger δ or U. Thus, the finite DMRG scheme introduces larger improvements where the infinite scheme is more in error, rendering the method almost equally accurate over the entire parameter range of U and δ.

To study the exciton binding, we must necessarily include at least the V term, namely, the nearest neighbor density-density interaction, which is the origin of attraction between electron and hole. This term represents a physics that is different from the Hubbard model in terms of the excitation spectra [123]. Generally speaking, the long-range character of the Coulomb interaction is essential for describing exciton binding. However, it is known that DMRG works extremely well for short-range potentials [65, 69]; this is the reason why we have chosen to keep only the nearest-neighbour interaction term in our studies. This model contains the minimum physics required to support a bound exciton and at the same time renders itself to a numerically accurate study. The importance of the bond-alternation parameter δ has been emphasized by Soos, Ramasesha and Galvao [107]; it provides the simplest way to incorporate the molecular structure in a model study and rationalizes interesting features associated

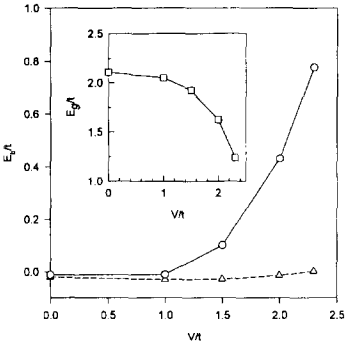

Figure 14: Dependence of the $1B_u$ binding energy (E_b) on V/t for $U/t = 5.0$. Circles represent $\delta = 0.2$ and triangles $\delta = 0.0$. The inset shows the dependence of the band gap (E_g) on V/t for $\delta = 0.0$.

with it. For instance, δ can induce a $2A/1B$ crossover, namely, for δ smaller than a critical value δ_c, $E(2A) < E(1B)$, *i.e.* the two-photon gap lies below the one-photon gap. We also note that the condition for spin-density-wave (SDW) or bond-order-wave (BOW) phase is $U > 2V$ [128] and conjugated polymers belong to this region of the phase space.

Pang and Liang have calculated the charge excitation gap for the Hubbard-Peierls model, which is defined for a neutral chain of N sites (number of electrons $N_e = N$) as $E_g(N) = E(N_e = N+1) + E(N_e = N-1) - 2E(N_e = N)$ [105]. We note that this is not the optical gap in the extended Hubbard-Peierls model, since the definition excludes the contribution due to Coulomb attraction between electron and hole. Instead, this quantity becomes our definition of charge excitation band gap which constitutes the continuum edge, the reason being, taht at the band edge, the electron and hole are uncorrelated

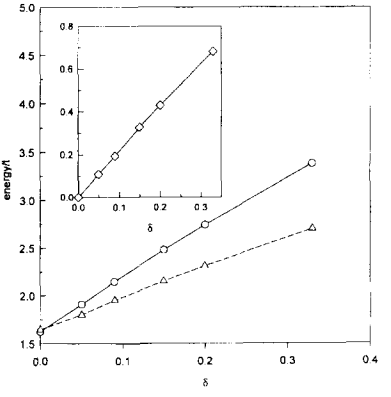

Figure 15: Dependence of band gap, E_g (circles), and $1B_u$ exciton energy (triangles) on alternation δ for $U/t = 5.0$ and $V/t = 2.0$. The inset shows the dependence of the binding energy E_b on δ.

and can be assumed to be on two different chains. This approximation implies that the charge gap provides an upper limit on the band edge. Thus, the exciton binding energy is defined as $E_b = E_g - E(1B_u)$. Strictly, this definition is only valid for an infinite chain; for a finite chain, the error is on the order of $1/N$. Besides, the exciton binding energy we calculate from this above definition of band edge should provide the upper limit for an isolated infinite chain. We note that finite-size effects for E_g are lower than for $E(1B_u)$, because $1B_u$ represents two charge carriers on a single chain, while for calculating E_g, there is only one additional charge; the chain ends have then a smaller effect. (As a result, within the Hubbard model where E_b is known to be zero, E_b as calculated with the DMRG method will actually be slightly negative and of the order of $1/N$.)

The DMRG cut-off is taken to be $100 \leq m \leq 150$ and since the

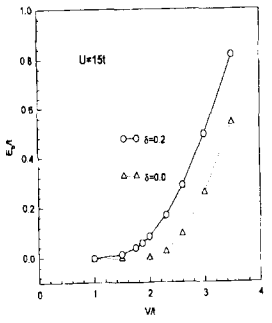

Figure 16: Dependence of the $1B_u$ exciton binding energy on V (with $U = 15t$) for $\delta = 0$ (dotted line) and $\delta = 0.2$ (solid line).

DMRG method is more accurate for stronger correlation, we choose smaller m values in the above range for larger U values. The accuracy is always high enough to give a definite answer concerning exciton binding energy, which contains an intrinsic error of $1/N$.

There exist two recent studies on exciton binding energies in the large U limit of the extended Hubbard-Peierls model, that aim at finding the critical V (V_c) value beyond which the binding energy increases with increasing V. Yu, Saxena and Bishop (YSB) [141] have applied a mean-field model in which the charge and spin degrees of freedom are separated in the large U limit and used a $t - matrix$ formulation in treating the V term as a perturbation; these authors find that V_c is equal to $4t^2(1 + \delta^2)/U$. In contrast to this result, Gallagher and Mazumdar (GM) [142] have performed a mapping of the model Hamiltonian in the subspace of $N_2 = 1(i.e.$, only one doubly occupied site) to a ferromagnetic Ising-Heisenberg spin model, which can be solved analytically for zero dimerization in the infinite

Table 1: $1B_u$ exciton binding energies and, in parentheses, $1B_u$ state energy (for $t = 1$); V/U is fixed at 0.4. If we take the experimental $1B_u$ energy values for PA ($\delta = 0.07$) and PPV ($\delta = 0.15 - 0.2$), then the E_b values can be scaled in absolute units (eV) and are given underlined.

δ	U	
	3	5
0.07	0.042	0.149
	(0.947)	(1.879)
	<u>0.080</u>	<u>0.143</u>
0.15	0.123	0.328
	(1.327)	(2.152)
	<u>0.222</u>	<u>0.366</u>
0.20	0.18	0.430
	(1.54)	(2.312)
	<u>0.28</u>	<u>0.446</u>

U limit; these authors have found that the critical value of V_c is equal to $2t$ and decreases very slowly with increasing δ. The results of Yu, Saxena and Bishop are in disagreement with the Bethe *ansatz* results for $V = 0$, $\delta = 0$, where the band edge of the excited states should be at $U - 4t$ and not U; hence, the V_c value from their study is taken with much caution. The results of Gallagher and Mazumdar are exact for $\delta = 0$ in the large U limit and are consistent with earlier results.

Small to intermediate correlation regime: The main results of our study could be summarized as follows.

1. For $V = 0$, as expected for the Hubbard-Peierls model, the binding energy E_b is always calculated to be a small negative quantity $O(1/N)$ for any U and δ. This excellent agreement with the physical picture serves as a check on our numerical scheme.

2. For $\delta = 0$ and for fixed $U(= 5t)$, V does not induce any binding in the BOW phase ($V < U/2$). V lowers both the band gap

and the $1B_u$ exciton energy, see Fig. 14. The V term is the origin of exciton binding. However, V also increases electron delocalization by largely renormalizing the t term; this eventually increases the electron-hole seperation which is largest for $\delta = 0$.

3. For fixed electron correlation strength, E_b increases with increasing δ (Fig. 15). This implies that the larger the δ value, the more excitonic-like is the lowest charge excitation.

4. For fixed δ (*e.g.*, 0.2), small V values have little effect on E_b; however, a larger V strongly enhances E_b (see Fig. 14). We note that the exciton is bound only when V is large enough relative to U.

To relate our results with experimental findings, we present in Table 1 the DMRG results for the $1B_u$ exciton state and binding energies for three sets of correlation strengths and bond alternation parameters. The alternation parameter for polyacetylene (PA) is 0.07 from its bond-length data. Soos *et al.* have proposed an effective δ of 0.2 for systems containing phenylene rings [143]. We assume that poly(paraphenylene vinylene), PPV, can be described in an effective way as a regular copolymer of poly(paraphenylene) and polyacetylene, PA [144]; thus, we consider the effective bond alternation for PPV to be within the range $0.15 - 0.2$. Note that V/U is fixed at 0.4 in Table 1. In a one-dimensional correlated system, it has been shown that the $1B_u$ state is nearly responsible for all the oscillator strength of the system and the continuum band states hardly show up in linear absorption [123]; as a result, we take the optical absorption data to set the $1B_u$ state energy: 1.8 eV for PA and 2.4 eV for PPV. We then set the t values for different (U, V)'s using these experimental optical gaps [145]; namely the actual t value for PA and PPV are evaluated as $E^{exp}(1B_u)/E^{theo(t=1)}(1B_u)$. The binding energies corresponding to these t values are also reported in Table 1.

For PA, we have already noted that earlier quantum-chemical calculations gave a range of large E_b values, while the experimental estimate corresponds to an E_b value as small as about 0.1 eV within the whole range of parameters given in Table 1. Another quantity of interest is the ratio of exciton binding energy to the optical gap,

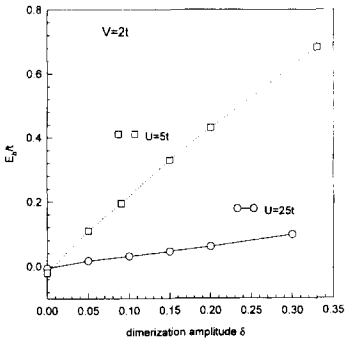

Figure 17: Dependence of the $1B_u$ exciton binding energy on δ (with $V = 2t$): solid line for $U = 25t$ and dotted line for $U = 5t$.

which we also present in Table 1. The theoretical ratio for PA is in good agreement with experiments. For PPV also, the $E_b/E(1B_u)$ ratios are in agreement with the experimental findings by Campbell *et al.* [134], Friend *et al.* [135] and Kersting *et al.* [136], as well as the results of the phenomenological calculations by Gomes da Costa and Conwell [137]. The DMRG E_b values are thus in the weak to intermediate range. We would like, however, to draw attention to the fact that interchain interactions as well as intrachain relaxations are neglected in the DMRG study.

One of the limitations of our study in the case of PPV is that the actual geometry (topology) of the polymer is not taken into account. Besides, it is also known that the actual polyenes have correlations which extend beyond the nearest neighbour. It is not possible to parametrize the "U-V" model such that the full excitation spectrum is in good agreement with the Pariser-Parr-Pople model values. This factor could also influence the exciton binding energy significantly as

we will discover below.

Large correlation regime: Numerically, we extend the U parameter to a much larger magnitude range, in order to compare the DMRG results with those of the recent results of GM and YSB based on the large U limit. It is known that DMRG works better for stronger correlation strengths. Thus, the numerical accuracy is extremely good in this limit.

In Figure 16, we present the relation between the $1B_u$ binding energy and V for $U = 15t$ for two different dimerization amplitudes (δ=0 and 0.2) at a chain length of $N = 60$. The result for δ=0 confirms the conclusion of GM that the critical V value is $V_c = 2t$. This critical value decreases as soon as the dimerization, δ, is included. This casts much doubt on the validity of the results of YSB, in which the critical point occurs at $4t^2(1+\delta^2)/U$: this value is quantitatively too small and shows the opposite trend with δ: instead of V_c decreasing, it increases with δ.

We note that even for such a large $U(= 15t)$ value, the V_c value is quite sensitive to δ, even though it is more weakly dependent on δ than in the case of the smaller $U(= 5t)$ used in the study of PA and PPV discussed above. From Figure 16, the V_c value is found to be around $1.7t$ for $\delta = 0.2$, which differs significantly from $2t$ in comparison with GM's V_c value of $1.97t$ for this value of δ; this implies that even at $U = 15t$, we have not reached the infinite U limit. In other words, the argument that the large U behavior is already shown for $U > 4t$ [142] is highly questionable.

As demonstrated in the above, the dependence of E_b on δ is rather strong (as shown for U=5t in Figure 15); this is in sharp contrast to, and actually constitutes the major point of disagreement with GM's work. In Figure 17, we present again the E_b *vs.* δ curve for an even larger value of $U = 25t$, in order to compare with the previously chosen $U = 5t$ case. It is clearly seen that the δ-dependence of E_b is strongly suppressed by U. Thus, the applicability of the strongly correlated picture should be considered with much caution when dealing with real polymers.

Most interestingly, we find that the Hubbard U decreases drastically the $1B_u$ exciton binding energy. We have shown the U-dependence of E_b in Figure 18. In fact, this result does clarify the

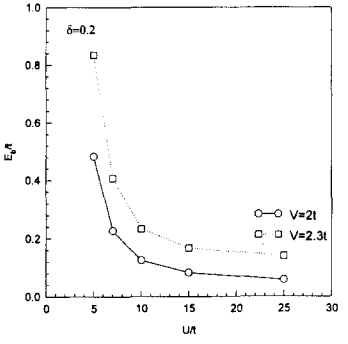

Figure 18: Dependence of the $1B_u$ exciton binding energy on U (with $\delta = 0.2$) for $V = 2t$ (solid line) and $V = 2.3t$ (dotted line).

quantitative disagreement with GM. For instance, for $V = 2.3t$ and $\delta = 0.2$, the E_b value decreases from $0.82t$ at $U = 5t$ to $0.14t$ for $U = 25t$, in good agreement with GM's $0.1t$ value for infinite U. This behavior is actually rather counter-intuitive: exciton binding is a correlation effect, the Hubbard U would be expected to increase it, as argued by GM. More work is definitely required to clarify this intriguing point.

7.3 U-V and Pariser-Parr-Pople Model Studies on the Ordering of Lowest Excited States

The prospect of potential applications due to the extraordinary luminescence properties of conjugated organic materials have underscored the importance of gaining insights into the structure of low-lying electronic excited states of these systems. Specifically, a major issue is the relative ordering of the lowest dipole allowed singlet ($1^1B_u^-$) state

and the lowest dipole forbidden singlet ($2^1A_g^+$) state, in the light of Kasha's rule which relates molecular fluorescence to the lowest excited singlet state.

It is well established that correlated electron systems behave differently from independent electron systems, especially in the case of electronic excitations. Earlier experimental work has shown that the lowest optically forbidden excited state, $2A$, lies below the optically allowed excited state, $1B$, in polyene molecules [146] (thus preventing any significant luminescence in such compounds), while an independent electron model gives the opposite picture; similar results have been found by Periasamy *et al.* in the case of polycrystalline sexithienyl [147] or Lawrence *et al.*, in single crystal polydiacetylene [148]. When going from oligomer to polymer chains, continuum band states are formed, derived from higher-lying excited states of oligomers, while the $1B$ and $2A$ states keep an excitonic character. However, it is important to stress that the electronic and optical properties of conjugated oligomers and polymers differ, depending on whether the compounds are in the gas phase, in solution, or in the solid state [149]. The chemical environment affects the geometric structure as well as the electron correlation strength, the latter *via* dielectric screening [121]. Furthermore, the characteristics of the conjugation defects present in oligomers depend on chain length, which emphasizes the influence of quantum size effects [150]. In view of these features, we believe that these three factors: (i) geometric structure, (ii) strength of electron correlation, and (iii) quantum confinement, are most relevant for the study of the photo- and electro-luminescence response in organic conjugated chains.

Previous studies of the $1B/2A$ crossover behavior have been carried out for short-chain systems. In the independent electron limit, the $2A$ energy is significantly higher than that of $1B$ due to the discreteness of the molecular orbital energy spectrum; in this zero U limit, the $2A$ state corresponds to single HOMO to LUMO-1 (or HOMO+1 to LUMO) excitation while $1B$ is a HOMO to LUMO excitation. According to previous results [151, 128], as electron correlation U is turned on, the gap between the ground state and the $2A$ state narrows while the gap to the 1B state increases; the states thus cross at a critical Hubbard correlation strength U_c. This, we

refer to as the "*U-crossover*". However, for an infinite chain, the $2A$ and $1B$ states both occur at the same energy in the Hückel limit ($U = 0$). If the $2A$ and $1B$ states were evolving in a manner identical to that in the short chains, these states would never cross with increasing U. Thus, for a given U, there must occur a crossover from the short-chain behavior to the long-chain behavior; this, we refer to as the "*N-crossover*".

It was noted by Soos, Ramasesha and Galváo [107] from exact diagonalization studies of short chains that a similar crossover occurred with variation of the bond-alternation parameter δ, which we refer to as the "*δ-crossover*". The *δ-crossover* was studied by monitoring the optical gap and the lowest singlet-triplet (spin) gap; the critical δ_c for a given correlation strength was determined by the value of δ at which the optical gap equals twice the spin gap. These authors further described the system as behaving band-like for δ values above δ_c and correlated-like for δ values below δ_c. However, as was pointed out earlier [152], increasing bond alternation does not lead to the band picture, because the binding energy of the $1B$ exciton increases with increasing δ, which indicates that electron correlation also increases at the same time. Here, we present a detailed SDMRG study that encompasses the three kinds of crossovers, namely the U, N and *δ-crossovers* in conjugated chains. We first discuss an extended Hubbard-Peierls study of the three kinds of crossover behaviors.

Crossover behaviors: We contrast the "*U-crossover*" for short (N=8) and long (N=80) chains for fixed alternation $\delta = 0.07$ in Fig. 19. It is well known that in the strong correlation limit, the $2A$ state becomes a spin excitation which is gapless in the limit (V, δ)=0 and this state can be described as composed of two triplets, as suggested earlier by Tavan and Schulten [130, 153]. Thus, increase in correlation strength should lead to a decrease in the $2A$ energy [153]. However, we note that in the N=8 chain, the energy of the two-photon state remains nearly constant before decreasing for values of U/t larger than 2.0. In longer chains, the $2A_g$ energy increases even more rapidly with increasing correlation strength, than the $1B_u$ energy. This implies a substantial ionic contribution to the $2A_g$ state in long chains besides the covalent triplet-triplet contribution. This result constitutes the first clear illustration of the importance of quantum

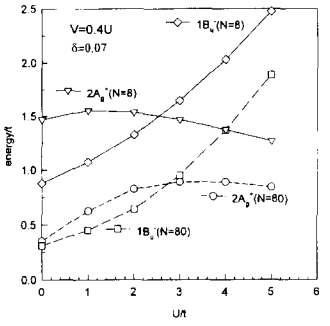

Figure 19: Crossover on U for $\delta = 0.07$ and $V/U = 0.4$.

size effects. We find, however, that the critical correlation strength, U_c, at which the crossover occurs is nearly independent of the chain length N; in both N=8 and N=80 cases, U_c is around $2.5t$.

For fixed correlation strength ($U/t = 3$ and 4), we present the "δ-*crossover*" results for N=8 and 80 in both Fig. 20 and Fig. 21 for two values of U. We find that the critical δ value, δ_c, strongly depends on chain length. For U/t=3, the δ_c values are found to be 0.15 and 0.09 for N=8 and 80, respectively; for U/t=4, they are 0.32 and 0.22. Thus, δ_c has both strong N and U dependence. We also show in Fig. 20 and Fig. 21 the crossover behavior between the $1B_u$ energy and twice the lowest triplet energy, E_T. This crossover occurs at systematically smaller δ values, again emphasizing the larger ionic character present in the $2A_g$ state compared to the lowest triplet state.

Most interestingly, the "*N-crossover*" behavior is found in the case of intermediate U/t and medium to large δ values. We observe that the $1B_u$ and $2A_g$ states cross over for fixed U/t and δ as a

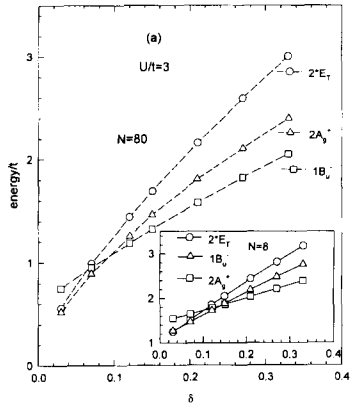

Figure 20: Crossover on δ for $U/t = 3$.

function of N, the chain length. The critical lengths are actually fairly insensitive to U and δ. For U/t=3, δ=0.12 we find the crossover for N=14 (Fig. 22) and for U/t=4.0, δ=0.27, the crossover occurs at N=12 (Fig. 23). This is a direct theoretical observation of quantum confinement induced crossover. It is related to the fact that the $2A_g$ excitation is more local in character with a shorter characteristic length than the $1B_u$ state. Thus, the $1B_u$ excitation is stabilized over longer length scales than the $2A_g$ excitation. This is seen as a more rapid saturation in the $2A_g$ energy compared to the $1B_u$ energy, as a function of chain length. We note that this crossover can also be seen from Fig. 20 and Fig. 21 where the δ_c values show a decrease in going from N=8 to N=80. This behavior can only exist for intermediate correlation strength: for weak correlation, there does not exist any crossover and $2A_g$ lies above the $1B_u$ state for all chain lengths as seen from Fig. 19; at large values of U/t, we are in the atomic limit, a crossover is not expected and the quantum size effects are largely suppressed. It has been widely accepted that the conju-

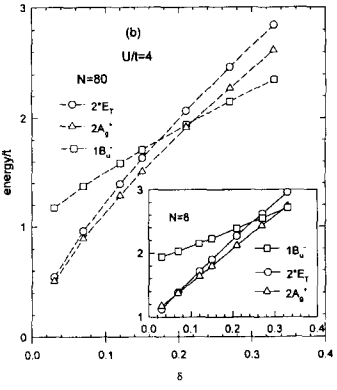

Figure 21: Crossover on δ for $U/t = 4$.

gated molecules fall in the intermediate correlation regime; thus, the confinement-induced crossover is realistic.

Note that, we have not included the points for N=2. We stress that the dimer limit (N=2) constitutes a special case, which cannot be extrapolated to longer chains, as far as the $2A_g$ state is concerned. In the dimer limit, the exact solution for the energies of the four states at half-filling are given by $E(1A_g) = -\epsilon$; $E(Triplet) = 0$; $E(1B_u) = U - V$; $E(2A_g) = \epsilon + U - V$, where $\epsilon = -(U - V)1/2(\sqrt{(U-V)^2 + 16t^2(1+\delta)^2} - (U - V))$. In fact, $2A_g$ in the dimer is always higher than $1B_u$ regardless of the parameters U and V. In the strong correlation limit ($4t/(U - V) \to 0$, $\epsilon \to 0^+$), we note that $E(1B_u)$ becomes degenerate with $E(2A_g)$ from below. From Fig. 19, the "*covalent*" $E(2A_g)$ should come down well below $E(1B_u)$. The calculated $2A_g$ state in the dimer limit has a totally different character from that in cases $N > 2$. In fact, in a two-site system, there is no space to construct two coupled triplet states; as a result, the $2A_g$ state then corresponds to an higher-lying ionic ex-

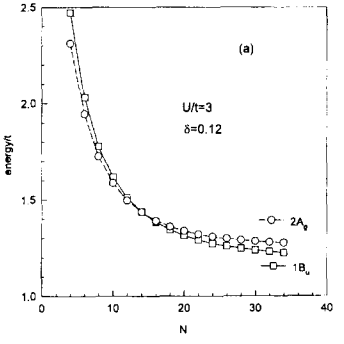

Figure 22: Crossover on N for $U/t = 3$ and $\delta = 0.12$.

citonic mA_g state of long chains, as discussed in Ref. [123], a feature which deserves further study.

PPP model studies of $1B_u/2A_g$ crossover in polyenes:

We here investigate in more depth the specific case of polyene molecules. Contradictory theoretical results have been found in the literature concerning the ordering of $2A_g$ and $1B_u$ states, due to difficulties in treating electron correlation effects with traditional approaches, even for polyenes with moderate sizes, e.g. $N \sim 20$. The limited experimental data indicate that the $2A_g$ state is below $1B_u$ starting from $N = 6$ [154]. Most interestingly, extrapolation of the N=6 to N=16 results indicate that the gap between $1B_u$ and $2A_g$ increases as the chain length increases [155, 154]. A rough extrapolation by Kohler placed the $2A_g$ state energy at half of that of $1B_u$ in long chain limit [156].

We have studies finite polyenes with long chain lengths employing the PPP model with Ohno parametrization. Even for the long range Ohno potential, the SDMRG results are found to be nearly exact

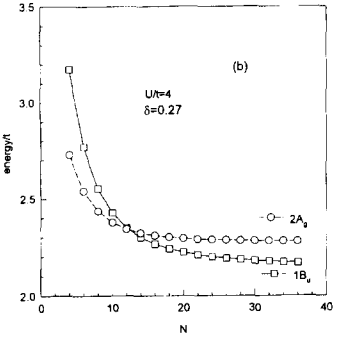

Figure 23: Crossover on N for $U/t = 4$ and $\delta = 0.27$.

for the ground state and a few excited states from comparison with model exact results for $N \leq 14$ sites. The accuracy of the calculations can be gauged from the fact that the energy of the targeted state converges with the increase in
the order (the cut-off, m) of the truncated density matrix eigenstates; for instance, the ground state energy changes by less than a ppm when the cut-off, m, is increased. The reason for this accuracy could be that the interaction part is diagonal in the real space representation.

The evolution with chain length of the lowest-lying excited states of polyenes within the PPP model is depicted in Figure 24. For the chosen set of parameters, namely, t=-2.4 eV, δ=0.07, U=11.26 eV (with the widely used Ohno-Klopman potential, see Eq. (8)), there does not exist any *N-crossover*, namely, for all systems, the covalent $2A_g$ is always below $1B_u$. (Note that the "*exotic*" $2A_g$ state for N=2 is shown in Fig. 24; it is much higher in energy than both $1B_u$ and twice the lowest triplet state). Most interestingly, we find that the

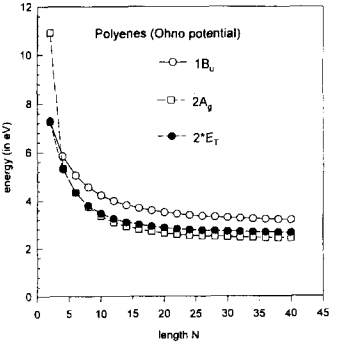

Figure 24: Pariser-Parr-Pople evolution of the $2A_g$ and $1B_u$ states in polyenes as a function of chain length.

difference between $1B_u$ and $2A_g$ increases with chain length in the short-chain regime, then levels off, and finally starts decreasing (see Fig. 25). In Table 2, we present the DMRG results which we believe represent the most accurate theoretical calculations to date.

As mentioned above, Kohler developed an extrapolation model from short-chain data and concluded that in the long-chain limit, the $2A_g$ state energy should appear at only half that of $1B_u$. Since the model is not size-consistent (because the ground state is mixed up with the lowest doubly excited configuration in his theoretical model) and the data being limited to short chains, it is not unexpected that such an extrapolation is in sharp contradiction with the results of our accurate calculations. In fact, if we extrapolate to polyacetylene our data on the long polyenes, the $1B_u$ and $2A_g$ state energies are found to be 2.92eV and 2.31eV, respectively (the difference thus being 0.61eV). The 2.92eV value for the $1B_u$ energy is about 1eV higher than the experimental result for polyacetylene in the solid

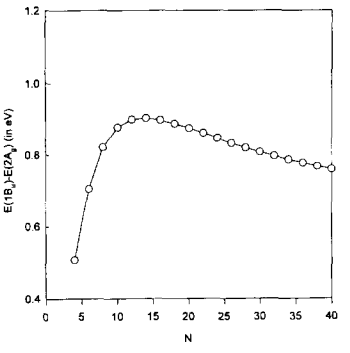

Figure 25: Evolution of $E(1B_u) - E(2A_g)$, as a function of polyene chain length, in the Pariser-Parr-Pople model.

state. The discrepancy can be ascribed to solid-state polarization effects (or to the inadequacy of molecular parameters for solids). The solid-state polarization effects should be smaller for the $2A_g$ state than for $1B_u$, because the former is "*covalent*" while the latter is "*ionic*"; the $1B_u - 2A_g$ should thus reduce in going from gas phase to solid state. Another aspect is that the solid-state polarization affects more an anion or cation state (thus, the continuum bandgap) than the $1B_u$ state, which is a bound state of two opposite charges; this argument leads Moore and Yaron to stress that the polarization effect should act to decreas the $1B_u$ exciton binding energy [157].

7.4 DMRG studies of the Lattice Relaxation

One of the interesting predictions of the Su-Schrieffer-Heeger model [158, 159] is that the electronic excitations are closely related to the topological distortions of the conjugated polyene chain. It is predicted that solitons are the elementary excitations both for optical

Table 2: SDMRG results for the lowest-lying excited state energies (in eV) of polyenes with 4 to 30 carbons. All the values correspond to the vertical transition energies from the $1A_g$ ground state.

N	4	6	10	16	18	20	24	28	30
$1B_u$	5.84	5.05	4.23	3.69	3.59	3.51	3.39	3.32	3.29
$2A_g$	5.33	4.35	3.35	2.79	2.70	2.63	2.55	2.50	2.48
$1T$	2.66	2.17	1.73	1.50	1.46	1.43	1.39	1.36	1.36

excitation and for charge doping. Su and Schrieffer further proposed photoexcitation-induced soliton creation, which is now known as the Su-Schrieffer mechanism [160]. According to this mechanism, photoexcited states can relax to a pair of separated positively and negatively charged solitons; unlike the doping process, this mechanism will generate solitons of both charges. This mechanism, if operating, should show a similarity between the spectra of photogenerated states obtained from a pump-probe experiment and the absorption spectra of doped polyacetylene. Unfortunately, a straightforward comparison of the photogenerated gap states and states of the doped systems, is not possible since with doping counter-ions are present which provide an electrostatic potential for the charged solitons and thereby shift the solitonic absorption energy [128, 161, 162]. We note that there were claims that the optically excited state also relaxed to a pair of neutral solitons except that the yield in this channel was claimed to be $\approx 1\%$ the yield in the charged solitonic channels [163, 164]. However, it is difficult to rationalize this situation theoretically since the coupling between the $1B_u$ state and a pair of neutral solitons requires breaking electron - hole symmetry and neither electron correlation nor electron-phonon coupling can break this symmetry. However, it is worth recalling at this point that the electron - hole symmetry is an idealized symmetry although the nonideality of the experimental situation may not be sufficient to provide observable yields in the two-neutral soliton channel. The charged solitonic states have also been studied by both Raman and infrared spectroscopies to elucidate the nature of electron-phonon coupling and the

nature of distortion surrounding the charge [163, 164, 165, 166, 167].

The state that is expected to decay into two neutral solitons is the lowest triplet state. The spins constituting the triplet state can dissociate to give rise to two neutral solitons each with spin-$\frac{1}{2}$ [168]. There have been studies of the triplet state [169, 135, 170], with this idea in focus employing the optically detected magnetic resonance technique [171]. Another excited state that has been discussed in the context of solitons is the 2^1A_g state. It was shown by Tavan and Schulten in the context of finite polyenes that this state could be regarded as composed of two triplets [153]. This was also later studied by others with a view to find the relaxation products of the 2^1A_g state. It is worth mentioning that among these studies, the work of Su dealt with longer polyene chains. Su [172] who employed a degenerate perturbation approach in both the weak correlation limit (U as perturbation) and the strong correlation limit (spin-lattice model), found that in both limits the $2A_g$ state relaxed to four solitons. However, it should be pointed out that the perturbation theory employed by Su is not size-consistent, because the double excitation configuration has been mixed with the ground state configuration. Thus, his result for N=80 is not reliable in the weak correlation limit. In the strong correlation limit, it is now well established that employing spin models is quite inappropriate [152, 173].

In the SSH model, both neutral and charged solitons will show an absorption peak at half the energy gap between HOMO and LUMO. Experimentally, both charged solitons and neutral solitons are claimed to be photogenerated and they show absorption features which are distinct and at two different frequencies [174, 175]. This feature is believed to be due to electron-electron interactions. It is by now well established that electron correlations remove the notion of a mid-gap state in the neutral odd-polyene compounds; this is demonstrated by the fact that in undistorted finite polyenes, the optical gap of both odd and even polyenes plotted as inverse chain length, fall on the same straight line in the PPP and the Hubbard models [176] and extrapolate to the same infinite chain value. In the dimerized case, while the odd and even chains extrapolate differently [177], the optical gap in the infinite chain limit are quite close in value. However, in the SSH model, the odd and even car-

bon polyenes would extrapolate differently and for zero dimerization, the extrapolated gap would be zero while for non zero dimerization, the gap for even carbon polyenes would be twice that of the odd carbon polyene, in the limit of infinite chain length. With regard to the doped states, it is well established, experimentally, that the neutral, positively charged, and negatively charged solitons absorb at different energies [178].

Thus, in so far as energetics of low-lying excited states of odd and even carbon systems and doped systems are concerned, once electron correlations are introduced, the notion of solitons as elementary electronic excitations becomes somewhat blurred [128]. Moreover, it is important to evaluate whether the associated topological features of the low-lying excitations survive when we introduce realistic electron-electron correlations. The purpose of this chapter is to study the equilibrium geometries of excitations in the Peierls-PPP model and discover if there is a relation between the relaxed geometries and the topological lattice distortions associated with solitons in the presence of realistic electron correlations.

We have employed the PPP model with independent bond distortions for a fixed electron-phonon coupling constant. The distortions of the bond lead to change in the corresponding transfer integrals. The bond distortions are introduced such that the total bond-order of the chain remains a constant. In the absence of this constraint, the purely π electron Hamiltonian would lead to a collapse of the chain to a point since the total energy of the system tends to decrease with decrease in chain length; equivalently, the π electron Hamiltonian does not have an in-built repulsive term which keeps the atoms apartsince this term comes from the σ framework and the internuclear potentials. Imposition of the constraint of constant total bond-order serves the purpose of the σ framework and the inter-nuclear potentials.

The model Hamiltonian including the electron-phonon coupling is given by:

$$H = \sum_i (1+\delta_i)(\hat{E}_{i,i+1} + h.c.) + \frac{U}{2}\sum_i n_i(n_i - 1) + \sum_{ij} V_{ij}(n_i - 1)(n_j - 1) + \frac{1}{\pi\lambda}\sum_i \delta_i^2 \qquad (43)$$

where λ is the dimensionless coupling constant, δ_i represents the deviation of the transfer integral for the $i, i+1$ bond from uniform transfer integral. All the interaction integrals appearing in the Hamiltonian are scaled in units of the uniform transfer integral. The form of λ can be obtained by noting that the alternation in the transfer integral $\delta = \alpha x/t_0$, where α is the electron- phonon coupling constant and x is the bond displacement. The strain energy is given by $\frac{1}{2}kx^2/t_0$, where k is the force constant of the bond. The strain energy can be rewritten as $\frac{1}{2}k\delta^2 t_0/\alpha^2$ and equating it to the strain term in the Hamiltonian, namely $1/\pi\lambda\delta^2$ one obtains for the coupling constant $\lambda = 2\alpha^2/\pi k t_0$.

The constraint of constant total bond-order is introduced via the method of Lagrange undetermined multiplier, so that the functional that is minimized with respect to δ_i is $F = H + L$, where $L = \zeta \sum_i \delta_i$, ζ being the undetermined multiplier.

$$\frac{\delta < F >}{\delta(\delta_i)} = -\sum_{\sigma} < (c^{\dagger}_{i\sigma} c_{i+1\sigma} + c^{\dagger}_{i+1\sigma} c_{i\sigma}) > + \frac{2}{\pi\lambda}\delta_i + \zeta = 0 \tag{44}$$

The Lagrange multiplier ζ turns out to be the average bond order $\bar{p}$ and we get:

$$\delta_i = \pi\lambda(p_i - \bar{p}); p_i = 1/2 \sum_{\sigma} < c^{\dagger}_i c_{i+1} + h.c. > \tag{45}$$

In the actual calculations, we start with either $\delta_i = 0$ or the δ_i value corresponding to the ground state and iterate on the δ_i values obtained from the desired eigenstate until the bond order profile δ_i vs i converges.

The π coherence length for a reasonable value of the electron-phonon coupling constant of $\lambda = 0.1$ is rather large, implying the need to study fairly long chains in the regange $40 \leq N \leq 60$, where the usual quantum chemical or related many-body methods for obtaining the ground and excited states to reliable accuracy fail. However, the SDMRG method can be applied to this problem since the distortion does not break any of the crucial symmetries of the undistorted model. We have used the finite SDMRG algorithm in all the

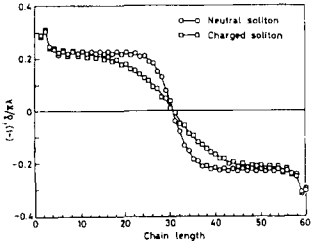

Figure 26: Bond order profile for neutral (squares) and charged (triangles) solitons for a polyene chain of 61 carbon atoms.

calculations to enhance the accuracy of our computations over and above what is inherent in the infinite SDMRG method for these systems. Besides, in the finite DMRG iteration, we obtain the bond orders of the newly introduced bonds at each stage of the iteration to modify the transfer integrals corresponding to those bonds at the next stage of the iteration. The finite DMRG iterations are continued until the bond order profile converges. Our calculations for the excited states start with the relaxed ground state geometry and hence can give the vertical excitation energies. Besides, the calculations for the self- consistently relaxed geometries give us the relaxation energies for various states.

We have studied the geometries of four states, namely, the ground state, the lowest one-photon state, the lowest two-photon state, and the lowest triplet state. We have studied the excited states in both the unrelaxed geometry (corresponding to the geometry of the ground state) and the relaxed geometry, for various chain lengths. We have

also studied the relaxed geometries of the neutral and charged solitonic configurations, corresponding to the ground state of an odd-polyene chain and its ion, respectively. For a value of the coupling constant $\lambda = 0.1$, we find that the ground state of the polyene has a bond alternation of $\delta = 0.07$, which is in agreement with experiments. The magnitude of bond alternation scales linearly with λ for $0 \leq \lambda \leq 0.2$. We have carried out all our studies fixing the value of λ to be 0.1.

In Fig. 26, we show the equilibrium bond order profile for the neutral and charged solitons in a polyene of 61 carbon atoms. We find the typical tangent hyperbolic dependence of the bond order as a function of bond number, barring the chain-end effects. What is interesting to find is the fact that the soliton width of the neutral soliton is lesser than that of the charged soliton. In fact, this agrees with the earlier quantim chemical calculation by Boudreaux et al. This is purely a correlation effect and the bond lengths are rearranged over a longer length of the chain to accommodate the excess charge in the charged soliton. We also find that the relaxation energy associated with the neutral soliton is smaller than that associated with the charged soliton. The energy of the charged soliton state is now dependent upon the nature of the charge and thus lifts the degeneracy of the positively and negatively charged solitons.

In Fig. 27, the relaxation energy of the $2A_g$ and $1B_u$ states as well as the relaxation energy of the polaronic ground state are plotted for various chain lengths, for an electron- phonon coupling constant $\lambda = 0.1$. The $2A_g$ relaxation energy is 0.8 ± 0.06 eV for all chain lengths studied and is in fact the largest in magnitude of all the states considered in this study. The relaxation energy of the $1B_u$ state is 0.2 ± 0.01 eV while the polaron relaxation energy is about 0.04 eV in the long chain limit, which is about the same as in original SSH model. Note that in SSH model, the relaxation energy of $1B_u$ is about 0.56 eV, thus correlation which induces eletron hole binding, tends to reduce the relaxation energy of this excitation.

In order to understand these relaxation energies, we need to look at the bond-order profiles of these states, see Fig. 28. The ground-state equilibrium geometry corresponds to an almost ideal bond alternation pattern along the entire length of the chain, except for

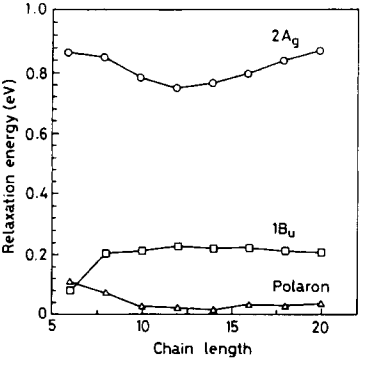

Figure 27: Relaxation energies of the $2A_g$, $1B_u$, and polaronic states as a function of chain length.

some chain-end effects. The $1B_u$ excitation shows an almost gradual distortion of the profile with the largest change in bond order for the central bonds is about 0.15 (while at the ends the difference in the bond order profiles of the $1A_g$ state and the $1B_u$ state is much less). In contrast, the $2A_g$ profile is very different from the ground state bond order profile. In fact, the bond order profile of this two-photon state shows the signature of *two* soliton-antisoliton pairs; the bond profile of the triplet state shows *one* soliton-antisoliton pair. The rather large deviation of the bond order profiles is consistent with the fact that the relaxation energies associated with these states are considerably larger than the relaxation energy of the $1B_u$ state.

In the original SSH model, the relaxation of the $1B_u$ state goes to a charged (S^+/S^-) soliton pair. However, once electron correlation effect is taken into account, the negative and positive solitons appear to attract one another to form an exciton. Nevertheless, ex-

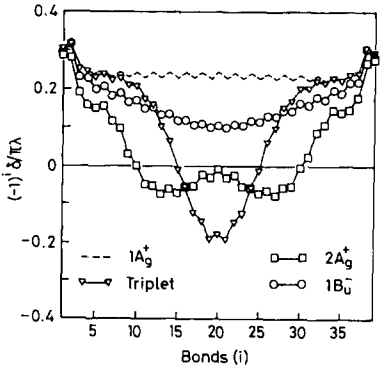

Figure 28: Bond order profile for the $1A_g$, $2A_g$, $1B_u$ and lowest triplet states as a function of bonds in the chain for the N=40 chain.

perimentally, photo-excited charged solitons have been observed. We can reconcile these contradicting results by recalling that the exciton binding energy for polyacetylene has been found to be small (less than 0.1 eV). Thus, the appearance of photo-induced charged solitons can be due to the relaxation of higher B_u states which form a continuum band and where the electron-hole separation is large so that correlation is very small. Thus, the main conclusions from the SSH model does hold for these band states.

8 Concluding remark

To summarize, we have presented a review on the renormalization group theory in the reduced many-body density matrix basis (DMRG method), and we have applied it to conjugated organic systems, with both short range and long range Coulomb interaction potentials. We

have developed the symmetry adaptation in the DMRG framework which enormously facilitates the computations of excited states and therefore the evaluation of the linear and nonlinear optical properties.

It has been shown that the ground state and the lower-lying excited states can be calculated for rather large systems (up to about 80 carbons), with extremely high accuracy. The nonlinear optical properties of conjugated chain can be evaluated through the correction vector method. Both the linear and nonlinear optical excitation spectra have been obtained and highlight several features of the excited state structures. The $1B_u$ exciton binding energy has been evaluated in the Peierls-Hubbard model. For a wide range of parameters, our results agree with the experimental data on polyacetylene ($E_b \approx 0.1$ eV). In the case of poly-(paraphenylene vinylene), the DMRG results support experimental findings which have shown the exciton binding energy to be 0.2 - 0.4 eV. Three kinds of cross-over behavior in the $1B_u/2A_g$ ordering have been demonstrated as a function of: correlation strength (U-crossover), geometry (δ-crossover), and most importantly system size (N-crossover). For a set of parameters adapted to polyenes, we find that $2A_g$ is always below $1B_u$, and as chain length increases, their difference first increases, then levels off, and finally decreases. We have also investigated the lattice relaxations in various excited states, which manifest the competing electron-electron and electron-phonon interactions: (i) the $1B_u$ state induces a more or less uniform reduction of bond-length alternation, with a relaxation energy around 0.2 eV; it does not lead to the formation of soliton-antisoliton pair as predicted in one-electron theory; (ii) the $2A_g$ state corresponds to a four-soliton structure, with a large relaxation energy of about 0.8 eV; (iii) the lowest triplet state corresponds to a well-confined soliton-antisoliton pair.

Although, throughout this work, we have presented results obtained on linear structures, the DMRG method is more general. In a recent study, the actual chemical structures of poly-paraphenylene and PPV have been taken into account [67]. The principle of the DMRG iterations for such systems is sketched in Fig. 29. Even though the 2-dimensional nature of the phenylene rings appear to contribute to a reduction in the DMRG accuracy, the one-dimensional extension of the polymers compensates for it. The general applica-

tion of DMRG for arbitrary structures deserves further study and is actively pursued.

Acknowledgements

We thank H. R. Krishnamurthy, Diptiman Sen, Kunj S. Tandon and Y. Anusooya, for many collaborations involving the development and applications of the DMRG method. The work in India is supported by the Department of Science and Technology, India and Indo-French Center for the Promotion of Advanced Research. The work in Mons is partly supported by the Belgian Prime Minister Services for Scientific, Technical, and Cultural Affairs (Pôle d'Attraction Interuniversitaires in Supramoleculare Chemistry and Catalysis), FNRS/FRFC, and an IBM Academic Joint Study. SR also thanks FNRS for a visiting Professorship.

References

[1] *Conjugated Polymers*, eds. J. L. Brédas and R. Silbey, Kluwer, Dordrecht, The Netherlands (1991); *Conjugated Polymers, Oligomers, and Dendrimers: From Polyacetylene to DNA*, ed. J. L. Brédas, DeBoeck Université, Louvain-la-Neuve, 1999.

[2] *Conjugated Conducting Polymers*, ed. H. Kiess, Springer Series in Solid State Sciences, Vol. 102, Springer-Verlag, Berlin (1992).

[3] E. Hückel, Z. *Physik* **70**, 204 (1931); **72**, 310 (1932).

[4] L. Salem, *Molecular Orbital Theory of Conjugated Systems*, Benjamin, New York (1966).

[5] R. E. Peierls, *Quantum Theory of Solids*, Clarendon Press, London (1955).

[6] See, for instance, the Proceedings of recent International Conference on Synthetic Metals (ICSM), Synth. Met. **83-85**, (1997); *Handbook of Conducting Polymers*, second edition, eds. T. A. Skotheim, R. L. Elsenbaumer, and J. R. Reynolds, Marcel Dekker, New York, 1998.

[7] Sirringhus, N. Tessler, R. H. Friend, to appear in Science.

[8] J. W. Perry, K. Mansour, I. Y. S. Lee, X. L. Wu, P. V. Bedworth, C. T. Chen, D. Ng, S. R. Marder, P. Milles, T. Wada, M. Tian, and H. Sasabe, Science **273**, 1533 (1996); .

[9] B. Kippelen, S. R. Marder, E. Hendrickx, J. L. Maldonado, G. Guillemet, B. L. Volodin, D. D. Steele, Y. Enami, Sandalphon, Y. J. Yao, J. F. Wang, H. Rockel, L. Erskine, and N. Peyghambarian, Science **279**, 54 (1998).

[10] J. Oddershede, P. Jorgensen, and D. L. Yeager, Computer Phys. Rept. **2**, 33 (1984).

[11] J. Cizek, Adv. Chem. Phys. **14**, 35 (1969); G. D. Purvis, III, and R. J. Bartlett, J. Chem. Phys. **76**, 1910(1982); J. Noga and R. J. Bartlett, J. Chem. Phys. **86**, 7041 (1987); S. A. Kucharski and R. J. Bartlett, J. Chem. Phys. **97**, 4282 (1992); J. F. Stanton and R. J. Bartlett, J. Chem. Phys. **98**, 7029 (1993).

[12] D. Yaron, E. E. Moore, Z. Shuai, and J. L. Brédas, J. Chem. Phys. **108**, 7451 (1998).

[13] A. Szabo and N. S. Ostlund, *Modern Quantum Chemistry*, Macmillan, London (1982).

[14] J. N. Murrell, *The Theory of Electronic Spectra of Organic Molecules*, Wiley, New York (1973).

[15] For a review see, S. Ramasesha, *Chemistry of Advanced Materials*, ed. C. N. R. Rao, Blackwell Scientific Publications, 237 (1993).

[16] J. A. Pople and S. H. Walmsley, Mol. Phys. **5**, 15 (1962).

[17] B. E. Kohler, Chem. Rev. **93**, 41 (1993), and references therein.

[18] M. Fedin, E. Bagryanskaya and P. Purtov, J. Chem. Phys. **111**, 5491 (1999).

[19] J. Kanamori, Prog. Theor. Phys. (Kyoto) **30**, 275 (1963).

[20] M. Gutzwiller, Phys. Rev. Lett. **10**, 159 (1963).

[21] J. Hubbard, Proc. Roy. Soc. A **276**, 238 (1964); A **277**, 237 (1964); A **281**, 401 (1964).

[22] Y. Nagaoka, Phys. Rev. **147**, 392 (1966); D. R. Penn, Phys. Rev. **142**, 350 (1966).

[23] N. F. Mott, *Metal-Insulator Transitions*, Taylor and Francis, London (1990); P. W. Anderson, Science **235**, 1196 (1987).

[24] W. Metzner and D. Vollhardt, Phys. Rev. Lett. **62**, 324 (1989) ; A. Georges and W. Krauth, Phys. Rev. Lett. **69**, 1240 (1992); M. Jarrel, Phys. Rev. Lett. **69**, 168 (1992); M. J. Rozenberg, X. Y. Zhang and G. Kotliar, Phys. Rev. Lett. **69**, 1236 (1992).

[25] R. G. Parr, J. Chem. Phys. **20**, 239 (1952); J. A. Pople and D. L. Beveridge, *Approximate Molecular Orbital Theory*, McGraw Hill, New York (1970).

[26] E. H. Lieb and F. Y. Wu, Phys. Rev. Lett. **25**, 1445 (1968); A. A. Ovchinnikov, Soviet Physics JETP **30**, 1160 (1970).

[27] For a review see, *The Hubbard Model: Recent Results*, ed. M. Rasetti, World Scientific, Singapore (1991).

[28] R. Pariser and R. G. Parr, J. Chem. Phys. **21**, 466 (1953).

[29] J. A. Pople, Trans. Farad. Soc. **49**, 1375 (1953).

[30] K. Ohno, Theor. Chem. Acta **2**, 219 (1964); G. Klopman, J. Am. Chem. Soc. **86**, 4550 (1964).

[31] N. Mataga and K. Nishimoto, Z. Physik. Chem. **12**, 335 (1957); **13**, 140 (1957).

[32] Z. G. Soos and S. Ramasesha, Chem. Phys. Lett. **101**, 34 (1983); S. Ramasesha and Z. G. Soos, Synth. Metals **9**, 283 (1984).

[33] S. Ramasesha and Z. G. Soos, Chem. Phys. **91**, 35 (1984).

[34] V. J. Emery, in *Highly Conducting One-Dimensional Solids*, ed. by J. T. Devreese, Plenum, New York (1979); K. Kuroki, K. Kusakabe and H. Aoki, Phys. Rev. B, **50**, 575 (1994).

[35] For a review, see R. Micnas, J. Ranninger and S. Robaszkiewicz, Rev. Mod. Phys. **62**, 113 (1990).

[36] J. E. Hirsch, Phys. Rev. Lett. **53**, 2327 (1984); H. Q. Lin and J. E. Hirsh, Phys. Rev. B **33**, 8155 (1986).

[37] M. del Bosch and L. M. Falikov, Phys. Rev. B **37**, 6073 (1988); J. Callaway, D. P. Chen, D. G. Kanhere, and Q. Li, Phys. Rev. B **42**, 465 (1990).

[38] A. F. Garito and A. J. Heeger, Acc. Chem. Res. **7**, 232 (1974); Z. G. Soos, S. Kuwajima and R. H. Harding, J. Chem. Phys. **85**, 601 (1986).

[39] W. Heisenberg, Z. Phys. **38**, 411 (1928); *ibid.* **49**, 619 (1929); P. A. M. Dirac, Proc. Roy. Soc. A **123**, 714 (1929); J. H. van Vleck, *Theory of Electric and Magnetic Susceptibilities*, Oxford Univ. Press, London (1932).

[40] H. A. Bethe, Z. Physik **71**, 205 (1931).

[41] L. Hulthen, Ark. Mat. Astron. Fysik A **26**, no.11 (1938).

[42] J. des Cloizeaux and J. J. Pearson, Phys. Rev. **128**, 2131 (1962); J. des Cloizeaux and M. Gaudin, J. Math. Phys. **7**, 1384 (1966).

[43] S. Ramasesha and Z. G. Soos, Int. J. Quant. Chem. **25**, 1003 (1984); J. Chem. Phys. **80**, 3278 (1984).

[44] For a review see, Z. G. Soos and S. Ramasesha, in *Valence Bond Theory and Chemical Structure*, eds., D. J. Klein and N. Trinajstic, Elsevier, Amsterdam, p. 81 (1990).

[45] G. Rumer, Nachr. Chem. Tech. Goettingen, 377 (1932).

[46] L. Pauling, J. Chem. Phys. **1**, 180 (1933); L. Pauling and G. W. Wheland *ibid*, 362 (1933).

[47] Z. G. Soos and S. Ramasesha, J. Chem. Phys. **90**, 1067 (1989).

[48] S. Rettrup, J. Comput. Phys. **45**, 100 (1982).

[49] T. De Neef, Phys. Lett. A **47**, 51 (1974).

[50] H. J. Blote, Physica B **93**, 93 (1978).

[51] R. Botet and R. Jullien, Phys. Rev. B **27**, 613 (1983); R. Botet, R. Jullien and M. Kolb, *ibid* **28**, 3914 (1983).

[52] J. B. Parkinson and J. C. Bonner, Phys. Rev. B **32**, 4703 (1985).

[53] A. Moreo, Phys. Rev. B **35** 8562 (1987).

[54] M. Takahashi, Phys. Rev. Lett. **62**, 2313 (1989); Phys. Rev. B **48**, 311 (1993).

[55] O. Golinelli, Th. Jolicoeur and R. Racaze, Phys. Rev. B **50**, 3037 (1994).

[56] H. F. Trotter, Proc. Am. Math. Soc. **10**, 545 (1959).

[57] M. Suzuki, Prog. Theor. Phys. **56**, 1454 (1976); M. Suzuki, S. Miyashita and A. Kuroda, Prg. Theor. Phys. **58**, 1377 (1977).

[58] J. Hubbard, Phys. Rev. Lett. **3**, 77 (1959); R. Stratonovich, Dokl. Akad. Nauk. SSSR **1115**, 1097 (1957).

[59] B. Srinivasan, S. Ramasesha and H. R. Krishnamurthy, Phys. Rev. B **56**, 6542 (1997).

[60] S. Zhang, J. Carlson and J. E. Gubernatis, Phys. Rev. Lett. **74**, 3652 (1995).

[61] J. E. Hirsch, D. J. Scalapino, R. L. Sugar and R. Blankenbecler, Phys. Rev. Lett. **47**, 1628 (1981); J. E. Hirsch, R. L. Sugar, D. J. Scalapino and R. Blankenbecler, Phys. Rev. B **26**, 5033 (1982).

[62] K. G. Wilson, Rev. Mod. Phys. **47**, 773 (1975).

[63] J. W. Bray and S. T. Chui, Phys. Rev. B **19**, 4876 (1979); J. E. Hirsh, Phys. Rev. B **22**, 5259 (1980).

[64] S. R. White and R. M. Noack, Phys. Rev. Lett. **68**, 3487 (1992).

[65] S. R. White, Phys. Rev. Lett. **69**, 2863 (1992); Phys. Rev. B **48**, 10345 (1993).

[66] R. McWeeny and B. T. Sutcliffe, *Methods of Molecular Quantum Mechanics*, Academic Press, London (1969).

[67] Y. Anusooya, Swapan K. Pati and S. Ramasesha, J. Chem. Phys. **106**, 1 (1997).

[68] S. R. White, Phys. Rev. Lett. **45**, 5752 (1992).

[69] S. R. White and D. A. Huse, Phys. Rev. B **48**, 3844 (1993); E. S. Sorensen and I. Affleck, Phys. Rev. Lett. **71**, 1633 (1993).

[70] E. S. Sorensen and I. Affleck, Phys. Rev. B **49**, 13235 (1994); Phys. Rev. B **49**, 15771 (1994).

[71] R. Chitra, Swapan K. Pati, H. R. Krishnamurthy, D. Sen and S. Ramasesha, Phys. Rev. B **52**, 6581 (1995); Swapan K. Pati, R. Chitra, D. Sen, H. R. Krishnamurthy and S. Ramasesha, Europhys. Lett. **33**, 707 (1996).

[72] U. Schollwock and Th. Jolicoeur, Europhys. Lett. **30**, 493 (1995); Y. Nishiyama, K. Totsuka, N. Hatano and M. Suzuki, J. Phys. Soc. Jap. **64**, 414 (1995)

[73] Y. Kato and A. Tanaka, J. Phys. Soc. Jap. **63**, 1277 (1994); U. Schollwock, Th. Jolicoeur and T. Garel, Phys. Rev. B **53**, 3304 (1996).

[74] R. J. Bursill, T. Xiang and G. A. Gehring, J. Phys. A **28**, 2109 (1994); R. J. Bursill, G. A. Gehring, D. J. Farnell, J. B. Parkinson, T. Xiang and C. Zeng, J. Phys. C **7**, 8605 (1995).

[75] S. R. White, R. M. Noack and D. J. Scalapino, Phys. Rev. Lett. **73**, 886 (1994); M. Azzouz, L. Chen and S. Moukouri, Phys. Rev. B **50**, 6223 (1994).

[76] T. Narushima, T. Nakamura and S. Takada, J. Phys. Soc. Jap. **64**, 4322 (1995); U. Schollwock and D. Ko, Phys. Rev. B **53**, 240 (1996).

[77] S. J. Qin, S. D. Liang, Z. B. Su, and L. Yu, Phys. Rev. B **52**, R5475 (1995).

[78] S. Moukouri, L. Chen, and L. G. Caron, Phys. Rev. B **53**, R488 (1996); L. Chen and S. Moukouri, Phys. Rev. B **53**, 1866 (1996).

[79] C. C. Yu and S. R. White, Phys. Rev. Lett. **71**, 3866 (1993); *ibid.*, Physica B **199**, 454 (1994); M. Guerrero and C. C. Yu, Phys. Rev. B **51**, 10301 (1995).

[80] S. Moukouri and L. G. Caron, Phys. Rev. B **52**, 15723 (1995); N. Shibata, T. Nishino, K. Veda and C. Ishii, Phys. Rev. B **53**, R8828 (1996).

[81] M. Guerrero and R. M. Noack, Phys. Rev. B **53**, 3707 (1996).

[82] S. Moukouri, L. G. Caron, C. Bourbonnais and L. Hubert, Phys. Rev. B **51**, 15920 (1995); H. Otsuka and T. Nishino, Phys. Rev. B **52**, 15066 (1995).

[83] R. M. Noack, S. R. White and D. J. Scalapino, Phys. Rev. Lett. **73**, 882 (1994); S. R. White, R. M. Noack, and D. J. Scalapino, J. Low Temp. Phys. **99**, 593 (1995).

[84] C. A. Hayward, D. Poilblanc, R. M. Noack, D. J. Scalapino and W. Hanke, Phys. Rev. Lett. **75**, 926 (1995); R. M. Noack, S. R. White and D. J. Scalapino, Europhys. Lett. **30**, 163 (1995).

[85] T. A. Costi, P. Schmitteckert, J. Kroma and P. Wolfle, Phys. Rev. Lett. **73**, 1275 (1994); S. Eggert and I. Affleck, Phys. Phys. Lett. **75**, 934 (1995); E. S. Sorensen and I. Affleck, Phys. Rev. B **51**, 16115 (1995).

[86] X. Q. Wang and S. Mallwitz, Phys. Rev. B **53**, R492 (1996); W. Wang, S. J. Qin, Z. Y. Lu, L. Yu and Z. B. Su, Phys. Rev. B **53**, 40 (1996).

[87] K. Hida, J. Phys. Soc. Japn. **65**, 895 (1996).

[88] P. Schmitteckert and U. Eckern, Phys. Rev. B **53**, 15397 (1996).

[89] R. V. Pai, R. Pandit, H. R. Krishnamurthy, and S. Ramasesha, Phys. Rev. Lett. **76**, 2937 (1996).

[90] S. J. Qin, T. K. Ng and Z. B. Su, Phys. Rev. B **52**, 12844 (1995).

[91] H. B. Pang, H. Akhlaghpour and M. Jarrel, Phys. Rev. B **53**, 5086 (1996).

[92] K. A. Hallberg, Phys. Rev. B **52**, R9827 (1995).

[93] Swapan K. Pati, S. Ramasesha, Z. Shuai and J. L. Brédas, to be published.

[94] L. J. Caron and S. Moukouri, Phys. Rev. Lett. **77**, 4640 (1996).

[95] Swapan K. Pati, S. Ramasesha and D. Sen, Phys. Rev. B **55**, 8894 (1997); J. Phys. Condens. Matt. **9**, 8707 (1997).

[96] L. G. Caron and S. Moukouri, Phys. Rev. Lett. **76**, 4050 (1996).

[97] S. Ramasesha, Swapan K. Pati, H. R. Krishnamurthy, Z. Shuai and J. L. Brédas, Phys. Rev. B **54**, 7598 (1996); Synth. Metals **85**, 1019 (1997).

[98] Z. Shuai, Swapan K. Pati, J. L. Brédas and S. Ramasesha, Phys. Rev. B **56**, 9298 (1997); Synth. Metals, **85**, 1011 (1997).

[99] T. Nishino and K. Okunishi, J. Phys. Soc. Japn. **64**, 4084 (1995).

[100] T. Nishino and K. Okunishi, J. Phys. Soc. Japn. **65**, 891 (1996).

[101] R. M. Noack and S. R. White, Phys. Rev. B **47**, 9243 (1993)

[102] E. S. Sorenson and I. Affleck, Phys. Rev. B **49**, 15771 (1994)

[103] R. Chitra, Swapan K Pati, H. R. Krishnamurthy, Diptiman Sen and S. Ramasesha, Phys. Rev. B **52**, 6581 (1995).

[104] Hanbin Pang, Shoudan Liang and James F. Annett, Phys. Rev. Lett. **71**, 4377 (1993).

[105] Hanbin Pang and Shoudan Liang, Phys. Rev. B **51**, 10287 (1995).

[106] Z. G. Soos and S. Ramasesha, Phys. Rev. B **29**, 5410 (1984).

[107] Z. G. Soos, S. Ramasesha and D. S. Galvao, Phys. Rev. Lett. **71**, 1609 (1993).

[108] S. Ramasesha and Swapan K. Pati, unpublished results.

[109] S. Etemad and Z. G. Soos, in *Spectroscopy of Advanced Materials*, ed. R. J. H. Clark and R. E. Hester, Wiley, New York (1991), p. 87.

[110] Z. G. Soos and G. W. Hayden, in *Electroresponsive Molecular and Polymeric Systems*, ed. T. A. Skotheim, Dekker, New York (1988), Vol. 1, p. 197, and references therein.

[111] S. Ramasesha, Kunj S. Tandon, Y. Anusooya and Swapan K. Pati, Proceedings of SPIE **3145**, 282 (1997).

[112] *Nonlinear Optical Properties of Organic Molecules and Crystals*, ed. D. S. Chemla and J. Zyss, Academic, New York (1987).

[113] *Materials for Nonlinear Optics: Chemical Perspectives*, edited by S. R. Marder, J. E. Sohn, and G. D. Stucky, American Chemical Society, Washington DC, 1991, vol. 455.

[114] P. W. Langhoff, S. T. Epstein and M. Karplus, Rev. Mod. Phys. **44**, 602 (1972); B. J. Orr and J. F. Ward, Mol. Phys. **20**, 513 (1971).

[115] See *The Recursion Method and Its Applications*, eds. D. G. Pettifor and D. L. Weaire, Springer, Berlin-Heidelberg (1985).

[116] E. Dagotto, Rev. Mod. Phys. **66**, 763 (1994)

[117] S. Ramasesha, Z. Shuai and J. L. Brédas, Chem. Phys. Lett. **245**, 224 (1995).

[118] S. Ramasesha, J. Comput. Chem. **11**, 545 (1990).

[119] K. Hallberg, Phys. Rev. B **52**, 9827 (1995).

[120] Z. Shuai, S. Ramasesha and J. L. Brédas, Chem. Phys. Lett. **250**, 14 (1996).

[121] S. R. Marder, C. B. Gorman, F. Meyers, J. W. Perry, G. Bourhill, J. L. Brédas and B. M. Pierce, Science **265**, 632 (1994).

[122] J. R. Heflin, K. Y. Wong, O. Zamani-Khamiri, and A. F. Garito, Phys. Rev. B **38**, 1573 (1988).

[123] D. Guo, S. Mazumdar, S. N. Dixit, F. Kajzar, F. Jarka, Y. Kawabe, and N. Peyghambarian, Phys. Rev. B **48**, 1433 (1993).

[124] B. E. Kohler and V. Terpougov, J. Chem. Phys. **104**, 9297 (1996).

[125] D. Guo and S. Mazumdar, J. Chem. Phys. **97**, 2170 (1992).

[126] F. Guo, D. Guo, and S. Mazumdar, Phys. Rev. B **49**, 10102 (1994).

[127] D. Beljonne, J. Cornil, Z. Shuai, J. L. Brédas, F. Rohlfing, D. D. C. Bradley, V. Ricci, W. E. Torruellas, and G. I. Stegeman, Phys. Rev. B **55**, 1505 (1997).

[128] C. Q. Wu, X. Sun and K. Nasu, Phys. Rev. Lett. **59**, 831 (1987); S. Mazumdar and D. K. Campbell, *ibid.*, **55**, 2067 (1985); J. L. Brédas, and A. J. Heeger, *ibid.* **63**, 2534 (1989).

[129] S. Ramasesha and Z. G. Soos, J. Chem. Phys. **80**, 3278 (1984); D. Baeriswyl and K. Maki, Phys. Rev. B **31**, 6633 (1985).

[130] P. Tavan and K. Schulten, Phys. Rev. B **36**, 4337 (1987).

[131] S. N. Dixit, D. Guo and S. Mazumdar, Phys. Rev. B **43**, 6781 (1991); S. Abe, J. Yu and W. P. Su, *ibid.* **45**, 8264 (1992); Z. Shuai, D. Beljonne, and J. L. Brédas, J. Chem. Phys. **97**, 1132 (1992).

[132] C. R. Fincher Jr., M. Ozaki, M. Tanaka, D. Peebles, L. Lauchlan, A. J. Heeger, and A. G. MacDiarmid, Phys. Rev. B **20**, 1589 (1979).

[133] C. H. Lee, G. Yu and A. J. Heeger, Phys. Rev. B **47**, 15543 (1993).

[134] I. H. Campbell, T. W. Hagler, D. L. Smith, and J. P. Ferraris, Phys. Rev. Lett. **76**, 1900 (1996).

[135] R. H. Friend, D. D. C. Bradley, and P. D. Townsend, J. Phys. D: Appl. Phys. **20**, 1367 (1987).

[136] R. Kersting, U. Lemmer, M. Deussen, H. J. Bakker, R. F. Mahrt, H. Kurz, V. I. Arkhipov, H. Bässler, E. O. Gobel, Phys. Rev. Lett. **73**, 1440 (1994).

[137] P. Gomes da Costa and E. M. Conwell, Phys. Rev. B **48**, 1993 (1993).

[138] M. Chandross, S. Mazumdar, M. Liess, P. A. Lane, Z. V. Vardeny, M. Hamaguchi, and K. Yoshino, Phys. Rev. B **50**, 14702 (1994); J. M. Leng et al., Phys. Rev. Lett. **72**, 156 (1994).

[139] C. M. Liegener, J. Chem. Phys. **88**, 6999 (1988); S. Suhai, Int. J. Quant. Chem. **29**, 469 (1986).

[140] M. Kertesz, Chem. Phys. **44**, 349 (1979).

[141] Z. G. Yu, A. B. Saxena, and A. R. Bishop, Phys. Rev. B **56**, 3697 (1997).

[142] F. B. Gallagher and S. Mazumdar, Phys. Rev. B **56**, 15025 (1997).

[143] Z. G. Soos, S. Ramasesha, D. S. Galvao, and S. Etemad, Phys. Rev. B **47**, 1742 (1993); D. Mukhopadhyay, G. W. Hayden and Z. G. Soos, *ibid.* **51**, 9476 (1995).

[144] M. Fahlman, M. Lögdlund, S. Stafström, W. R. Salaneck, R. H. Friend, P. L. Burn, A. B. Holmes, K. Kaeriyama, Y. Sonoda, O. Lhost, F. Meyers, and J. L. Brédas, Macromolecules **28**, 1959 (1995).

[145] Actually, t is a bare value in the Hamiltonian. When a one-electron picture is taken, $4t$ is the bandwidth. However, electron-electron interaction can largely renormalize t. This fact allows us to apply different t for different (U, V) pairs in estimating both exciton energy and its binding energy when comparing with experiment.

[146] B. S. Hudson and B. E. Kohler, Chem. Phys. Lett. **14**, 229 (1972); J. Chem. Phys. **59**, 4984 (1973).

[147] N. Periasamy, R. Danieli, G. Ruani, R. Zamboni, and C. Taliani, Phys. Rev. Lett. **68**, 919 (1992).

[148] B. Lawrence, W. E. Torruellas, M. Cha, M. L. Sundheimer, G. I. Stegeman, J. Meth, S. Etemad, and G. L. Baker, Phys. Rev. Lett. **73**, 597 (1994).

[149] O. Dippel, V. Brandl, H. Bässler, R. Danieli, R. Zamboni, and C. Taliani, Chem. Phys. Lett. **216**, 418 (1993).

[150] J. L. Brédas and A. J. Heeger, Chem. Phys. Lett. **154**, 56 (1989).

[151] G. W. Hayden and E. J. Mele, Phys. Rev. B **34**, 5484 (1986).

[152] Z. Shuai, S. K. Pati, W. P. Su, J. L. Brédas, and S. Ramasesha, Phys. Rev. B. **55**, 15368 (1997).

[153] P. Tavan and K. Schulten, J. Chem. Phys. **85**, 6602 (1986).

[154] B. E. Kohler, J. Chem. Phys. **93**, 5838 (1990).

[155] R. J. Cave and E. R. Davidson, J. Phys. Chem. **92**, 2173 (1988).

[156] B. E. Kohler, J. Chem. Phys. **88**, 2788 (1988).

[157] E. Moore, B. Gherman and D. Yaron, J. Chem. Phys. **106**, 4216 (1997); E. Moore and D. Yaron, Synth. Met. **85**, 1023 (1997).

[158] W. P. Su, J. R. Schrieffer and A. J. Heeger, Phys. Rev. B **22**, 2099 (1980); Phys. Rev. B **28**, 1138 (1983) (erratum).

[159] A. J. Heeger, S. Kivelson, J. R. Schrieffer and W. P. Su, Rev. Mod. Phys. **60**, 781 (1988).

[160] W. P. Su and J. R. Schrieffer, Proc. Natl. Acad. Sci. U.S.A. **77**, 5626 (1980).

[161] B. Horovitz, Solid State Commun. **41**, 729 (1982).

[162] A. Terai and Y. Ono, J. Phys. Soc. Jpn. **55**, 213 (1986).

[163] H. E. Schaffer, R. H. Friend and A. J. Heeger, Phys. Rev. B **36**,7537 (1987).

[164] Z. Vardeny, E. Ehrenfreund, O. Brafman, B. Horovitz, Phys. Rev. Lett. **54**, 75 (1985).

[165] Z. Vardeny, E. Ehrenfreund, O. Brafman, B. Horovitz, Phys. Rev. Lett. **57**, 2995 (1986).

[166] E. J. Mele, in *Handbook of Conducting Polymers*, first edition, ed. T. Skotheim, (Dekker, New York, 1986), p. 795.

[167] J. C. Hicks, J. T. Gammel, H. Y. Choi and E. J. Mele, Synth. Met. **17**, 57 (1987).

[168] W. P. Su, Phys. Rev. B **34**, 2988 (1986).

[169] M. J. Rice and I. A. Howard, Phys. Rev. B **28**, 6089 (1983).

[170] B. S. Hudson and B. E. Kohler, Annu. Rev. Phys. Chem. **25**, 437 (1974).

[171] L. Robins, J. Orenstein and R. Superfine, Phys. Rev. Lett. **56**, 1850 (1986).

[172] W. P. Su, Phys. Rev. Lett. **74**, 1167 (1995).

[173] Z. Shuai, J. L. Brédas, S. K. Pati, and S. Ramasesha, Phys. Rev. B **56**, 9298 (1997).

[174] L. Rothberg, T. M. Jedju, P. D. Townsend, S. Etamad and G. L. Baker, Phys. Rev. Lett. **65**, 100 (1990).

[175] X. Wei, B. C. Hess, Z. V. Vardeny and F. Wudl, Phys. Rev. Lett. **68**, 666 (1992).

[176] Z. G. Soos and S. Ramasesha, Phys. Rev. Lett. **51**, 2374 (1983).

[177] S. Mazumdar and S. N. Dixit, Synth. Met. **28** D463 (1989).

[178] J. Orenstein and G. L. Baker, Phys. Rev. Lett. **49**, 1043 (1982).

COUPLING CONSTANT INTEGRATION ANALYSIS OF DENSITY FUNCTIONALS FOR SUBSYSTEMS

Roman F. Nalewajski

K. Gumiński Department of Theoretical Chemistry,
Jagiellonian University, 30-060 Cracow, Poland

ADVANCES IN QUANTUM CHEMISTRY, VOLUME 38

0065-3276/01 $35.00

OUTLINE

Density functionals defined within the Kohn-Sham theory for the complementary subsytems are investigated using the familiar coupling constant integration technique, linking the Kohn-Sham subsystems, consisting of the non-interacting electrons, and the subsystems in the real system of the fully interacting electrons. The formal definition of the nonadditive functionals is given, using the constrained search construction of Levy, appropriately reformulated in the subsystem resolution. Selected paths of scaling the intra- and inter-subsystem electron repulsions are examined. They correspond to both uniform and nonuniform scalings of electronic charges in subsystems. Integration of the Hellmann-Feynman theorem for the scaled Hamiltonians, and the relevant partitioning of the exchange correlation hole into the intra- and inter-subsystem contributions, give rise to integral expressions for the nonadditive kinetic energy and various components of the exchange-correlation energy in the subsystem resolution. General implications of these formulas are examined.

1. INTRODUCTION

The *density functional theory* (DFT) of Hohenberg, Kohn and Sham (1-5) has effected a progress in the theory of chemical reactivity by generating new *reactivity criteria* and novel descriptions of reactive systems at typical stages of the reorganization in the electronic structure of reactants: the electrostatic, polarization and charge-transfer (3,6-11). It has provided, within the *charge sensitivity analysis* (CSA) (6,7), a thermodynamic-like perspective on the reactant responses to changes in their environment caused by the presence of the reaction partner. The predictive potential of the semiempirically parametrized CSA in *atomic resolution* in diagnosing the reactivity preferences in large model chemisorption systems (9,10,12,13) has prompted a progress towards the corresponding orbitally resolved *ab initio* formulation in the so called *local resolution* (6,10,11,14).

The Kohn-Sham (KS) theory for sybsystems (10,11,14, 15), a direct analog of the corresponding Hartree-Fock approach (16,17), which can be used to define the chemical potential, hardness/softness or the *Fukui function* (FF) characteristics of reactants (10,11), involves the so called *nonadditive kinetic energy functional* of the non-interacting system (14), the structure of which is still little understood. Similar nonadditive contributions to the exchange-correlation energy may play a vital role in the DFT treatment of the reactive systems, van der Waals

complexes and in uderstanding the dynamical (short-range) vs. nondynamical (long-range) correlation effects in DFT (18). The eventual use of the DFT calculations in determining the relevant correlation components of the potential energy surfaces may facilitate a better analytical modeling of the electronic energy sufaces for chemical reactions, e.g., using the atomic/diatomic cluster expansion of the *many-body* (MB) and *double many-body* (DMBE) expansions (19).

The present work focuses on the *coupling constant integration* (CCI) analysis (20-22) of such nonadditive functionals. After a brief summary of elements of the electronic structure theory for complementary subsystems and the relevant forms of the Hellmann-Feynman theorem, the constrained search construction of nonadditive functionals is outlined. They are defined as differences between the corresponding functionals of the sum of the subsystem densities (corresponding to the equilibrium state of the mutually open subsystems for this constrained overall density) and densities of the mutually closed, polarized subsystems (corresponding to the intra-subsystem equilibria). Several CCI-paths are explored in the plane of subsystem coupling constants, controlling both the intra- and inter-subsystem electron repulsions. They correspond to both the uniform and nonuniform scalings of electronic charges in the two subsystems, and they expose various contributions to the overal exchange-correlation hole. The CCI integrations provide integral constraints on the functional for the overall exchange-correlation energy

in the subsystem resolution and on its effective intra- and inter-subsystem contributions. The atomic units are used throughout the paper.

2. SUBSYSTEMS AND NONADDITIVE FUNCTIONALS

2.1. Complementary Subsystems in $\mathcal{M} = (\mathcal{A}|\mathcal{B})$

Consider two complementary subsytems $\mathcal{A}$ and $\mathcal{B}$ of the combined molecular system $\mathcal{M} = (\mathcal{A}|\mathcal{B})$; these fragments consisting of $N_{\mathcal{A}}$ and $N_{\mathcal{B}}$ electrons, respectively, moving in the fixed external potential $v(\mathbf{r})$ due to the nuclei of both subsystems, are mutually closed but interacting. We shall denote such a combined system as $(\mathcal{A}|\mathcal{B})$, with the perpendicular full line symbolizing that the flow of electrons between the two subsystems is prevented by a hypothetical barrier, e.g., between reactants at the polarization stage of a reaction or between an adsorbate and a substrate in the physisorption system.

At the quantum-mechanical level two subsystems are distinct, when each is described by "its own" wavefunction or density matrix. In the pure-state description the $\mathcal{M}$ wavefunction is the "symmetry-adapted" (inter-reactant antisymmetrized) product of the subsystem wavefunctions, each individually normalized and antisymmetric (16,17),

$$\Psi^{\mathcal{M}}(\mathbf{x}^{\mathcal{A}}, \mathbf{x}^{\mathcal{B}}) \equiv \Psi^{\mathcal{M}}(\mathbf{x}^{\mathcal{M}})$$

$$= \mathcal{N} \hat{\mathrm{A}}_{\mathcal{A},\mathcal{B}}\{\Psi^{\mathcal{A}}(\mathbf{x}^{\mathcal{A}}) \Psi^{\mathcal{B}}(\mathbf{x}^{\mathcal{B}})\} \equiv \Psi^{\mathcal{M}}(\Psi^{\mathcal{A}}, \Psi^{\mathcal{B}}); \qquad (1)$$

here $\mathbf{x}^{\mathcal{A}} = (\mathbf{x}_1, \ldots, \mathbf{x}_{N_{\mathcal{A}}})$ and $\mathbf{x}^{\mathcal{B}} = (\mathbf{x}_{N_{\mathcal{A}}+1}, \ldots, \mathbf{x}_{N=N_{\mathcal{A}}+N_{\mathcal{B}}})$ are the space-spin coordinates of electrons in $\mathcal{A}$ and $\mathcal{B}$, respectively, $\mathcal{N}$ is the normalizing factor and $\hat{\mathrm{A}}_{\mathcal{A},\mathcal{B}}$ denotes the partial antisymmetrizer including all transpositions that exchange the electronic spin-position arguments between the two groups of electrons (see Appendix). The ensembles of such states, defining the group density matrices, involve mixtures of such functions defined by the relevant equilibrium state probabilities.

The ground state $\Psi^{\mathcal{M}}(\Psi^{\mathcal{A}}, \Psi^{\mathcal{B}})$ follows from the stationary-value problem of the expectation value of the electronic energy $E^{\mathcal{M}}[\Psi^{\mathcal{A}}, \Psi^{\mathcal{B}}] \equiv E^{\mathcal{M}}[\Psi^{\mathcal{M}}]$:

$$\delta E^{\mathcal{M}}[\Psi^{\mathcal{A}}, \Psi^{\mathcal{B}}] \equiv \delta\{\langle\Psi^{\mathcal{M}}|\hat{\mathrm{H}}^{\mathcal{M}}|\Psi^{\mathcal{M}}\rangle/\langle\Psi^{\mathcal{M}}|\Psi^{\mathcal{M}}\rangle\} = 0. \qquad (2a)$$

At the optimum $\Psi^{\mathcal{M}}(\Psi^{\mathcal{A}}, \Psi^{\mathcal{B}})$ this wavefunction energy functional must be stationary with respect to the first-order variation of $\Psi^{\mathcal{M}}$, i.e., for variations preserving the number of electrons in each subsystem. This variational principle is thus satisfied in the subspace of variational functions represented by the limited, *polarization* CI expansion with the fixed partitioniong of the electrons into groups, disregarding the possibility of the *charge transfer* between orbitals of both subsystems.

In the subspace of the trial functions defined by Eq. (1) the first-order variation of $\Psi^{\mathcal{M}}$ can be realized by variations of either $\Psi^{\mathcal{A}}$ or $\Psi^{\mathcal{B}}$, subject to orthonormality of the two functions. In other words, since each variation of the subsystem function makes its own first-order change in the system energy, we have to consider only one at a time. A variation $\delta\Psi^{\mathcal{X}}$ is constructed from the $\mathcal{X}$-group orbitals alone, these being orthogonal to the $\mathcal{Y}(\neq\mathcal{X})$-group orbitals, so that $\Psi^{\mathcal{X}}$ will remain strong-orthogonal to $\Psi^{\mathcal{Y}}$.

For the $(\delta\Psi^{\mathcal{M}})^*$ variations the stationary value problem of Eq.(2a), $\langle\delta\Psi^{\mathcal{M}}|\hat{H}^{\mathcal{M}} - E^{\mathcal{M}}|\Psi^{\mathcal{M}}\rangle = 0$, is therefore equivalent to the *$\mathcal{M}$-Schrödinger equation*:

$$\hat{H}^{\mathcal{M}}\ \Psi^{\mathcal{M}} = E^{\mathcal{M}}\ \Psi^{\mathcal{M}}, \tag{2b}$$

which can be recast into the corresponding eigenvalue problems of the effective hamiltonians of subsystems (17), i.e., the *effective subsystem Schrödinger equations*.

Let us write the electronic hamiltonian of $\mathcal{M}$ as the sum of the hamiltonians for the separate group of electrons by themselves, and the remaining inter-group electron repulsion operator,

$$\hat{H}^{\mathcal{M}}(\mathbf{x}^{\mathcal{A}}, \mathbf{x}^{\mathcal{B}}) = \hat{H}^{\mathcal{A}}(\mathbf{x}^{\mathcal{A}}) + \hat{H}^{\mathcal{B}}(\mathbf{x}^{\mathcal{B}}) + \hat{V}_{ee}^{\mathcal{A},\mathcal{B}}(\mathbf{x}^{\mathcal{A}}, \mathbf{x}^{\mathcal{B}}), \tag{3a}$$

where the subsystem hamiltonian $\hat{H}^{\mathcal{X}}(\mathbf{x}^{\mathcal{X}})$ groups the kinetic $(\hat{T}_e^{\mathcal{X}})$, external potential $(\hat{V}_{ext}^{\mathcal{X}})$, and the *intra*-$\mathcal{X}$ electron repulsion $(\hat{V}_{ee}^{\mathcal{X}})$ energy operators,

$$\hat{H}^{\mathcal{X}}(\mathbf{x}^{\mathcal{X}}) = -\frac{1}{2}\sum_{i\in\mathcal{X}}\Delta_i + \sum_{i\in\mathcal{X}} v(\mathbf{r}_i) + \sum_{i\in\mathcal{X}}\sum_{j(>i)\in\mathcal{X}} |\mathbf{r}_i - \mathbf{r}_j|^{-1}$$

$$\equiv \sum_{i\in\mathcal{X}} \hat{h}^{\mathcal{X}}(i) + \sum_{i\in\mathcal{X}}\sum_{j(>i)\in\mathcal{X}} g(i,\ j)$$

$$\equiv [\hat{T}_e^{\mathcal{X}}(\mathbf{x}^{\mathcal{X}}) + \hat{V}_{ext}^{\mathcal{X}}(\mathbf{x}^{\mathcal{X}})] + \hat{V}_{ee}^{\mathcal{X}}(\mathbf{x}^{\mathcal{X}}) \equiv \hat{\mathcal{H}}^{\mathcal{X}}(\mathbf{x}^{\mathcal{X}}) + \hat{V}_{ee}^{\mathcal{X}}(\mathbf{x}^{\mathcal{X}});\quad (3b)$$

here

$$v(\mathbf{r}) = -\sum_{\mathcal{X}=\mathcal{A},\mathcal{B}}\{\sum_{X\in\mathcal{X}} Z_X/|\mathbf{r} - \mathbf{R}_X|\} \equiv \sum_{\mathcal{X}=\mathcal{A},\mathcal{B}} v^{\mathcal{X}}(\mathbf{r}) \qquad (3c)$$

is the system external potential due to the nuclei of both subsystems and

$$\hat{V}_{ee}^{\mathcal{A},\mathcal{B}} = \sum_{i\in\mathcal{A}}\sum_{j\in\mathcal{B}} g(i,\ j). \qquad (3d)$$

The electronic energy $E^{\mathcal{M}}$ can be also expressed as the sum of the energy $E^{\mathcal{Y}}$ of electrons of the $\mathcal{Y}$-group alone in the field of nuclei, and the effective energy $E_{eff}^{\mathcal{X}}$ of electrons of the other group $\mathcal{X}$ in the field of the nuclei and in the presence of electrons belonging to group $\mathcal{Y}$:

$$E^{\mathcal{M}} = E^{\mathcal{Y}} + E_{eff}^{\mathcal{X}}, \qquad (4a)$$

where:

$$E^{\mathcal{Y}} = \langle\Psi^{\mathcal{Y}}|\hat{H}^{\mathcal{Y}}|\Psi^{\mathcal{Y}}\rangle/\langle\Psi^{\mathcal{Y}}|\Psi^{\mathcal{Y}}\rangle, \qquad (4b)$$

$$E_{eff}^{\mathcal{X}} = \langle\Psi^{\mathcal{M}}|\hat{H}^{\mathcal{X}} + \hat{V}_{ee}^{\mathcal{A},\mathcal{B}}|\Psi^{\mathcal{M}}\rangle/\langle\Psi^{\mathcal{M}}|\Psi^{\mathcal{M}}\rangle$$

$$= \langle\Psi^{\mathcal{X}}|\hat{H}_{eff}^{\mathcal{X}}|\Psi^{\mathcal{X}}\rangle/\langle\Psi^{\mathcal{X}}|\Psi^{\mathcal{X}}\rangle, \qquad (4c)$$

$$\hat{H}^{\mathcal{X}}_{eff}(\mathbf{x}^{\mathcal{X}}) = \hat{\mathcal{H}}^{\mathcal{X}}_{eff}(\mathbf{x}^{\mathcal{X}}) + \hat{V}^{\mathcal{X}}_{ee}(\mathbf{x}^{\mathcal{X}}) \equiv \hat{H}^{\mathcal{X}}_{eff}[\Psi^{\mathcal{Y}}], \tag{4d}$$

$$\hat{\mathcal{H}}^{\mathcal{X}}_{eff}(\mathbf{x}^{\mathcal{X}}) \equiv \hat{\mathcal{H}}^{\mathcal{X}}(\mathbf{x}^{\mathcal{X}}) + \langle \Psi^{\mathcal{M}} | \hat{V}^{\mathcal{A},\mathcal{B}}_{ee} | \Psi^{\mathcal{M}} \rangle_{\mathbf{x}^{\mathcal{Y}}}, \tag{4e}$$

and the symbol $\langle\rangle_{\mathbf{z}}$ stands for the integration over the subset $\mathbf{z}$ of $\mathbf{x}^{\mathcal{M}}$.

The subsystem wavefunction $\Psi^{\mathcal{X}}$ then satisfies the effective stationary value problem for the fixed $\Psi^{\mathcal{Y}}$:

$$\delta E^{\mathcal{X}}_{eff}[\Psi^{\mathcal{X}};\ \Psi^{\mathcal{Y}}] \equiv \delta\{\langle\Psi^{\mathcal{X}}|\hat{H}^{\mathcal{X}}_{eff}[\Psi^{\mathcal{Y}}]|\Psi^{\mathcal{X}}\rangle/\langle\Psi^{\mathcal{X}}|\Psi^{\mathcal{X}}\rangle\} = 0, \tag{5a}$$

or equivalently $\langle\delta\Psi^{\mathcal{X}}|\hat{H}^{\mathcal{X}}_{eff}[\Psi^{\mathcal{Y}}] - E^{\mathcal{X}}_{eff}[\Psi^{\mathcal{Y}}]|\Psi^{\mathcal{X}}\rangle = 0$, i.e., the effective subsystem Schrödinger equation:

$$\hat{H}^{\mathcal{X}}_{eff}[\Psi^{\mathcal{Y}}]\ \Psi^{\mathcal{X}} = E^{\mathcal{X}}_{eff}[\Psi^{\mathcal{Y}}]\ \Psi^{\mathcal{X}}. \tag{5b}$$

One can also consider the eigenvalue problem of the hamiltonian $\hat{H}^{\mathcal{X}}$, of $\mathcal{X}$-group electrons alone in the external potential generated by the nuclei of both subsystems [Eqs.(3b),(4b)].

$$\hat{H}^{\mathcal{X}}(\mathbf{x}^{\mathcal{X}})\ \Psi^{\mathcal{X}}_{S}(\mathbf{x}^{\mathcal{X}}) = E^{\mathcal{X}}_{S}\ \Psi^{\mathcal{X}}_{S}(\mathbf{x}^{\mathcal{X}}). \tag{6}$$

This is equivalent to scaling down the electronic charges in the other subsystem to zero. For the external potential of the isolated fragment $\mathcal{X}$, $v(\mathbf{r}) = v^{\mathcal{X}}(\mathbf{r})$, due to the nuclei belonging to $\mathcal{X}$ alone, this equation represents the *separate fragment* Schrödinger equation.

2.2. Hellmann-Feynman Theorem

Let us further assume that the fragment hamiltonians $\{\hat{H}^{\mathcal{X}}, \hat{H}^{\mathcal{X}}_{eff}, \mathcal{X} = \mathcal{A}, \mathcal{B}\}$ depend on parameters $\lambda_{\mathcal{A}}$ and $\lambda_{\mathcal{B}}$, e.g., those scaling the electron interactions inside $\mathcal{A}$ and $\mathcal{B}$, respectively, corresponding to the $\lambda_{\mathcal{A}}^{-1/2}$ and $\lambda_{\mathcal{B}}^{-1/2}$ scalings of the respective electronic charges:

$$\hat{H}^{\mathcal{X}} = \hat{H}^{\mathcal{X}}(\lambda_{\mathcal{X}}), \quad \hat{H}^{\mathcal{X}}_{eff} = \hat{H}^{\mathcal{X}}_{eff}(\lambda_{\mathcal{A}}, \lambda_{\mathcal{B}}), \qquad \mathcal{X} = \mathcal{A}, \mathcal{B}. \tag{7}$$

Then the subsystem energies are functions of these parameters:

$$E_s^{\mathcal{X}}(\lambda_{\mathcal{X}}) = \langle\Psi_s^{\mathcal{X}}(\lambda_{\mathcal{X}})|\hat{H}^{\mathcal{X}}(\lambda_{\mathcal{X}})|\Psi_s^{\mathcal{X}}(\lambda_{\mathcal{X}})\rangle / \langle\Psi_s^{\mathcal{X}}(\lambda_{\mathcal{X}})|\Psi_s^{\mathcal{X}}(\lambda_{\mathcal{X}})\rangle,$$

$$E_{eff}^{\mathcal{X}}(\lambda_{\mathcal{A}},\lambda_{\mathcal{B}}) = \langle\Psi^{\mathcal{X}}_{\lambda_{\mathcal{A}},\lambda_{\mathcal{B}}}|\hat{H}^{\mathcal{X}}_{eff}(\lambda_{\mathcal{A}},\lambda_{\mathcal{B}})|\Psi^{\mathcal{X}}_{\lambda_{\mathcal{A}},\lambda_{\mathcal{B}}}\rangle \times \langle\Psi^{\mathcal{X}}_{\lambda_{\mathcal{A}},\lambda_{\mathcal{B}}}|\Psi^{\mathcal{X}}_{\lambda_{\mathcal{A}},\lambda_{\mathcal{B}}}\rangle^{-1}.$$

It immediately follows from the hermitian character of the respective subsystem hamiltonians and their eigenvalue equations that these energy functions satisfy the following differential Hellmann-Feynman theorems:

$$\partial E_s^{\mathcal{X}}(\lambda_{\mathcal{X}})/\partial\lambda_{\mathcal{X}} = \langle\Psi_s^{\mathcal{X}}(\lambda_{\mathcal{X}})|\partial\hat{H}^{\mathcal{X}}(\lambda_{\mathcal{X}})/\partial\lambda_{\mathcal{X}}|\Psi_s^{\mathcal{X}}(\lambda_{\mathcal{X}})\rangle \times \langle\Psi_s^{\mathcal{X}}(\lambda_{\mathcal{X}})|\Psi_s^{\mathcal{X}}(\lambda_{\mathcal{X}})\rangle^{-1}, \tag{8a}$$

$$\partial E^{\chi}_{eff}(\lambda_{\mathcal{A}},\lambda_{\mathcal{B}})/\partial\lambda_{\mathcal{Y}} = \langle\Psi^{\chi}_{\lambda_{\mathcal{A}},\lambda_{\mathcal{B}}}|\partial\hat{H}^{\chi}_{eff}(\lambda_{\mathcal{A}},\lambda_{\mathcal{B}})/\partial\lambda_{\mathcal{Y}}|\Psi^{\chi}_{\lambda_{\mathcal{A}},\lambda_{\mathcal{B}}}\rangle$$

$$\times \langle\Psi^{\chi}_{\lambda_{\mathcal{A}},\lambda_{\mathcal{B}}}|\Psi^{\chi}_{\lambda_{\mathcal{A}},\lambda_{\mathcal{B}}}\rangle^{-1},\ \chi,\ \mathcal{Y} = \mathcal{A},\ \mathcal{B}. \quad (8b)$$

For example, the differentiation of $E^{\chi}_{S}(\lambda_{\chi})$ and use of Eq.(6) directly give Eq.(8a):

$$(\partial E^{\chi}_{S}(\lambda_{\chi})/\partial\lambda_{\chi})\ \langle\Psi^{\chi}_{S}(\lambda_{\chi})|\Psi^{\chi}_{S}(\lambda_{\chi})\rangle$$

$$+ E^{\chi}_{S}(\lambda_{\chi})\ \partial/\partial\lambda_{\chi}\langle\Psi^{\chi}_{S}(\lambda_{\chi})|\Psi^{\chi}_{S}(\lambda_{\chi})\rangle$$

$$= \langle\Psi^{\chi}_{S}(\lambda_{\chi})|\partial\hat{H}^{\chi}(\lambda_{\chi})/\partial\lambda_{\chi}|\Psi^{\chi}_{S}(\lambda_{\chi})\rangle$$

$$+ E^{\chi}_{S}(\lambda_{\chi})\ \partial/\partial\lambda_{\chi}\langle\Psi^{\chi}_{S}(\lambda_{\chi})|\Psi^{\chi}_{S}(\lambda_{\chi})\rangle.$$

Similarly, differentiating $E^{\chi}_{eff}(\lambda_{\mathcal{A}},\lambda_{\mathcal{B}})$ with respect to a single scaling factor and using Eq.(5b) leads to Eq.(8b).

An analogous theorem,

$$\partial E^{\mathcal{M}}(\lambda_{\mathcal{A}},\lambda_{\mathcal{B}})/\partial\lambda_{\chi} = \langle\Psi^{\mathcal{M}}_{\lambda_{\mathcal{A}},\lambda_{\mathcal{B}}}|\partial\hat{H}^{\mathcal{M}}(\lambda_{\mathcal{A}},\lambda_{\mathcal{B}})/\partial\lambda_{\chi}|\Psi^{\mathcal{M}}_{\lambda_{\mathcal{A}},\lambda_{\mathcal{B}}}\rangle$$

$$\times \langle\Psi^{\mathcal{M}}_{\lambda_{\mathcal{A}},\lambda_{\mathcal{B}}}|\Psi^{\mathcal{M}}_{\lambda_{\mathcal{A}},\lambda_{\mathcal{B}}}\rangle^{-1}. \quad (8c)$$

is satisfied by the total energy of $\mathcal{M}$ [Eqs.(2),(4a)]:

$$E^{\mathcal{M}}(\lambda_{\mathcal{A}},\lambda_{\mathcal{B}}) = \langle\Psi^{\mathcal{M}}_{\lambda_{\mathcal{A}},\lambda_{\mathcal{B}}}|\hat{H}^{\mathcal{M}}(\lambda_{\mathcal{A}},\lambda_{\mathcal{B}})|\Psi^{\mathcal{M}}_{\lambda_{\mathcal{A}},\lambda_{\mathcal{B}}}\rangle/\langle\Psi^{\mathcal{M}}_{\lambda_{\mathcal{A}},\lambda_{\mathcal{B}}}|\Psi^{\mathcal{M}}_{\lambda_{\mathcal{A}},\lambda_{\mathcal{B}}}\rangle.$$

2.3. Kohn-Sham Scheme

In the KS orbital approximation the strong-orthogonal group functions are the *Slater determinants* $\Phi^{\mathcal{A}}(\{\phi_a\}) \equiv \Phi^{\mathcal{A}}(\phi^{\mathcal{A}})$ and $\Phi^{\mathcal{B}}(\{\phi_b\}) \equiv \Phi^{\mathcal{B}}(\phi^{\mathcal{B}})$, defined by the disjoint subsets of the ortonormal subsystem occupied *spinorbitals* (SO): $\phi^{\mathcal{X}} = (\phi_x, \phi_{x'}, \ldots)$, $\mathcal{X} = \mathcal{A}, \mathcal{B}$. These group functions determine the overall wavefunction [Eq. (1)] of $\mathcal{M} = (\mathcal{A}|\mathcal{B})$, $\Psi^{\mathcal{M}} = \Psi^{\mathcal{M}}(\Phi^{\mathcal{A}}, \Phi^{\mathcal{B}})$. Let $\varphi^{\mathcal{X}} = (\varphi_x, \varphi_{x'}, \ldots)$ and $\zeta^{\mathcal{X}} = (\zeta_x, \zeta_{x'}, \ldots)$ denote the row vectors of the spatial parts (*orbitals*) and spinfunctions of the subsystem SO: $\{\phi_x(\mathbf{x}) = \varphi_x(\mathbf{r})\zeta_x(\sigma), x \in \mathcal{X} = (\mathcal{A}, \mathcal{B})\}$. We shall denote by $\mathbf{n}^{\mathcal{X}} = (n_x, n_{x'}, \ldots)$ their electron occupations. Here $\zeta_x(\sigma)$ is the spin function for either the spin-up ($\zeta_x = \alpha$) or spin-down ($\zeta_x = \beta$) electrons. For the given sets of the spin components the subsystem Slater determinants are dependent upon the shapes of the occupied orbitals, $\Phi^{\mathcal{A}} \equiv \Phi^{\mathcal{A}}(\varphi^{\mathcal{A}})$ and $\Phi^{\mathcal{B}} \equiv \Phi^{\mathcal{B}}(\varphi^{\mathcal{B}})$, which determine the *subsystem electron densities* $\{\rho_{\mathcal{X}}(\mathbf{r})\}$,

$$\rho_{\mathcal{X}}(\mathbf{r}) = \sum_{x \in \mathcal{X}} n_x |\varphi_x(\mathbf{r})|^2, \qquad \mathcal{X} = \mathcal{A}, \mathcal{B}, \tag{9}$$

and hence also the *overall electron density* of $\mathcal{M} = (\mathcal{A}|\mathcal{B})$:

$$\rho(\mathbf{r}) = \rho_{\mathcal{A}}(\mathbf{r}) + \rho_{\mathcal{B}}(\mathbf{r}).$$

The subsystem SO, $\phi = (\phi^{\mathcal{A}}, \phi^{\mathcal{B}}) = (\phi_1, \phi_2, \ldots, \phi_N)$, must be othonormal, $\{\langle\phi_i|\phi_j\rangle = \delta_{i,j}\}$, and their occupations should fall into the physically acceptable Pauli limits: $0 \le n_i \le 1$; here the subscripts i and j

extend over all SO in $\mathcal{M}$. Therefore the orbitals should be orthogonal both *internally* (intra-subsystem),

$$\langle \phi_a | \phi_{a'} \rangle = \delta_{a,a'}, \qquad (a, a') \in \mathcal{A},$$

$$\langle \phi_b | \phi_{b'} \rangle = \delta_{b,b'}, \qquad (b, b') \in \mathcal{B}, \tag{10a}$$

and *externally* (inter-subsystem),

$$\langle \phi_a | \phi_b \rangle = 0. \tag{10b}$$

Recently, a construction of such subsystem orbitals from the overlaping densities $\rho_{\mathcal{A}}$ and $\rho_{\mathcal{B}}$ (Fig. 1A) has been proposed (15), on the basis of the earlier developments (23-27) for the overall density ρ. Such density conserving orbitals can be used to describe the sybsystem wavefunctions that yield the prescribed densities of these complementary framgments of $\mathcal{M}$, e.g., in the subsystem application (15) of the Levy (28) constrained search construction of the functional for the sum of the electronic kinetic and repulsion energies.

The KS equations for the optimum orbitals of the polarized subsystems in $\mathcal{M}$ are (10,11,14,15):

$$\hat{h}_s^{\mathcal{X}}(\mathbf{r})\, \varphi_x(\mathbf{r}) = e_x\, \varphi_x(\mathbf{r}), \qquad x \in \mathcal{X} = \mathcal{A}, \mathcal{B}, \tag{11}$$

where the subsystem KS one-electron hamiltonian

$$\hat{h}_s^{\mathcal{X}}(\mathbf{r}) = -\frac{1}{2}\Delta + v_{eff}^{\mathcal{X}}(\mathbf{r}), \tag{12}$$

corresponds to the hypothetical, *separable* system of $N_{\mathcal{X}}$ noninteracting electrons moving in the *subsystem effective*

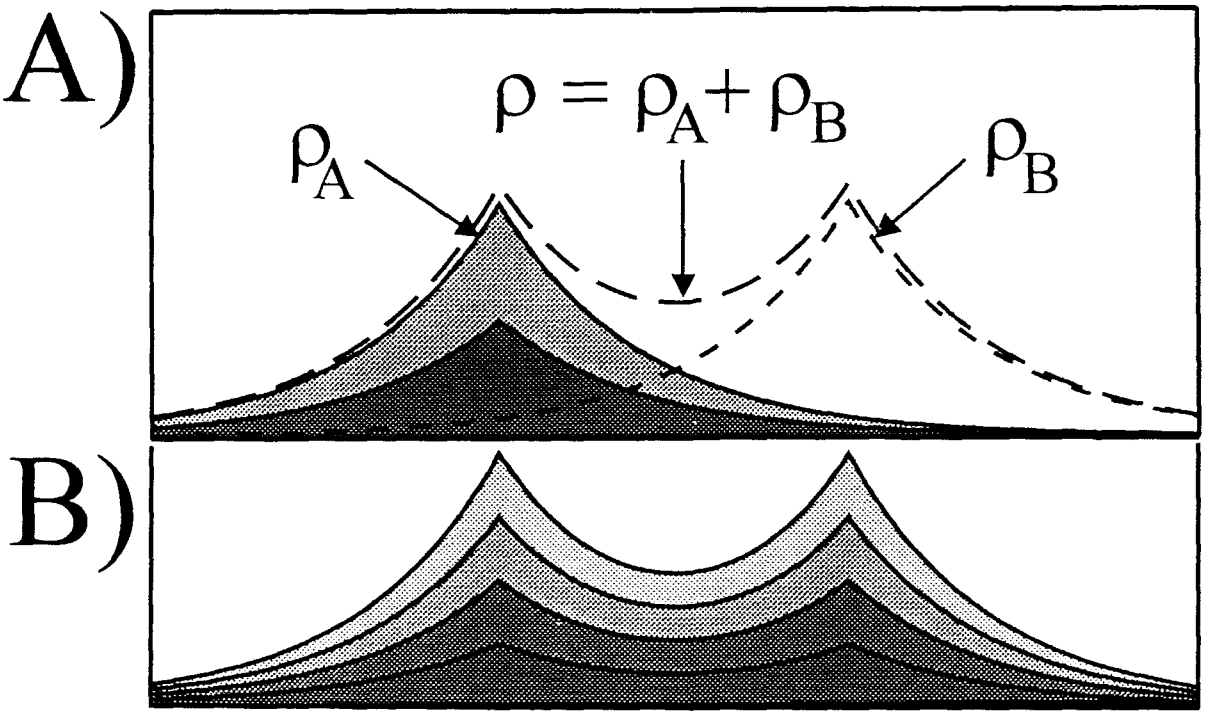

Figure 1. Schematic diagram showing the densities of orbitals conserving the prescribed subsystem density (panel A) and overall density (panel B), which are used in the constrained search constructions of Eqs. (25) and (23), respectively.

one-body potential

$$v^{\mathcal{X}}_{eff}(\mathbf{r}) = v^{\mathcal{X}}_{eff}[\rho_{\mathcal{A}}, \rho_{\mathcal{B}}; \mathbf{r}]$$

$$= v(\mathbf{r}) + \int \rho(\mathbf{r}') \, |\mathbf{r} - \mathbf{r}'|^{-1} \, d\mathbf{r}' + v^{\mathcal{X}}_{xc}[\rho_{\mathcal{A}}, \rho_{\mathcal{B}}; \mathbf{r}]$$

$$\equiv v_H[\rho; \mathbf{r}] + v^{\mathcal{X}}_{xc}[\rho_{\mathcal{A}}, \rho_{\mathcal{B}}; \mathbf{r}]. \tag{13}$$

The latter consists of the *Hartree potential*, $v_H[\rho; \mathbf{r}]$, generated by the system nuclei and the overall electron density $\rho(\mathbf{r})$, and the *subsystem exchange-correlation potential*, $v^{\mathcal{X}}_{xc}[\rho_{\mathcal{A}}, \rho_{\mathcal{B}}; \mathbf{r}]$, including a correction due to the *nonadditive kinetic energy* $T_s^{nadd}[\rho_{\mathcal{A}}, \rho_{\mathcal{B}}]$ (14) defined as the difference between the kinetic energy of noninteracting electrons of both fragments in $\mathcal{M}$, $T_s^{\mathcal{M}}[\rho_{\mathcal{A}}, \rho_{\mathcal{B}}] = T_s[\rho_{\mathcal{A}} + \rho_{\mathcal{B}}]$, and its additive part, $T_s^{add}[\rho_{\mathcal{A}}, \rho_{\mathcal{B}}] = T_s[\rho_{\mathcal{A}}] + T_s[\rho_{\mathcal{B}}]$:

$$T_s^{nadd}[\rho_{\mathcal{A}}, \rho_{\mathcal{B}}] = T_s[\rho_{\mathcal{A}} + \rho_{\mathcal{B}}] - T_s[\rho_{\mathcal{A}}] - T_s[\rho_{\mathcal{B}}], \tag{14}$$

$$v^{\mathcal{X}}_{eff}[\rho_{\mathcal{A}}, \rho_{\mathcal{B}}; \mathbf{r}] = \delta/\delta\rho_{\mathcal{X}}(\mathbf{r}) \, \{E_v^{\mathcal{M}}[\rho_{\mathcal{A}}, \rho_{\mathcal{B}}] - T_s[\rho_{\mathcal{A}}] - T_s[\rho_{\mathcal{B}}]\}$$

$$= \frac{\delta}{\delta\rho(\mathbf{r})}\{(E_{ext}[\rho] + J[\rho] + E_{xc}[\rho]) + \frac{\delta T_s^{nadd}[\rho_{\mathcal{A}}, \rho_{\mathcal{B}}]}{\delta\rho_{\mathcal{X}}(\mathbf{r})}$$

$$\equiv v_{eff}[\rho; \mathbf{r}] + \frac{\delta T_s^{nadd}[\rho_{\mathcal{A}}, \rho_{\mathcal{B}}]}{\delta\rho_{\mathcal{X}}(\mathbf{r})}$$

$$= \frac{\delta}{\delta\rho(\mathbf{r})}(E_{ext}[\rho] + J[\rho]) + \frac{\delta}{\delta\rho_{\mathcal{X}}(\mathbf{r})}(E_{xc}[\rho] + T_s^{nadd}[\rho_{\mathcal{A}}, \rho_{\mathcal{B}}])$$

$$\equiv v_H[\rho;\ \mathbf{r}] + \delta E_{XC}^{\mathcal{M}}[\rho_{\mathcal{A}},\ \rho_{\mathcal{B}}]/\delta\rho_{\chi}(\mathbf{r})$$

$$\equiv v_H[\rho;\ \mathbf{r}] + v_{XC}^{\chi}[\rho_{\mathcal{A}},\ \rho_{\mathcal{B}};\ \mathbf{r}]. \tag{15}$$

Here the energy density functionals have their usual meaning: $E_{ext}[\rho]$ is the attraction energy between electrons and nuclei,

$$E_{ext}[\rho] = \int \mathbf{dr}\ \rho(\mathbf{r})\ v(\mathbf{r})\ \mathbf{dr}, \tag{16}$$

$\{T_S[\rho_{\chi}]\}$ are the subsystem kinetic energies of independent electrons, $J[\rho]$ stands for the classical coulombic repulsion energy of all electrons,

$$J[\rho] = \frac{1}{2} \int\int \rho(\mathbf{r})\ \rho(\mathbf{r}')\ |\mathbf{r} - \mathbf{r}'|^{-1}\ \mathbf{dr}\ \mathbf{dr}', \tag{17}$$

and $E_{XC}[\rho]$ is the exchange-correlation energy for the overall electronic density.

Let the vector $\psi^{\mathcal{M}}[\rho] = (\psi_1[\rho],\ \psi_2[\rho],\ \ldots)$ groups the occupied orbitals for all N electrons (Fig. 1B), defining the determinant $\Phi^{\mathcal{M}}(\psi^{\mathcal{M}}[\rho_{\mathcal{M}}])$ of $\mathcal{M}$ as a whole, which gives rise to the sum of subsystem densities, $\Phi^{\mathcal{M}}(\psi^{\mathcal{M}}) \rightarrow \rho_{\mathcal{M}}$, for the specified occupation numbers $\mathbf{d} = (d_1,\ d_2,\ \ldots)$:

$$\rho(\mathbf{r}) = \sum_i d_i\,|\psi_i(\mathbf{r})|^2 \equiv \sum_i \rho_i(\mathbf{r}) = \rho_{\mathcal{A}} + \rho_{\mathcal{B}}. \tag{18}$$

These orbitals result from the Levy constrained density search.

It should be emphasized at this point that $\rho_{\mathcal{M}}$ is

different from the optimum density ρ^* for the internally open $\mathcal{M}^* = (\mathcal{A}\,|\,\mathcal{B})$, i.e. for the *equilibrium* density of $\mathcal{M}$ as whole, in which the barrier preventing the charge transfer between the two fragments has been removed. In other words, the overall density of $\mathcal{M}$ at the *polarizational stage* is different from that at the *charge transfer stage*. The same is true for the corresponding orbitals and the determinants they define:

$$\psi^{\mathcal{M}}[\rho_{\mathcal{M}}] \neq \bar{\psi}^{\mathcal{M}}[\rho^*] \equiv (\bar{\psi}_1[\rho^*],\ \bar{\psi}_2[\rho^*],\ \ldots,\ \bar{\psi}_N[\rho^*]),$$

$$\Phi^{\mathcal{M}}(\psi^{\mathcal{M}}[\rho_{\mathcal{M}}]) \neq \Phi^{\mathcal{M}^*}(\psi^{\mathcal{M}^*}[\rho^*]).$$

Above the functional relation $\bar{\psi}^{\mathcal{M}}[\rho^*]$ implies

$$\rho^*(\mathbf{r}) = \sum_i \bar{d}_i\,|\bar{\psi}_i(\mathbf{r})|^2 \equiv \sum_i \bar{\rho}_i(\mathbf{r}),$$

with the row vector $\bar{\mathbf{d}} \equiv (\bar{d}_1,\ \bar{d}_2,\ \ldots)$ grouping the occupations of the KS orbitals $\bar{\psi}^{\mathcal{M}}$.

The optimum orbitals $\bar{\psi}^{\mathcal{M}}[\rho^*]$ satisfy the familiar KS equations:

$$\hat{h}_S(\mathbf{r})\ \bar{\psi}_i(\mathbf{r}) = \varepsilon_i\ \bar{\psi}_i(\mathbf{r}), \qquad i = 1,\ 2,\ \ldots, \tag{19}$$

with the effective one-electron hamiltonian

$$\hat{h}_S(\mathbf{r}) = -\frac{1}{2}\,\Delta + v_{eff}[\rho^*;\ \mathbf{r}]. \tag{20}$$

2.4. Nonadditive Functionals

The kinetic energies defining the nonadditive functional of Eq.(14) are known functionals of the optimum KS orbitals of $\mathcal{M} = (\mathcal{A}|\mathcal{B})$ as a whole, $\psi^{\mathcal{M}} = \psi^{\mathcal{M}}[\rho = \rho_{\mathcal{A}} + \rho_{\mathcal{B}}]$, and those of the individual subsystems in $\mathcal{M}$, $\varphi^{\mathcal{X}} = \varphi^{\mathcal{X}}[\rho_{\mathcal{A}}, \rho_{\mathcal{B}}]$, $\mathcal{X} = \mathcal{A}, \mathcal{B}$:

$$T_s^{add}[\rho_{\mathcal{A}}, \rho_{\mathcal{B}}] = \sum_{\mathcal{X}=\mathcal{A},\mathcal{B}} \sum_{x\in\mathcal{X}} n_x \langle \varphi_x[\rho_{\mathcal{A}}, \rho_{\mathcal{B}}] | -\frac{1}{2}\Delta | \varphi_x[\rho_{\mathcal{A}}, \rho_{\mathcal{B}}]\rangle, \tag{21}$$

$$T_s^{\mathcal{M}}[\rho_{\mathcal{A}}, \rho_{\mathcal{B}}] \equiv T_s[\rho] = \sum_i d_i \langle \psi_i[\rho] | -\frac{1}{2}\Delta | \psi_i[\rho]\rangle. \tag{22}$$

These optimum obitals, which yield the prescribed density ρ of $\mathcal{M}$ (Fig. 1B) or densities $\{\rho_{\mathcal{A}}, \rho_{\mathcal{B}}\}$ of its subsystems (Fig. 1A), can be formally defined as the corresponding density functionals (15) via the relevant Levy (28) constructions, respectively searching over the Slater determinants conserving the overal density, $\Phi^{\mathcal{M}}(\psi^{\mathcal{M}} \rightarrow \rho = \rho_{\mathcal{A}} + \rho_{\mathcal{B}})$,

$$\begin{aligned} F_{KS}[\rho] &\equiv T_s[\rho] + J[\rho] + E_{xc}[\rho] \\ &= \min_{\psi^{\mathcal{M}}\rightarrow\rho} \langle \Phi^{\mathcal{M}}(\psi^{\mathcal{M}}) | \hat{T}_e + \hat{V}_{ee} | \Phi^{\mathcal{M}}(\psi^{\mathcal{M}})\rangle \\ &\equiv \langle \Phi^{\mathcal{M}}(\psi^{\mathcal{M}}[\rho]) | \hat{T}_e + \hat{V}_{ee} | \Phi^{\mathcal{M}}(\psi^{\mathcal{M}}[\rho])\rangle, \end{aligned} \tag{23}$$

and over all the antisymmetrized products of the subsystem Slater determinants [Eq.(1)], $\Psi^{\mathcal{M}}(\Phi^{\mathcal{A}}(\varphi^{\mathcal{A}}), \Phi^{\mathcal{B}}(\varphi^{\mathcal{B}})) \equiv \Psi^{\mathcal{M}}(\varphi^{\mathcal{A}}, \varphi^{\mathcal{B}})$, preserving the subsystem densities, $\Psi^{\mathcal{M}}(\Phi^{\mathcal{A}}(\varphi^{\mathcal{A}} \rightarrow \rho_{\mathcal{A}}), \Phi^{\mathcal{B}}(\varphi^{\mathcal{B}} \rightarrow \rho_{\mathcal{B}})) \equiv \Psi^{\mathcal{M}}(\varphi^{\mathcal{A}} \rightarrow \rho_{\mathcal{A}}, \varphi^{\mathcal{B}} \rightarrow \rho_{\mathcal{B}})$,

$$F_{KS}^{\mathcal{M}}[\rho_{\mathcal{A}}, \rho_{\mathcal{B}}] \equiv T_s^{add}[\rho_{\mathcal{A}}, \rho_{\mathcal{B}}] + J[\rho] + (E_{xc}[\rho] + T_s^{nadd}[\rho_{\mathcal{A}}, \rho_{\mathcal{B}}])$$

$$\equiv T_s^{add}[\rho_{\mathcal{A}}, \rho_{\mathcal{B}}] + J[\rho] + E_{xc}^{\mathcal{M}}[\rho_{\mathcal{A}}, \rho_{\mathcal{B}}] \qquad (24)$$

$$= \min_{\varphi^{\mathcal{A}} \to \rho_{\mathcal{A}}} \min_{\varphi^{\mathcal{B}} \to \rho_{\mathcal{B}}} \langle \Psi^{\mathcal{M}}(\Phi^{\mathcal{A}}(\varphi^{\mathcal{A}}), \Phi^{\mathcal{B}}(\varphi^{\mathcal{B}})) | \hat{T}_e + \hat{V}_{ee} | \Psi^{\mathcal{M}}(\Phi^{\mathcal{A}}(\varphi^{\mathcal{A}}), \Phi^{\mathcal{B}}(\varphi^{\mathcal{B}})) \rangle$$

$$= \langle \Psi^{\mathcal{M}}(\varphi^{\mathcal{A}}[\rho_{\mathcal{A}}, \rho_{\mathcal{B}}], \varphi^{\mathcal{B}}[\rho_{\mathcal{A}}, \rho_{\mathcal{B}}]) | \hat{T}_e + \hat{V}_{ee} | \Psi^{\mathcal{M}}(\varphi^{\mathcal{A}}[\rho_{\mathcal{A}}, \rho_{\mathcal{B}}], \varphi^{\mathcal{B}}[\rho_{\mathcal{A}}, \rho_{\mathcal{B}}]) \rangle. \qquad (25)$$

Above the kinetic energy ($\hat{T}_e$) and electron repulsion ($\hat{V}_{ee}$) operators, correspond to all N electrons in $\mathcal{M}$,

$$\hat{T}_e = -\frac{1}{2} \sum_{i=1}^{N} \Delta_i, \qquad (26)$$

$$\hat{V}_{ee} = \sum_{i=1}^{N-1} \sum_{j=i+1}^{N} |\mathbf{r}_i - \mathbf{r}_j|^{-1} \equiv \sum_{i=1}^{N-1} \sum_{j=i+1}^{N} g(i, j), \qquad (27)$$

The density functionals for the optimum KS determinant of $\mathcal{M}$ as a whole, $\Phi^{\mathcal{M}}[\rho_{\mathcal{A}} + \rho_{\mathcal{B}}] = \Phi^{\mathcal{M}}(\psi^{\mathcal{M}}[\rho_{\mathcal{A}} + \rho_{\mathcal{B}}])$, and the two subsystem determinants $\Phi^{\mathcal{A}}[\rho_{\mathcal{A}}, \rho_{\mathcal{B}}] = \Phi^{\mathcal{A}}(\varphi^{\mathcal{A}}[\rho_{\mathcal{A}}, \rho_{\mathcal{B}}])$ and $\Phi^{\mathcal{B}}[\rho_{\mathcal{A}}, \rho_{\mathcal{B}}] = \Phi^{\mathcal{B}}(\varphi^{\mathcal{B}}[\rho_{\mathcal{A}}, \rho_{\mathcal{B}}])$, which determine the resulting functional for the KS-type wavefunction describing the subsystem electrons,

$$\Psi^{\mathcal{M}}[\rho_{\mathcal{A}}, \rho_{\mathcal{B}}] \equiv N \hat{A}_{\mathcal{A},\mathcal{B}} \{\Phi^{\mathcal{A}}[\rho_{\mathcal{A}}, \rho_{\mathcal{B}}] \Phi^{\mathcal{B}}[\rho_{\mathcal{A}}, \rho_{\mathcal{B}}]\}, \qquad (28)$$

then allow one to formally define nonadditive density functionals of a general physical property A through its known dependence on the wave function, $A[\Psi] = \langle\Psi|\hat{A}|\Psi\rangle / \langle\Psi|\Psi\rangle$:

$$A^{nadd}[\rho_{\mathcal{A}}, \rho_{\mathcal{B}}] = A[\Psi^{\mathcal{M}}[\rho_{\mathcal{A}}, \rho_{\mathcal{B}}]] - A[\Phi^{\mathcal{A}}[\rho_{\mathcal{A}}, \rho_{\mathcal{B}}]] - A[\Phi^{\mathcal{B}}[\rho_{\mathcal{A}}, \rho_{\mathcal{B}}]]. \qquad (29)$$

The corresponding definition of the nonadditive component of a property $B[\rho]$, defined by an explicit density functional, is:

$$B^{nadd}[\rho_{\mathcal{A}}, \rho_{\mathcal{B}}] = B[\rho_{\mathcal{A}} + \rho_{\mathcal{B}}] - B[\rho_{\mathcal{A}}] - B[\rho_{\mathcal{B}}]. \qquad (30)$$

For example, in the particular case of the classical electron repulsion energy $J[\rho]$ one identifies the classical electron repulsion energy between the two subsystems in $\mathcal{M}$, $J_{\mathcal{A},\mathcal{B}}[\rho_{\mathcal{A}}, \rho_{\mathcal{B}}]$, as the non-additive part of this energy contribution:

$$J^{nadd}[\rho_{\mathcal{A}}, \rho_{\mathcal{B}}] \equiv J[\rho_{\mathcal{A}} + \rho_{\mathcal{B}}] - J[\rho_{\mathcal{A}}] - J[\rho_{\mathcal{B}}]$$

$$= \int\int \rho_{\mathcal{A}}(\mathbf{r})\, \rho_{\mathcal{B}}(\mathbf{r}')\, |\mathbf{r} - \mathbf{r}'|^{-1}\, d\mathbf{r}\, d\mathbf{r}' \equiv J_{\mathcal{A},\mathcal{B}}[\rho_{\mathcal{A}}, \rho_{\mathcal{B}}]. \qquad (31)$$

Similarly,

$$E_{xc}^{nadd}[\rho_{\mathcal{A}}, \rho_{\mathcal{B}}] \equiv E_{xc}[\rho_{\mathcal{A}} + \rho_{\mathcal{B}}] - E_{xc}[\rho_{\mathcal{A}}] - E_{xc}[\rho_{\mathcal{B}}], \qquad (32)$$

$$F^{nadd}[\rho_{\mathcal{A}}, \rho_{\mathcal{B}}] \equiv J_{\mathcal{A},\mathcal{B}}[\rho_{\mathcal{A}}, \rho_{\mathcal{B}}] + E_{xc}^{nadd}[\rho_{\mathcal{A}}, \rho_{\mathcal{B}}] + T_S^{nadd}[\rho_{\mathcal{A}}, \rho_{\mathcal{B}}], \quad \text{etc.} \qquad (33)$$

It should be emphasized that in the Kohn-Sham description of the ground-state in $\mathcal{M} = (\mathcal{A}|\mathcal{B})$, the subsystem electrons in fact represent two distinct components exhibiting different levels of the chemical potential,

$$\mu_{\mathcal{A}} \equiv \partial E_v(N_{\mathcal{A}}, N_{\mathcal{B}})/\partial N_{\mathcal{A}}\Big|_v \neq \mu_{\mathcal{B}} \equiv \partial E_v(N_{\mathcal{A}}, N_{\mathcal{B}})/\partial N_{\mathcal{B}}\Big|_v , \quad (34)$$

identified by the highest occupied KS orbital eigenvalues in $\mathcal{A}$ and $\mathcal{B}$, respectively (4,11). Therefore, we must admit that the subsystem electronic densities can be coupled in the scaled interaction systems to the separate, generally different *scaled external potentials*: $\rho_{\mathcal{A}}$ - to $v^{\mathcal{A}}$ and $\rho_{\mathcal{B}}$ - to $v^{\mathcal{B}}$. The overall density $\rho = \rho_{\mathcal{A}} + \rho_{\mathcal{B}}$, representing a single electronic component, is coupled to the common external potential $v^{\mathcal{AB}}$: $v^{\mathcal{A}} = v^{\mathcal{B}} = v^{\mathcal{AB}}$. In such a general case of the intrareactant equilibria the energy contribution $E_{ext}[\rho_{\mathcal{A}}, \rho_{\mathcal{B}}]$, due to the interaction between the subsystem electrons and their respective external potentials,

$$E_{ext}^{nadd}[\rho_{\mathcal{A}}, \rho_{\mathcal{B}}] = E_{ext}[\rho_{\mathcal{A}} + \rho_{\mathcal{B}}] - E_{ext}[\rho_{\mathcal{A}}] - E_{ext}[\rho_{\mathcal{B}}]$$

$$= \int\{[\rho_{\mathcal{A}}(\mathbf{r}) + \rho_{\mathcal{B}}(\mathbf{r})]v^{\mathcal{AB}}(\mathbf{r}) - \rho_{\mathcal{A}}(\mathbf{r})\, v^{\mathcal{A}}(\mathbf{r}) - \rho_{\mathcal{B}}(\mathbf{r})\, v^{\mathcal{B}}(\mathbf{r})\}\, d\mathbf{r}. \quad (35)$$

The additive character of this energy contribution is thus obtained only for the common external potential coupled to both subsystem densities, equal to that corresponding to

the overall density ρ: $v^{\mathcal{A}} = v^{\mathcal{B}} = v^{\mathcal{AB}}$. This is the case in the unscaled molecular system, consisting of the fully interacting electrons, in which both subsystem densities are coupled to the external potential due to all nuclei in $\mathcal{M}$: $v^{\mathcal{A}} = v^{\mathcal{B}} = v^{\mathcal{AB}} = v$.

3. SCALED HAMILTONIANS

Let us combine the subsystem operators for the kinetic, external potential and the electron repulsion components, respectively, in the electronic hamiltonian of Eq.(3) [see also the definitions of Eqs.(26) and (27)]:

$$\hat{H}^{\mathcal{M}}(N_{\mathcal{A}}, v^{\mathcal{A}}; N_{\mathcal{B}}, v^{\mathcal{B}}) = [\hat{T}_e^{\mathcal{A}}(N_{\mathcal{A}}) + \hat{T}_e^{\mathcal{B}}(N_{\mathcal{B}})] + [\hat{V}_{ext}^{\mathcal{A}}(N_{\mathcal{A}}, v^{\mathcal{A}}) + \hat{V}_{ext}^{\mathcal{B}}(N_{\mathcal{B}}, v^{\mathcal{B}})] + [\hat{V}_{ee}^{\mathcal{A}}(N_{\mathcal{A}}) + \hat{V}_{ee}^{\mathcal{B}}(N_{\mathcal{B}}) + \hat{V}_{ee}^{\mathcal{A},\mathcal{B}}(N_{\mathcal{A}}, N_{\mathcal{B}})]$$

$$\equiv \hat{T}_e^{\mathcal{M}}(N_{\mathcal{A}}, N_{\mathcal{B}}) + \hat{V}_{ext}^{\mathcal{M}}(N_{\mathcal{A}}, v^{\mathcal{A}}; N_{\mathcal{B}}, v^{\mathcal{B}}) + \hat{V}_{ee}^{\mathcal{M}}(N_{\mathcal{A}}, N_{\mathcal{B}}). \quad (36)$$

We shall also distinguish the corresponding operators in the hamiltonian of the $\mathcal{AB}$ system as a whole:

$$\hat{H}(N, v^{\mathcal{AB}}) = \hat{T}_e(N) + \sum_{i=1}^{N} v^{\mathcal{AB}}(\mathbf{r}_i) + \hat{V}_{ee}(N)$$

$$\equiv \hat{T}_e(N) + \hat{V}_{ext}(N, v^{\mathcal{AB}}) + \hat{V}_{ee}(N). \quad (37)$$

3.1. Uniform Scaling of Electronic Charges in Subsystems

The familiar technique of the coupling constant integration (20-22) provides a link between the hypothetical Kohn-Sham system of noninteracting electrons and the real fully interacting system. It also represents an attractive tool for a direct investigation of the exchange-correlation functional. In the subsystem resolution one can envisage a similar *uniform scaling* of *all* electron repulsions $\{g(i, j)\}$ using the common *coupling constant* $0 \le \lambda \le 1$ for both subsystems. This is equivalent to the $\lambda^{1/2}$ scaling of the electronic charges in the *uniformly scaled hamiltonian*

$$\hat{H}^{\mathcal{M}}_{\lambda}(N_{\mathcal{A}}, v^{\mathcal{A}}_{\lambda}; N_{\mathcal{B}}, v^{\mathcal{B}}_{\lambda}) \equiv \hat{H}^{\mathcal{M}}_{\lambda}$$
$$= \hat{T}^{\mathcal{M}}_{e}(N_{\mathcal{A}}, N_{\mathcal{B}}) + \hat{V}^{\mathcal{M}}_{ext}(N_{\mathcal{A}}, v^{\mathcal{A}}_{\lambda}; N_{\mathcal{B}}, v^{\mathcal{B}}_{\lambda}) + \lambda \hat{V}^{\mathcal{M}}_{ee}(N_{\mathcal{A}}, N_{\mathcal{B}})$$
$$\equiv \hat{T}^{\mathcal{M}}_{e} + \hat{V}^{\mathcal{M}}_{ext}(\lambda) + \lambda \hat{V}^{\mathcal{M}}_{ee}, \qquad (38)$$

where the operator of the interaction energy between electrons and the *scaled external potentials of subsystems*, $\{v^{\mathcal{X}}_{\lambda}(\mathbf{r})\}$,

$$\hat{V}^{\mathcal{M}}_{ext}(\lambda) = \sum_{\mathcal{X}=\mathcal{A},\mathcal{B}} \sum_{i \in \mathcal{X}} v^{\mathcal{X}}_{\lambda}(\mathbf{r}_i) \equiv \sum_{\mathcal{X}=\mathcal{A},\mathcal{B}} \hat{V}^{\mathcal{X}}_{ext}(\lambda). \qquad (39)$$

We shall denote the scaled molecular system $\mathcal{M}_{\lambda}$, described by the hamiltonian of Eq.(38), by $\mathcal{M}(\lambda, \lambda)$ to explicitly indicate that the charges of electrons in both subsystems are scaled by the same factor $\lambda^{1/2}$.

By hypothesis the potentials $\{v_\lambda^{\mathcal{X}}(\mathbf{r})\}$ are chosen in such a way that the *scaled ground-state densities* of subsystems in $\mathcal{M}(\lambda, \lambda)$,

$$\rho_\lambda^{\mathcal{X}}(\mathbf{r}) = \langle\Psi_\lambda^{\mathcal{M}}|\hat{\rho}_{\mathcal{X}}(\mathbf{r})|\Psi_\lambda^{\mathcal{M}}\rangle = \langle\Psi_\lambda^{\mathcal{X}}|\hat{\rho}_{\mathcal{X}}(\mathbf{r})|\Psi_\lambda^{\mathcal{X}}\rangle,$$

$$\hat{\rho}_{\mathcal{X}}(\mathbf{r}) = \sum_{i\in\mathcal{X}} \delta(\mathbf{r}_i - \mathbf{r}), \qquad \mathcal{X} = \mathcal{A},\mathcal{B}, \tag{40}$$

corresponding to the *scaled ground state wavefunction* $\Psi_\lambda^{\mathcal{M}} = N\,\hat{A}_{\mathcal{A},\mathcal{B}}\{\Psi_\lambda^{\mathcal{A}}\,\Psi_\lambda^{\mathcal{B}}\}$ and energy $E^{\mathcal{M}}(\lambda) = \langle\Psi_\lambda^{\mathcal{M}}|\hat{H}_\lambda^{\mathcal{M}}|\Psi_\lambda^{\mathcal{M}}\rangle$ are both independent of λ and identical with the exact ground-state subsystem densities of the interacting system $\mathcal{M}(1, 1)$:

$$\rho_\lambda^{\mathcal{X}}(\mathbf{r}) = \rho_{\lambda=1}^{\mathcal{X}}(\mathbf{r}) \equiv \rho_{\mathcal{X}}(\mathbf{r}), \qquad \mathcal{X} = \mathcal{A},\ \mathcal{B}. \tag{41}$$

In other words, the two scaled subsystem external potentials are defined to give rise to the true ground state densities of interacting subsystems, irrespectively of the current value of the the scaled electronic charge, which we indicate by the following mapping relation:

$$[v_\lambda^{\mathcal{A}},\ v_\lambda^{\mathcal{B}}] \leftrightarrow [\rho_{\mathcal{A}},\ \rho_{\mathcal{B}}].$$

It should be noticed that in general, due to different effective contributions from the kinetic energy functional [Eq.(15)], the two scaled external potentials for subsystems differ from each other for $0 \le \lambda < 1$. The scaled ground state wavefunction $\Psi_\lambda^{\mathcal{M}}$ is the lowest energy eigenfunction of $\hat{H}_\lambda^{\mathcal{M}}$ [see Eq.(2b)]:

$$\hat{H}_\lambda^{\mathcal{M}}\,\Psi_\lambda^{\mathcal{M}} = E^{\mathcal{M}}(\lambda)\,\Psi_\lambda^{\mathcal{M}}. \tag{42a}$$

The scaled subsystem wavefunctions $\Psi_\lambda^{\mathcal{A}}$ and $\Psi_\lambda^{\mathcal{B}}$ are the ground states of the corresponding scaled effective hamiltonians $\{\hat{H}_{eff}^{\mathcal{X}}(\lambda)\}$ of subsystems in $\mathcal{M}(\lambda, \lambda)$ [see Eqs. (4d,e) and (5b)],

$$\begin{aligned}\hat{H}_{eff}^{\mathcal{X}}(\lambda) \equiv \hat{H}_{eff}^{\mathcal{X}}[\lambda, \rho^{\mathcal{Y}}; \mathbf{x}^{\mathcal{X}}] &= \{\hat{T}_e^{\mathcal{X}}(\mathbf{x}^{\mathcal{X}}) + [\hat{V}_{ext}^{\mathcal{X}}(\lambda, \mathbf{x}^{\mathcal{X}}) \\ &\quad + \lambda\langle\Psi_\lambda^{\mathcal{M}}(\mathbf{x}^{\mathcal{M}})|\hat{V}_{ee}^{\mathcal{A},\mathcal{B}}(\mathbf{x}^{\mathcal{M}})|\Psi_\lambda^{\mathcal{M}}(\mathbf{x}^{\mathcal{M}})\rangle_{\mathbf{x}^{\mathcal{Y}}}]\} + \lambda\hat{V}_{ee}^{\mathcal{X}}(\mathbf{x}^{\mathcal{X}}) \\ &\equiv \{\hat{T}_e^{\mathcal{X}}(\mathbf{x}^{\mathcal{X}}) + \hat{V}_{eff}^{\mathcal{X}}[\lambda, \rho_{\mathcal{Y}}; \mathbf{x}^{\mathcal{X}}]\} + \lambda\hat{V}_{ee}^{\mathcal{X}}(\mathbf{x}^{\mathcal{X}}) \\ &\equiv \hat{\mathcal{H}}_{eff}^{\mathcal{X}}[\lambda, \rho_{\mathcal{Y}}] + \lambda\hat{V}_{ee}^{\mathcal{X}} \\ &\equiv \{\hat{T}_e^{\mathcal{X}} + \hat{V}_{ext}^{\mathcal{X}}(\lambda)\} + \lambda\hat{V}_{ee,\mathcal{X}}^{eff}[\lambda, \rho_{\mathcal{Y}}], \end{aligned} \tag{43}$$

$$\begin{aligned}\hat{H}_{eff}^{\mathcal{X}}[\lambda, \rho^{\mathcal{Y}}; \mathbf{x}^{\mathcal{X}}]\,\Psi_\lambda^{\mathcal{X}}[\rho^{\mathcal{Y}}; \mathbf{x}^{\mathcal{X}}] &\equiv \hat{H}_{eff}^{\mathcal{X}}(\lambda)\,\Psi_\lambda^{\mathcal{X}} \\ &= E_{eff}^{\mathcal{X}}[\lambda, \rho^{\mathcal{Y}}]\,\Psi_\lambda^{\mathcal{X}}[\rho^{\mathcal{Y}}; \mathbf{x}^{\mathcal{X}}] \equiv E_{eff}^{\mathcal{X}}(\lambda)\,\Psi_\lambda^{\mathcal{X}}, \\ &\qquad (\mathcal{X} \neq \mathcal{Y}) = \mathcal{A}, \mathcal{B}. \end{aligned} \tag{42b}$$

The above definition of the scaled external potentials of subsystems immediately implies their shapes for the limiting values of λ (see Fig. 2):

$$\begin{aligned} v_{\lambda=0}^{\mathcal{X}}(\mathbf{r}) &= v_{eff}^{\mathcal{X}}[\rho_{\mathcal{A}}, \rho_{\mathcal{B}}; \mathbf{r}], \\ v_{\lambda=1}^{\mathcal{X}}(\mathbf{r}) &= v(\mathbf{r}). \qquad\qquad \mathcal{X} = \mathcal{A}, \mathcal{B}. \end{aligned} \tag{44}$$

Such a uniform scaling of electronic charges in $\mathcal{M}(\lambda, \lambda)$ corresponds to the *path 1* in Fig. 2.

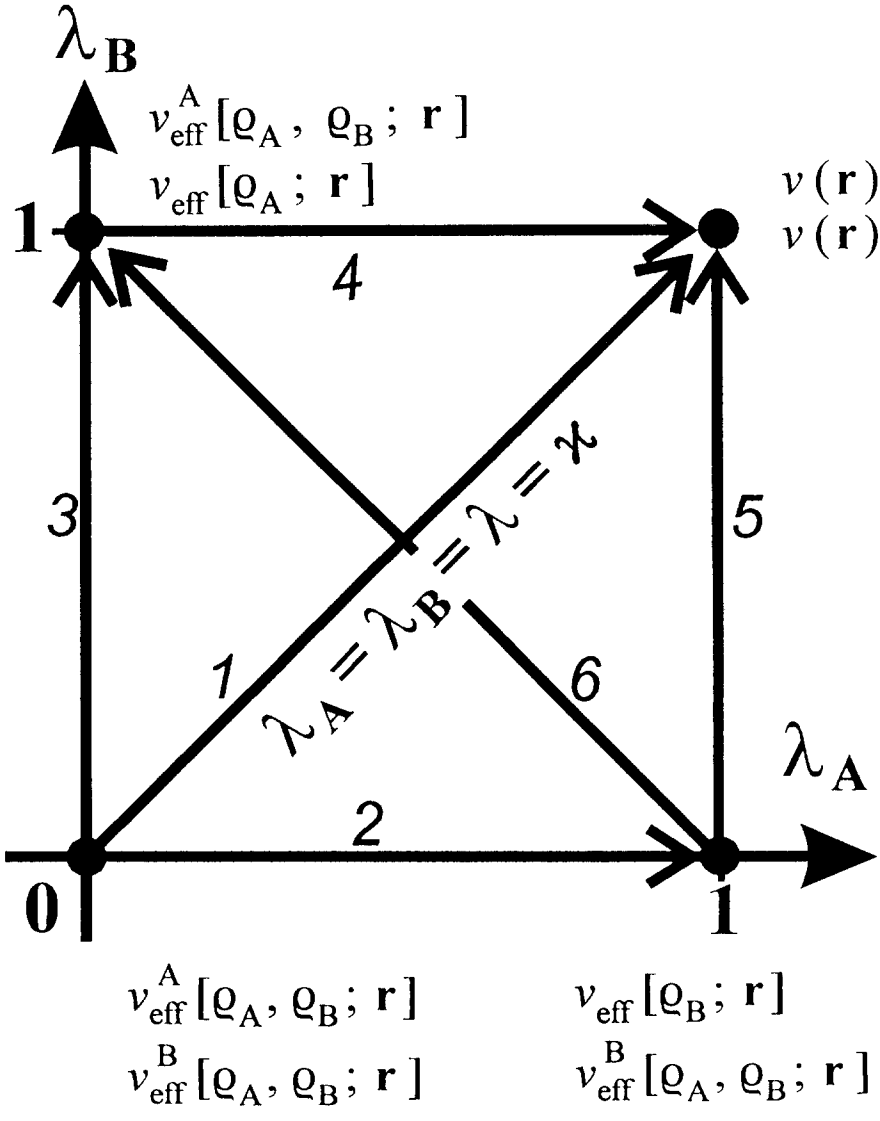

Figure 2. Uniform (1) and nonuniform (2-6) scaling paths of electronic charges in the complementary subsystems of $\mathcal{M} = (\mathcal{A}|\mathcal{B})$. The subsystem external potentials of the scaled hamiltonians for the starting and end points of each path are also listed, with the upper (lower) entries corresponding to $\mathcal{A}$ ($\mathcal{B}$).

3.2. Separate Scalings of Electronic Charges in Subsystems

In the KS theory for subsystems one can also envisage the *non-uniform scalings* of electronic interactions (charges), defined by the separate coupling constants for each subsystem: $0 \le \lambda_{\mathcal{A}} \le 1$ and $0 \le \lambda_{\mathcal{B}} \le 1$. The resulting *non-uniformly scaled hamiltonian*,

$$\hat{H}^{\mathcal{M}}_{\lambda_{\mathcal{A}},\lambda_{\mathcal{B}}}(N_{\mathcal{A}},\ v^{\mathcal{A}}_{\lambda_{\mathcal{A}},\lambda_{\mathcal{B}}};\ N_{\mathcal{B}},\ v^{\mathcal{B}}_{\lambda_{\mathcal{A}},\lambda_{\mathcal{B}}}) \equiv \hat{H}^{\mathcal{M}}_{\lambda_{\mathcal{A}},\lambda_{\mathcal{B}}}$$

$$= \hat{T}^{\mathcal{M}}_{e}(N_{\mathcal{A}},\ N_{\mathcal{B}}) + \hat{V}^{\mathcal{M}}_{ext}(N_{\mathcal{A}},\ v^{\mathcal{A}}_{\lambda_{\mathcal{A}},\lambda_{\mathcal{B}}};\ N_{\mathcal{B}},\ v^{\mathcal{B}}_{\lambda_{\mathcal{A}},\lambda_{\mathcal{B}}})$$

$$\lambda_{\mathcal{A}}\hat{V}^{\mathcal{A}}_{ee}(N_{\mathcal{A}}) + (\lambda_{\mathcal{A}}\lambda_{\mathcal{B}})^{1/2}\hat{V}^{\mathcal{A},\mathcal{B}}_{ee}(N_{\mathcal{A}},\ N_{\mathcal{B}}) + \lambda_{\mathcal{B}}\hat{V}^{\mathcal{B}}_{ee}(N_{\mathcal{B}}), \quad (45)$$

defining the subsystems in $\mathcal{M}(\lambda_{\mathcal{A}},\ \lambda_{\mathcal{B}})$, includes the intra-subsystem electron interactions $\hat{V}^{\mathcal{A}}_{ee}$ and $\hat{V}^{\mathcal{B}}_{ee}$, scaled by the corresponding subsystem coupling constants, the geometric average of which provides the scaling factor for the inter-subsystem electron repulsion operator $\hat{V}^{\mathcal{A},\mathcal{B}}_{ee}$.

It is again assumed that the scaled hamiltonian $\hat{H}^{\mathcal{M}}_{\lambda_{\mathcal{A}},\lambda_{\mathcal{B}}}$ includes the appropriately modified external potentials $\{v^{\mathcal{X}}_{\lambda_{\mathcal{A}},\lambda_{\mathcal{B}}}(\mathbf{r})\}$, coupled to the respective subsystem densities $\{\rho^{\mathcal{X}}_{\lambda_{\mathcal{A}},\lambda_{\mathcal{B}}}(\mathbf{r})\}$, in the external potential operator

$$\hat{V}^{\mathcal{M}}_{ext}(N_{\mathcal{A}},\ v^{\mathcal{A}}_{\lambda_{\mathcal{A}},\lambda_{\mathcal{B}}};\ N_{\mathcal{B}},\ v^{\mathcal{B}}_{\lambda_{\mathcal{A}},\lambda_{\mathcal{B}}}) \equiv \hat{V}^{\mathcal{M}}_{ext}(\lambda_{\mathcal{A}},\ \lambda_{\mathrm{B}})$$

$$= \sum_{\mathcal{X}=\mathcal{A},\mathcal{B}}[\sum_{i\in\mathcal{X}} v^{\mathcal{X}}_{\lambda_{\mathcal{A}},\lambda_{\mathcal{B}}}(\mathbf{r}_i)] \equiv \sum_{\mathcal{X}=\mathcal{A},\mathcal{B}} \hat{V}^{\mathcal{X}}_{ext}(\lambda_{\mathcal{A}},\ \lambda_{\mathcal{B}}). \quad (46)$$

They are chosen in such a way that the ground-state densities of subsystems in $\mathcal{M}(\lambda_{\mathcal{A}}, \lambda_{\mathcal{B}})$,

$$\rho^{\mathcal{X}}_{\lambda_{\mathcal{A}},\lambda_{\mathcal{B}}}(\mathbf{r}) = \langle \Psi^{\mathcal{M}}_{\lambda_{\mathcal{A}},\lambda_{\mathcal{B}}} | \hat{\rho}_{\mathcal{X}}(\mathbf{r}) | \Psi^{\mathcal{M}}_{\lambda_{\mathcal{A}},\lambda_{\mathcal{B}}} \rangle$$

$$= \langle \Psi^{\mathcal{X}}_{\lambda_{\mathcal{A}},\lambda_{\mathcal{B}}} | \hat{\rho}_{\mathcal{X}}(\mathbf{r}) | \Psi^{\mathcal{X}}_{\lambda_{\mathcal{A}},\lambda_{\mathcal{B}}} \rangle, \qquad \mathcal{X} = \mathcal{A}, \mathcal{B}, \tag{47}$$

for the scaled ground state wavefunction of subsystems

$$\Psi^{\mathcal{M}}_{\lambda_{\mathcal{A}},\lambda_{\mathcal{B}}} = \mathcal{N} \hat{\mathrm{A}}_{\mathcal{A},\mathcal{B}} \{ \Psi^{\mathcal{A}}_{\lambda_{\mathcal{A}},\lambda_{\mathcal{B}}} \Psi^{\mathcal{B}}_{\lambda_{\mathcal{A}},\lambda_{\mathcal{B}}} \}, \tag{48}$$

are both independent of the two coupling constants and identical with the true ground-state densities of the fully interacting electrons in $\mathcal{M}(1, 1)$:

$$\rho^{\mathcal{X}}_{\lambda_{\mathcal{A}},\lambda_{\mathcal{B}}}(\mathbf{r}) = \rho^{\mathcal{X}}_{\lambda_{\mathcal{A}}=1,\lambda_{\mathcal{B}}=1}(\mathbf{r}) \equiv \rho_{\mathcal{X}}(\mathbf{r}), \qquad \mathcal{X} = \mathcal{A}, \mathcal{B}. \tag{49}$$

This assumption can again be summarized by the following ground state mapping between the external potentials of subsystems in $\mathcal{M}(\lambda_{\mathcal{A}}, \lambda_{\mathcal{B}})$ and the exact subsystem densities in $\mathcal{M}(1, 1)$:

$$[v^{\mathcal{A}}_{\lambda_{\mathcal{A}},\lambda_{\mathcal{B}}}, v^{\mathcal{B}}_{\lambda_{\mathcal{A}},\lambda_{\mathcal{B}}}] \leftrightarrow [\rho_{\mathcal{A}}, \rho_{\mathcal{B}}]. \tag{50}$$

As in the uniform scaling case the subsystem scaled wavefunctions in Eq. (48) are the grounds states of the respective scaled effective hamiltonians:

$$\hat{H}^{\mathcal{X}}_{eff}(\lambda_{\mathcal{A}}, \lambda_{\mathcal{B}}) = \hat{H}^{\mathcal{X}}_{eff}[\lambda_{\mathcal{A}}, \lambda_{\mathcal{B}}, \rho^{\mathcal{Y}}; \mathbf{x}^{\mathcal{X}}]$$

$$= \{\hat{T}^{\mathcal{X}}_{e} + [\hat{V}^{\mathcal{X}}_{ext}(\lambda_{\mathcal{A}}, \lambda_{\mathcal{B}}) + (\lambda_{\mathcal{A}}\lambda_{\mathcal{B}})^{1/2} \langle \Psi^{\mathcal{M}}_{\lambda_{\mathcal{A}},\lambda_{\mathcal{B}}} | \hat{V}^{\mathcal{A},\mathcal{B}}_{ee} | \Psi^{\mathcal{M}}_{\lambda_{\mathcal{A}},\lambda_{\mathcal{B}}} \rangle_{\mathbf{x}^{\mathcal{Y}}}]\}$$

$$+ \lambda_{\mathcal{X}} \hat{V}^{\mathcal{X}}_{ee}$$

$$\equiv \hat{\mathcal{H}}^{\mathcal{X}}_{eff}[\lambda_{\mathcal{A}}, \lambda_{\mathcal{B}}, \rho_{\mathcal{Y}}] + \lambda_{\mathcal{X}} \hat{V}^{\mathcal{X}}_{ee}$$

$$\equiv \{\hat{T}^{\mathcal{X}}_{e} + \hat{V}^{\mathcal{X}}_{ext}(\lambda_{\mathcal{A}}, \lambda_{\mathcal{B}})\} + \lambda_{\mathcal{X}} \hat{V}^{eff}_{ee,\mathcal{X}}[\lambda_{\mathcal{A}}, \lambda_{\mathcal{B}}, \rho_{\mathcal{Y}}], \qquad (51)$$

$$\hat{H}^{\mathcal{X}}_{eff}(\lambda_{\mathcal{A}}, \lambda_{\mathcal{B}})\, \Psi^{\mathcal{X}}_{\lambda_{\mathcal{A}},\lambda_{\mathcal{B}}} = E^{\mathcal{X}}_{eff}(\lambda_{\mathcal{A}}, \lambda_{\mathcal{B}})\, \Psi^{\mathcal{X}}_{\lambda_{\mathcal{A}},\lambda_{\mathcal{B}}},$$

$$(\mathcal{X} \neq \mathcal{Y}) = \mathcal{A}, \mathcal{B}. \qquad (52)$$

The above definition of the external potentials coupled to densities of the nonuniformly scaled electronic charges of subsystems in $\mathcal{M}(\lambda_{\mathcal{A}}, \lambda_{\mathcal{B}})$ again implies for the two extreme uniform scaling points [see Fig. 2 and Eq.(44)]:

$$v^{\mathcal{X}}_{\lambda_{\mathcal{A}}=0,\lambda_{\mathcal{B}}=0}(\mathbf{r}) = v^{\mathcal{X}}_{eff}[\rho_{\mathcal{A}}, \rho_{\mathcal{B}}; \mathbf{r}],$$

$$v^{\mathcal{X}}_{\lambda_{\mathcal{A}}=1,\lambda_{\mathcal{B}}=1}(\mathbf{r}) = v(\mathbf{r}), \qquad \mathcal{X} = \mathcal{A}, \mathcal{B}. \qquad (53)$$

Consider now a case when the charges of electrons in one subsystem, say $\mathcal{A}$, are scaled to zero: $\lambda_{\mathcal{A}} = 0$. Since then electrons in $\mathcal{A}$ do not interact both among themselves, $\lambda_{\mathcal{A}}\, \hat{V}^{\mathcal{A}}_{ee} = 0$, and with the other, $\mathcal{B}$-group of electrons, $(\lambda_{\mathcal{A}}\lambda_{\mathcal{B}})^{1/2}\, \hat{V}^{\mathcal{A},\mathcal{B}}_{ee} = 0$, for any value of $\lambda_{\mathcal{B}}$,

$$v^{\mathcal{A}}_{\lambda_{\mathcal{A}}=0,\lambda_{\mathcal{B}}}(\mathbf{r}) = v^{\mathcal{A}}_{eff}[\rho_{\mathcal{A}}, \rho_{\mathcal{B}}; \mathbf{r}], \qquad 0 \le \lambda_{\mathcal{B}} \le 1. \tag{54a}$$

Similarly, in the $\lambda_{\mathcal{B}} = 0$ case,

$$v^{\mathcal{B}}_{\lambda_{\mathcal{A}},\lambda_{\mathcal{B}}=0}(\mathbf{r}) = v^{\mathcal{B}}_{eff}[\rho_{\mathcal{A}}, \rho_{\mathcal{B}}; \mathbf{r}], \qquad 0 \le \lambda_{\mathcal{A}} \le 1. \tag{54b}$$

For the ($\lambda_{\mathcal{A}} = 0$, $\lambda_{\mathcal{B}} = 1$) point in Fig. 2 the scaled external potential for electrons in $\mathcal{B}$ corresponds to the fully interacting electrons of this subsystem moving in the the effective potential due to nuclei of $\mathcal{M}$ and electrons in $\mathcal{A}$:

$$v^{\mathcal{B}}_{\lambda_{\mathcal{A}}=0,\lambda_{\mathcal{B}}=1}(\mathbf{r}) = v_H[\rho_{\mathcal{A}}; \mathbf{r}] + v_{xc}[\rho_{\mathcal{A}}; \mathbf{r}] \equiv v_{eff}[\rho_{\mathcal{A}}; \mathbf{r}]. \tag{55a}$$

The same reasoning identifies the following scaled external potential coupled to $\rho_{\mathcal{A}}$ in the ($\lambda_{\mathcal{A}} = 1$, $\lambda_{\mathcal{B}} = 0$) point of Fig. 2:

$$v^{\mathcal{A}}_{\lambda_{\mathcal{A}}=1,\lambda_{\mathcal{B}}=0}(\mathbf{r}) = v_H[\rho_{\mathcal{B}}; \mathbf{r}] + v_{xc}[\rho_{\mathcal{B}}; \mathbf{r}] \equiv v_{eff}[\rho_{\mathcal{B}}; \mathbf{r}]. \tag{55b}$$

Examples of a non-uniform scaling of the subsystem electronic charges are represented by the *paths 2-6* in Fig. 2; we have summarized in the figure Eqs. (44) and (53)-(55) identifying the subsystem scaled external potentials corresponding to the four points defining these scaling trajectories.

3.3. Uniform Scaling of Electronic Charges in $\mathcal{M}$ as a Whole

The third coupling-constant hamiltonian to be considered [see Eq.(37)], again with all electron-electron repulsions scaled uniformly in accordance with the global factor $0 \leq \kappa \leq 1$ (*path 1* in Fig. 2),

$$\hat{H}_\kappa(N, v_\kappa) \equiv \hat{H}_\kappa = \hat{T}_e(N) + \hat{V}_{ext}(N, v_\kappa^{\mathcal{AB}}) + \kappa\hat{V}_{ee}(N)$$

$$\equiv \hat{T}_e + \hat{V}_{ext}(\kappa) + \kappa\hat{V}_{ee}, \tag{56}$$

includes yet another *scaled external potential* $v_\kappa^{\mathcal{AB}}$, coupled to the overall density of $\mathcal{M}$, $\rho = \rho_{\mathcal{A}} + \rho_{\mathcal{B}}$, which defines the operator $\hat{V}_{ext}(\kappa) = \sum_{i=1}^{N} v_\kappa^{\mathcal{AB}}(\mathbf{r}_i)$. The hamiltonian of Eq.(56) represents the scaled system $\mathcal{M}(\kappa)$.

For the current value of the scaling factor κ the potential $v_\kappa^{\mathcal{AB}}$ is defined by the requirement that the scaled density

$$\rho_\kappa(\mathbf{r}) \equiv \langle\Psi_\kappa|\hat{\rho}_{\mathcal{A}}(\mathbf{r}) + \hat{\rho}_{\mathcal{B}}(\mathbf{r})|\Psi_\kappa\rangle = \langle\Psi_\kappa|\hat{\rho}(\mathbf{r})|\Psi_\kappa\rangle, \tag{57}$$

of the ground state $\Psi_\kappa(\mathbf{x}^{\mathcal{M}})$ of the scaled hamiltonian $\hat{H}_\kappa(\mathbf{x}^{\mathcal{M}})$,

$$\hat{H}_\kappa \Psi_\kappa = E(\kappa)\, \Psi_\kappa, \tag{58}$$

is equal to the overall density ρ of the fully interacting system $\mathcal{M}(1) = \mathcal{M}(1, 1)$:

$$\rho_{\kappa}(\mathbf{r}) = \rho_{\kappa=1}(\mathbf{r}) = \rho(\mathbf{r}) = \rho_{\mathcal{A}}(\mathbf{r}) + \rho_{\mathcal{B}}(\mathbf{r}). \tag{59}$$

This definition is therefore summarized by the mapping:

$$v_{\kappa}^{\mathcal{AB}} \leftrightarrow \rho.$$

It immediately follows from the above hypothesis that

$$v_{\kappa=1}^{\mathcal{AB}}(\mathbf{r}) = v(\mathbf{r}) \quad \text{and} \quad v_{\kappa=0}^{\mathcal{AB}}(\mathbf{r}) = v_{eff}[\rho;\ \mathbf{r}]. \tag{60}$$

4. COUPLING CONSTANT INTEGRATIONS

4.1. Uniform Scaling of Electronic Charges

The Hellmann-Feynman theorem for the uniform, λ-scaling scheme of electronic interactions/charges in the scaled ground state $\Psi_{\lambda}^{\mathcal{M}}[\rho_{\mathcal{A}},\ \rho_{\mathcal{B}}] = \Psi_{\lambda}^{\mathcal{M}}(\Psi_{\lambda}^{\mathcal{A}}[\rho_{\mathcal{A}},\rho_{\mathcal{B}}],\ \Psi_{\lambda}^{\mathcal{B}}[\rho_{\mathcal{A}},\rho_{\mathcal{B}}])$ of the two subsystems in $\mathcal{M}(\lambda,\ \lambda)$ reads:

$$dE^{\mathcal{M}}(\lambda)/d\lambda = \langle\Psi_{\lambda}^{\mathcal{M}}[\rho_{\mathcal{A}},\ \rho_{\mathcal{B}}]|\,\partial\hat{H}_{\lambda}^{\mathcal{M}}/\partial\lambda\,|\Psi_{\lambda}^{\mathcal{M}}[\rho_{\mathcal{A}},\ \rho_{\mathcal{B}}]\rangle$$

$$= \sum_{\mathcal{X}=\mathcal{A},\mathcal{B}} \int \rho_{\mathcal{X}}(\mathbf{r})\ [\partial v_{\lambda}^{\mathcal{X}}(\mathbf{r})/\partial\lambda]\ d\mathbf{r}$$

$$+ \langle\Psi_{\lambda}^{\mathcal{M}}[\rho_{\mathcal{A}},\ \rho_{\mathcal{B}}]|\,\hat{V}_{ee}^{\mathcal{M}}\,|\Psi_{\lambda}^{\mathcal{M}}[\rho_{\mathcal{A}},\ \rho_{\mathcal{B}}]\rangle$$

$$\equiv \sum_{\mathcal{X}=\mathcal{A},\mathcal{B}} \int \rho_{\mathcal{X}}(\mathbf{r})\ [\partial v_{\lambda}^{\mathcal{X}}(\mathbf{r})/\partial\lambda]\ d\mathbf{r} + V_{ee}^{\mathcal{M}}[\rho_{\mathcal{A}},\ \rho_{\mathcal{B}},\ \lambda]. \tag{61}$$

Its integration along the *path 1* in Fig. 2 gives the following expression for the change in the ground state electronic energy $E^{\mathcal{M}}(1)$, of the real, interacting system $\mathcal{M}(1, 1)$,

$$E^{\mathcal{M}}(1) - E^{\mathcal{M}}(0) = \int_0^1 \left(dE^{\mathcal{M}}(\lambda)/d\lambda\right) d\lambda$$

$$= \sum_{\mathcal{X}=\mathcal{A},\mathcal{B}} \int \rho_{\mathcal{X}}(\mathbf{r}) \left(v(\mathbf{r}) - v^{\mathcal{X}}_{eff}[\rho_{\mathcal{A}}, \rho_{\mathcal{B}}; \mathbf{r}]\right) d\mathbf{r}$$

$$+ \int_0^1 V^{\mathcal{M}}_{ee}[\rho_{\mathcal{A}}, \rho_{\mathcal{B}}, \lambda] \, d\lambda, \qquad (62)$$

relative to the energy $E^{\mathcal{M}}(0)$ of the noninteracting electrons in $\mathcal{M}(0, 0)$ [see Eq.(28)],

$$E^{\mathcal{M}}(0) \equiv E^{\mathcal{M}}_S[\rho_{\mathcal{A}}, \rho_{\mathcal{B}}]$$

$$= \langle \Psi^{\mathcal{M}}(\Phi^{\mathcal{A}}, \Phi^{\mathcal{B}}) | \sum_{i=1}^{N_{\mathcal{A}}} \hat{h}^{\mathcal{A}}_S(\mathbf{r}_i) + \sum_{i=N_{\mathcal{A}}+1}^{N} \hat{h}^{\mathcal{B}}_S(\mathbf{r}_i) | \Psi^{\mathcal{M}}(\Phi^{\mathcal{A}}, \Phi^{\mathcal{B}}) \rangle$$

$$\equiv \langle \Psi^{\mathcal{M}}(\Phi^{\mathcal{A}}, \Phi^{\mathcal{B}}) | \hat{H}^{\mathcal{M}}_S(\mathbf{r}^{\mathcal{A}}, \mathbf{r}^{\mathcal{B}}) | \Psi^{\mathcal{M}}(\Phi^{\mathcal{A}}, \Phi^{\mathcal{B}}) \rangle$$

$$= \sum_{i=1}^{N} \left\{ \frac{N_{\mathcal{A}}}{N} \langle \varphi_i | \hat{h}^{\mathcal{A}}_S | \varphi_i \rangle + \frac{N_{\mathcal{B}}}{N} \langle \varphi_i | \hat{h}^{\mathcal{B}}_S | \varphi_i \rangle \right\}$$

$$= \sum_{\mathcal{X}=\mathcal{A},\mathcal{B}} \left\{ T_S[\rho_{\mathcal{X}}] + \int \rho_{\mathcal{X}}(\mathbf{r}) \, v^{\mathcal{X}}_{eff}[\rho_{\mathcal{A}}, \rho_{\mathcal{B}}; \mathbf{r}] \, d\mathbf{r} \right\}. \qquad (63)$$

The last equation implies that the non-additive kinetic energy functional must be explicitly dependent upon the numbers of electrons in subsystems (29).

Hence the total energy of the real, fully interacting system is given by the functional:

$$E^{\mathcal{M}}(1) = T_S[\rho_{\mathcal{A}}] + T_S[\rho_{\mathcal{B}}] + \int \rho(\mathbf{r})\, v(\mathbf{r})\, d\mathbf{r} + \int_0^1 V_{ee}^{\mathcal{M}}[\rho_{\mathcal{A}}, \rho_{\mathcal{B}}, \lambda]\, d\lambda. \quad (64)$$

This energy is independently defined by the following density functionals [see Eq.(15)] (10,11,14):

$$E^{\mathcal{M}}(1) = E_v^{\mathcal{M}}[\rho_{\mathcal{A}}, \rho_{\mathcal{B}}]$$

$$= T_S[\rho_{\mathcal{A}}] + T_S[\rho_{\mathcal{B}}] + \int \rho(\mathbf{r})\, v(\mathbf{r})\, d\mathbf{r} + J[\rho] + E_{XC}^{\mathcal{M}}[\rho_{\mathcal{A}}, \rho_{\mathcal{B}}]$$

$$= T_S^{\mathcal{M}}[\rho_{\mathcal{A}}, \rho_{\mathcal{B}}] + \int \rho(\mathbf{r})\, v(\mathbf{r})\, d\mathbf{r} + J[\rho] + E_{XC}[\rho]. \quad (65)$$

Following the Appendix let us introduce the resultant scaled exchange-correlation hole $h_{XC}^{\mathcal{X}}[\rho_{\mathcal{A}}, \rho_{\mathcal{B}}, \lambda; \mathbf{r}, \mathbf{r}']$, around an electron of the subsystem $\mathcal{X}$ in $\mathcal{M}(\lambda, \lambda)$ [Eq. (A16a)]. The overall exchange-correlation energy $E_{XC}^{\mathcal{M}}[\rho_{\mathcal{A}}, \rho_{\mathcal{B}}, \lambda]$ for the scaled ground state $\Psi_\lambda^{\mathcal{M}}$ can then be expressed as the sum of the corresponding resultant contributions of subsystems [see Eq.(A17a)]:

$$E_{XC}^{\mathcal{M}}[\rho_{\mathcal{A}}, \rho_{\mathcal{B}}, \lambda] \equiv \lambda \{V_{ee}^{\mathcal{M}}[\rho_{\mathcal{A}}, \rho_{\mathcal{B}}, \lambda] - J[\rho_{\mathcal{A}} + \rho_{\mathcal{B}}]\}$$

$$\equiv \lambda\, \mathcal{E}_{XC}^{\mathcal{M}}[\rho_{\mathcal{A}}, \rho_{\mathcal{B}}, \lambda]$$

$$= \frac{\lambda}{2} \iint \{\rho_{\mathcal{A}}(\mathbf{r})\, h_{XC}^{\mathcal{A}}[\rho_{\mathcal{A}}, \rho_{\mathcal{B}}, \lambda; \mathbf{r}, \mathbf{r}'] + \rho_{\mathcal{B}}(\mathbf{r})\, h_{XC}^{\mathcal{B}}[\rho_{\mathcal{A}}, \rho_{\mathcal{B}}, \lambda; \mathbf{r}, \mathbf{r}']\}\, |\mathbf{r} - \mathbf{r}'|^{-1}\, d\mathbf{r}\, d\mathbf{r}'$$

$$\equiv E_{XC}^{\mathcal{A}}[\rho_{\mathcal{A}}, \rho_{\mathcal{B}}, \lambda] + E_{XC}^{\mathcal{B}}[\rho_{\mathcal{A}}, \rho_{\mathcal{B}}, \lambda]. \quad (66)$$

Integration of $\mathcal{E}^{\mathcal{M}}_{xc}[\rho_{\mathcal{A}}, \rho_{\mathcal{B}}, \lambda]$ over the coupling constant λ in the whole range from $\lambda = 0$ to $\lambda = 1$ gives the overall exchange-correlation energy of $\mathcal{M}(1, 1)$ (20-22) in terms of the average holes of subsystems, $h^{\chi}_{av}(\mathbf{r}, \mathbf{r}') \equiv h^{\chi}_{av(1)}[\rho_{\mathcal{A}}, \rho_{\mathcal{B}}; \mathbf{r}, \mathbf{r}']$ [Eq.(A18)], averaged over the *Path 1* section:

$$E^{\mathcal{M}}_{xc}[\rho_{\mathcal{A}}, \rho_{\mathcal{B}}] = \int_0^1 \mathcal{E}^{\mathcal{M}}_{xc}[\rho_{\mathcal{A}}, \rho_{\mathcal{B}}, \lambda]\, d\lambda$$

$$\equiv \frac{1}{2} \sum_{\chi=\mathcal{A},\mathcal{B}} \iint \rho_{\chi}(\mathbf{r}) \left\{\int_0^1 h^{\chi}_{xc}[\rho_{\mathcal{A}}, \rho_{\mathcal{B}}, \lambda; \mathbf{r}, \mathbf{r}']d\lambda\right\} |\mathbf{r} - \mathbf{r}'|^{-1} d\mathbf{r}d\mathbf{r}'$$

$$\equiv \frac{1}{2} \sum_{\chi=\mathcal{A},\mathcal{B}} \iint \rho_{\chi}(\mathbf{r})\, h^{\chi}_{av}[\rho_{\mathcal{A}}, \rho_{\mathcal{B}}; \mathbf{r}, \mathbf{r}']|\mathbf{r} - \mathbf{r}'|^{-1} d\mathbf{r}d\mathbf{r}'. \quad (67)$$

Alternatively, the above equation can be interpreted as defining the nonadditive kinetic energy functional itself [see Eq. (15)]:

$$T_s^{nadd}[\rho_{\mathcal{A}}, \rho_{\mathcal{B}}] = E^{\mathcal{M}}_{xc}[\rho_{\mathcal{A}}, \rho_{\mathcal{B}}] - E_{xc}[\rho]$$

$$= \int_0^1 \{V^{\mathcal{M}}_{ee}[\rho_{\mathcal{A}}, \rho_{\mathcal{B}}, \lambda] - V_{ee}[\rho, \lambda]\}\, d\lambda$$

$$= \frac{1}{2} \sum_{\chi=\mathcal{A},\mathcal{B}} \iint \rho_{\chi}(\mathbf{r})\, |\mathbf{r} - \mathbf{r}'|^{-1}$$

$$\times \left\{\int_0^1 (h^{\chi}_{xc}[\rho_{\mathcal{A}}, \rho_{\mathcal{B}}, \lambda; \mathbf{r}, \mathbf{r}'] - h_{xc}[\rho, \lambda; \mathbf{r}, \mathbf{r}'])\, d\lambda\right\} d\mathbf{r}\, d\mathbf{r}'$$

$$\equiv \frac{1}{2} \sum_{\chi=\mathcal{A},\mathcal{B}} \iint \rho_{\chi}(\mathbf{r})\, |\mathbf{r} - \mathbf{r}'|^{-1}$$

$$\times \left\{\int_0^1 h^{nadd}_{\chi}[\rho_{\mathcal{A}}, \rho_{\mathcal{B}}, \lambda; \mathbf{r}, \mathbf{r}']\, d\lambda\right\} d\mathbf{r}\, d\mathbf{r}'$$

$$= \frac{1}{2} \sum_{\chi=\mathcal{A},\mathcal{B}} \iint \rho_\chi(\mathbf{r}) \, |\mathbf{r} - \mathbf{r}'|^{-1} \times \{h^{\chi}_{av}[\rho_{\mathcal{A}},\rho_{\mathcal{B}};\ \mathbf{r},\mathbf{r}'] - h_{av}[\rho;\ \mathbf{r},\mathbf{r}']\} \, d\mathbf{r}d\mathbf{r}'$$

$$\equiv \frac{1}{2} \sum_{\chi=\mathcal{A},\mathcal{B}} \iint \rho_\chi(\mathbf{r}) \, h^{nadd}_{\chi,av}[\rho_{\mathcal{A}},\rho_{\mathcal{B}};\ \mathbf{r},\mathbf{r}']|\mathbf{r} - \mathbf{r}'|^{-1} \, d\mathbf{r}d\mathbf{r}'. \tag{68}$$

Indeed, within the κ-scaling integration scheme along the same *path 1* in Fig. 2 one similarly arrives at the associated relation for the overall density of Eq. (57):

$$E_{xc}[\rho] = \int_0^1 V_{ee}[\rho;\ \kappa] \, d\kappa - J[\rho]$$

$$= \frac{1}{2} \iint \rho(\mathbf{r}) \{\int_0^1 h_{xc}[\rho,\ \kappa;\ \mathbf{r},\ \mathbf{r}'] \, d\kappa\} \, |\mathbf{r} - \mathbf{r}'|^{-1} \, d\mathbf{r} \, d\mathbf{r}'$$

$$\equiv \frac{1}{2} \iint \rho(\mathbf{r}) \, h_{av}[\rho;\ \mathbf{r},\ \mathbf{r}'] \, |\mathbf{r} - \mathbf{r}'|^{-1} \, d\mathbf{r} \, d\mathbf{r}', \tag{69}$$

where $V_{ee}[\rho;\ \kappa] = \langle \Psi_\kappa[\rho] | \hat{V}_{ee} | \Psi_\kappa[\rho] \rangle$ and $\Psi_\kappa[\rho] = \Psi_\kappa$ denotes the ground state of $\hat{H}_\kappa$ giving rise to the overall density $\rho = \rho_{\mathcal{A}} + \rho_{\mathcal{B}}$.

It should be observed, that the corresponding exact expectation values of $\hat{V}_{ee}$,

$$V^{\mathcal{M}}_{ee}[\rho_{\mathcal{A}},\ \rho_{\mathcal{B}},\ \lambda = 1] = \langle \Psi^{\mathcal{M}}_1[\rho_{\mathcal{A}},\ \rho_{\mathcal{B}}] | \hat{V}_{ee} | \Psi^{\mathcal{M}}_1[\rho_{\mathcal{A}},\ \rho_{\mathcal{B}}] \rangle$$

$$\equiv J[\rho_{\mathcal{A}} + \rho_{\mathcal{B}}] + \bar{E}^{\mathcal{M}}_{xc}[\rho_{\mathcal{A}},\ \rho_{\mathcal{B}}], \tag{70}$$

and

$$V^{\mathcal{M}}_{ee}[\rho,\ \kappa = 1] = \langle \Psi_1[\rho] | \hat{V}_{ee} | \Psi_1[\rho] \rangle \equiv J[\rho] + \bar{E}_{xc}[\rho], \tag{71}$$

in the fully interacting systems $\mathcal{M}(1, 1)$ and $\mathcal{M}(1)$, respectively, do not include the corresponding correlation contributions to the kinetic energy of electrons:

$$T_c^{\mathcal{M}}[\rho_{\mathcal{A}}, \rho_{\mathcal{B}}] \equiv \bar{T}_e^{\mathcal{M}}[\rho_{\mathcal{A}}, \rho_{\mathcal{B}}] - T_s^{\mathcal{M}}[\rho_{\mathcal{A}}, \rho_{\mathcal{B}}]$$

$$= E_{xc}^{\mathcal{M}}[\rho_{\mathcal{A}}, \rho_{\mathcal{B}}] - \bar{E}_{xc}^{\mathcal{M}}[\rho_{\mathcal{A}}, \rho_{\mathcal{B}}] - T_s^{nadd}[\rho_{\mathcal{A}}, \rho_{\mathcal{B}}], \qquad (72)$$

$$T_c[\rho] \equiv \bar{T}_e[\rho] - T_s[\rho] = E_{xc}[\rho] - \bar{E}_{xc}[\rho]. \qquad (73)$$

Here, $\bar{T}_e^{\mathcal{M}}[\rho_{\mathcal{A}}, \rho_{\mathcal{B}}] \equiv \langle \Psi_1^{\mathcal{M}}[\rho_{\mathcal{A}}, \rho_{\mathcal{B}}] | \hat{T}_e | \Psi_1^{\mathcal{M}}[\rho_{\mathcal{A}}, \rho_{\mathcal{B}}] \rangle$ and $\bar{T}_e[\rho] \equiv \langle \Psi_1[\rho] | \hat{T}_e | \Psi_1[\rho] \rangle$ are the exact kinetic energies of electrons, for the correlated ground state wavefunctions in $\mathcal{M} = (1, 1)$ and $\mathcal{M}(1)$, accordingly.

It should also be realized, that the CI expansions of $\Psi_1^{\mathcal{M}}[\rho_{\mathcal{A}}, \rho_{\mathcal{B}}]$ and $\Psi_1[\rho]$ wavefunctions, in terms of configurations generated by the subsystem orbitals, differ by the *charge tramsfer* (CT) terms, which change the number of electrons in subsystems. Such configurations are neglected in the polarization-only expansion of the generalized product function $\Psi_1^{\mathcal{M}}[\rho_{\mathcal{A}}, \rho_{\mathcal{B}}]$. Therefore, the above functionals of the overall density $\rho(\mathbf{r})$, $\bar{T}_e[\rho]$ and $\bar{E}_{xc}[\rho]$, differ from their corresponding subsystem resolved analogs, $\bar{T}_e^{\mathcal{M}}[\rho_{\mathcal{A}}, \rho_{\mathcal{B}}]$ and $\bar{E}_{xc}^{\mathcal{M}}[\rho_{\mathcal{A}}, \rho_{\mathcal{B}}]$, by the relevant CT electron correlation terms:

$$T_{c,CT}^{\mathcal{M}}[\rho_{\mathcal{A}}, \rho_{\mathcal{B}}] \equiv \bar{T}_e[\rho] - \bar{T}_e^{\mathcal{M}}[\rho_{\mathcal{A}}, \rho_{\mathcal{B}}], \qquad (74)$$

$$E_{c,CT}^{\mathcal{M}}[\rho_{\mathcal{A}}, \rho_{\mathcal{B}}] \equiv \bar{E}_{xc}[\rho] - \bar{E}_{xc}^{\mathcal{M}}[\rho_{\mathcal{A}}, \rho_{\mathcal{B}}]. \qquad (75)$$

4.2. Separate Scalings of Subsystem Electronic Charges

The Hellmann-Feynman theorem now reads [see Eq.(8c)]:

$$\partial E^{\mathcal{M}}(\lambda_{\mathcal{A}},\lambda_{\mathcal{B}})/\partial\lambda_{\mathcal{X}}$$

$$= \langle\Psi^{\mathcal{M}}_{\lambda_{\mathcal{A}},\lambda_{\mathcal{B}}}[\rho_{\mathcal{A}},\ \rho_{\mathcal{B}}]\,|\,\partial\hat{H}^{\mathcal{M}}_{\lambda_{\mathcal{A}},\lambda_{\mathcal{B}}}/\partial\lambda_{\mathcal{X}}\,|\,\Psi^{\mathcal{M}}_{\lambda_{\mathcal{A}},\lambda_{\mathcal{B}}}[\rho_{\mathcal{A}},\ \rho_{\mathcal{B}}]\rangle$$

$$= \sum_{\mathcal{Z}=\mathcal{A},\mathcal{B}} \int \rho_{\mathcal{Z}}(\mathbf{r})\ (\partial v^{\mathcal{Z}}_{\lambda_{\mathcal{A}},\lambda_{\mathcal{B}}}(\mathbf{r})/\partial\lambda_{\mathcal{X}})\ d\mathbf{r} + V^{\mathcal{X}}_{ee}[\rho_{\mathcal{A}},\rho_{\mathcal{B}},\lambda_{\mathcal{A}},\lambda_{\mathcal{B}}]$$

$$+ \frac{1}{2}\,(\lambda_{\mathcal{Y}}/\lambda_{\mathcal{X}})^{1/2}\ V^{\mathcal{A},\mathcal{B}}_{ee}[\rho_{\mathcal{A}},\rho_{\mathcal{B}},\lambda_{\mathcal{A}},\lambda_{\mathcal{B}}],\quad (\mathcal{Y}\neq\mathcal{X})=\mathcal{A},\ \mathcal{B}, \tag{76}$$

where:

$$V^{\mathcal{X}}_{ee}[\rho_{\mathcal{A}},\rho_{\mathcal{B}},\lambda_{\mathcal{A}},\lambda_{\mathcal{B}}] \equiv \langle\Psi^{\mathcal{M}}_{\lambda_{\mathcal{A}},\lambda_{\mathcal{B}}}[\rho_{\mathcal{A}},\ \rho_{\mathcal{B}}]\,|\,\hat{V}^{\mathcal{X}}_{ee}\,|\,\Psi^{\mathcal{M}}_{\lambda_{\mathcal{A}},\lambda_{\mathcal{B}}}[\rho_{\mathcal{A}},\ \rho_{\mathcal{B}}]\rangle, \tag{77}$$

$$V^{\mathcal{A},\mathcal{B}}_{ee}[\rho_{\mathcal{A}},\rho_{\mathcal{B}},\lambda_{\mathcal{A}},\lambda_{\mathcal{B}}] \equiv \langle\Psi^{\mathcal{M}}_{\lambda_{\mathcal{A}},\lambda_{\mathcal{B}}}[\rho_{\mathcal{A}},\ \rho_{\mathcal{B}}]\,|\,\hat{V}^{\mathcal{A},\mathcal{B}}_{ee}\,|\,\Psi^{\mathcal{M}}_{\lambda_{\mathcal{A}},\lambda_{\mathcal{B}}}[\rho_{\mathcal{A}},\ \rho_{\mathcal{B}}]\rangle. \tag{78}$$

For definiteness let us assume $\mathcal{X} = \mathcal{A}$ and integrate the above theorem over the whole range of $\lambda_{\mathcal{A}}$ for the fixed value of $\lambda_{\mathcal{B}}$. This procedure gives the following expression for the $E^{\mathcal{M}}(1,\ \lambda_{\mathcal{B}})$-cut of the ground state energy function $E^{\mathcal{M}}(\lambda_{\mathcal{A}},\ \lambda_{\mathcal{B}})$:

$$E^{\mathcal{M}}(1,\ \lambda_{\mathcal{B}}) = E^{\mathcal{M}}(0,\ \lambda_{\mathcal{B}}) + \int_0^1 (dE^{\mathcal{M}}(\lambda_{\mathcal{A}},\ \lambda_{\mathcal{B}})/d\lambda_{\mathcal{A}})\ d\lambda_{\mathcal{A}}$$

$$= E^{\mathcal{M}}(0,\ \lambda_{\mathcal{B}}) + \sum_{\mathcal{Z}=\mathcal{A},\mathcal{B}} \int \rho_{\mathcal{Z}}(\mathbf{r})\ [v^{\mathcal{Z}}_{1,\lambda_{\mathcal{B}}}(\mathbf{r}) - v^{\mathcal{Z}}_{0,\lambda_{\mathcal{B}}}(\mathbf{r})]\ d\mathbf{r}$$

$$+ \int_0^1 \{V^{\mathcal{A}}_{ee}[\rho_{\mathcal{A}},\rho_{\mathcal{B}},\lambda_{\mathcal{A}},\lambda_{\mathcal{B}}] + \frac{1}{2}(\lambda_{\mathcal{B}}/\lambda_{\mathcal{A}})^{1/2} V^{\mathcal{A},\mathcal{B}}_{ee}[\rho_{\mathcal{A}},\rho_{\mathcal{B}},\lambda_{\mathcal{A}},\lambda_{\mathcal{B}}]\}\ d\lambda_{\mathcal{A}}. \tag{79}$$

Table 1. Summary of energy changes corresponding to the scaling paths of Fig. 2.

$$E^{\mathcal{M}}(0,0) = \sum_{\mathcal{X}=\mathcal{A},\mathcal{B}} \{T_s[\rho_{\mathcal{X}}] + \int \rho_{\mathcal{X}}(\mathbf{r})\, v^{\mathcal{X}}_{eff}[\rho_{\mathcal{A}}, \rho_{\mathcal{B}}; \mathbf{r}]\, d\mathbf{r}\}$$

$$\Delta E^{\mathcal{M}}_1 = E^{\mathcal{M}}(1,1) - E^{\mathcal{M}}(0,0) = \sum_{\mathcal{X}=\mathcal{A},\mathcal{B}} \int \rho_{\mathcal{X}}(\mathbf{r}) \{v(\mathbf{r}) - v^{\mathcal{X}}_{eff}[\rho_{\mathcal{A}}, \rho_{\mathcal{B}}; \mathbf{r}]\}\, d\mathbf{r} + \int_0^1 V^{\mathcal{M}}_{ee}[\rho_{\mathcal{A}}, \rho_{\mathcal{B}}, \lambda]\, d\lambda$$

$$= \int \rho(\mathbf{r}) \{v(\mathbf{r}) - v_{eff}[\rho; \mathbf{r}]\}\, d\mathbf{r} + \int_0^1 V_{ee}[\rho; \kappa]\, d\kappa$$

$$\Delta E^{\mathcal{M}}_2 \equiv E^{\mathcal{M}}(1,0) - E^{\mathcal{M}}(0,0) = \int \rho_{\mathcal{A}}(\mathbf{r}) \{v_{eff}[\rho_{\mathcal{B}}; \mathbf{r}] - v^{\mathcal{A}}_{eff}[\rho_{\mathcal{A}}, \rho_{\mathcal{B}}; \mathbf{r}]\}\, d\mathbf{r} + \int_0^1 V^{\mathcal{A}}_{ee}[\rho_{\mathcal{A}}, \rho_{\mathcal{B}}, \lambda_{\mathcal{A}}, 0]\, d\lambda_{\mathcal{A}}$$

$$\Delta E^{\mathcal{M}}_3 \equiv E^{\mathcal{M}}(0,1) - E^{\mathcal{M}}(0,0) = \int \rho_{\mathcal{B}}(\mathbf{r}) \{v_{eff}[\rho_{\mathcal{A}}; \mathbf{r}] - v^{\mathcal{B}}_{eff}[\rho_{\mathcal{A}}, \rho_{\mathcal{B}}; \mathbf{r}]\}\, d\mathbf{r} + \int_0^1 V^{\mathcal{B}}_{ee}[\rho_{\mathcal{A}}, \rho_{\mathcal{B}}, 0, \lambda_{\mathcal{B}}]\, d\lambda_{\mathcal{B}}$$

$$\Delta E^{\mathcal{M}}_4 \equiv E^{\mathcal{M}}(1,1) - E^{\mathcal{M}}(0,1) = \int \rho_{\mathcal{A}}(\mathbf{r}) \{v(\mathbf{r}) - v^{\mathcal{A}}_{eff}[\rho_{\mathcal{A}}, \rho_{\mathcal{B}}; \mathbf{r}]\}\, d\mathbf{r} + \int \rho_{\mathcal{B}}(\mathbf{r}) \{v(\mathbf{r}) - v_{eff}[\rho_{\mathcal{A}}; \mathbf{r}]\}\, d\mathbf{r} + \int_0^1 \{V^{\mathcal{A}}_{ee}[\rho_{\mathcal{A}}, \rho_{\mathcal{B}}, \lambda_{\mathcal{A}}, 1] + \frac{1}{2} \lambda_{\mathcal{A}}^{-1/2} V^{\mathcal{A},\mathcal{B}}_{ee}[\rho_{\mathcal{A}}, \rho_{\mathcal{B}}, \lambda_{\mathcal{A}}, 1]\}\, d\lambda_{\mathcal{A}}$$

$$\Delta E^{\mathcal{M}}_4 = \Delta E^{\mathcal{M}}_1 - \Delta E^{\mathcal{M}}_3 = \int \rho_{\mathcal{A}}(\mathbf{r}) \{v(\mathbf{r}) - v^{\mathcal{A}}_{eff}[\rho_{\mathcal{A}}, \rho_{\mathcal{B}}; \mathbf{r}]\}\, d\mathbf{r} + \int \rho_{\mathcal{B}}(\mathbf{r}) \{v(\mathbf{r}) - v_{eff}[\rho_{\mathcal{A}}; \mathbf{r}]\}\, d\mathbf{r} + \int_0^1 V^{\mathcal{M}}_{ee}[\rho_{\mathcal{A}}, \rho_{\mathcal{B}}, \lambda]\, d\lambda - \int_0^1 V^{\mathcal{B}}_{ee}[\rho_{\mathcal{A}}, \rho_{\mathcal{B}}, 0, \lambda_{\mathcal{B}}]\, d\lambda_{\mathcal{B}}$$

Table 1. Continued.

$$\Delta E_5^{\mathcal{M}} \equiv E^{\mathcal{M}}(1,1) - E^{\mathcal{M}}(1,0)$$

$$= \int \rho_{\mathcal{A}}(\mathbf{r}) \{v(\mathbf{r}) - v_{eff}[\rho_{\mathcal{B}}; \mathbf{r}]\} \, d\mathbf{r} + \int \rho_{\mathcal{B}}(\mathbf{r}) \{v(\mathbf{r}) - v_{eff}^{\mathcal{B}}[\rho_{\mathcal{A}}, \rho_{\mathcal{B}}; \mathbf{r}]\} \, d\mathbf{r}$$

$$+ \int_0^1 \{V_{ee}^{\mathcal{B}}[\rho_{\mathcal{A}}, \rho_{\mathcal{B}}, 1, \lambda_{\mathcal{B}}] + \frac{1}{2} \lambda_{\mathcal{B}}^{-1/2} V_{ee}^{\mathcal{A},\mathcal{B}}[\rho_{\mathcal{A}}, \rho_{\mathcal{B}}, 1, \lambda_{\mathcal{B}}]\} \, d\lambda_{\mathcal{B}}$$

$$\Delta E_5^{\mathcal{M}} = \Delta E_1^{\mathcal{M}} - \Delta E_2^{\mathcal{M}} = \int \rho_{\mathcal{A}}(\mathbf{r}) \{v(\mathbf{r}) - v_{eff}[\rho_{\mathcal{B}}; \mathbf{r}]\} \, d\mathbf{r} + \int \rho_{\mathcal{B}}(\mathbf{r}) \{v(\mathbf{r}) - v_{eff}^{\mathcal{B}}[\rho_{\mathcal{A}}, \rho_{\mathcal{B}}; \mathbf{r}]\} \, d\mathbf{r}$$

$$+ \int_0^1 V_{ee}^{\mathcal{M}}[\rho_{\mathcal{A}}, \rho_{\mathcal{B}}, \lambda] \, d\lambda - \int_0^1 V_{ee}^{\mathcal{A}}[\rho_{\mathcal{A}}, \rho_{\mathcal{B}}, \lambda_{\mathcal{A}}, 0] \, d\lambda_{\mathcal{A}}$$

$$\Delta E_6^{\mathcal{M}} \equiv E^{\mathcal{M}}(0,1) - E^{\mathcal{M}}(1,0)$$

$$= \int \rho_{\mathcal{A}}(\mathbf{r}) \{v_{eff}^{\mathcal{A}}[\rho_{\mathcal{A}}, \rho_{\mathcal{B}}; \mathbf{r}] - v_{eff}[\rho_{\mathcal{B}}; \mathbf{r}]\} \, d\mathbf{r} - \int \rho_{\mathcal{B}}(\mathbf{r}) \{v_{eff}^{\mathcal{B}}[\rho_{\mathcal{A}}, \rho_{\mathcal{B}}; \mathbf{r}] - v_{eff}[\rho_{\mathcal{A}}; \mathbf{r}]\} \, d\mathbf{r}$$

$$+ \int_0^1 \{V_{ee}^{\mathcal{B}}[\rho_{\mathcal{A}}, \rho_{\mathcal{B}}, 1 - \lambda_{\mathcal{B}}, \lambda_{\mathcal{B}}] - V_{ee}^{\mathcal{A}}[\rho_{\mathcal{A}}, \rho_{\mathcal{B}}, 1 - \lambda_{\mathcal{B}}, \lambda_{\mathcal{B}}]$$

$$+ \frac{1}{2}(1 - 2\lambda_{\mathcal{B}})[\lambda_{\mathcal{B}}(1 - \lambda_{\mathcal{B}})]^{-1/2} V_{ee}^{\mathcal{A},\mathcal{B}}[\rho_{\mathcal{A}}, \rho_{\mathcal{B}}, 1 - \lambda_{\mathcal{B}}, \lambda_{\mathcal{B}}]\} \, d\lambda_{\mathcal{B}}$$

$$\Delta E_6^{\mathcal{M}} = \Delta E_3^{\mathcal{M}} - \Delta E_2^{\mathcal{M}}$$

$$= \int \rho_{\mathcal{A}}(\mathbf{r}) \{v_{eff}^{\mathcal{A}}[\rho_{\mathcal{A}}, \rho_{\mathcal{B}}; \mathbf{r}] - v_{eff}[\rho_{\mathcal{B}}; \mathbf{r}]\} \, d\mathbf{r} + \int \rho_{\mathcal{B}}(\mathbf{r}) \{v_{eff}[\rho_{\mathcal{A}}; \mathbf{r}] - v_{eff}^{\mathcal{B}}[\rho_{\mathcal{A}}, \rho_{\mathcal{B}}; \mathbf{r}]\} \, d\mathbf{r}$$

$$- \int_0^1 V_{ee}^{\mathcal{A}}[\rho_{\mathcal{A}}, \rho_{\mathcal{B}}, \lambda_{\mathcal{A}}, 0] \, d\lambda_{\mathcal{A}} + \int_0^1 V_{ee}^{\mathcal{B}}[\rho_{\mathcal{A}}, \rho_{\mathcal{B}}, 0, \lambda_{\mathcal{B}}] \, d\lambda_{\mathcal{B}}$$

The explicit expressions obtained from this integrated Hellmann-Feynman theorem for the energy changes corresponding to the *paths 2-5* are reported in Table 1, where we have summarized the CCI formulas for the energy changes corresponding to all integration paths shown in Fig. 2.

Following the Appendix we now express the intra- and inter-subsystem scaled exchange-correlation energies in terms of the corresponding scaled, subsystem-resolved holes:

$$E_{xc}^{\mathcal{X},\mathcal{X}}[\rho_{\mathcal{A}},\rho_{\mathcal{B}},\lambda_{\mathcal{A}},\lambda_{\mathcal{B}}] = \lambda_{\mathcal{X}}\{V_{ee}^{\mathcal{X}}[\rho_{\mathcal{A}},\rho_{\mathcal{B}},\lambda_{\mathcal{A}},\lambda_{\mathcal{B}}] - J[\rho_{\mathcal{X}}]\}$$

$$\equiv \lambda_{\mathcal{X}}\, \mathcal{E}_{xc}^{\mathcal{X}}[\rho_{\mathcal{A}},\rho_{\mathcal{B}},\lambda_{\mathcal{A}},\lambda_{\mathcal{B}}]$$

$$= \frac{\lambda_{\mathcal{X}}}{2} \int\int \rho_{\mathcal{X}}(\mathbf{r})\, h_{xc}^{\mathcal{X},\mathcal{X}}[\rho_{\mathcal{A}},\rho_{\mathcal{B}},\lambda_{\mathcal{A}},\lambda_{\mathcal{B}};\ \mathbf{r},\mathbf{r}']\, |\mathbf{r} - \mathbf{r}'|^{-1}\, d\mathbf{r}d\mathbf{r}',$$

$$\mathcal{X} = \mathcal{A},\ \mathcal{B}; \qquad (80)$$

$$E_{xc}^{\mathcal{A},\mathcal{B}}[\rho_{\mathcal{A}},\rho_{\mathcal{B}},\lambda_{\mathcal{A}},\lambda_{\mathcal{B}}] = (\lambda_{\mathcal{A}}\lambda_{\mathcal{B}})^{1/2}\{V_{ee}^{\mathcal{A},\mathcal{B}}[\rho_{\mathcal{A}},\rho_{\mathcal{B}},\lambda_{\mathcal{A}},\lambda_{\mathcal{B}}] - J_{\mathcal{A},\mathcal{B}}[\rho_{\mathcal{A}},\rho_{\mathcal{B}}]\}$$

$$= \frac{1}{2}\,(\lambda_{\mathcal{A}}\lambda_{\mathcal{B}})^{1/2} \int\int \{\rho_{\mathcal{A}}(\mathbf{r})\, h_{xc}^{\mathcal{A},\mathcal{B}}[\rho_{\mathcal{A}},\ \rho_{\mathcal{B}},\ \lambda_{\mathcal{A}},\ \lambda_{\mathcal{B}};\ \mathbf{r},\ \mathbf{r}']$$

$$+\ \rho_{\mathcal{B}}(\mathbf{r}) h_{xc}^{\mathcal{B},\mathcal{A}}[\rho_{\mathcal{A}},\rho_{\mathcal{B}},\lambda_{\mathcal{A}},\lambda_{\mathcal{B}};\ \mathbf{r},\mathbf{r}']\}\, |\mathbf{r} - \mathbf{r}'|^{-1}\, d\mathbf{r}d\mathbf{r}'. \qquad (81)$$

Consider now a special case of $\lambda_{\mathcal{B}} = 0$ (*path 2* in Fig. 2). The relevant scaled external potentials for the limiting points $(0,\ 0)$ and $(1,\ o)$ of this integration are given by Eqs. (54b) and (55b); they are also explicitly listed in Fig. 2. Using these expressions in the above Hellmann-Feynman theorem for the path 2 in Fig. 2 gives:

$$E^{\mathcal{M}}(1,\ 0) = E^{\mathcal{M}}(0,\ 0) + \int_0^1 V_{ee}^{\mathcal{A}}[\rho_{\mathcal{A}},\rho_{\mathcal{B}},\lambda_{\mathcal{A}},\ 0]\ d\lambda_{\mathcal{A}}$$

$$+ \int \rho_{\mathcal{A}}(\mathbf{r})\ \left(v_{eff}[\rho_{\mathcal{B}};\ \mathbf{r}] - v_{eff}^{\mathcal{A}}[\rho_{\mathcal{A}},\ \rho_{\mathcal{B}};\ \mathbf{r}]\right)\ d\mathbf{r}, \qquad (82)$$

where the starting point energy $E^{\mathcal{M}}(0,\ 0) = E^{\mathcal{M}}(0)$ of the noninteracting electrons is defined in Eq.(63).

The end-point energy $E^{\mathcal{M}}(1,\ 0)$ corresponds to the vanishing interaction between the $\mathcal{A}$- and $\mathcal{B}$-group electrons. Therefore, it can be expressed as the sum of the relevant additive subsystem energies $\{E_{\chi}^{\mathcal{M}}(1,\ 0)\}$:

$$E^{\mathcal{M}}(1,\ 0) = E_{\mathcal{A}}^{\mathcal{M}}(1,\ 0) + E_{\mathcal{B}}^{\mathcal{M}}(1,\ 0). \qquad (83)$$

In $\mathcal{M}(1,\ 0)$ the $\mathcal{A}$-group electrons are fully interacting with one another, moving in the effective one-body potential due to the nuclei and the $\mathcal{B}$-group electrons. Hence, the energy $E_{\mathcal{A}}^{\mathcal{M}}(1,\ 0)$ is given by the functional

$$E_{\mathcal{A}}^{\mathcal{M}}(1,\ 0) = \langle \Psi_{1,0}^{\mathcal{M}}[\rho_{\mathcal{A}},\ \rho_{\mathcal{B}}] | \hat{T}_e^{\mathcal{A}}(\mathbf{x}^{\mathcal{A}}) + \hat{V}_{ee}^{\mathcal{A}}(\mathbf{x}^{\mathcal{A}})$$

$$+ \sum_{i=1}^{N_{\mathcal{A}}} v_{eff}[\rho_{\mathcal{B}};\ \mathbf{r}_i] | \Psi_{1,0}^{\mathcal{M}}[\rho_{\mathcal{A}},\ \rho_{\mathcal{B}}] \rangle$$

$$= T_S[\rho_{\mathcal{A}}] + \int \rho_{\mathcal{A}}(\mathbf{r})\ v_{eff}[\rho_{\mathcal{B}};\ \mathbf{r}]\ d\mathbf{r} + J[\rho_{\mathcal{A}}] + E_{xc}^{\mathcal{M}}[\rho_{\mathcal{A}}], \qquad (84)$$

in which the exchange-correlation energy $E_{xc}^{\mathcal{M}}[\rho_{\mathcal{A}}]$ includes the relevant correlation correction to the kinetic energy of electrons in $\mathcal{A}$, $T_c[\rho_{\mathcal{A}}]$. The $\mathcal{B}$-group electrons do not interact in $\mathcal{M}(1,\ 0)$, moving independently in the effective potential due to nuclei and electrons of both groups. Hence the expression for $E_{\mathcal{B}}^{\mathcal{M}}(1,\ 0)$:

$$E^{\mathcal{M}}_{\mathcal{B}}(1,\ 0) \equiv E^{\mathcal{B}}_{S}[\rho_{\mathcal{A}},\ \rho_{\mathcal{B}}]$$

$$\equiv \langle \Psi^{\mathcal{M}}_{1,0}[\rho_{\mathcal{A}},\ \rho_{\mathcal{B}}] |\ \sum_{i=N_{\mathcal{A}}+1}^{N} \hat{h}^{\mathcal{B}}_{S}[\rho_{\mathcal{A}},\ \rho_{\mathcal{B}};\ \mathbf{r}_i]\ | \Psi^{\mathcal{M}}_{1,0}[\rho_{\mathcal{A}},\ \rho_{\mathcal{B}}] \rangle$$

$$\equiv \langle \Psi^{\mathcal{M}}_{1,0}[\rho_{\mathcal{A}},\ \rho_{\mathcal{B}}] | \hat{H}^{\mathcal{B}}_{S}(\mathbf{r}^{\mathcal{B}}) | \Psi^{\mathcal{M}}_{1,0}[\rho_{\mathcal{A}},\ \rho_{\mathcal{B}}] \rangle$$

$$= T_S[\rho_{\mathcal{B}}] + \int \rho_{\mathcal{B}}(\mathbf{r})\ v^{\mathcal{B}}_{eff}[\rho_{\mathcal{A}},\ \rho_{\mathcal{B}};\ \mathbf{r}]\ d\mathbf{r}. \qquad (85)$$

Equations (63), (82)-(85), (A16a), and (A20a) give the following expression for $E^{\mathcal{M}}_{xc}[\rho_{\mathcal{A}}]$:

$$E^{\mathcal{M}}_{xc}[\rho_{\mathcal{A}}] = \int_0^1 V^{\mathcal{A}}_{ee}[\rho_{\mathcal{A}},\ \rho_{\mathcal{B}},\ \lambda_{\mathcal{A}},\ 0]\ d\lambda_{\mathcal{A}} - J[\rho_{\mathcal{A}}]$$

$$= \frac{1}{2} \iint \rho_{\mathcal{A}}(\mathbf{r}) \left\{ \int_0^1 h^{\mathcal{A},\mathcal{A}}_{xc}[\rho_{\mathcal{A}},\rho_{\mathcal{B}},\lambda_{\mathcal{A}},0;\ \mathbf{r},\ \mathbf{r}']d\lambda_{\mathcal{A}} \right\} |\mathbf{r} - \mathbf{r}'|^{-1} d\mathbf{r}d\mathbf{r}'$$

$$\equiv \frac{1}{2} \iint \rho_{\mathcal{A}}(\mathbf{r})\ h^{\mathcal{A},\mathcal{A}}_{av(2)}(\lambda_{\mathcal{B}} = 0;\ \mathbf{r},\ \mathbf{r}')\ |\mathbf{r} - \mathbf{r}'|^{-1}\ d\mathbf{r}d\mathbf{r}'. \qquad (86)$$

It expresses the exchange-correlation energy in the subsystem $\mathcal{A}$ of $\mathcal{M}(1,\ 0)$ in terms of the *exchange-correlation hole* $h^{\mathcal{A},\mathcal{A}}_{av(2)}(\lambda_{\mathcal{B}} = 0;\ \mathbf{r},\ \mathbf{r}') \equiv h^{\mathcal{A},\mathcal{A}}_{av(2)}(\mathbf{r},\ \mathbf{r}')$ *for the non-interacting electrons in* $\mathcal{B}$ ($\lambda_{\mathcal{A}}$-averaged).

Clearly, the $\lambda_{\mathcal{B}}$-integration for the fixed $\lambda_{\mathcal{A}} = 0$, along the *path 3* in Fig. 2, will give rise to the corresponding expressions for the exhange-correlation energy of $\mathcal{B}$ in $\mathcal{M}(0,\ 1)$:

$$E^{\mathcal{M}}_{xc}[\rho_{\mathcal{B}}] = \int_0^1 V^{\mathcal{B}}_{ee}[\rho_{\mathcal{A}},\ \rho_{\mathcal{B}},\ 0,\ \lambda_{\mathcal{B}}]\ d\lambda_{\mathcal{B}} - J[\rho_{\mathcal{B}}]$$

$$= \frac{1}{2} \iint \rho_{\mathcal{B}}(\mathbf{r}) \left\{ \int_0^1 h^{\mathcal{B},\mathcal{B}}_{xc}[\rho_{\mathcal{A}},\rho_{\mathcal{B}},0,\lambda_{\mathcal{B}};\ \mathbf{r},\ \mathbf{r}']d\lambda_{\mathcal{B}} \right\} |\mathbf{r} - \mathbf{r}'|^{-1}\ d\mathbf{r}d\mathbf{r}'$$

$$\equiv \frac{1}{2} \iint \rho_{\mathcal{B}}(\mathbf{r})\ h^{\mathcal{B},\mathcal{B}}_{av(3)}(\lambda_{\mathcal{A}} = 0;\ \mathbf{r},\ \mathbf{r}')\ |\mathbf{r} - \mathbf{r}'|^{-1}\ d\mathbf{r}d\mathbf{r}', \qquad (87)$$

as a functional of the *exchange correlation hole* $h^{\mathcal{B},\mathcal{B}}_{av(3)}(\lambda_{\mathcal{A}} = 0;\ \mathbf{r},\ \mathbf{r}') \equiv h^{\mathcal{B},\mathcal{B}}_{av(3)}(\mathbf{r},\ \mathbf{r}')$ *for the non-interacting electrons in* $\mathcal{A}$ ($\lambda_{\mathcal{B}}$-averaged). The corresponding energy for the end point of *path 3* in Fig. 2 is:

$$E^{\mathcal{M}}(0,\ 1) = E^{\mathcal{M}}_{\mathcal{A}}(0,\ 1) + E^{\mathcal{M}}_{\mathcal{B}}(0,\ 1), \tag{83a}$$

where:

$$E^{\mathcal{M}}_{\mathcal{B}}(0,\ 1) = \langle \Psi^{\mathcal{M}}_{0,1}[\rho_{\mathcal{A}},\ \rho_{\mathcal{B}}] |\ \hat{T}^{\mathcal{B}}_{e}(\mathbf{x}^{\mathcal{B}}) + \hat{V}^{\mathcal{B}}_{ee}(\mathbf{x}^{\mathcal{B}}) + \sum_{i=N_{\mathcal{A}}+1}^{N} v_{eff}[\rho_{\mathcal{A}};\ \mathbf{r}_i]\ |\Psi^{\mathcal{M}}_{0,1}[\rho_{\mathcal{A}},\ \rho_{\mathcal{B}}]\rangle$$

$$= T_S[\rho_{\mathcal{B}}] + \int \rho_{\mathcal{B}}(\mathbf{r})\ v_{eff}[\rho_{\mathcal{A}};\ \mathbf{r}]\ d\mathbf{r} + J[\rho_{\mathcal{B}}] + E^{\mathcal{M}}_{xc}[\rho_{\mathcal{B}}], \tag{84a}$$

$$E^{\mathcal{M}}_{\mathcal{A}}(0,\ 1) \equiv E^{\mathcal{A}}_{S}[\rho_{\mathcal{A}},\ \rho_{\mathcal{B}}]$$

$$\equiv \langle \Psi^{\mathcal{M}}_{0,1}[\rho_{\mathcal{A}},\ \rho_{\mathcal{B}}] | \sum_{i=1}^{N_{\mathcal{A}}} \hat{h}^{\mathcal{A}}_{S}[\rho_{\mathcal{A}},\ \rho_{\mathcal{B}};\ \mathbf{r}_i] | \Psi^{\mathcal{M}}_{0,1}[\rho_{\mathcal{A}},\ \rho_{\mathcal{B}}]\rangle$$

$$\equiv \langle \Psi^{\mathcal{M}}_{0,1}[\rho_{\mathcal{A}},\ \rho_{\mathcal{B}}] | \hat{H}^{\mathcal{A}}_{S}(\mathbf{r}^{\mathcal{A}}) | \Psi^{\mathcal{M}}_{0,1}[\rho_{\mathcal{A}},\ \rho_{\mathcal{B}}]\rangle$$

$$= T_S[\rho_{\mathcal{A}}] + \int \rho_{\mathcal{A}}(\mathbf{r})\ v^{\mathcal{A}}_{eff}[\rho_{\mathcal{A}},\ \rho_{\mathcal{B}};\ \mathbf{r}]\ d\mathbf{r}. \tag{85a}$$

Two additional examples of the nonuniform scaling paths corresponding to an integration over the whole range of the coupling constant of one reactant for the fixed value of the coupling constant of the other reactant are represented by the *paths 4* and *5* in Fig. 2. The corresponding energy changes from the Hellmann-Feynman theorem are reported in Table 1.

Let us consider an integration over $\lambda_{\mathcal{A}}$ along the *path 4* for constant $\lambda_{\mathcal{B}} = 1$, i.e. between the points (*0*, *1*) and

$(1, 1)$ in the $(\lambda_{\mathcal{A}}, \lambda_{\mathcal{B}})$-plane. In these two points the exchange-correlation energy is given by the $E_{xc}^{\mathcal{M}}[\rho_{\mathcal{B}}]$ and $E_{xc}^{\mathcal{M}}[\rho_{\mathcal{A}}, \rho_{\mathcal{B}}]$ functionals, respectively. Hence, the CCI relation expressing their difference:

$$E_{xc}^{\mathcal{M}}[\rho_{\mathcal{A}}, \rho_{\mathcal{B}}] - E_{xc}^{\mathcal{M}}[\rho_{\mathcal{B}}] = \int_0^1 V_{ee}^{\mathcal{A}}[\rho_{\mathcal{A}}, \rho_{\mathcal{B}}, \lambda_{\mathcal{A}}, 1]\, d\lambda_{\mathcal{A}} - J[\rho_{\mathcal{A}}]$$

$$+ \frac{1}{2} \int_0^1 (\lambda_{\mathcal{A}})^{-1/2}\, V_{ee}^{\mathcal{A},\mathcal{B}}[\rho_{\mathcal{A}}, \rho_{\mathcal{B}}, \lambda_{\mathcal{A}}, 1]\, d\lambda_{\mathcal{A}} - J_{\mathcal{A},\mathcal{B}}[\rho_{\mathcal{A}}, \rho_{\mathcal{B}}]. \quad (88)$$

Equation (88) can be further transformed by integrating the second integral by parts and using the partitioning of $E_{xc}^{\mathcal{M}}[\rho_{\mathcal{A}}, \rho_{\mathcal{B}}]$ in accordance with Eq.(A15) of the Appendix:

$$E_{xc}^{\mathcal{A},\mathcal{A}}[\rho_{\mathcal{A}}, \rho_{\mathcal{B}}] + E_{xc}^{\mathcal{B},\mathcal{B}}[\rho_{\mathcal{A}}, \rho_{\mathcal{B}}] - E_{xc}^{\mathcal{M}}[\rho_{\mathcal{B}}]$$

$$= \int_0^1 V_{ee}^{\mathcal{A}}[\rho_{\mathcal{A}}, \rho_{\mathcal{B}}, \lambda_{\mathcal{A}}, 1]\, d\lambda_{\mathcal{A}} - J[\rho_{\mathcal{A}}]$$

$$- \int_0^1 (\lambda_{\mathcal{A}})^{1/2}\, (\partial V_{ee}^{\mathcal{A},\mathcal{B}}[\rho_{\mathcal{A}}, \rho_{\mathcal{B}}, \lambda_{\mathcal{A}}, 1]/\partial\lambda_{\mathcal{A}})\, d\lambda_{\mathcal{A}}. \quad (89)$$

The l.h.s. of Eq.(88) can be conveniently partitioned into contributions in the subsystem resolution [Eqs.(80), (81), (A15), and (A17)], which can in turn be expressed in terms of the corresponding average holes [Eqs. (67), (68), (87), and (A20a)]. The resulting functional for this energy difference is:

$$E_{xc}^{\mathcal{M}}[\rho_{\mathcal{A}}, \rho_{\mathcal{B}}] - E_{xc}^{\mathcal{M}}[\rho_{\mathcal{B}}] = E_{xc}^{\mathcal{M}}[\rho_{\mathcal{A}}] + E_{xc}^{\mathcal{A},\mathcal{B}}[\rho_{\mathcal{A}}, \rho_{\mathcal{B}}]$$

$$= \frac{1}{2}\int\int\{\rho_{\mathcal{A}}(\mathbf{r})[h_{av(4)}^{\mathcal{A},\mathcal{A}}(\mathbf{r}, \mathbf{r}') + h_{av(4)}^{\mathcal{A},\mathcal{B}}(\mathbf{r}, \mathbf{r}')]$$

$$+ \rho_{\mathcal{B}}(\mathbf{r})h_{av(4)}^{\mathcal{B},\mathcal{A}}(\mathbf{r}, \mathbf{r}')\} \, |\mathbf{r} - \mathbf{r}'|^{-1} \, d\mathbf{r} \, d\mathbf{r}'. \qquad (88a)$$

It provides a transparent physical interpretation of the integral in the r.h.s. of Eq. (88).

Obviously, interchanging the subsystem indices in Eqs.(88) and (88a) gives the corresponding relation which results from the *path 5* integration, in the whole range of $\lambda_{\mathcal{B}}$ for constant $\lambda_{\mathcal{A}} = 1$:

$$E_{xc}^{\mathcal{M}}[\rho_{\mathcal{A}}, \rho_{\mathcal{B}}] - E_{xc}^{\mathcal{M}}[\rho_{\mathcal{A}}] = E_{xc}^{\mathcal{M}}[\rho_{\mathcal{B}}] + E_{xc}^{\mathcal{A},\mathcal{B}}[\rho_{\mathcal{A}}, \rho_{\mathcal{B}}]$$

$$= \frac{1}{2}\int\int\{\rho_{\mathcal{B}}(\mathbf{r}) \, [h_{av(5)}^{\mathcal{B},\mathcal{B}}(\mathbf{r}, \mathbf{r}') + h_{av(5)}^{\mathcal{B},\mathcal{A}}(\mathbf{r}, \mathbf{r}')]$$

$$+ \rho_{\mathcal{A}}(\mathbf{r}) \, h_{av(5)}^{\mathcal{A},\mathcal{B}}(\mathbf{r}, \mathbf{r}')\} \, |\mathbf{r} - \mathbf{r}'|^{-1} \, d\mathbf{r} \, d\mathbf{r}'$$

$$= \int_0^1 \{V_{ee}^{\mathcal{B}}[\rho_{\mathcal{A}}, \rho_{\mathcal{B}}, 1, \lambda_{\mathcal{B}}] + \frac{1}{2}(\lambda_{\mathcal{B}})^{-1/2} V_{ee}^{\mathcal{A},\mathcal{B}}[\rho_{\mathcal{A}}, \rho_{\mathcal{B}}, 1, \lambda_{\mathcal{B}}]\} \, d\lambda_{\mathcal{B}}$$

$$- J[\rho_{\mathcal{B}}] - J_{\mathcal{A},\mathcal{B}}[\rho_{\mathcal{A}}, \rho_{\mathcal{B}}]. \qquad (88b)$$

The final *path 6* of Fig. 2 corresponds to a simultaneous integration over the two subsystem scaling factors, similarly to the previously discussed integration along the *path 1*. The CCI trajectory 6 can be considered as defined by the *progress parameter* $\lambda_{\mathcal{B}}$, in the range from *0* to *1*, since $\lambda_{\mathcal{A}} = \lambda_{\mathcal{A}}(\lambda_{\mathcal{B}}) = 1 - \lambda_{\mathcal{B}}$. In such a case the full

derivative of the scaled hamiltonian with respect to $\lambda_{\mathcal{B}}$ includes the contributions from the partial differentiations with respect to both $\lambda_{\mathcal{A}}$ and $\lambda_{\mathcal{B}}$:

$$d\hat{H}^{\mathcal{M}}_{\lambda_{\mathcal{A}},\lambda_{\mathcal{B}}}/d\lambda_{\mathcal{B}} = \partial\hat{H}^{\mathcal{M}}_{\lambda_{\mathcal{A}},\lambda_{\mathcal{B}}}/\partial\lambda_{\mathcal{B}} + (\partial\hat{H}^{\mathcal{M}}_{\lambda_{\mathcal{A}},\lambda_{\mathcal{B}}}/\partial\lambda_{\mathcal{A}})\,(d\lambda_{\mathcal{A}}/d\lambda_{\mathcal{B}})$$

$$= \partial\hat{H}^{\mathcal{M}}_{\lambda_{\mathcal{A}},\lambda_{\mathcal{B}}}/\partial\lambda_{\mathcal{B}} - \partial\hat{H}^{\mathcal{M}}_{\lambda_{\mathcal{A}},\lambda_{\mathcal{B}}}/\partial\lambda_{\mathcal{A}}. \qquad (90)$$

Hence the relevant Hellmann-Feynman theorem for the *path 6* in Fig. 2 is [see Eqs.(76)-(78)]:

$$\frac{\partial E^{\mathcal{M}}(1-\lambda_{\mathcal{B}},\lambda_{\mathcal{B}})}{\partial\lambda_{\mathcal{B}}} = \langle\Psi^{\mathcal{M}}_{1-\lambda_{\mathcal{B}},\lambda_{\mathcal{B}}}[\rho_{\mathcal{A}},\rho_{\mathcal{B}}]\,|\,(\partial\hat{H}^{\mathcal{M}}_{\lambda_{\mathcal{A}},\lambda_{\mathcal{B}}}/\partial\lambda_{\mathcal{B}})_{\lambda_{\mathcal{A}}=1-\lambda_{\mathcal{B}}}$$

$$- (\partial\hat{H}^{\mathcal{M}}_{\lambda_{\mathcal{A}},\lambda_{\mathcal{B}}}/\partial\lambda_{\mathcal{A}})_{\lambda_{\mathcal{A}}=1-\lambda_{\mathcal{B}}}\,|\,\Psi^{\mathcal{M}}_{1-\lambda_{\mathcal{B}},\lambda_{\mathcal{B}}}[\rho_{\mathcal{A}},\rho_{\mathcal{B}}]\rangle$$

$$= \sum_{\mathcal{Z}=\mathcal{A},\mathcal{B}} \int \rho_{\mathcal{Z}}(\mathbf{r})\,\{(\partial v^{\mathcal{Z}}_{\lambda_{\mathcal{A}},\lambda_{\mathcal{B}}}(\mathbf{r})/\partial\lambda_{\mathcal{B}})$$

$$- (\partial v^{\mathcal{Z}}_{\lambda_{\mathcal{A}},\lambda_{\mathcal{B}}}(\mathbf{r})/\partial\lambda_{\mathcal{A}})\}_{\lambda_{\mathcal{A}}=1-\lambda_{\mathcal{B}}}\,d\mathbf{r}$$

$$+ V^{\mathcal{B}}_{ee}[\rho_{\mathcal{A}},\,\rho_{\mathcal{B}},\,1-\lambda_{\mathcal{B}},\,\lambda_{\mathcal{B}}] - V^{\mathcal{A}}_{ee}[\rho_{\mathcal{A}},\,\rho_{\mathcal{B}},\,1-\lambda_{\mathcal{B}},\,\lambda_{\mathcal{B}}]$$

$$+ \tfrac{1}{2}(1-2\lambda_{\mathcal{B}})[\lambda_{\mathcal{B}}(1-\lambda_{\mathcal{B}})]^{-1/2}\,V^{\mathcal{A},\mathcal{B}}_{ee}[\rho_{\mathcal{A}},\,\rho_{\mathcal{B}},\,1-\lambda_{\mathcal{B}},\,\lambda_{\mathcal{B}}]. \qquad (91)$$

The coupling constant functional for the *path 6* energy difference, $E^{\mathcal{M}}(0,\,1) - E^{\mathcal{M}}(1,\,0)$, can be obtained either by a direct integration of Eq.(91) (see Table 1) or, alternatively, from the already derived energy

expressions. summarized in Eqs.(83)-(85), their (*0*, *1*)-analogs [Eqs.(83a)-(85a)], and in Eqs. (86), (87), *Paths 2* and *3*). The latter route gives:

$$
\begin{aligned}
&E^{\mathcal{M}}(0,\,1) - E^{\mathcal{M}}(1,\,0) \\
&\quad = \int \{\rho_{\mathcal{A}}(\mathbf{r})\,(v^{\mathcal{A}}_{eff}[\rho_{\mathcal{A}},\,\rho_{\mathcal{B}};\,\mathbf{r}] - v_{eff}[\rho_{\mathcal{B}};\,\mathbf{r}]) \\
&\qquad\qquad - \rho_{\mathcal{B}}(\mathbf{r})\,(v^{\mathcal{B}}_{eff}[\rho_{\mathcal{A}},\,\rho_{\mathcal{B}};\,\mathbf{r}] - v_{eff}[\rho_{\mathcal{A}};\,\mathbf{r}])\}\,d\mathbf{r} \\
&\qquad + \int_0^1 V^{\mathcal{B}}_{ee}[\rho_{\mathcal{A}},\,\rho_{\mathcal{B}},\,0,\,\lambda_{\mathcal{B}}]\,d\lambda_{\mathcal{B}} - \int_0^1 V^{\mathcal{A}}_{ee}[\rho_{\mathcal{A}},\,\rho_{\mathcal{B}},\,\lambda_{\mathcal{A}},\,0]\,d\lambda_{\mathcal{A}} \\
&\quad = \int \{\rho_{\mathcal{A}}(\mathbf{r})\,(v^{\mathcal{A}}_{eff}[\rho_{\mathcal{A}},\,\rho_{\mathcal{B}};\,\mathbf{r}] - v_{eff}[\rho_{\mathcal{B}};\,\mathbf{r}]) \\
&\qquad\qquad - \rho_{\mathcal{B}}(\mathbf{r})\,(v^{\mathcal{B}}_{eff}[\rho_{\mathcal{A}},\,\rho_{\mathcal{B}};\,\mathbf{r}] - v_{eff}[\rho_{\mathcal{A}};\,\mathbf{r}])\}\,d\mathbf{r} \\
&\qquad + (J[\rho_{\mathcal{B}}] - J[\rho_{\mathcal{A}}]) + (E^{\mathcal{M}}_{xc}[\rho_{\mathcal{B}}] - E^{\mathcal{M}}_{xc}[\rho_{\mathcal{A}}]). \qquad (92)
\end{aligned}
$$

The direct integration of the Hellmann-Feynman theorem of Eq.(91) generates the following coupling constant functional:

$$
\begin{aligned}
&E^{\mathcal{M}}(0,\,1) - E^{\mathcal{M}}(1,\,0) \\
&\quad = \int\{\rho_{\mathcal{A}}(\mathbf{r})\,(v^{\mathcal{A}}_{eff}[\rho_{\mathcal{A}},\,\rho_{\mathcal{B}};\,\mathbf{r}] - v_{eff}[\rho_{\mathcal{B}};\,\mathbf{r}]) \\
&\qquad\qquad - \rho_{\mathcal{B}}(\mathbf{r})\,(v^{\mathcal{B}}_{eff}[\rho_{\mathcal{A}},\,\rho_{\mathcal{B}};\,\mathbf{r}] - v_{eff}[\rho_{\mathcal{A}};\,\mathbf{r}])\}\,d\mathbf{r} \\
&\qquad + \int_0^1 \{V^{\mathcal{B}}_{ee}[\rho_{\mathcal{A}},\,\rho_{\mathcal{B}},\,1-\lambda_{\mathcal{B}},\,\lambda_{\mathcal{B}}] - V^{\mathcal{A}}_{ee}[\rho_{\mathcal{A}},\,\rho_{\mathcal{B}},\,1-\lambda_{\mathcal{B}},\,\lambda_{\mathcal{B}}] \\
&\qquad + \tfrac{1}{2}(1-2\lambda_{\mathcal{B}})[\lambda_{\mathcal{B}}(1-\lambda_{\mathcal{B}})]^{-1/2} V^{\mathcal{A},\mathcal{B}}_{ee}[\rho_{\mathcal{A}},\,\rho_{\mathcal{B}},\,1-\lambda_{\mathcal{B}},\,\lambda_{\mathcal{B}}]\}\,d\lambda_{\mathcal{B}}. \qquad (93)
\end{aligned}
$$

A comparison between the last two equations implies the eguality between the electron repulsion energies from these two different integration routes:

$$\int_0^1 V_{ee}^{\mathcal{B}}[\rho_{\mathcal{A}}, \rho_{\mathcal{B}}, 0, \lambda_{\mathcal{B}}]\, d\lambda_{\mathcal{B}} - \int_0^1 V_{ee}^{\mathcal{A}}[\rho_{\mathcal{A}}, \rho_{\mathcal{B}}, \lambda_{\mathcal{A}}, 0]\, d\lambda_{\mathcal{A}}$$

$$= \int_0^1 \{V_{ee}^{\mathcal{B}}[\rho_{\mathcal{A}}, \rho_{\mathcal{B}}, 1 - \lambda_{\mathcal{B}}, \lambda_{\mathcal{B}}] - V_{ee}^{\mathcal{A}}[\rho_{\mathcal{A}}, \rho_{\mathcal{B}}, 1 - \lambda_{\mathcal{B}}, \lambda_{\mathcal{B}}]$$

$$+ \tfrac{1}{2}(1 - 2\lambda_{\mathcal{B}})[\lambda_{\mathcal{B}}(1 - \lambda_{\mathcal{B}})]^{-1/2} V_{ee}^{\mathcal{A},\mathcal{B}}[\rho_{\mathcal{A}}, \rho_{\mathcal{B}}, 1 - \lambda_{\mathcal{B}}, \lambda_{\mathcal{B}}]\}\, d\lambda_{\mathcal{B}}. \tag{94}$$

The addition to l.h.s. of Eq. (94) of the difference $(J[\rho_{\mathcal{A}}] - J[\rho_{\mathcal{B}}])$ gives [see Eqs. (86), (87)]:

$$E_{xc}^{\mathcal{M}}[\rho_{\mathcal{B}}] - E_{xc}^{\mathcal{M}}[\rho_{\mathcal{A}}] = \tfrac{1}{2} \iint \{\rho_{\mathcal{B}}(\mathbf{r})\, h_{av(3)}^{\mathcal{B},\mathcal{B}}(\mathbf{r}, \mathbf{r}')$$

$$- \rho_{\mathcal{A}}(\mathbf{r})\, h_{av(2)}^{\mathcal{A},\mathcal{A}}(\mathbf{r}, \mathbf{r}')\}\, |\mathbf{r} - \mathbf{r}'|^{-1}\, d\mathbf{r}\, d\mathbf{r}', \tag{95}$$

which does not include the inter-subsystem contribution. Performing the same manipulation on the r.h.s. of Eq. (94) gives:

$$E_{xc}^{\mathcal{M}}[\rho_{\mathcal{B}}] - E_{xc}^{\mathcal{M}}[\rho_{\mathcal{A}}] = \int_0^1 V_{ee}^{\mathcal{B}}[\rho_{\mathcal{A}}, \rho_{\mathcal{B}}, 1 - \lambda_{\mathcal{B}}, \lambda_{\mathcal{B}}]\, d\lambda_{\mathcal{B}} - J[\rho_{\mathcal{B}}]$$

$$- \{\int_0^1 V_{ee}^{\mathcal{A}}[\rho_{\mathcal{A}}, \rho_{\mathcal{B}}, 1 - \lambda_{\mathcal{B}}, \lambda_{\mathcal{B}}]\, d\lambda_{\mathcal{B}} - J[\rho_{\mathcal{A}}]\}$$

$$+ \frac{1}{2} \int_0^1 \frac{(1 - 2\lambda_{\mathcal{B}})}{[\lambda_{\mathcal{B}}(1 - \lambda_{\mathcal{B}})]^{1/2}} V_{ee}^{\mathcal{A},\mathcal{B}}[\rho_{\mathcal{A}}, \rho_{\mathcal{B}}, 1 - \lambda_{\mathcal{B}}, \lambda_{\mathcal{B}}]\, d\lambda_{\mathcal{B}}. \tag{95}$$

The CCI expressions in Table 1, for the energy changes along the specific paths of Fig. 2, include both the direct integral Hellmann-Feynman formula for the path under consideration and some alternative energy relations for the *paths 4-6*, obtained from selected integrations along indirect routes involving combinations of the *paths 1-3*. Clearly, such alternative expressions can also be given for $\Delta E_1^{\mathcal{M}}$, $\Delta E_2^{\mathcal{M}}$, and $\Delta E_3^{\mathcal{M}}$, e.g., for $\Delta E_1^{\mathcal{M}} = \Delta E_2^{\mathcal{M}} + \Delta E_5^{\mathcal{M}} = \Delta E_3^{\mathcal{M}} + \Delta E_4^{\mathcal{M}}$, $\Delta E_2^{\mathcal{M}} = \Delta E_1^{\mathcal{M}} - \Delta E_5^{\mathcal{M}} = \Delta E_3^{\mathcal{M}} - \Delta E_6^{\mathcal{M}}$, etc., using the direct expressions already listed in the table. Comparing the alternative CCI formulas for the change in the electron repulsion energy would then give a number of CCI identities, similar to that of Eq. (95), which provide additional, exact constraints on the exchange-correlation functionals in the subsystem resolution.

5. CONCLUSION

The theory of molecular interactions, and the theory of chemical reactivity in particular, deal with reactive systems consisting of complementary subsystems. One of major goals of the quantum chemistry is to determine various effects of their interaction, both intra- and inter-subsystem in character, and how they influence the ultimate reactivity trends. This can be studied, e.g., using the semi-empirically parametrized CSA in the atomic resolution. Its *first-principle*, local formulation in DFT

calls for the Kohn-Sham scheme for subsystems and thus for a theoretical investigation of the density functionals in this resolution. Such a subsystem development is a natural DFT extension of the familiar Hartree-Fock theory and provides a convenient framework for determining such subsystem properties as the electronegativity, hardness/softness and Fukui-function, the quantities systematically explored within CSA.

This article extends the Hellmann-Feynman analysis and the range of application of the related technique of the coupling constant integration, to studying the exchange-correlation density functionals in the subsystem resolution. In particular the nonadditive functionals have been examined in a more detail, with a special emphasis placed upon the density functional for the nonadditive kinetic energy of the noninteracting system, which appeares in the Kohn-Sham theory for subsystems.

The partitioning of the underlying exhange-correlation holes into the relevant intra- and inter-subsystem parts has been introduced. It has also been demonstrated how these various contributions can be "turned on" or "turned off" by a proper selection of the integration path in the plane of the scaling factors for the subsystem electronic charges. Several illustrative integration trajectories have been used to derive the corresponding exact integral expressions for combinations of various exchange-correlation functionals of densities of the complementary subsystems, or equivalently, the functionals involving the corresponding subsystem exchange-correlation holes.

6. APPENDIX: EXCHANGE-CORRELATION HOLES IN THE SUBSYSTEM RESOLUTION

Let us define the one- and two-electron densities of $\mathcal{M}$ described by the generalized product function of Eq.(1):

$$\Psi^{\mathcal{M}}(\mathbf{x}^{\mathcal{M}}) = N_{\mathcal{A},\mathcal{B}}\,\hat{A}_{\mathcal{A},\mathcal{B}}\{\Psi^{\mathcal{A}}(\mathbf{x}_1, \ldots, \mathbf{x}_{N_{\mathcal{A}}})\Psi^{\mathcal{B}}(\mathbf{x}_{N_{\mathcal{A}}+1}, \ldots, \mathbf{x}_N)\}$$

$$= \Psi^{\mathcal{M}}[\rho_{\mathcal{A}}, \rho_{\mathcal{B}}]. \qquad \text{(A1)}$$

The subsystem spin dependent and spinless one-electron densities, respectively, are given by the following expectation values:

$$\bar{\rho}_{\mathcal{A}}(\mathbf{x}) = N_{\mathcal{A}}\langle\Psi^{\mathcal{M}}|\delta(\mathbf{x}_1 - \mathbf{x})|\Psi^{\mathcal{M}}\rangle, \quad \rho_{\mathcal{A}}(\mathbf{r}) = \sum_{\sigma=-1/2}^{1/2}\rho_{\mathcal{A}}^{\sigma}(\mathbf{x}), \qquad \text{(A2)}$$

$$\bar{\rho}_{\mathcal{B}}(\mathbf{x}) = N_{\mathcal{B}}\langle\Psi^{\mathcal{M}}|\delta(\mathbf{x}_N - \mathbf{x})|\Psi^{\mathcal{M}}\rangle, \quad \rho_{\mathcal{B}}(\mathbf{r}) = \sum_{\sigma=-1/2}^{1/2}\rho_{\mathcal{B}}^{\sigma}(\mathbf{x}). \qquad \text{(A3)}$$

Similarly, the four elements of the matrix $\bar{\rho}_2^{\mathcal{M}}(\mathbf{x}, \mathbf{x}') \equiv \{\bar{\rho}_2^{\mathcal{X},\mathcal{Y}}(\mathbf{x}, \mathbf{x}'), \mathcal{X}, \mathcal{Y} = \mathcal{A}, \mathcal{B}\}$ defining the spin dependent two-electron densities in the subsystem resolution are defined by the following expectation values:

$$\bar{\rho}_2^{\mathcal{A},\mathcal{A}}(\mathbf{x}, \mathbf{x}') = N_{\mathcal{A}}(N_{\mathcal{A}} - 1)\langle\Psi^{\mathcal{M}}|\delta(\mathbf{x}_1 - \mathbf{x})\delta(\mathbf{x}_2 - \mathbf{x}')|\Psi^{\mathcal{M}}\rangle, \qquad \text{(A4)}$$

$$\bar{\rho}_2^{\mathcal{B},\mathcal{B}}(\mathbf{x}, \mathbf{x}') = N_{\mathcal{B}}(N_{\mathcal{B}} - 1)\langle\Psi^{\mathcal{M}}|\delta(\mathbf{x}_N - \mathbf{x})\delta(\mathbf{x}_{N-1} - \mathbf{x}')|\Psi^{\mathcal{M}}\rangle, \qquad \text{(A5)}$$

$$\bar{\rho}_2^{\mathcal{A},\mathcal{B}}(\mathbf{x}, \mathbf{x}') = N_{\mathcal{A}}N_{\mathcal{B}}\langle\Psi^{\mathcal{M}}|\delta(\mathbf{x}_1 - \mathbf{x})\delta(\mathbf{x}_N - \mathbf{x}')|\Psi^{\mathcal{M}}\rangle, \qquad \text{(A6)}$$

$$\bar{\rho}_2^{\mathcal{B},\mathcal{A}}(\mathbf{x}, \mathbf{x}') = N_{\mathcal{A}}N_{\mathcal{B}}\langle\Psi^{\mathcal{M}}|\delta(\mathbf{x}_N - \mathbf{x})\delta(\mathbf{x}_1 - \mathbf{x}')|\Psi^{\mathcal{M}}\rangle. \qquad \text{(A7)}$$

The corresponding matrix of the spinless two-electron densities $\rho_2^{\mathcal{M}}(\mathbf{r}, \mathbf{r}') \equiv \{\rho_2^{\mathcal{X},\mathcal{Y}}(\mathbf{r}, \mathbf{r}'), \mathcal{X}, \mathcal{Y} = \mathcal{A}, \mathcal{B}\}$ is obtained by summations over spins:

$$\rho_2^{\mathcal{A},\mathcal{A}}(\mathbf{r}, \mathbf{r}') = \sum_{\sigma=-1/2}^{1/2} \sum_{\sigma'=-1/2}^{1/2} \bar{\rho}_2^{\mathcal{A},\mathcal{A}}(\mathbf{x}, \mathbf{x}'). \text{ etc.} \tag{A8}$$

The matrices of the corresponding exchange correlation holes in the subsystem resolution,

$$\bar{\mathbf{h}}_{xc}^{\mathcal{M}}[\rho_{\mathcal{A}}, \rho_{\mathcal{B}}; \mathbf{x}, \mathbf{x}'] \equiv \bar{\mathbf{h}}_{xc}^{\mathcal{M}}(\mathbf{x}, \mathbf{x}') = \{\bar{h}_{xc}^{\mathcal{X},\mathcal{Y}}(\mathbf{x}, \mathbf{x}')\}, \tag{A9}$$

$$\mathbf{h}_{xc}^{\mathcal{M}}[\rho_{\mathcal{A}}, \rho_{\mathcal{B}}; \mathbf{r}, \mathbf{r}'] \equiv \mathbf{h}_{xc}^{\mathcal{M}}(\mathbf{r}, \mathbf{r}') = \{h_{xc}^{\mathcal{X},\mathcal{Y}}(\mathbf{r}, \mathbf{r}')\}, \tag{A10}$$

are then defined by the familiar relations [$(\mathcal{X},\mathcal{Y}) = \mathcal{A}, \mathcal{B}$]:

$$\bar{\rho}_2^{\mathcal{X},\mathcal{Y}}(\mathbf{x}, \mathbf{x}') \equiv \bar{\rho}_{\mathcal{X}}(\mathbf{x}) [\bar{\rho}_{\mathcal{Y}}(\mathbf{x}') + \bar{h}_{xc}^{\mathcal{X},\mathcal{Y}}(\mathbf{x}, \mathbf{x}')], \tag{A11}$$

$$\rho_2^{\mathcal{X},\mathcal{Y}}(\mathbf{r}, \mathbf{r}') \equiv \rho_{\mathcal{X}}(\mathbf{r}) [\rho_{\mathcal{Y}}(\mathbf{r}') + h_{xc}^{\mathcal{X},\mathcal{Y}}(\mathbf{r}, \mathbf{r}')]. \tag{A12}$$

These equations give rise to the corresponding expressions for the the intra- and inter-subsystem exchange-correlation energies [see Eqs. (3), (17), and (31)] in terms of the relevant exchange-correlation holes:

$$E_{xc}^{\mathcal{X},\mathcal{X}}[\rho_{\mathcal{A}}, \rho_{\mathcal{B}}] = \langle\Psi^{\mathcal{M}}[\rho_{\mathcal{A}}, \rho_{\mathcal{B}}]|\hat{V}_{ee}^{\mathcal{X}}|\Psi^{\mathcal{M}}[\rho_{\mathcal{A}}, \rho_{\mathcal{B}}]\rangle - J[\rho_{\mathcal{X}}]$$
$$= \frac{1}{2} \iint \rho_{\mathcal{X}}(\mathbf{r}) h_{xc}^{\mathcal{X},\mathcal{X}}(\mathbf{r}, \mathbf{r}') |\mathbf{r}-\mathbf{r}'|^{-1} d\mathbf{r}d\mathbf{r}', \quad \mathcal{X} = \mathcal{A}, \mathcal{B}; \tag{A13}$$

$$E_{xc}^{\mathcal{A},\mathcal{B}}[\rho_{\mathcal{A}}, \rho_{\mathcal{B}}] = \langle\Psi^{\mathcal{M}}[\rho_{\mathcal{A}}, \rho_{\mathcal{B}}]|\hat{V}_{ee}^{\mathcal{A},\mathcal{B}}|\Psi^{\mathcal{M}}[\rho_{\mathcal{A}}, \rho_{\mathcal{B}}]\rangle - J_{\mathcal{A},\mathcal{B}}[\rho_{\mathcal{A}}, \rho_{\mathcal{B}}]$$
$$= \frac{1}{2} \iint \{\rho_{\mathcal{A}}(\mathbf{r}) h_{xc}^{\mathcal{A},\mathcal{B}}(\mathbf{r}, \mathbf{r}') + \rho_{\mathcal{B}}(\mathbf{r}) h_{xc}^{\mathcal{B},\mathcal{A}}(\mathbf{r}, \mathbf{r}')\} |\mathbf{r}-\mathbf{r}'|^{-1} d\mathbf{r}d\mathbf{r}', \tag{A14}$$

defining the overall exchange-correlation energy in $\mathcal{M}$:

$$E_{xc}^{\mathcal{M}}[\rho_{\mathcal{A}}, \rho_{\mathcal{B}}] = E_{xc}^{\mathcal{A},\mathcal{A}}[\rho_{\mathcal{A}}, \rho_{\mathcal{B}}] + E_{xc}^{\mathcal{B},\mathcal{B}}[\rho_{\mathcal{A}}, \rho_{\mathcal{B}}] + E_{xc}^{\mathcal{A},\mathcal{B}}[\rho_{\mathcal{A}}, \rho_{\mathcal{B}}]. \tag{A15}$$

It should be noticed that for a given position of the first, $\mathcal{X}$-group electron at $\mathbf{r}$ the off-diagonal hole $h_{xc}^{\mathcal{X},\mathcal{Y}}(\mathbf{r}, \mathbf{r}')$ represents the correction to the probabilty of finding the second, $\mathcal{Y}$-group electron at $\mathbf{r}'$, due to the *inter-subsystem correlations*. Similarly, the diagonal hole $h_{xc}^{\mathcal{X},\mathcal{X}}(\mathbf{r}, \mathbf{r}')$ carries the related correction to the two-electron probabilities due to the *intra-$\mathcal{X}$ correlations*. Adding the holes in a single row of of the matrix $\mathbf{h}_{xc}^{\mathcal{M}}(\mathbf{r}, \mathbf{r}')$ gives the the *resultant exchange-correlation hole* of subsystems in $\mathcal{M}$, combining the intra- and inter-subsystem contributions,

$$\bar{h}_{xc}^{\mathcal{X}}(\mathbf{x}, \mathbf{x}') = \sum_{\mathcal{Y}=\mathcal{A},\mathcal{B}} \bar{h}_{xc}^{\mathcal{X},\mathcal{Y}}(\mathbf{x}, \mathbf{x}'),$$

$$h_{xc}^{\mathcal{X}}(\mathbf{r}, \mathbf{r}') = \sum_{\mathcal{Y}=\mathcal{A},\mathcal{B}} h_{xc}^{\mathcal{X},\mathcal{Y}}(\mathbf{r}, \mathbf{r}'). \tag{A16}$$

In terms of these resultant holes of subsystems the overall exchange-correlation energy of Eq.(A15) can be expressed as the sum of the resultant subsystem contributions:

$$E_{xc}^{\mathcal{M}}[\rho_{\mathcal{A}}, \rho_{\mathcal{B}}] = \frac{1}{2} \int\int \{\rho_{\mathcal{A}}(\mathbf{r})\, h_{xc}^{\mathcal{A}}[\rho_{\mathcal{A}}, \rho_{\mathcal{B}}; \mathbf{r}, \mathbf{r}'] + \rho_{\mathcal{B}}(\mathbf{r})\, h_{xc}^{\mathcal{B}}[\rho_{\mathcal{A}}, \rho_{\mathcal{B}}; \mathbf{r}, \mathbf{r}']\}\, |\mathbf{r} - \mathbf{r}'|^{-1}\, d\mathbf{r}\, d\mathbf{r}'$$

$$\equiv E_{xc}^{\mathcal{A}}[\rho_{\mathcal{A}}, \rho_{\mathcal{B}}] + E_{xc}^{\mathcal{B}}[\rho_{\mathcal{A}}, \rho_{\mathcal{B}}]. \tag{A17}$$

A substitution of the wavefunction $\Psi^{\mathcal{M}}[\rho_{\mathcal{A}}, \rho_{\mathcal{B}}]$ in Eqs. (A1)-(A13) by the scaled wavefunctions of Section 3, $\Psi^{\mathcal{M}}_{\lambda}[\rho_{\mathcal{A}}, \rho_{\mathcal{B}}]$ (or $\Psi_{\kappa}[\rho]$) and $\Psi^{\mathcal{M}}_{\lambda_{\mathcal{A}},\lambda_{\mathcal{B}}}[\rho_{\mathcal{A}}, \rho_{\mathcal{B}}]$, allows one to similarly define the corresponding *scaled exchange-correlation holes* discussed in Section 4. Since the former wavefunction, of the uniformly scaled system $\mathcal{M}(\lambda, \lambda)$, can be considered as a special case of the latter, for the nonuniformly scaled system $\mathcal{M}(\lambda_{\mathcal{A}}, \lambda_{\mathcal{B}})$, below summarized are the corresponding expressions for the exchange correlation energy and its subsystem contributions in terms of the *exchange-correlation hole matrix*

$$\mathbf{h}^{\mathcal{M}}_{xc}[\rho_{\mathcal{A}}, \rho_{\mathcal{B}}, \lambda_{\mathcal{A}}, \lambda_{\mathcal{B}}; \mathbf{r}, \mathbf{r}'] \equiv \mathbf{h}^{\mathcal{M}}_{xc}(\lambda_{\mathcal{A}}, \lambda_{\mathcal{B}}; \mathbf{r}, \mathbf{r}') = \{h^{\mathcal{X},\mathcal{Y}}_{xc}(\lambda_{\mathcal{A}}, \lambda_{\mathcal{B}}; \mathbf{r}, \mathbf{r}')\} \quad \text{(A10a)}$$

defined by the scaled wavefunction $[\rho_{\mathcal{A}}, \rho_{\mathcal{B}}]$ of the general nonuniform approach [see Eqs. (A2)-(A12)]. The scaled analogs of Eqs. (A13)-(A17) are:

$$E^{\mathcal{X},\mathcal{X}}_{xc}[\rho_{\mathcal{A}}, \rho_{\mathcal{B}}, \lambda_{\mathcal{A}}, \lambda_{\mathcal{B}}] = \lambda_{\mathcal{X}} \{\langle\Psi^{\mathcal{M}}_{\lambda_{\mathcal{A}},\lambda_{\mathcal{B}}}[\rho_{\mathcal{A}}, \rho_{\mathcal{B}}] | \hat{V}^{\mathcal{X}}_{ee} | \Psi^{\mathcal{M}}_{\lambda_{\mathcal{A}},\lambda_{\mathcal{B}}}[\rho_{\mathcal{A}}, \rho_{\mathcal{B}}]\rangle - J[\rho_{\mathcal{X}}]\}$$

$$= \frac{\lambda_{\mathcal{X}}}{2} \iint \rho_{\mathcal{X}}(\mathbf{r})\, h^{\mathcal{X},\mathcal{X}}_{xc}(\lambda_{\mathcal{A}}, \lambda_{\mathcal{B}}; \mathbf{r}, \mathbf{r}')\, |\mathbf{r} - \mathbf{r}'|^{-1}\, d\mathbf{r}\, d\mathbf{r}', \quad \mathcal{X} = \mathcal{A}, \mathcal{B}; \quad \text{(A13a)}$$

$$E^{\mathcal{A},\mathcal{B}}_{xc}[\rho_{\mathcal{A}}, \rho_{\mathcal{B}}, \lambda_{\mathcal{A}}, \lambda_{\mathcal{B}}] = (\lambda_{\mathcal{A}}\lambda_{\mathcal{B}})^{1/2} \times \{\langle\Psi^{\mathcal{M}}_{\lambda_{\mathcal{A}},\lambda_{\mathcal{B}}}[\rho_{\mathcal{A}}, \rho_{\mathcal{B}}] | \hat{V}^{\mathcal{A},\mathcal{B}}_{ee} | \Psi^{\mathcal{M}}_{\lambda_{\mathcal{A}},\lambda_{\mathcal{B}}}[\rho_{\mathcal{A}}, \rho_{\mathcal{B}}]\rangle - J_{\mathcal{A},\mathcal{B}}[\rho_{\mathcal{A}}, \rho_{\mathcal{B}}]\}$$

$$= \frac{1}{2}\,(\lambda_{\mathcal{A}}\,\lambda_{\mathcal{B}})^{1/2} \iint \{\rho_{\mathcal{A}}(\mathbf{r})\, h_{xc}^{\mathcal{A},\mathcal{B}}(\lambda_{\mathcal{A}}, \lambda_{\mathcal{B}}; \mathbf{r}, \mathbf{r}') + \rho_{\mathcal{B}}(\mathbf{r})\, h_{xc}^{\mathcal{B},\mathcal{A}}(\lambda_{\mathcal{A}}, \lambda_{\mathcal{B}}; \mathbf{r}, \mathbf{r}')\}\, |\mathbf{r} - \mathbf{r}'|^{-1}\, d\mathbf{r}\, d\mathbf{r}'; \quad \text{(A14a)}$$

$$E_{xc}^{\mathcal{M}}[\rho_{\mathcal{A}}, \rho_{\mathcal{B}}, \lambda_{\mathcal{A}}, \lambda_{\mathcal{B}}] = E_{xc}^{\mathcal{A},\mathcal{A}}[\rho_{\mathcal{A}}, \rho_{\mathcal{B}}, \lambda_{\mathcal{A}}, \lambda_{\mathcal{B}}] + E_{xc}^{\mathcal{B},\mathcal{B}}[\rho_{\mathcal{A}}, \rho_{\mathcal{B}}, \lambda_{\mathcal{A}}, \lambda_{\mathcal{B}}] + E_{xc}^{\mathcal{A},\mathcal{B}}[\rho_{\mathcal{A}}, \rho_{\mathcal{B}}, \lambda_{\mathcal{A}}, \lambda_{\mathcal{B}}]; \quad \text{(A15a)}$$

$$h_{xc}^{\mathcal{A}}(\lambda_{\mathcal{A}}, \lambda_{\mathcal{B}}; \mathbf{r}, \mathbf{r}')] = h_{xc}^{\mathcal{A},\mathcal{A}}(\lambda_{\mathcal{A}}, \lambda_{\mathcal{B}}; \mathbf{r}, \mathbf{r}') + (\lambda_{\mathcal{B}}/\lambda_{\mathcal{A}})^{1/2}\, h_{xc}^{\mathcal{A},\mathcal{B}}(\lambda_{\mathcal{A}}, \lambda_{\mathcal{B}}; \mathbf{r}, \mathbf{r}'),$$

$$h_{xc}^{\mathcal{B}}(\lambda_{\mathcal{A}}, \lambda_{\mathcal{B}}; \mathbf{r}, \mathbf{r}')] = h_{xc}^{\mathcal{B},\mathcal{B}}(\lambda_{\mathcal{A}}, \lambda_{\mathcal{B}}; \mathbf{r}, \mathbf{r}') + (\lambda_{\mathcal{A}}/\lambda_{\mathcal{B}})^{1/2}\, h_{xc}^{\mathcal{B},\mathcal{A}}(\lambda_{\mathcal{A}}, \lambda_{\mathcal{B}}; \mathbf{r}, \mathbf{r}'); \quad \text{(A16a)}$$

$$E_{xc}^{\mathcal{M}}[\rho_{\mathcal{A}}, \rho_{\mathcal{B}}, \lambda_{\mathcal{A}}, \lambda_{\mathcal{B}}] = \frac{1}{2} \iint \{\lambda_{\mathcal{A}}\, \rho_{\mathcal{A}}(\mathbf{r})\, h_{xc}^{\mathcal{A}}[\lambda_{\mathcal{A}}, \lambda_{\mathcal{B}}; \mathbf{r}, \mathbf{r}'] + \lambda_{\mathcal{B}}\, \rho_{\mathcal{B}}(\mathbf{r})\, h_{xc}^{\mathcal{B}}[\lambda_{\mathcal{A}}, \lambda_{\mathcal{B}}; \mathbf{r}, \mathbf{r}']\}\, |\mathbf{r} - \mathbf{r}'|^{-1}\, d\mathbf{r}\, d\mathbf{r}'$$
$$\equiv E_{xc}^{\mathcal{A}}[\rho_{\mathcal{A}}, \rho_{\mathcal{B}}, \lambda_{\mathcal{A}}, \lambda_{\mathcal{B}}] + E_{xc}^{\mathcal{B}}[\rho_{\mathcal{A}}, \rho_{\mathcal{B}}, \lambda_{\mathcal{A}}, \lambda_{\mathcal{B}}]. \quad \text{(A17a)}$$

Expressing the scaled off-diagonal holes through the subsystem effective and diagonal holes [using Eq.(16a)] gives:

$$h_{xc}^{\mathcal{A},\mathcal{B}}(\lambda_{\mathcal{A}}, \lambda_{\mathcal{B}}; \mathbf{r}, \mathbf{r}') \equiv (\lambda_{\mathcal{A}}/\lambda_{\mathcal{B}})^{1/2}[h_{xc}^{\mathcal{A}}(\lambda_{\mathcal{A}}, \lambda_{\mathcal{B}}; \mathbf{r}, \mathbf{r}') - h_{xc}^{\mathcal{A},\mathcal{A}}(\lambda_{\mathcal{A}}, \lambda_{\mathcal{B}}; \mathbf{r}, \mathbf{r}')],$$

$$h_{xc}^{\mathcal{B},\mathcal{A}}(\lambda_{\mathcal{A}}, \lambda_{\mathcal{B}}; \mathbf{r}, \mathbf{r}') \equiv (\lambda_{\mathcal{B}}/\lambda_{\mathcal{A}})^{1/2}[h_{xc}^{\mathcal{B}}(\lambda_{\mathcal{A}}, \lambda_{\mathcal{B}}; \mathbf{r}, \mathbf{r}') - h_{xc}^{\mathcal{B},\mathcal{B}}(\lambda_{\mathcal{A}}, \lambda_{\mathcal{B}}; \mathbf{r}, \mathbf{r}')], \quad \text{(A16b)}$$

A subsequent use of these relations in Eq.(A14a) gives yet another expression for the scaled intersubsystem exchange-correlation energy:

$$E_{xc}^{\mathcal{A},\mathcal{B}}[\rho_{\mathcal{A}}, \rho_{\mathcal{B}}, \lambda_{\mathcal{A}}, \lambda_{\mathcal{B}}]$$

$$= \frac{1}{2} \int\int\{\lambda_{\mathcal{A}}\, \rho_{\mathcal{A}}(\mathbf{r})\, [h_{xc}^{\mathcal{A}}(\lambda_{\mathcal{A}}, \lambda_{\mathcal{B}}; \mathbf{r}, \mathbf{r}') - h_{xc}^{\mathcal{A},\mathcal{A}}(\lambda_{\mathcal{A}}, \lambda_{\mathcal{B}}; \mathbf{r}, \mathbf{r}')]$$

$$+ \lambda_{\mathcal{B}}\, \rho_{\mathcal{B}}(\mathbf{r})\, [h_{xc}^{\mathcal{B}}(\lambda_{\mathcal{A}}, \lambda_{\mathcal{B}}; \mathbf{r}, \mathbf{r}') - h_{xc}^{\mathcal{B},\mathcal{B}}(\lambda_{\mathcal{A}}, \lambda_{\mathcal{B}}; \mathbf{r}, \mathbf{r}')]\}$$

$$\times |\mathbf{r} - \mathbf{r}'|^{-1}\, d\mathbf{r}\, d\mathbf{r}'; \qquad \text{(A14b)}$$

The average holes for a given trajectory in Fig. 2 are obtained by integration over the corresponding cut of the $(\lambda_{\mathcal{A}}, \lambda_{\mathcal{B}})$-plane. In particular, for the uniform scaling *path 1* the average hole [Eqs.(67)-(69)] results from the integration over the common scale factor $\lambda = \lambda_{\mathcal{A}} = \lambda_{\mathcal{B}}$, e.g.,

$$h_{av(1)}^{\mathcal{X},\mathcal{Y}}(\mathbf{r}, \mathbf{r}') = \int h_{xc}^{\mathcal{X},\mathcal{Y}}(\lambda, \lambda; \mathbf{r}, \mathbf{r}')\, d\lambda$$

$$\equiv \int h_{xc}^{\mathcal{X},\mathcal{Y}}(\lambda; \mathbf{r}, \mathbf{r}')\, d\lambda \equiv h_{av}^{\mathcal{X},\mathcal{Y}}(\mathbf{r}, \mathbf{r}'). \qquad \text{(A18)}$$

Similarly, for the *path 6* the averaging involves the integration over the independend scale factor $\lambda_{\mathcal{B}} = 1 - \lambda_{\mathcal{A}}$, e.g.,

$$h_{av(6)}^{\mathcal{X},\mathcal{Y}}(\mathbf{r}, \mathbf{r}') = \int h_{xc}^{\mathcal{X},\mathcal{Y}}(1 - \lambda_{\mathcal{B}}, \lambda_{\mathcal{B}}; \mathbf{r}, \mathbf{r}')\, d\lambda_{\mathcal{B}}. \qquad \text{(A19)}$$

Finally, for the scaling *paths 2-5*, corresponding to the fixed scaling factor of one subsystem, $\lambda_{\mathcal{B}} = \lambda^{0}_{\mathcal{B}}$ (*paths 2* and *4*) or $\lambda_{\mathcal{A}} = \lambda^{0}_{\mathcal{A}}$ (*paths 3* and *5*), the hole averaging is defined by the integration over the scaling factor of the other subsystem, e.g.,

$$h^{\mathcal{X},\mathcal{Y}}_{av(2,4)}(\lambda^{0}_{\mathcal{B}};\ \mathbf{r},\ \mathbf{r}') = \int h^{\mathcal{X},\mathcal{Y}}_{xc}(\lambda_{\mathcal{A}},\ \lambda^{0}_{\mathcal{B}};\ \mathbf{r},\ \mathbf{r}')\ d\lambda_{\mathcal{A}}, \qquad \text{(A20a)}$$

$$h^{\mathcal{X},\mathcal{Y}}_{av(3,5)}(\lambda^{0}_{\mathcal{A}};\ \mathbf{r},\ \mathbf{r}') = \int h^{\mathcal{X},\mathcal{Y}}_{xc}(\lambda^{0}_{\mathcal{A}},\ \lambda_{\mathcal{B}};\ \mathbf{r},\ \mathbf{r}')\ d\lambda_{\mathcal{B}}. \qquad \text{(A20b)}$$

ACKNOWLEDGMENTS

This work was partly supported by a research grant from the State Committee for Scientific Research in Poland.

REFERENCES

(1) Hohenberg, P.; Kohn W. *Phys. Rev.* **1964,** *136B*, 864.

(2) Kohn, W.; Sham L.J. *Phys. Rev.* **1965,** *140A*, 1133.

(3) Parr, R.G.; Yang, W. "Density Functional Theory of Atoms and Molecules"; Oxford University Press: New York, 1989.

(4) Dreizler, R.M.; Gross, E.K.U. "Density Functional Theory: An Approach to the Quantum Many-Body Problem"; Springer-Verlag, Berlin, 1990.

(5) "Topics in Current Chemistry: Density Functional Theory I-IV"; Nalewajski, R.F., Ed.; Springer-Verlag: Heidelberg, 1996; Vols. 180-183.

(6) Nalewajski, R.F.; Korchowiec, J. "Charge Sensitivity Approach to Electronic Structure and Chemical Reactivity"; World-Scientific: Singapore, 1997.

(7) Nalewajski, R.F.; Korchowiec, J.; Michalak A. In "Topics in Current Chemistry: Density Functional Theory IV: Theory of Chemical Reactivity"; Nalewajski, Ed.; Springer-Verlag, Heidelberg, 1996; Vol. 183, 25-141; R. F. Nalewajski, *Phys. Chem. Chem. Phys.*("Chemical Reaction Theory"), **1999**, *1*, in press.

(8) Cohen, M.H. In "Topics in Current Chemistry: Density Functional Theory IV: Theory of Chemical Reactivity", Nalewajski, Ed.; Springer-Verlag, Heidelberg, 1996; Vol. 183, 143-173.

(9) Nalewajski, R.F. *Int. J. Quantum Chem.* **1997**, *61*, 181; Chandra, A.K.; Michalak, A.; Nguyen, M.T.; Nalewajski, R.F.*J. Phys. Chem. A* **1998**, *102*, 10182; Michalak, A.; De Proft, F.; Geerlings P.; Nalewajski R.F. *J. Phys. Chem. A* **1999**, *103*, 762.

(10) Nalewajski, R. F. In "Developments in the Theory of Chemical Reactivity and Heterogeneous Catalysis"; Mortier, W.M.; Schoonheydt, R.A.,Eds.; Research Signpost, Trivandrum, 1997; 135-196.

(11) Nalewajski, R.F. *Int. J. Quantum Chem.* **1998**, *69*, 591; *Polish J. Chem.* **1998**, *72*, 1763.

(12) Nalewajski, R.F.; Korchowiec, J. *J. Mol. Catal.* **1996**, *112*, 167.

(13) Nalewajski, R.F.; Michalak, A. *J. Phys. Chem. A* **1996,** *100*,20076; **1998,** *102*, 636.

(14) Wesołowski, T.A.; Warshel, A. *J. Phys. Chem.* **1993,** *97*, 8050; Wesołowski, T.A.; Weber, J. *Chem. Phys. Lett.* **1996,** *248*, 71.

(15) Nalewajski, R.F. *Theochem.* (R. Gaspar Issue), submitted.

(16) Parr, R.G.; Ellison, F.O.; Lykos, P.G. *J. Chem. Phys.* **1956,** *24*, 1106; Lykos, P.G.; Parr, R.G. *J. Chem. Phys.* **1956,** *24*, 1166;

(17) Klessinger, M.; McWeeny, R.J. *Chem. Phys.* **1965,** *42*, 3343; McWeeny, R. "Methods of Molecular Quantum Mechanics"; Academic Press: London, 1989.

(18) Mok, D.K.W.; Neumann, R.; Handy, N.C. *J. Phys. Chem.* **1996,** *100*, 6225.

(19) Murrell, J.N.; Carter, S.; Farantos, S.C.; Huxley, P.; Varandas, A.J.C. "Molecular Potential Energy Functions"; Wiley: Chichester, 1984; Varandas, A.J.C. *Advan. Chem. Phys.* **1988,** *74*, 255.

(20) Harris, J.; Jones, R.O. *J. Phys.* **1974,** *F4*, 1170; Harris, *J. Phys. Rev.* **1984,** *A29*, 1648.

(21) (a) Langreth, D.C.; Perdew, J.P. *Solid State Commun.* **1975,** *17*, 1425; *Phys. Rev.* **1976,** *B13*, 4274; (b) Perdew, J.P. In "Density Functional Methods in Physics", Dreizler, R.M.; da Providencia, J., Eds.; Plenum Press: New York, 1985); NATO ASI Series Vol. B123, 265-308.

(22) Gunnarson, O.; Lundqvist, B.I. *Phys. Rev.* **1976,** *B13*, 4274.

(23) Macke, W. *Ann. Phys. Leipzig* **1955,** *17*, 1.

(24) Gilbert, T.L. *Phys. Rev.* **1975,** *B12*, 2111.

(25) Harrimann, J. E. *Phys. Rev.* **1981,** *A24*, 680.

(26) March, N.H. *Phys. Rev.* **1982,** *A26*, 1845.

(27) Zumbach, G.; Maschke, K. *Phys. Rev.* **1984,** *A28*, 544; **1984,** *A29*, 1585.

(28) Levy, M. *Proc. Natl. Acad. Sci. USA* **1979,** *76*, 6062.

(29) Nalewajski, R.F. *Int. J. Quantum Chem.* (K. Ruedenberg Issue), submitted.

Subject Index

E

F

G

H

I

K

L

M

N

O

P

Q

R

S

T

U

V